



THE UNIVERSITY
of ADELAIDE

Liquid chemical looping gasification

Mohammad Mohsen Sarafraz

School of Mechanical Engineering, The University of Adelaide, Australia

A thesis submitted in fulfilment of the requirements for the degree of Ph.D. in
Mechanical Engineering

2019

Abstract

Combustion of fossil fuel for energy production is not a sustainable method since it releases CO₂, particulate materials and greenhouse gases such as NO_x into the atmosphere, which causes environmental pollution and global warming. Additionally, fossil fuel resources are limited, thus reliance on fossil fuels is not sustainable. To address this, special attention has recently been paid to renewable energy resources as alternatives for fossil fuels. However, it requires the development of new processes, or to integrate systems to produce energy through clean technologies aimed at the reduction of carbon dioxide emissions. One promising method is to convert fossil fuels, or biomass, to synthetic fuel referred to as “syngas”.

Gasification is an established method for producing syngas from a carbonaceous fuel. The conventional gasification pathways employ air to supply the required oxygen for the reactions, however, due to the presence of the nitrogen in the gaseous products, the quality of the syngas (molar ratio of H₂: CO) is relatively low. Thus, a new process for the production of syngas has been developed, referred to as a “chemical looping gasification” process, which uses solid metal oxide as the oxygen carrier. This process prevents direct contact between the feedstock and the air, addressing the challenge of the presence of nitrogen in the product. However, there are some disadvantages associated with the use of solid metal oxides, such as sintering, breakage of the particle, agglomeration and the deposition of the carbon on the oxygen carrier particles. Therefore, one potential solution to address the aforementioned challenges is to use a liquid metal oxide as an oxygen carrier instead of solid particles in a new process referred to as Liquid Chemical Looping Gasification (LCLG).

To assess the LCLG system, a thermodynamic model was developed to simulate the reactions occurring in a chemical looping gasification system with a liquid metal, such as copper oxide, as the oxygen carrier. To identify other suitable oxygen carriers, a thermodynamic model and a selection procedure were also developed to assess the chemical performance of the system

with various metal oxides. Copper, lead, antimony and bismuth oxides were potential options. Amongst them, lead oxide was assessed for integration of the system with a supercritical steam turbine cycle for the co-production of work and syngas. Bismuth oxide was thermodynamically and experimentally assessed for the gasification of biomass, coal and natural gas. To validate the developed models and to demonstrate the liquid chemical looping process, a series of experiments were conducted using a thermo-gravimetric analyser. Experiments were performed to assess the reduction and oxidation reactions of bismuth oxide with a graphitic carbon and air by measuring the mass change of the samples in the nitrogen and the air environments. The activation energy and reaction constant for the reduction and oxidation reactions were measured experimentally. The results obtained with the thermodynamic models for the bismuth oxide were in good agreement with those obtained with the experiments.

Thesis Declaration

I certify that this work contains no material which has been accepted for the award of any other degree or diploma in my name, in any university or other tertiary institution and, to the best of my knowledge and belief, contains no material previously published or written by another person, except where due reference has been made in the text. In addition, I certify that no part of this work will, in the future, be used in a submission in my name, for any other degree or diploma in any university or other tertiary institution without the prior approval of the University of Adelaide and where applicable, any partner institution responsible for the joint-award of this degree.

I acknowledge that copyright of published works contained within this thesis resides with the copyright holder(s) of those works.

I also give permission for the digital version of my thesis to be made available on the web, via the University's digital research repository, the Library Search and also through web search engines, unless permission has been granted by the University to restrict access for a period of time.

I acknowledge the support I have received for my research through the provision of an Australian Government Research Training Program Scholarship.

Mohammad Mohsen Sarafraz

Acknowledgements

I would like to express the deepest appreciation and sincere gratitude to my principal supervisor A/Prof Maziar Arjomandi. Without his guidance, this thesis would not have been possible. Special thanks and appreciation with deep love to my amazing wife, Maryam, who has always been a supportive friend and heart-warming company. Special thanks to my family, my mother and father, two real angels, and my beautiful little sister for their support and help. I have to show my gratitude to my friends Sina, Amin, Ali, Yousef, Amir, Mina and others who I cannot list here. Their unconditional support helped me get through the ups and downs of this journey.

I would also like to show my appreciation for my best ever supervising panel Maziar Arjomandi, Mehdi Jafarian and Graham Nathan for their great guidance, insightful inputs, encouragement, endless support and friendship. This supervising panel was a gift from heaven that you cannot find anywhere else.

I have also had amazing support and encouragement from the Workshop staff: Ian Linke, Phil, Joseph and Norio, along with great help and guidance.

Table of Contents

Abstract.....	I
Thesis Declaration	III
Acknowledgments.....	IV
Table of Contents.....	V
Chapter 1 Introduction.....	1
1.1. Background and motivation.....	1
1.2. Objectives of the research.....	6
1.3. Structure of the thesis.....	8
1.4. Publications arising from this thesis	11
1.4.1. Published journal papers	11
1.4.2. Conference presentation.....	12
1.5. Thesis format	12
References.....	13
Chapter 2 Literature review	15
2.1. Background.....	15
2.2. Chemical looping combustion	18
2.3. Chemical looping reforming	22
2.4. Chemical looping gasification	23
2.5. Thermodynamic and experimental assessments on chemical looping gasification	26
2.6. Influence of type of feedstock on performance of chemical looping gasification	32
2.7. Solid oxygen carrier.....	34
2.8. Particle size models for solid-gas reactions	34
2.8.1. Changing grain size model.....	34
2.8.2. Shrinking core model.....	35
2.9. Challenges associated with the solid oxygen carriers	36
2.10. Liquid oxygen carriers for chemical looping combustion	42
2.11. Liquid metals for hydrogen and syngas production	44
2.12. Kinetics of reaction with carbon in liquid metal.....	55
2.13. Summary and discussion of identified gaps.....	59
References.....	63
Chapter 3 development of a model for liquid chemical looping gasification.....	73
3.1. Chapter overview	73

Statement of Authorship	74
Chapter 4 Performance assessment of various oxygen carriers for chemical looping gasification process	89
4.1. Chapter overview	89
Statement of Authorship	91
Chapter 5 Co-production of syngas and power with liquid chemical looping gasification process	106
5.1. Chapter overview	106
Statement of Authorship	108
Chapter 6 Syngas production from biomass using liquid chemical looping gasification	126
6.1. Chapter overview	126
Statement of Authorship	128
Chapter 7 Experimental investigation of the reduction of liquid bismuth oxide with graphite	144
7.1. Chapter overview	144
Statement of Authorship	146
Chapter 8 Conclusion and future works	157
8.1. Significance of the present study	157
8.2. Recommendations for future works	161
8.2.1. Experimental analysis of the outlet gases	162
8.2.2. Plausible application of concentrated solar thermal energy	162
8.2.3. Heat and mass transfer within a bubbling regime	163
8.2.4. Development of an ash separator	164
8.2.5. Fabrication of a small-scale LCLG plant	164
References	165

Chapter 1 Introduction

1.1. Background and motivation

Sustainable production of energy is by far one of the greatest challenges in the world and various methods for producing energy have been developed to satisfy the demands and requirements for social and economic development. Hence, developing an economically viable and reliable energy production system and decreasing its contribution to climate change are the two barriers towards a sustainable future (Owusu & Asumadu-Sarkodie, 2016). Currently, fossil fuels (carbonaceous fuels) are the main resources for energy production, however, reliance on fossil fuels is not sustainable since they are limited and pollute the environment.

Combustion is an established method to release energy from the carbonaceous feedstock accompanying the emission of CO₂ and other greenhouse gases. A census has been reached that the emission of CO₂ into the environment is one of the major reasons for global warming. Hence, seeking for an alternative source of energy and/or an alternative energy production method have been targeted by researchers to address the aforementioned challenges.

Australia is one of the main exporters of coal in the world and has the fifth largest resources of black coal. The black and brown coal account for ~75% of total electricity production in Australia (Burnard & Bhattacharya, 2011). However, the combustion of coal produces various pollutants, such as sulphur-based products, heavy metals and some trace elements, such as arsenic. These trace elements, together with other components, are pollutants, which directly (or indirectly) influence the environment. Some are known to cause cancer and respiratory illnesses, while some of them influence decision-making and the brain inside the human body. Thus, release of particulate materials and chemical compounds, together with carbon dioxide, are the main challenges associated with the use of fossil fuels for energy production in the majority of industrial sectors in Australia.

To overcome the pollution and CO₂ emissions, one potential solution is to convert fossil fuels

such as coal into cleaner products, such as liquid fuels or hydrogen. Liquid fuels, such as alcohols, generate lower pollution levels and do not release trace elements into the atmosphere. To convert coal to liquid fuel or hydrogen, an intermediate product is required. Synthetic gas (referred to as syngas: a mixture of hydrogen, carbon monoxide, a small amount of methane and other gaseous components) is the main product of the gasification process, which can be converted to liquid fuels via Fischer-Tropsch and syngas-to-liquid processes.

Gasification comprises a chain of reactions in which a carbonaceous feedstock is partially oxidised and converted to H₂, CO and other gaseous products. During the gasification of feedstock, the following reactions occur:



The net enthalpy of reaction for the above reactions is positive and as a result, gasification is an endothermic process. Therefore, for gasification reactions to proceed, thermal energy must be supplied to the gasifier. Hence, in a conventional gasification process, part of the feedstock is combusted to meet the thermal energy required for driving the gasification process, thereby requiring more feedstock to be combusted and gasified.

To provide sufficient oxygen for the gasification process, air is blown into the gasifier, which not only produces a bubbly and/or fluidised medium for better heat and mass transfer, but also supplies the required oxygen for the gasification reactions. Furthermore, the ratio of air to inlet feedstock has always been a determining parameter for the gasification process. If the ratio of

the inlet air to feedstock equals the stoichiometric value, the feedstock is completely combusted, however if the ratio of air to feedstock is less than the stoichiometric value, the feedstock is gasified into CO, H₂ and other gaseous products. Despite the fact that air is a suitable candidate for gasification, it introduces nitrogen into the gasifier. As a result, the final gas product includes a large portion of nitrogen (e.g. ~30%), which not only reduces the purity of the syngas, but also reduces the quality of the syngas and limits its application. For example, a syngas with the molar ratio of H₂: CO~2.01 can be used in fuel cells and Fischer-Tropsch processes (Riedel et al., 1999). However, if the molar ratio is H₂: CO~1, the syngas has more limited applications, such as combustion of syngas (Karimipour, Gerspacher, Gupta, & Spiteri, 2013). Hence, the presence of nitrogen in syngas (referred to as nitrogen dilution) is another challenge associated with conventional gasification processes (Prathap, Ray, & Ravi, 2008).

To address the nitrogen dilution issue, a chemical looping gasification process has recently been developed (Fan, Li, & Ramkumar, 2008; Li et al., 2009), which prevents direct contact between the air and fuel, thereby hindering syngas dilution. This concept employs solid metal oxide particles to supply the oxygen required for the gasification reactions. Particles are circulated between two reactors, namely the air and the gasification reactors, as shown in Figure 1.1. In the gasification reactor, a chain of reactions occurs between the feedstock and metal oxide particles and the feedstock is partially oxidised. During the partial oxidation of the feedstock, the metal oxide releases its oxygen content and a reduced metal oxide forms in the reactor. The syngas is produced in the gasifier and leaves the reactor. The molar ratio of H₂: CO is highly dependent on the molar ratio of the oxygen carrier to the feedstock. The higher the molar ratio of metal oxide particle to feedstock, the lower the mole fraction of CO and H₂. Instead, the combustion reaction proceeds, resulting in an increase in the mole fraction of CO₂ and H₂O.

The reduced metal oxide is transported to the air reactor, in which air is introduced to react

with the reduced metal oxide. The reaction in this reactor is highly exothermic and the oxygen of the oxygen carrier is recovered. The outlet from the air reactor contains hot air with a mole fraction of oxygen $\ll 0.21$, which is referred to as “vitiated air”. Notably, to enrich the syngas and to increase its calorific value (giving a lower heating value), steam is injected into the gasification reactor. This has two advantages: 1) enriching the hydrogen content of the syngas, and 2) fluidising and changing the physical properties and porosity of the feedstock, which facilitate the heat and mass transfer within the reactor.

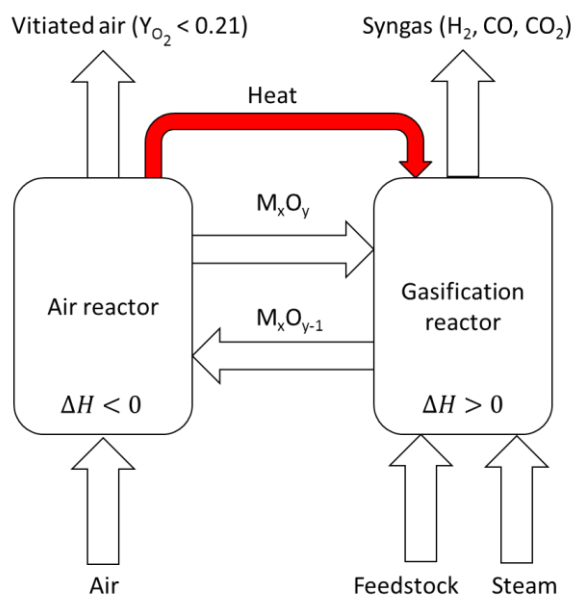


Figure 1.1 A schematic diagram of the chemical looping gasification process for syngas production with steam.

Despite the advantages associated with the use of chemical looping gasification, the reactivity of solid metal oxides is gradually reduced due to the occurrence of sintering, attrition and agglomeration of particles. The sintering of the solid metal oxide particles results in the formation of the clog and the agglomeration of the particles within the reactors, which not only devastate the reaction sites on the external layer of the particles, but also change the size of the metal oxides after several cycles (Ku et al., 2017). Since the kinetic of the solid-gas systems is highly dependent on the size and specific surface area of the particles, the reactivity of the

particles decreases. The challenge is more pronounced when particles are exposed to a carbon-containing feedstock. In this condition, carbon deposition worsens the scenario by covering the irregularities and reaction sites of the particles. This results in a drastic reduction in the reactivity of the oxygen carrier. For example, in a study conducted by Ku et al. (Ku et al., 2017), CuO was utilised as an oxygen carrier in a chemical looping process at temperatures ranging between 1000°C and 1300°C. Figure 1.2 presents the results of a visualisation study on the morphology of CuO metal oxides as an oxygen carrier in a chemical looping process.

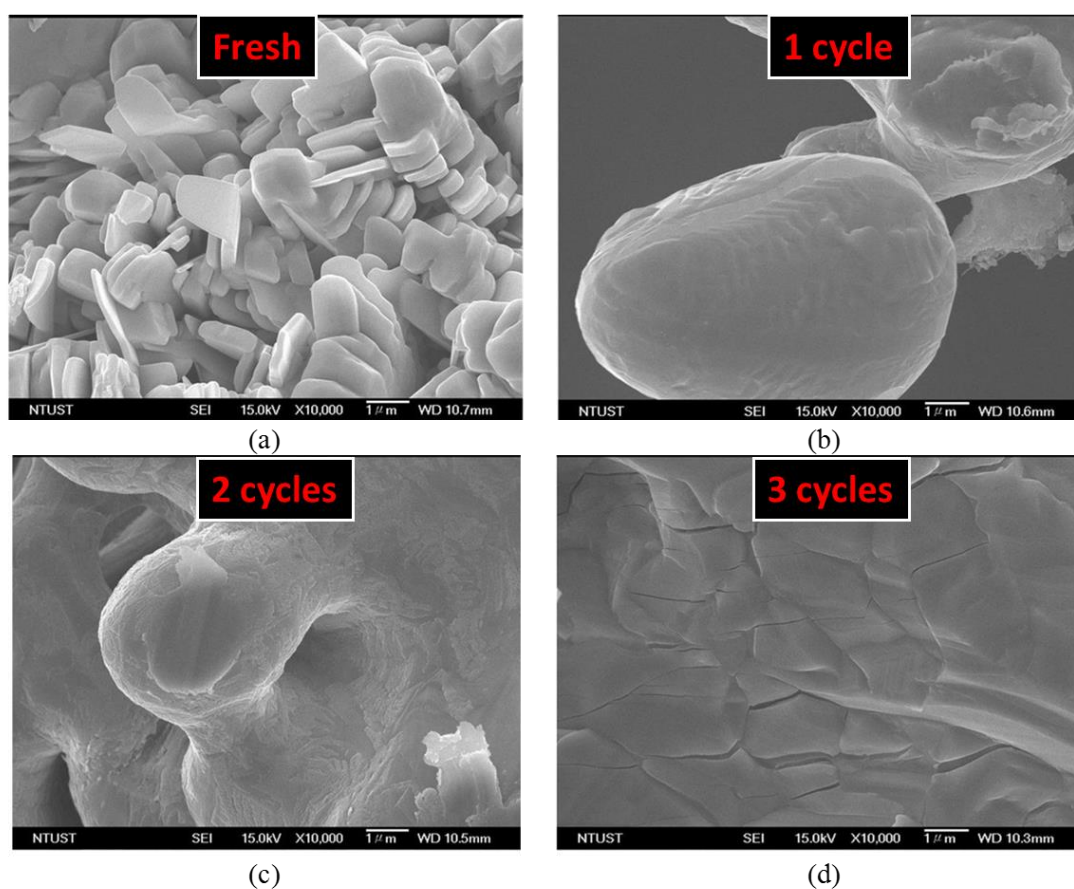


Figure 1.2 Scanning electron microscopic images of CuO metal oxide particles used as an oxygen carrier in a chemical looping process. Images are adapted from (Ku et al., 2017), a) fresh CuO, b) CuO after one cycle, c) CuO after two cycles and d) CuO after three cycles.

As shown in Figure 1.2, after several cycles of operation, the morphology of the CuO particles

was changed. The mean size, the average surface area together with the general structure of the particles, were destroyed due to the occurrence of attrition, sintering and agglomeration. In addition, they showed that the challenges are more pronounced at high temperatures.

One potential solution to address the challenges associated with the utilisation of solid metal oxides in chemical looping systems is to use liquid metal oxides as an oxygen carrier instead of solid metal oxide particles. By doing this, not only challenges such as sintering, attrition and agglomeration are addressed, but also the phase of reactions in the gasification reactor is changed from a solid (feedstock)-solid (oxygen carrier)-gas (gasifying agent) reaction to a solid (feedstock)-liquid (oxygen carrier)-gas (gasifying agent) reaction. The latter can present better heat and mass transfer in comparison with the former. This is because the thermal conductivity of liquid metals is high (e.g. 394 W/m. K for copper oxide, or 36 W/m. K for lead oxide). Moreover, the mass transfer in liquid metals is plausible (Dunn, Bonilla, Ferstenberg, & Gross, 1956). Such characteristics can enlist the liquid metals as a plausible oxygen carrier to be utilised in an LCLG process.

The primary motivation of this study is to develop a new understanding and a well-resolved model to investigate the plausible application of liquid metal oxides for the gasification of carbonaceous feedstock in a chemical looping gasification process. The research goals are not only to develop a thermo-chemical equilibrium model for the gasification of feedstock with liquid metal oxides but also to determine the potential thermodynamic parameters for operating and controlling the chemical looping gasification process.

1.2. Objectives of the research

The primary objective of the present research is to develop a thermochemical equilibrium model for the gasification of carbon-containing components with liquid metal oxides in a chemical looping gasification. This is because the lack of knowledge in this area is seen and a

detailed assessment of the process is required. To achieve this objective, it is necessary to model the system using thermo-equilibrium techniques such as Gibbs' minimisation method to determine the composition of the solid, liquid and gas phases before and after the gasification process. It is expected that at certain temperatures above the melting point of a liquid metal oxide, oxygen is released from the liquid metal oxide and reacts with the feedstock to produce carbon monoxide. Likewise, the reaction between the gasifying agent (e.g. steam) and feedstock, together with liquid metal oxide, produces hydrogen and CO, which are the main components of a synthetic gas. Therefore, the Gibbs free energy of all components, enthalpy of reactions and equilibrium constant of the reactions need to be estimated using an accurately developed model.

The secondary objective of this work is to assess the chemical performance and potential of various liquid metal oxides as an oxygen carrier in liquid chemical looping gasification thermodynamically. This can be achieved by assessing different metal oxides against criteria such as the Gibbs free energy of oxidation and reduction reaction, enthalpy of reaction, melting point, oxygen molar content, syngas quality and chemical performance. The thermodynamic selecting procedure will identify plausible oxygen carriers for the chemical looping gasification process.

The third objective is to assess the thermodynamic potential of liquid metal oxides identified in the previous tasks for the co-production of syngas and work via a power cycle connected to the process through vitiated air. To improve the energetic performance of the system, a liquid chemical looping gasification system is proposed, to be connected to a combined cycle power block through the air reactor to produce work together with syngas production from the gasification reactor. For this purpose, it is essential to assess the exergy of the process, together with energetic analysis.

The last objective of this work is to conduct thermodynamic modelling to assess the potential

application of liquid chemical looping gasification for producing syngas with a high molar ratio of H_2/CO from low-grade feedstock such as biomass. In addition, a set of experiments will be conducted using high-fidelity instruments to validate the outcome of the models and to partially prove the gasification of carbonaceous feedstock with liquid metal oxides. To achieve this, a thermo-gravimetric analyser together with x-ray diffraction tests will be employed to demonstrate the reduction and oxidation of a liquid metal oxide with feedstock and air. The activation energy and the reaction constant of the reduction and oxidation reactions will be measured experimentally and the liquid metal oxide characterised before and after the experiments. Results of the experiments will be used to validate both the models and the results obtained from the previous tasks.

1.3. Structure of the thesis

The structure of this thesis is briefly discussed in this section. The template of this thesis is formatted as a collection of manuscripts that have been published or are currently under review in peer-reviewed journals. At first, an introductory chapter discusses the motivation behind this research. A literature review is also added as an independent chapter (Chapter 2). The published papers and those under review form the foundation and the basis of this thesis and constitute other chapters, which show the progress of the current study sequentially.

In chapter 2 of this thesis, a deep literature review was conducted to determine the key questions and gaps in the existing knowledge to establish a detailed framework of this study. Initially, the fundamentals and basics of the gasification process were studied, to discuss the chemical and thermodynamic parameters associated with the gasification process. The advantages and limitations of conventional gasification processes were elaborated and the importance of the employment of the chemical looping process was highlighted. Then, various configurations of chemical looping, including chemical looping combustion, chemical looping

reforming and chemical looping gasification, were elaborated. Again, the advantages and drawbacks of each process was described. Finally, a review was conducted on the state-of-the-art studies on the potential application of liquid metal oxides for hydrogen and syngas production.

In chapter 3, a thermodynamic model was presented, through which the potential of a liquid metal oxide for the gasification of a carbonaceous feedstock was assessed. The influence of different parameters such as temperature, pressure, partial pressure of oxygen and the molar ratio of the liquid oxygen carrier to the feedstock and the steam to the feedstock on the composition of the syngas product was investigated thermodynamically. The lower heating value of syngas (the exergy partitioned in the syngas) was also assessed for various operating conditions.

In chapter 4, a thermodynamic model was developed to analyse various pairs of metal oxides to identify the most suitable candidates for the LCLG. To achieve this, the chemical and thermodynamic potential of different liquid metals were assessed against criteria such as melting temperature, the Gibbs free energy of oxidation and reduction reactions, enthalpy of reactions, oxygen molar content, the quality of the syngas (the molar ratio of H_2 : CO), the molar ratio of CO/CO₂ and the exergy partitioned in the syngas. This assessment narrowed down a wide range of metal oxides to a few options. Finally, selected metal oxides were suggested for combustion and gasification applications based on their thermodynamic potential and lower heating value, the quality of the syngas and the composition of the exhausted gases.

In chapter 5, the thermodynamic potential of lead oxide was investigated for the co-production of syngas and work with a power block connected to the liquid chemical looping gasification process. For this purpose, a supercritical steam power block was connected to the air reactor through the vitiated air for producing steam in a supercritical condition, while syngas was produced through the gasification reactor. The influence of different operating parameters such

as the liquid oxygen carrier to the feedstock, the steam to the feedstock and also the molar ratio of CO₂ to the feedstock on the quality of syngas, exergy and thermal energy of the system was investigated.

In chapter 6, the potential of liquid metal oxide for the gasification of biomass, coal and natural gas was investigated thermodynamically to produce syngas with a high molar ratio of H₂: CO (> 3). Such syngas can have wide applications in hydrogen production, clean fuel production, fuel cells and Fischer-Tropsch processes. In this chapter, based on the phase diagram of liquid bismuth oxide, a suitable gasification regime was identified and, with the use of excess steam, the quality of the syngas was set to > 3. An exergy analysis was performed to evaluate the portion of exergy partitioned in the syngas. The biomass conversion was calculated and the quality of the syngas product was compared with the results reported in the literature.

A set of experiments was conducted and discussed in Chapter 7 to demonstrate the reduction and oxidation of a liquid metal oxide with graphitic carbon and air respectively. To conduct the experimental investigation, a thermo-gravimetric analyser was used to monitor the mass change during the gasification of bismuth oxide with carbon. The mass change was evaluated at various ratios of bismuth oxide to graphite and temperatures. The activation energy of the reaction and oxidation reactions, together with the reaction constant were measured experimentally and a first-order kinetic of reaction of liquid bismuth with carbon and air was developed experimentally using the Kissinger method. This not only validated the thermodynamic models developed for the process, but also produced some novel data on the kinetics of the reaction of bismuth with carbon, which to the best of the author's knowledge is not available in the literature.

The final chapter is chapter 8, which includes the key findings obtained in each chapter, conclusions drawn during the modelling and experimental investigations and suggestions for future research.

1.4. Publications arising from this thesis

The research conducted in this thesis has led to several publications. Some of them have been published in well-known peer-reviewed journals and peer-reviewed conference proceedings and some of them are still under review for possible publication in high impact journals. The following is the list of papers published and under consideration for possible publication:

1.4.1. Published journal papers

M.M. Sarafraz, M. Jafarian, M. Arjomandi, G.J. Nathan, Potential use of liquid metal oxides for chemical looping gasification: A thermodynamic assessment, *Applied Energy*, 195, 2017, 702-712.

M.M. Sarafraz, Mehdi Jafarian, Maziar Arjomandi, Graham J. Nathan, The relative performance of alternative oxygen carriers for liquid chemical looping combustion and gasification, *International Journal of Hydrogen Energy*, 42, 2017, 16396-16407.

M.M. Sarafraz, M. Jafarian, M. Arjomandi, G.J. Nathan, Potential of molten lead oxide for liquid chemical looping gasification (LCLG): A thermochemical analysis, *International Journal of Hydrogen Energy*, Volume 43, 2018, 4195-4210.

M.M. Sarafraz, M. Jafarian, M. Arjomandi, G.J. Nathan, The thermochemical potential liquid chemical looping gasification with bismuth oxide, *International Journal of Hydrogen Energy*, 44, (2019) 8038-8050.

M.M. Sarafraz, M. Jafarian, M. Arjomandi, G.J. Nathan, M. M. Sarafraz, M. Jafarian, M. Arjomandi, G. J. Nathan, Experimental investigation of the reduction of liquid bismuth oxide with graphite, *Fuel Processing Technology*, 188, (2019) 110-117.

1.4.2. Conference presentation

M.M. Sarafraz, M. Jafarian, M. Arjomandi, G.J. Nathan, Solar Liquid Chemical Looping Gasification for syngas production-A thermodynamic assessment, Asia-Pacific Solar Research Conference 2017, Melbourne, Oral presentation.

M.M. Sarafraz, M. Jafarian, M. Arjomandi, G.J. Nathan, Potential application of liquid antimony oxide for solar-aided hydrogen production, Asia-Pacific Solar Research Conference 2017, Melbourne, Oral presentation.

1.5. Thesis format

This thesis is based on the collection of the manuscripts produced during the course of the research and has been submitted according to the format approved by the University of Adelaide. The thesis is provided and available in both hard and soft copy which are identical. The soft copy is available online at the University of Adelaide Library and can be viewed using Adobe Reader.

References

- Burnard, K. and S. Bhattacharya (2011). "Power generation from coal."
- Dunn, W., C. Bonilla, C. Ferstenberg and B. Gross (1956). "Mass transfer in liquid metals." *AIChE Journal* **2**(2): 184-189.
- Fan, L., F. Li and S. Ramkumar (2008). "Utilization of chemical looping strategy in coal gasification processes." *Particuology* **6**(3): 131-142.
- Karimipour, S., R. Gerspacher, R. Gupta and R. J. Spiteri (2013). "Study of factors affecting syngas quality and their interactions in fluidized bed gasification of lignite coal." *Fuel* **103**: 308-320.
- Ku, Y., S.-H. Shiu, Y.-C. Liu, H.-C. Wu, Y.-L. Kuo and H.-Y. Lee (2017). "Liquid sintering behavior of Cu-based oxygen carriers for chemical looping process." *Catalysis Communications* **92**: 70-74.
- Li, F., H. R. Kim, D. Sridhar, F. Wang, L. Zeng, J. Chen and L.-S. Fan (2009). "Syngas chemical looping gasification process: oxygen carrier particle selection and performance." *Energy & fuels* **23**(8): 4182-4189.
- Owusu, P. A. and S. Asumadu-Sarkodie (2016). "A review of renewable energy sources, sustainability issues and climate change mitigation." *Cogent Engineering* **3**(1): 1167990.
- Prathap, C., A. Ray and M. Ravi (2008). "Investigation of nitrogen dilution effects on the laminar burning velocity and flame stability of syngas fuel at atmospheric condition." *Combustion and Flame* **155**(1-2): 145-160.
- Riedel, T., M. Claeys, H. Schulz, G. Schaub, S.-S. Nam, K.-W. Jun, M.-J. Choi, G. Kishan and K.-W. Lee (1999). "Comparative study of Fischer–Tropsch synthesis with H₂/CO and H₂/CO₂ syngas using Fe- and Co-based catalysts." *Applied Catalysis A: General* **186**(1-2): 201-213.

Chapter 2 Literature review

2.1. Background

Since the industrial revolution in the eighteenth and nineteenth centuries, dependence on fossil fuels by the industrial sectors have been anomalously increased. Much effort has been made to employ other energy resources, such as nuclear or renewables (e.g. wind or solar thermal and/or electrical energy) to lower the reliance on fossil fuel. However, more than 90% of the world's energy demand is anticipated to be met by fossil fuels until 2030 (Conti et al., 2016; Gaffney & Marley, 2009; IEA., 2017; Velazquez-Vargas, 2007). A consensus has been reached that the presence of CO₂ in the atmosphere can gradually increase the mean temperature of the atmosphere around the earth. According to a study conducted by the US Energy Information Administration (EIA), as represented in Figure 2.1, by 2030, the energy demand will reach ~700 quadrillion BTU, increasing by ~28% in comparison with the current world energy demand. Fossil fuel resources are limited resources, hence, this is a driver to seek alternative fuels or to develop new pathways for combusting fossil fuels with a view to lowering the emissions of greenhouse gases and pollutants to the environment (Change, 2007).

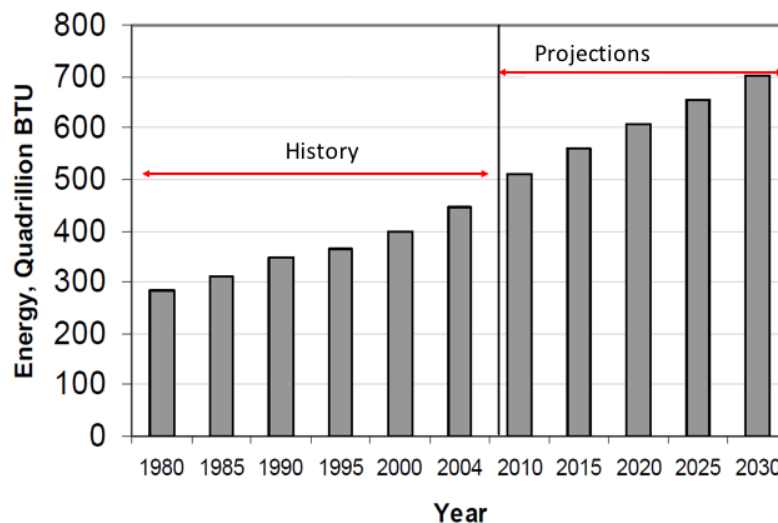


Figure 2.1. World energy consumption from 1980 to 2030 adapted from Outlook(Outlook, 2007).

To address the environmental challenges associated with the combustion of fossil fuels, one potential solution is to convert the fossil fuels into clean products, such as liquid fuels or hydrogen. However, liquid fuels are not a natural resource; hence, energy needs to be consumed to convert fossil fuels to these products. Thus, the conversion of a fossil fuel to a clean fuel requires an intermediate product such as synthetic gas (Woolcock & Brown, 2013).

Syngas can be converted to other renewable fuels such as hydrogen (with a CO sweeping process) or liquid fuels (with a Fischer-Tropsch process). Apart from this, a synthetic gas has many applications in the industrial sectors. It is usually used in internally combusting engines for electricity production or is employed for producing the thermal energy for high-temperature process heat (Lieuwen, Yetter, & Yang, 2009). Since the combustion temperature of syngas is higher than that of fossil fuels, therefore, in those processes with syngas as a primary fuel, the thermal efficiency of the process can be higher than for those with lower combustion temperatures. Direct combustion of syngas can also be used in equipment such as steam boilers, cement kilns and dryers (Rostrup-Nielsen, 2002). Given the fact that the syngas can be subject to a chemical transformation process, it can also have wide range of other applications in the automotive, plastic, hygiene and transportation sectors.

The conventional method for producing a hydrogen-enriched syngas from a gaseous fuel is to use an air/steam reforming process, while another well-established method to produce syngas from a solid feedstock is the gasification process. Both processes are very similar and the main differences lie in the type of fuel and the configuration of the reactors used for the process.

During the gasification process, a partial oxidation of carbon occurs and the hydrogen content of the feedstock is released. The molar ratio of the produced hydrogen to carbon monoxide, referred to as the syngas quality, is a critical parameter determining the application of syngas (Rostrup-Nielsen, 2002). For example, if $H_2: CO \sim 2$, syngas can be used in a Fischer-Tropsch

process plant, however, if $H_2: CO \sim 1$, it can be used for direct combustion. In most of the carbonaceous fuels and biomass feedstock, the hydrogen content is not normally sufficient to enrich the syngas and increase its quality. Therefore, a gasifying agent such as steam is used not only to increase the mixing inside the reactor, but to enhance the molar ratio of $H_2: CO$.

The simplest configuration of a gasifier is an air gasifier, which employs air to gasify a carbonaceous fuel. For this configuration, air is blown into the gasifier to provide agitation and mixing of the feedstock with air. The air gasification process normally occurs at $> 900^\circ C$ to achieve a high conversion rate of feedstock to syngas. Since there are some impurities in the feedstock, a cyclonic ash separator is used to separate the ash materials and unreacted feedstock. Although the use of air for gasification is cost-effective and simple, nitrogen dilution is the main challenge associated with the air-blown gasifiers. This is because nitrogen appears in the syngas product, resulting in the dilution of the syngas (Prathap et al., 2008). This limits the application of the syngas product. Therefore, direct contact between air and fuel in the gasification reactor must be avoided. The chemical looping process is a recently developed technology, which provides conditions to avoid direct contact between air and fuel.

A chemical looping process employs two reactors referred to as the air and the fuel reactor. An oxygen carrier is employed to absorb the oxygen in the air reactor and release it in the fuel reactor. The released oxygen from the oxygen carrier is used to drive the combustion and/or gasification reaction. The reduced particles are sent to the air reactor and their oxygen content is recovered via oxidation reaction with air. By doing this, direct contact between the air and the fuel is prevented, resulting in the production of syngas with a higher molar ratio of $H_2: CO$. Hence, depending on the application of the chemical looping, it can be classified into different processes as follows:

2.2. Chemical looping combustion

The main purpose of a Chemical Looping Combustion (CLC) process is to release the energy of a carbonaceous fuel to produce heat that can be used in further applications (e.g. heat exchanging media) or other endothermic processes (Adánez et al., 2004; Adánez et al., 2005; de Noronha, Miranda, Cavalca, Memmott, & Ramesh, 2014; Hatanaka, Matsuda, & Hatano, 1997; Ishida & Jin, 1994; Kim, Go, Jeon, & Park, 2010; Lyngfelt, Kronberger, Adanez, Morin, & Hurst, 2004). A CLC process usually consists of two interconnected reactors, namely fuel and air reactors. The complete oxidation of fuel occurs in the reduction reactor resulting in the production of CO₂ and H₂O. To achieve the complete conversion of fuel, oxygen needs to be supplied to the fuel reactor at its stoichiometric value. Solid metal oxides are utilised as the oxygen carrier to provide the required oxygen for the combustion process. Consuming the oxygen in the fuel reactor, the particles are reduced and subsequently conveyed to the air reactor. In the air reactor, the reduced particles are exposed to a large amount of air to absorb the oxygen in the air and to produce the metal oxide. The process of circulation of the oxygen carrier between reactors in a CLC continues repeatedly without using air in the fuel reactor. Notably, the outlet from the fuel reactor is carbon dioxide and water that can be captured and stored. Hence, CLC is inherently a carbon capture process. Likewise, the combustion reaction in the fuel reactor is endothermic, while the oxidation reaction in the air reactor is exothermic. Hence, the oxygen carrier can be utilised to transfer the released heat in the air reactor to the fuel reactor. Figure 2.2 presents a schematic diagram of the CLC process.

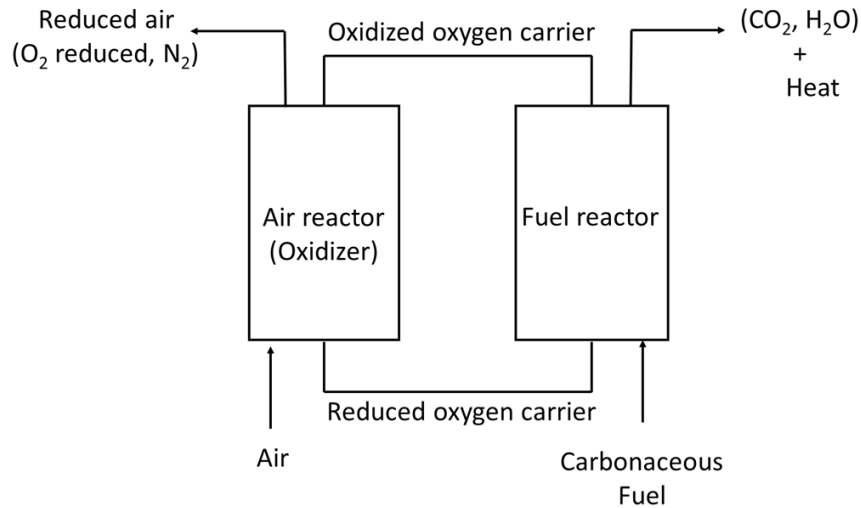


Figure 2.2. A schematic diagram of a chemical looping combustion system.

In the fuel reactor, the rate of heat and mass transfer is a key parameter, which influences the configuration and chemical performance of the CLC. This is because it directly influences the residence time, size and type of the reactor. Better heat and mass transfer inside the reactor results in a decrease in the required residence time and, subsequently, the size of the reactor is decreased. It is worth mentioning that the type of reactor depends on the kinetics of the reactions and the operating conditions. A fluidized bed is a plausible reactor for the CLC process, as it facilitates effective phase contact and sufficient residence time (Pan, Velo, Roca, Manyá, & Puigjaner, 2000). The effective phase contact between the reactants enhances the heat and mass transfer between the components inside the reactor.

In the air reactor, the reduced metal oxide is exposed to a high flow rate of air to provide sufficient fluidisation and better solid-gas contact. Hence, a high-velocity reactor is a plausible configuration for the air reactor. Notably, the rate of the oxidation reaction is relatively higher than that reported for the reduction reaction. Thus, the configuration of the air reactor and the fuel reactor might not be the same. Therefore, many studies have been conducted to assess the various configurations for the air and fuel reactors in a chemical looping combustion process, which are reviewed as follows:

At first, chemical looping combustion was designed and fabricated to work with gaseous fuels

such as natural gas under atmospheric pressure. Hence, much effort was made to identify the best plausible configurations for an atmospheric CLC system working with natural gas. For example, Lyngfelt et al. (Lyngfelt, Leckner, & Mattisson, 2001) proposed a basic design for the recirculation of an oxygen carrier in fluidised bed reactors referred to as a “circulating fluidised bed configuration”. The proposed system showed a plausible rate of heat and mass transfer between the oxygen carrier and the gaseous fuel. This was attributed to the superior surface contact between the solid particles and the gaseous fuel due to the uniform fluidisation of the solid phase. Other configurations were also assessed, considering high-velocity risers and low-velocity bubbling reactors (Johansson, Lyngfelt, Mattisson, & Johnsson, 2003; Kronberger et al., 2004; Kronberger, Lyngfelt, Löffler, & Hofbauer, 2005) and almost the same results were reported. It was found that CLC has the ability to work at different configurations, however, depending on the performance required from the process, specific configurations and oxygen carriers need to be matched and employed. In fact, the type of fuel and the rate of the reaction between the oxygen carrier and the fuel were determining parameters for the design of the CLC (Lyngfelt & Thunman, 2005b; H.-J. Ryu, Jin, & Yi, 2005). All of them noticed that for most solid-gas reactions, the mass transfer resistance is relatively higher than that measured for the liquid-gas reactions. Hence, more residence time is required for the solid-gas reactions to proceed. Therefore, it was concluded that the riser configuration can not only provide sufficient residence time for the reduction of the oxygen carrier but also provide sufficient driving force for the circulation of the oxygen carrier. These features are also offered by bubbling fluidised regimes (Adánez, Gayán, et al., 2006; H. Ryu, Jo, Park, Bae, & Kim, 2010). The dual fluidised bed configuration is another plausible option, which was proposed and tested at the Technology University of Vienna (TUWIEN), in which two bubbling fluidised bed reactors were employed for the air and fuel reactors. The test rig was designed based on a 120 kW thermal input (Kolbitsch, Pröll, Bolhar-Nordenkampf, & Hofbauer, 2009). To achieve

higher thermal and chemical performances, a turbulent bubbling regime was identified. In this regime, sufficient heat and mass transfer between the oxygen carrier and gaseous fuel was provided. A pneumatic system was used to recirculate the oxygen carriers between the reactors, while providing a bubbling regime in both reactors. To control the solid holdup, a direct hydraulic link between the two reactors was provided. It was found that the circulation of the oxygen carrier strongly depends on the flow rate of the air and the gaseous fuel.

At IFP France, a new concept of two interconnected bubbling beds with an independent solid flow control was developed at a scale of 10kW thermal input. To provide sufficient oxygen in the fuel reactor, a rapid circulation system, independent from the gas flow rate, was developed (Shen, Wu, Xiao, Song, & Xiao, 2009). Later, Ryu et al. (H. Ryu et al., 2010) modified the concept developed by Shen et al. (Shen et al., 2009) at 50 kWth and implemented some injection nozzles inside each reactor. This further enhanced the mixing and the circulation of the oxygen carrier within the reactors.

ALSTOM developed a new concept for the hybrid gasification and combustion of carbonaceous fuel including natural gas and solid feedstock (Abdulally et al., 2011). The proposed configuration implements a chemical looping system to circulate the oxygen carriers between the air and fuel reactor, and the sorbent calciner. The whole process occurs at high temperatures $> 1000^{\circ}\text{C}$ (Joshi, Lou, Neuschaefer, Chaudry, & Quinn, 2012). Li and Fan (Li & Fan, 2008) developed a moving bed system for the CLC process. By doing this, they reduced the required volume for the fuel and the air reactors because the plug flow of the oxygen carrier resulted in a higher conversion of the reaction between the fuel and the oxygen carrier in comparison with the fluidized bed. Recently, a parallel arrangement of a moving bed fuel reactor and a fluidised bed air reactor has been suggested by Schwebel et al. (Schwebel, Wiedenmann, & Krumm, 2010). They recommended that this configuration is suitable for the gasification of biomass with chemical looping gasification.

To increase the thermodynamic efficiency of the CLC, it was proposed to feed the vitiated air from the air reactor and the exhaust gases from the fuel reactor to a power cycle to co-produce heat and power. Importantly, to achieve higher efficiency, not only the power cycle but also the CLC should work at higher temperatures and pressures (Brandvoll & Bolland, 2002; Noorman, van Sint Annaland, & Kuipers, 2010; Wolf, Anheden, & Yan, 2001). Thus, the idea of running the chemical looping system at high pressures was developed. However, it was identified that the circulation of the oxygen carrier at high temperatures and pressures is technically challenging due to sintering, agglomeration and particle breakage.

Faced with the above literature, the configuration and operating condition of a CLC system is highly dependent on the type of fuel and the application of the exhaust and vitiated gases from the reactors (Brown, Dennis, Scott, Davidson, & Hayhurst, 2010; Scott, Dennis, Hayhurst, & Brown, 2006). For solid fuels, such as carbon particles or biomass, a moving bed together with a fluidised bed is a plausible configuration that can be used for CLC. A moving bed provides sufficient residence time and better chemical conversion of fuel, while a fluidised bed is also a plausible configuration since it offers great surface contact between the solid oxygen carrier and the fuel.

For all the chemical looping configurations discussed here, the circulation rate is a key parameter influencing the chemical performance and working mode of the system. If the circulation rate of the oxygen carrier is sufficient that the quantity of oxygen reaches the stoichiometric value, the system operates as chemical looping combustion. However, if the circulation ratio is not sufficient and is below the stoichiometric value, the system operates as chemical looping gasification (if the feedstock is solid) or chemical looping reforming (if the feedstock is natural gas). The main product of chemical looping reforming and gasification is syngas or hydrogen.

2.3. Chemical looping reforming

Chemical Looping Reforming (CLR) is a process utilized for syngas and hydrogen production. Auto-thermal and steam chemical looping reforming are two well-established configurations of CLR. (Kim et al., 2010; Wang, Yu, Qin, Hou, & Duan, 2015). For CLR, a gaseous fuel such as natural gas is utilised as a fuel and partial oxidation of fuel inside the fuel reactor provides conditions for the reforming reactions to occur, which produce hydrogen, H₂O, CO, and CO₂. By controlling the amount of oxygen released in the fuel reactor, the composition of the product is also controlled (Ahmad, Zawawi, Kasim, Inayat, & Khasri, 2016). In some cases, steam is used as the reforming agent not only to produce more hydrogen but also to increase the mixing inside the reactor and to maintain the temperature of the reactor. Notably, a CLR employs the adsorption technique to remove CO₂ and CO from the gas products to produce pure hydrogen. Figure 2.2 presents a schematic diagram of a chemical looping reforming process and methane as a fuel.

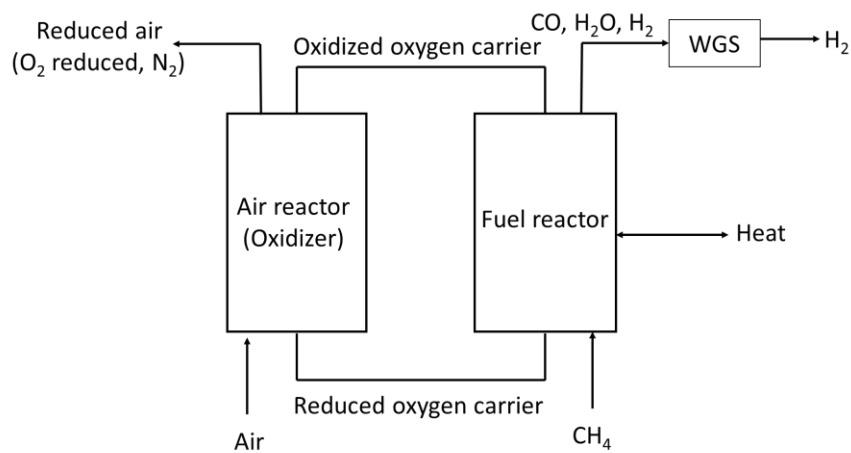


Figure 2.2. Schematic diagram of chemical looping reforming.

If the fuel of the system is a solid feedstock, the process is referred to as “chemical looping gasification”, which is described in the following section.

2.4. Chemical looping gasification

To mitigate the challenge of the nitrogen dilution in syngas production and to avoid direct contact between the air and the feedstock, one potential option is to employ a chemical looping gasification (CLG) process. CLG is a recently developed process, employing metal oxide particles to transport oxygen between the reactors. In a chemical looping gasification system, there are two reactors, namely the air and the gasification reactors. The operation of the CLG is similar to CLR, however, instead of a gaseous fuel, a solid feedstock such as coal or biomass is employed. Figure 2.3 presents a schematic diagram of the chemical looping gasification process.

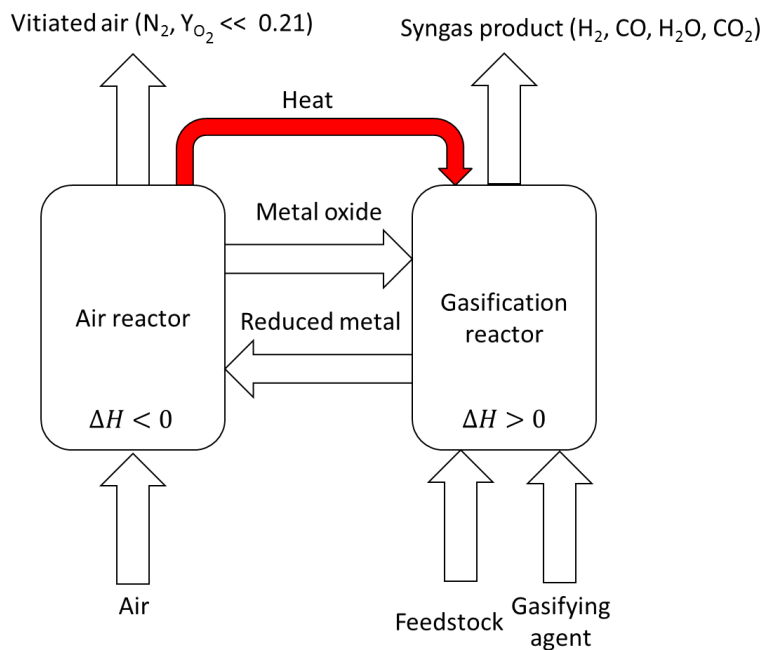


Figure 2.3. A schematic diagram of the chemical looping gasification system for syngas production.

In the fuel reactor, which is referred to as “gasification reactor”, the metal oxide is reduced and oxygen is released to react with the carbonaceous feedstock and the gasifying agent. A gasifying agent is injected into the gasification reactor not only to improve the mixing but also to increase the content of hydrogen (if the gasifying agent is steam) and/or CO content (if the gasifying agent is CO_2) in syngas. The reduced metal oxide is transported to the air reactor in

which the reduced metal oxide is oxidised with air to recover the consumed oxygen. The regenerated metal oxide is transported to the gasification reactor again and this process continues repeatedly. Figure 2.4 presents the general scheme of a chemical looping gasification system for a solid feedstock.

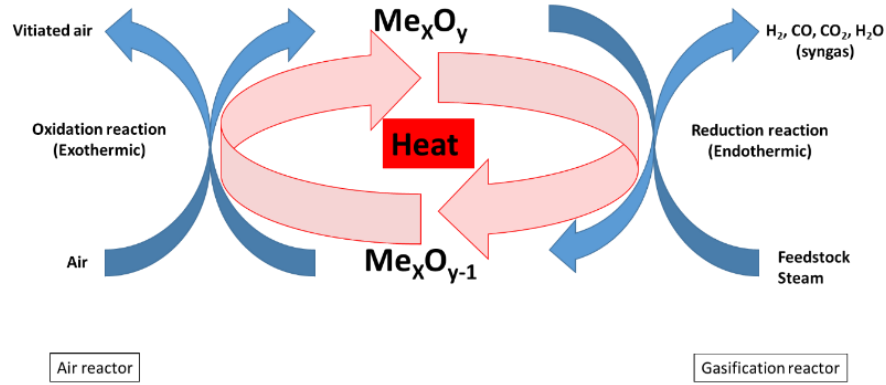


Figure 2.4. A schematic diagram of the steam chemical looping gasification process.

Gasification reactions in the gasifier include several main reactions namely, the Boudouard reaction, water-gas shift, steam gasification, methane reforming and methanation, as presented in Table 2.1.

Table 2.1. The reactions occurring in the gasification reactor (Kern, Pfeifer, & Hofbauer, 2013; Kumar, Jones, & Hanna, 2009).

Name of reaction	Chemical equation	Enthalpy (kJ/mol)	No.
Gasification (A)	$C(s)+H_2O(g) \leftrightarrow CO(g)+H_2(g)$	+118.5	(1)
Gasification (B)	$C(s)+2H_2O(g) \leftrightarrow CO_2(g)+2H_2(g)$	+103	(2)
Boudouard	$C(s)+CO_2(g) \leftrightarrow 2CO(g)$	+159.9	(3)
Methanation	$C(s)+2H_2(g) \leftrightarrow CH_4(g)$	-87.5	(4)
Complete combustion	$C(s)+O_2(g) \leftrightarrow CO_2(g)$	-393.5	(5)
Partial combustion	$C(s)+0.5O_2(g) \leftrightarrow CO(g)$	-123.1	(6)
Water-gas shift	$CO(g)+H_2O(g) \leftrightarrow CO_2(g)+H_2(g)$	-40.9	(7)
Methane reforming	$CH_4(g)+H_2O(g) \leftrightarrow CO(g)+3H_2(g)$	+225	(8)

The studies conducted on the kinetics of the gasification have shown that the temperature and

pressure of the gasifier (Adanez, Abad, Garcia-Labiano, Gayan, & Luis, 2012), the content of the ash (Adanez et al., 2012; Brown et al., 2010) and the quantity of oxygen in the gasifier are effective parameters. These parameters can determine the dominant reactions in the gasifier (see Table 2.1) (Irfan, Usman, & Kusakabe, 2011; Johnson, 1974; Kirubakaran et al., 2009). Amongst these parameters, temperature is the key parameter. It determines the composition and yield of the syngas product and the activation energy and the conversion extent of the feedstock. Many investigations have been conducted to identify the role of temperature on the yield of CO and H₂ (Corella, Aznar, Delgado, & Aldea, 1991; Herguido, Corella, & Gonzalez-Saiz, 1992; Turn, Kinoshita, Zhang, Ishimura, & Zhou, 1998). Notably, gasification at higher temperatures results in the production of small amounts of methane and other hydrocarbons (Kalinci, Hepbasli, & Dincer, 2009). For example, Nipattummakul et al. (Kalinci et al., 2009) and Shen et al. (Shen, Gao, & Xiao, 2008) demonstrated that the rate of production for CO₂ and CH₄ is highly dependent on the temperature of the gasifier, such that with an increase in the temperature, the rate of production of CO₂ and CH₄ decreases. Identical behaviour was also reported by Chang et al. (Chang, Chang, Lin, Lin, & Chen, 2011) and Turn et al. (Turn et al., 1998), Gao et al. (Gao, Li, Quan, & Gao, 2008; Udomsirichakorn & Salam, 2014).

2.5. Thermodynamic and experimental assessments of chemical looping gasification

Several studies were conducted, thermodynamically and experimentally, to assess the influence of different operating parameters on the syngas yield, the molar ratio of H₂: CO, and the energy demands of the process. In most of them, the content of oxygen was identified as a determinative parameter influencing the performance of the chemical looping gasification. To understand the role of oxygen on the chemical performance of CLG, it is necessary to define a parameter which relates the content of oxygen in the oxygen carrier to the performance of the system (Abad et al., 2007). R_o is the oxygen transport capability, which is defined as follows:

$$R_o = \frac{m_o - m_r}{m_o} \quad (9)$$

Here, m is the instantaneous mass of the oxygen carrier for the oxidation (o) and the reduction (r) states. Figure 2.5 presents the values of the oxygen transport capability for various metal oxides. As can be seen, some of the metal oxides presented in the Fig. 2.5 are not suitable for gasification, as they release a large amount of oxygen in the reactor (e.g. nickel or iron). Therefore, they can be used in chemical looping combustion. Likewise, there are other metals (e.g. cobalt), which release a small amount of oxygen during the reduction reaction and can be used for chemical looping gasification.

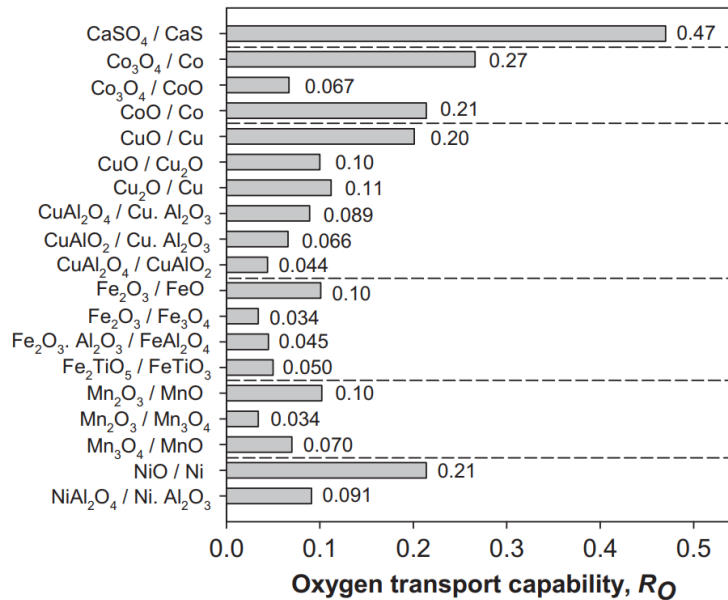


Figure 2.5. The oxygen transport capability for different metal oxides adapted from (Adanez et al., 2012).

Hence, not only the oxygen content of the oxygen carrier particles influences the chemical performance of the CLG but also the circulation rate affects its chemical performance. The circulation rate is important because it changes the amount of sensible heat transported from the air reactor to the gasification reactor. As discussed before, in the air reactor, the reactions

are exothermic, thus, thermal energy is released, which can be employed in the gasification reactor. However, the net energy demand for the process is highly dependent on both the circulation and the flow rate of the feedstock.

Figure 2.6 presents the dependence of the energy demand of the chemical looping gasification system on the circulation ratio and the oxygen content of the gasification reactor obtained by Ortiz et al. (Ortiz et al., 2011). They showed that the net thermal energy required for chemical looping gasification is a function of the circulation rate, such that, with an increase in the circulation rate, the thermal energy required for the system greatly changes. For example, for a molar ratio of oxygen to fuel=1, at circulation rate=0.5 kg/s, the net enthalpy of the system is ~58 kJ/s, however, at circulation ratio=4 kg/s, it is ~25 kJ/s.

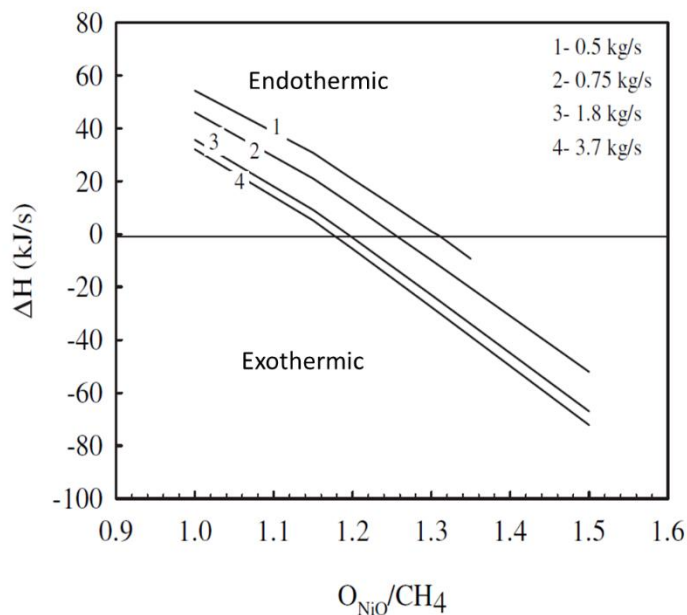


Figure 2.6. Dependence of the energy demand for a chemical looping gasification system on the circulation rate of oxygen available in the gasifier for various circulation rates, adapted from (Ortiz et al., 2011).

The molar ratio of the oxygen carrier to fuel is also a determining parameter in chemical looping gasification and chemical looping combustion systems. Jafarian et al. (Jafarian, Arjomandi, & Nathan, 2014) conducted a thermodynamic analysis on the potential of different

oxygen carriers to be employed in hybrid solar chemical looping combustion. They assessed five metal oxides for three different fuels, including carbon monoxide, natural gas and hydrogen. They identified that the ratio of oxygen carrier to fuel can be a determining parameter on the performance of the chemical looping process. Likewise, the type of reaction of the oxygen carrier with the fuel was another key parameter. Their calculations showed that the highest system's Carnot efficiency could be achieved with cobalt, followed by nickel and iron, while the highest solar share was achieved with iron oxide. This was attributed to the type of reaction of iron, which is highly endothermic. In another study, Wang et al. (Wang, Yu, Qin, Hou, & Duan, 2016) found that the ratio of steam to feedstock is another determining parameter for operating the CLG system, which considerably influences the gas yield and its composition. Figure 2.7 presents the dependence of the yield of gas products on temperature for various steam to fuel ratios.

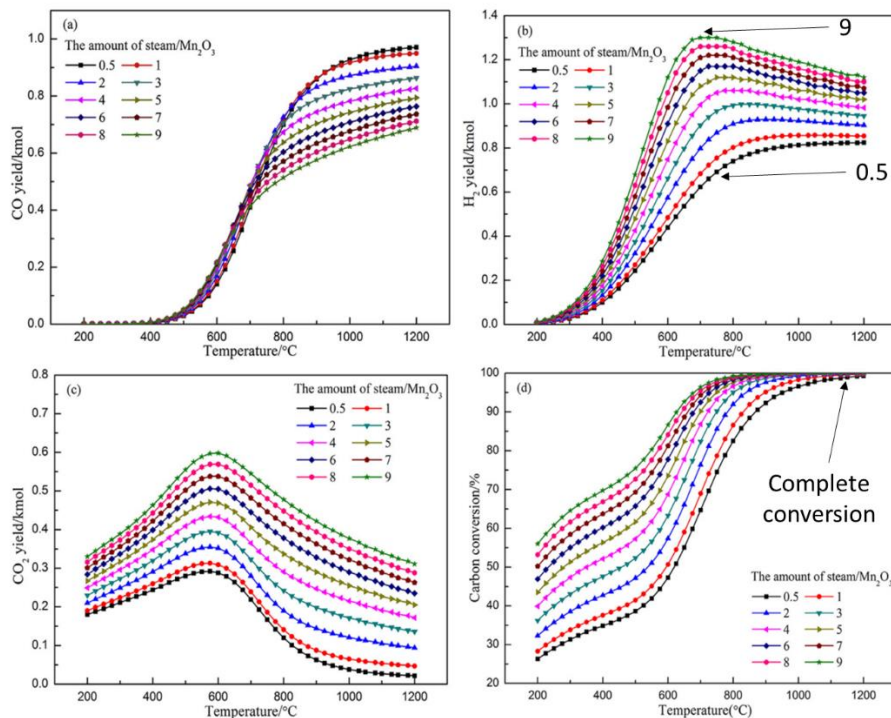


Figure 2.7. Dependence of CO, CO₂ and H₂ yields on the temperature for various steam to fuel ratios in a chemical looping gasification system, working with Mn₂O₃ metal oxide particles.

As can be seen, with an increase in the molar ratio of steam to fuel, the CO yield decreases, while the H₂ yield increases. This causes an increase in the ratio of H₂: CO. It was also found that the carbon conversion extent is increased with an increase in the ratio of steam to fuel, reaching 100% at T > 800°C for steam to fuel ratio=9. Likewise, the quality of syngas decreases with an increase in the temperature of the gasifier. This is because the CO yield increases with temperature and this decreases the ratio of H₂: CO at high temperatures, such as 1000°C. Overall, Mn₂O₃ showed a potential to be used in CLG and the molar ratios of the oxygen carrier to the fuel and the steam to the fuel were the key thermodynamic parameters controlling the gas yield and thermal energy required for the process.

Feasibility of the co-production of hydrogen and electricity with CLG has also been assessed in the literature. For example, using iron oxide as the solid oxygen carrier, a cyclic oxidation and reduction of iron with carbonaceous feedstock has been investigated thermodynamically by Li et al. (Li, Zeng, Velazquez-Vargas, Yoscovits, & Fan, 2010). The Gibbs minimisation method was applied to the process using an Aspen software package and the results were verified using a moving bed reactor. They showed that the moving bed gasifier has better heat and mass transfer, together with a higher carbon conversion, in comparison with the fluidised bed gasifier. They conducted the experiments for ~15 hr and reached a conversion extent of > 99.5%. However, the recovery rate for the oxygen carrier was ~50%. The results obtained from the experiments clearly showed that the chemical looping process is feasible for syngas production, however, the oxygen carrier needs further improvement to be used for successive cycles (Li et al., 2010).

To overcome the issue of regeneration of the oxygen carrier and to enhance the quality of the syngas, chemical looping steam gasification was proposed. A set of experiments were conducted at various oxygen to carbon ratios in a fluidised bed reactor to produce high-quality syngas. Iron oxide was used as the oxygen carrier in the reactors (Guo, Cheng, Liu, Jia, & Ryu,

2013). They investigated the influence of different operating parameters, such as temperature, pressure and the molar ratio of the oxygen carrier to the feedstock to determine the optimized operating regime for the system. They also studied the influence of the number of reactive sites of the oxygen carrier on the gas yield and reaction mechanisms. They used steam as the mixing and gasifying agent and noticed that the presence of steam not only maintains a uniform temperature profile in the gasifier, but also increases the amount of hydrogen in the syngas. They also modified the iron oxide oxygen carrier with CaO and assessed the potential reactivity of CaO-decorated iron-based oxygen carrier particles in successive reactions. They reported that the carbon conversion could reach ~81% with an increase in the ratio of the oxygen carrier to the feedstock. The addition of CaO enhanced the carbon conversion and the gasification rate substantially and reduced the production of H₂S. They also used an x-ray diffraction instrument to assess the structure of the oxygen carrier before and after the experiments. They showed that a modified oxygen carrier with CaO was completely regenerated after six redox cycles.

The presence of steam in the gasifier fortifies the mixing inside the gasifier and increases the content of hydrogen via a water gas shift reaction. The effect of mixing of steam with the oxygen carrier was investigated by Huang et al. (Huang et al., 2016). They implemented the natural iron ore as an oxygen carrier for CLG of biomass char in a fixed-bed reactor. They noticed that the reduction-oxidation reactions between biomass char and iron ore occurs under the oxygen-depleted environment, however, due to the lack of oxygen, the conversion of char was low. In addition, the contact between the surfaces of the solid particles was not sufficient and, as the result, the chemical performance of the system was low. Thus, they used steam to enhance the mixing between the solid particles and to increase the temperature and hydrogen content of the gaseous products. They obtained the optimum oxygen carrier to char and steam to char ratios, in which the highest conversion of char can reach ~80%, whilst the gas yield was three times higher than for the case without steam. They reported that with an increase in the

number of working cycles, sintering and attrition occurred within the system, decreasing the lifetime of the particles. After 52 hours of operation, the iron oxide showed reasonable reactivity, however, it required further modifications to be able to use it for longer operating hours (Huang et al., 2016).

He et al. (He, Galinsky, & Li, 2013) modified the iron oxygen carrier with copper oxide to further improve both its oxygen molar ratio and its reaction. To achieve this, a set of experiments were conducted using a thermo-gravimetric analyser to assess the structure of the oxygen carrier before and after the experiments. They analysed the amount of oxygen released and absorbed from the oxygen carrier for various amounts of copper oxide mixed with iron oxide. The results showed that an oxygen carrier consisting of a small amount of CuO (5% by weight) is more effective for char conversion than an oxygen carrier without copper. Also, the mathematical modelling of the process showed that the presence of small amounts of copper results in the increase in the rate of H₂ production and its yield (He et al., 2013).

The type of feedstock was found to influence the yield of the gasification and syngas composition. Hence, extensive research has been conducted to evaluate the influence of feedstock on the chemical performance of the CLG, which is discussed as follows:

2.6. Influence of the type of feedstock on the performance of chemical looping gasification

Apart from natural gas, which is mainly used in the reforming process, coal and biomass are the main feedstocks for the gasification processes. Hence, it is important to understand the mechanism of gasification of coal and biomass. During the gasification of this feedstock with a gasifying agent, the following mechanistic steps occur:

- **Drying stage:** In this stage, the moisture content in coal or biomass is taken out of the feedstock in the form of water vapour. The drying process occurs under specific

conditions to prevent the feedstock from decomposing. Therefore, the temperature in the drying zone is not sufficiently high for pyrolysis of the feedstock.

- The pyrolysis stage is referred to as “de-volatilization”: This stage is the next step after the drying process, in which a dried biomass feedstock is decomposed into components with low molecular weight volatiles, including solid material referred to as char and tar. This process occurs in the absence of oxygen. Most reactions in this stage are endothermic and, as a result, the energy must be supplied from an external source or with pre-combustion of part of the feedstock.
- Combustion stage: In this stage, the volatiles are partially oxidised by the oxygen provided to the gasifier. Normally, carbon monoxide, carbon dioxide and water are the main components of this stage. Although the main reactions of this stage are combustion reactions and exothermic, this heat is normally consumed by the endothermic reactions in the gasification stage.
- Gasification stage: In the gasification stage, reactions occur in the absence of oxygen. This is because all the oxygen content in the system has been consumed by the combustion reactions. The gas products from this stage are carbon monoxide, hydrogen, methane and water, together with a small quantity of CO₂ produced from the combustion reactions.

Thus, the oxygen available in the system and the method by which the oxygen is introduced in the gasifier influences the products of the system. For chemical looping gasification, the oxygen carrier determines how much oxygen can be consumed in the combustion and/or gasification region. Therefore, the oxygen carrier must meet specific conditions and must have some thermodynamic features before it can be used in the CLG system.

2.7. Solid oxygen carrier

For each oxygen carrier, accomplishment of the following characteristics is necessary:

(1) An oxygen carrier must have good thermo-physical properties. Since heat transfer is one of the important phenomena in the gasification process, the oxygen carrier must have high thermal conductivity and heat capacity. (2) The oxygen carrier must have sufficient oxygen transport capacity to supply the required oxygen for gasification. (3) The reactions between the oxygen carrier and feedstock, oxygen carrier with steam and the reduction and oxidation reactions for the oxygen carrier must be sufficiently fast to avoid solid inventory inside the reactors. (4) The oxygen carrier must tolerate high-temperature and high-pressure conditions and can be used for successive reduction-oxidation cycles. The physical structure, together with the chemical performance of the oxygen carrier, must be constant over a long operation. (5) It is also crucial that the oxygen carrier has good fluidisation characteristics and must be resistant against issues such as sintering, particle breakage and abrasion. (6) Other factors such as cost and environmentally benign characteristics are important.

According to the above characteristics, in a CLG process, the solid oxygen carrier particles are subject to a chain of reactions. Therefore, the general kinetics of reaction and the performance of the gasifier is strongly influenced by the mechanism of reduction and oxidation of the oxygen carrier, the activation energy and temperature in which oxygen carrier is reduced or oxidised. Therefore, it is important to understand how an oxygen carrier participates in a reduction or oxidation reaction. Hence, different models have been proposed to predict the behaviour of oxygen carriers in a gasifier or an air reactor, as is briefly discussed in the following sub-sections.

2.8. Particle size models for solid-gas reactions

2.8.1. Changing grain size model

In the changing grain size model, it is assumed that the oxygen carrier is a spherical particle and several intermediate steps are considered until the reduction or the oxidation reaction is completed. It is also assumed that both the re-dox reactions occur inside the core of the particles and any reacting gas needs to overcome the mass transfer resistances. For instance, for an oxidation reaction, the following intermediate stages occur: (1) The bulk of the reacting gas (oxygen) diffuses through the surface of the solid reduced metal oxide and passes through the external layer of the particle. This stage is referred to as “film diffusion”. (2) The reacting gas is then diffused through the pores and irregularities of the oxygen carrier. It is also assumed that this porous region is a constant domain and porosity is constant during the diffusion phenomena. (3) The adsorption stage in which the reacting gas is adsorbed by the core of the particle where the main oxidation reaction occurs. (4) The general oxidation reaction, which occurs between the oxygen and the reduced metal oxide. As the reaction proceeds, the size of the particle increases. However, for the reduction reaction, while the porous region remains constant, the core of the particle shrinks, resulting in a reduction in the size of the particle.

2.8.2. Shrinking core model

In this model, initially, the reaction happens on the external surface of the spherical particle, with a small mass transfer resistance. During the reaction, a layer of the solid product is formed around the unreacted core inside the particle. At the same time, the size of the unreacted core reduces gradually. The border area between the unreacted core and the solid product is the exact location where the general reaction occurs. Hence, the reacting gas must overcome the following resistances before the reaction can occur via film transfer, diffusion through spaces such as pores, diffusion through the solid product layer and the chemical reaction on the interface. This model also supports the change in the particles’ size over the reaction time. Figure 2.8 presents schematically the mechanisms occurring during the changing grain size and

shrinking core models. Overall, both models support particle size changes during the reduction and the oxidation reactions and successive changes in the size of the particle can weaken its structure and deform its morphology.

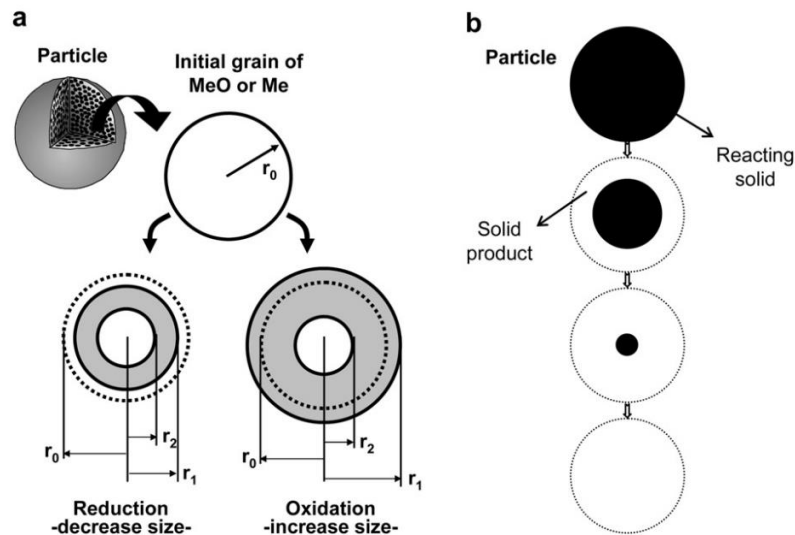


Figure 2.8. A schematic diagram of the different models for predicting particle size during the reaction, a) Changing grain size model (Szekely, Lin, & Sohn, 1973), b) Shrinking core model (Georgakis, Chang, & Szekely, 1979) adapted from the literature (Adanez et al., 2012).

2.9. Challenges associated with solid oxygen carriers

Fluidisation and interaction between particles at high temperatures result in the advent of some challenges, such as attrition and agglomeration. The attrition of an oxygen carrier particle is an important issue affecting the performance of chemical looping, especially for the fluidized-bed configurations. Attrition reduces the number of reactive sites on the external layer of an oxygen carrier, decreasing its reactivity over time. To evaluate the attrition, the crushing strength of an oxygen carrier particle is a preliminary indicator, which can be performed using standard test facilities. The results of the attrition assessment tests conducted on oxygen carriers used in

chemical looping systems show that at temperatures $\sim 700^{\circ}\text{C}$ and above, the friction between the particles due to particle collision and fluidisation can cause severe attrition, which directly influences the lifetime and operability of the chemical looping system.

Attrition can change the external layer of the particles and deform the reaction sites on the external surface of the particles. It also decreases the effective specific surface area of the particle by decreasing its external area. The lifetime of oxygen carriers is also important, since it relates to the economic viability and operation of the CLG. The lifetime of the oxygen-carriers can be defined as the average time in which a particle must be under reaction (reduction or oxidation) in the system, without any side reactions or structural losses that cause the particle to be removed or replaced. Generally, a reduction in the particle size to less than $45\mu\text{m}$ is referred to as “fine loss”. Table 2.2 presents the attrition measured for different oxygen carriers for various chemical looping systems.

Table 2.2. Attrition of diverse oxygen carriers in various chemical looping processes.

Solid oxygen carrier	concept	Test time /lifetime*(hrs)	attrition	Ref.
Iron	CLC	10/1600	0.0625	(Wu, Shen, Hao, & Gu, 2010)
CuO/NiO	CLC	67/2700	0.042	(Gayán et al., 2011)
CuO (on alumina)	CLC	100/2400	0.04	(Luis et al., 2007b)
NiO (on alumina)	CLC	100/40000	0.0023	(Lyngfelt & Thunman, 2005a)
NiO (on alumina)	CLG	37/NG*	-	(Rydén, Lyngfelt, & Mattisson, 2008)
NiO (on NiAl_2O_4)	CLG	160/4500	0.02	(Rydén et al., 2008)

*Estimated.

Agglomeration of the oxygen carrier is another issue associated with solid oxygen carriers, which must be avoided in chemical looping systems, particularly for fluidized bed systems, as it can devastate the fluidisation process, together with causing a massive reduction in the rate of heat and mass transfer. For a fixed bed reactor, agglomeration causes gas and/or liquid

entraining, channelling and high-pressure drop problems. Channelling decreases the heat and mass transfer and the contact between the gas and the particles. Agglomeration causes the particles to be attached to each other, creating larger clogs and clusters of particles with higher density. As a result, the clogs are deposited at the bottom of the reactor, decreasing the oxygen content over time. The rate of agglomeration depends on the structural strength of the particles, operating temperature and pressure and also the height of the reactor or tank in which the particles react or are stored (Adanez et al., 2012; Cao & Pan, 2006; Cuadrat et al., 2012; Hossain & de Lasa, 2008; Leion, Mattisson, & Lyngfelt, 2009; Luis et al., 2007b; Mattisson, Johansson, & Lyngfelt, 2004).

Much effort has been made to investigate the potential agglomeration of different oxygen carriers in a chemical looping gasification process. It was found that the combinations of metal oxide with a structural support, type of support and calcination conditions can avoid agglomeration problems in nickel-based, copper-based, zirconium-based and aluminium-based oxygen-carriers (Cho, Mattisson, & Lyngfelt, 2006; De Diego et al., 2004; Gayán et al., 2008; Mattisson, Johansson, & Lyngfelt, 2006). Ni-based oxygen carriers do not exhibit agglomeration problems at temperatures $\sim 950^{\circ}\text{C}$. In experimental work conducted by Liu et al. (Liu, Liao, Wu, & Ma, 2018), calcium ferrites (CaFe_2O_4) were adopted as the oxygen carrier to be tested in a chemical looping gasification and microalgae was selected as the fuel. Using a thermo-gravimetric analyser and FTIR instruments, the performance and characteristics of the system were assessed. The results showed that calcium ferrite has a lower oxidation capacity than iron oxide. The great selectivity of calcium ferrite was also verified. With steam, the chemical efficiency of gasification enhanced from 82.95% (with iron oxide) to 92.49% (with $\text{Ca}_2\text{Fe}_2\text{O}_5$) at 850°C . However, after one operating cycle, some of the CaFe_2O_4 particles agglomerated and formed larger clogs, and some parts of the tiny pores were extinguished, while larger pores were formed. The reason for the agglomeration was attributed to the

hydroxylation phenomena occurring on the external surface of the metal oxide, which led to the attachment of particles to one other.

Agglomeration is a serious challenge in CLC systems. During the operation of a CLC, the agglomeration phenomenon was clearly shown by Cho et al. (Cho et al., 2006). De-fluidization also occurred during the oxidation reaction in the air reactor (Mattisson et al., 2004). Similar results were found with the natural mineral ilmenite (FeTiO_3) for CLC applications (Leion, Lyngfelt, Johansson, Jerndal, & Mattisson, 2008). Adánez et al. (Adánez, Gayán, et al., 2006; Luis et al., 2007a) reported the same results for Cu-based oxygen carriers in a 10-kWth chemical looping combustion system. An oxygen carrier consisting of 60% NiO and 40% NiAl_2O_4 was used in a 10-kWth chemical looping combustion system for 160 h of operation with fuel. Agglomeration occurred inside the fuel reactor despite the fact that the flow rate and the temperature of the system were both maintained. While the exact reason and mechanism behind the agglomeration of the oxygen carrier was not discovered, it was found that the degree of oxidation has a direct influence on the agglomeration. It was also revealed that the reduced particles seem to agglomerate more easily. Importantly, the agglomeration was so massive that the circulation between the reactors could not be maintained. Finally, the fuel reactor had to be opened and the agglomerations crushed and re-introduced. The morphology and status of the particles before and after the test was evaluated using scanning electron microscopy. Figure 2.9 presents the results of the morphology test for a fresh particle and one typical agglomerated clog after 4 days of operation.

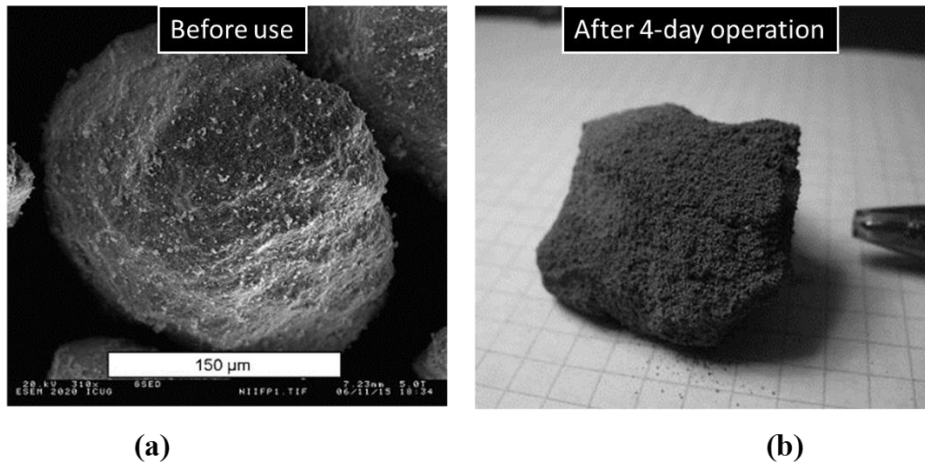


Figure 2.9. Scanning electron microscopic images before and after a 4-day operation in a chemical looping combustion system, a) a fresh particle; b) agglomerated particles after a 4-day operation.

Carbon deposition is another serious challenge associated with the use of a solid oxygen carrier in chemical looping gasification systems. In the gasifier, the external layer of the oxygen carrier is exposed to the carbonaceous feedstock. Since the temperature is high (e.g. 900°C), the exterior layer of the oxygen carrier is expanded along with the micro-cavities and irregularities, providing room for the deposition of the unreacted carbon. This results in a reduction in the capacity of the reduced metal oxide for absorbing the oxygen in the air reactor. The carbon deposited on the oxygen carrier can react with air in the oxidation reactor (air reactor), resulting in the production of CO₂.

Much effort has been expended to identify the effect of carbon deposition on the CLG process for various oxygen carriers (Adánez, García-Labiano, et al., 2006; Jerndal, Mattisson, & Lyngfelt, 2009; Jin, Okamoto, & Ishida, 1998; Mattisson, Johansson, Jerndal, & Lyngfelt, 2008). It has been shown that the rate of carbon deposition depends on the type of metal oxide, inert material and the molar ratio of the steam to fuel. They found that the main reason for the carbon deposition is the Boudouard reaction, which releases unreacted carbon material in the

reverse direction. Notably, the carbon formation strongly depends on the availability of oxygen. The formation of carbon on the oxygen carrier normally occurs at the end of the reduction period, when more than 80% of the available oxygen was consumed (Cho, Mattisson, & Lyngfelt, 2005). Similar phenomena were found for Cu-based oxygen carriers at carbon conversions higher than 75% (De Diego et al., 2005). Interestingly, for iron particles, a very small amount of carbon deposition was formed on the oxygen carrier (Cho et al., 2005).

Apart from the role of the availability of oxygen, the ratio of steam to fuel is another parameter affecting carbon deposition (Hoteit, Chandel, & Delebarre, 2009; Ishida, Jin, & Okamoto, 1998; H.-J. Ryu, Bae, & Jin, 2003).

To overcome the challenge of carbon deposition, one potential option is to use supportive materials such as zirconium or nickel to add some physical resistance to the body of the oxygen carrier and to strengthen its core. For this purpose, several methods such as doping, coating and synthesizing, or a combination of these methods, are applied to the oxygen carriers, using complex and need-specific technologies. These methods are not only expensive but at lab-scale, and need further development. Hence, this is another driver for seeking alternatives to solid oxygen carriers for chemical looping systems.

The application of solid metal oxides in chemical looping processes is thermodynamically limited. It means that the reduction and oxidation reactions of a metal oxide need a specific thermodynamic regime to proceed. Figure 2.10 presents the dependence of the Gibbs free energy of reaction on temperature for different reactions, including combustion and gasification. As can be seen, metal oxide is suitable for a CLC process if the Gibbs free energy of reaction between a metal oxide, fuel and the reacting gas (e.g. steam) equals the values represented by the blue colour. However, if the Gibbs free energy of the reaction equals the values represented with the orange colour, it can be used for the CLG process. Therefore, it is clear that a wider range of metal oxides can be employed for CLC, while a smaller number of

metal oxides are usable for the gasification process.

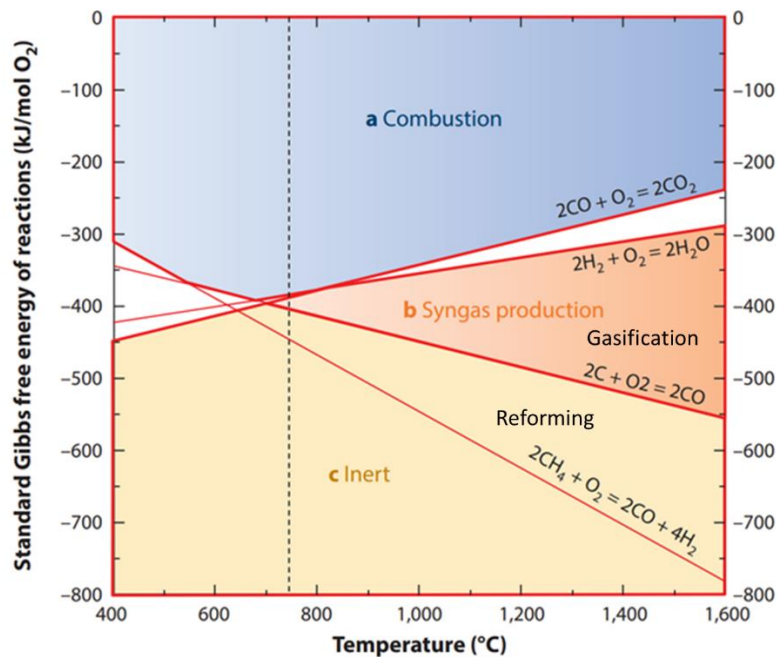


Figure 2.10. Dependence of Gibbs free energy of reaction on metal oxides at specific temperatures.

The use of a liquid metal oxide as the oxygen carrier, instead of solid metal oxide particles, can overcome the aforementioned challenges associated with the use of solid oxygen carriers. The following section highlights the state-of-the-art investigations conducted on the potential application of liquid oxygen carriers in chemical looping combustion processes.

2.10. Liquid oxygen carriers for chemical looping combustion

The application of liquid metal oxide in chemical looping combustion was first introduced by Ritcher and Knoche (Richter & Knoche, 1983). They developed a prototype of a CLC system that worked with cadmium as the oxygen carrier at an operating temperature higher than its melting point. The system was later improved by McGlashan (McGlashan, 2008). They demonstrated that the liquid/gas phase could be implemented for CLC processes to enhance the efficiency of the system. Then, it was found by McGlashan (McGlashan, 2008) that Na and

Zn can be utilized as an oxygen carrier. A new configuration of CLC was developed by Lamont (LaMont, Seaba, Latimer, & Platon, 2010), in which a liquid oxygen carrier was used in a semi-batch reactor. In a batch reactor, the reactants were first loaded into the reactor and then reactions were commenced. In comparison with the batch reactor, the semi-batch reactor showed features such as continuous addition/removal of one or more streams of components. In the proposed system, fuel entered the semi-batch reduction reactor, which was previously charged with active metal oxide for the reduction reaction to take place. Then, the fuel line was closed, and the air was injected into the reactor to recover the released oxygen and reactivate the reduced metal oxides. However, in contrast with the batch reactor, the quantity of reactants could be changed during the reaction, which increased the flexibility of the process. To validate the configuration, they evaluated other metal oxides, including Mn, Cr and Bi and showed that neither quenching nor endothermic reactions occurred during the gasification process. Later, they improved the system by using two inter-connected semi-batch reactors. However, the operating temperature of the improved system had an upper limit of 800°C, which caused lower efficiency as the temperature was relatively low in comparison with the temperature required for the power cycles. More importantly, this system was not appropriate for gas turbine power blocks due to the evaporation of the metals (LaMont et al., 2010). Recently, Jafarian et al. (Jafarian, Arjomandi, & Nathan, 2017) have proposed the concept of liquid chemical looping combustion working with liquid iron oxide, in which the proposed system is capable of working continuously using two interconnected bubble reactors. They showed that if the rate of circulation of liquid metal decreases between two reactors, the system can operate as chemical looping gasification, however, they did not assess the details of the gasification process using liquid metal oxides and did not prove the concept experimentally.

2.11. Liquid metals for hydrogen and syngas production

The potential application of liquid metal for the gasification of carbonaceous feedstock for hydrogen and syngas production has recently been investigated by several researchers worldwide. The first attempt to gasify a carbonaceous fuel with a molten metal was performed and patented by Tyrer et al. and, since then, much effort has been made to develop new systems for hydrogen and syngas production using molten metals (Daniel, 1931). For example, Steinberg et al. (Steinberg, 1999) developed a system for the decomposition of a carbonaceous fuel with liquid metal. They used liquid tin as a heat and mass transfer medium and natural gas was used as a carbonaceous fuel. Martynov et al. (Martynov, Gulevich, Orlov, & Gulevsky, 2005) and Gulevich et al. (Gulevich, Martynov, Gulevsky, & Ulyanov, 2008) proposed a novel system for producing H₂ via a liquid metal alloy (a mixture of lead and bismuth) by injecting the natural gas into the lower section of the reactor. They targeted the pyrolysis reaction and used the sensible heat carried by the liquid metal alloy to supply the required heat for the pyrolysis of methane. Paxman et al. (Paxman, Trottier, Nikoo, Secanell, & Ordorica-Garcia, 2014) reported some results based on the thermochemical equilibrium for cracking of methane in a bubble column reactor using various designs. They published their preliminary reports on the potential of liquid tin for hydrogen production. In their most recent study, they presented some experimental data obtained for methane cracking in a tubular reactor with and without applying the liquid metal. In another study conducted by Schultz et al. (Schultz & Agar, 2015), a new system for utilising a liquid metal in a capillary reactor was proposed. They demonstrated that at 1100°C, methane cracking conversion could reach ~32%. Interestingly, after 5 hours of operation, neither carbon deposition nor agglomeration was seen on the walls and in the liquid phase.

Gasification and hydrogen production in a bubble column reactor has been extensively investigated to demonstrate practically the capability of liquid metals to gasify a carbonaceous

feedstock (Geißler et al., 2015; Plevan et al., 2015; Schultz & Agar, 2015; Serban, Lewis, Marshall, & Doctor, 2003). For example, Serban et al. (Serban et al., 2003) conducted some experiments using a stainless steel-made micro reactor filled with liquid tin, liquid lead and a combination of tin/packed bed material. They used natural gas as a fuel and chose a bubbling regime for better mixing of the natural gas in the system. They reported a ~57% conversion of methane to hydrogen at temperatures around 750°C. They utilised a SiC-made packed bed material and noticed that tin can also be contained with SiC. Plevan et al. (Plevan et al., 2015) performed some experiments in a larger stainless steel reactor but with the same experimental conditions as those conducted by (Serban et al., 2003). They reached an 18% conversion at 900 °C. For similar experiments with liquid tin, Geißler et al. (Geißler et al., 2015) reported a conversion of 30% without any significant carbon deposition within the reactor. They used a quartz reactor. Again, a set of experiments was performed to investigate methane pyrolysis with liquid tin in a quartz-made bubble reactor. The reactor was filled with tin and some cylindrical quartz rings was used as a packed bed to increase the contact between the gas and the liquid. Tests were performed at different temperatures ranging between 930°C and 1175°C. Methane was bubbled within the column. The ratio of methane to liquid tin was also adjusted using dilution of the inlet gas with nitrogen. It was found that with an increase in the flow rate of methane, the yield of hydrogen also increased. Likewise, an increase in the temperature of liquid metal also resulted in an increase in the hydrogen yield. Interestingly, the hydrogen yield reached ~78% at 1175°C. The liquid phase was analysed using x-ray diffraction and it was found that only 1.5% of the liquid metal could be converted to other tin-related products, such as SnC alloy. The carbon formed a flake-shaped ash on the surface of the tin. The agglomeration was also seen during the experiments with a mean size of 40 nm to 100 nm. Interestingly, due to the significant difference between the density of carbon and liquid tin, carbon was easily separated from the molten tin. Also, due to the bubbling regime, carbon

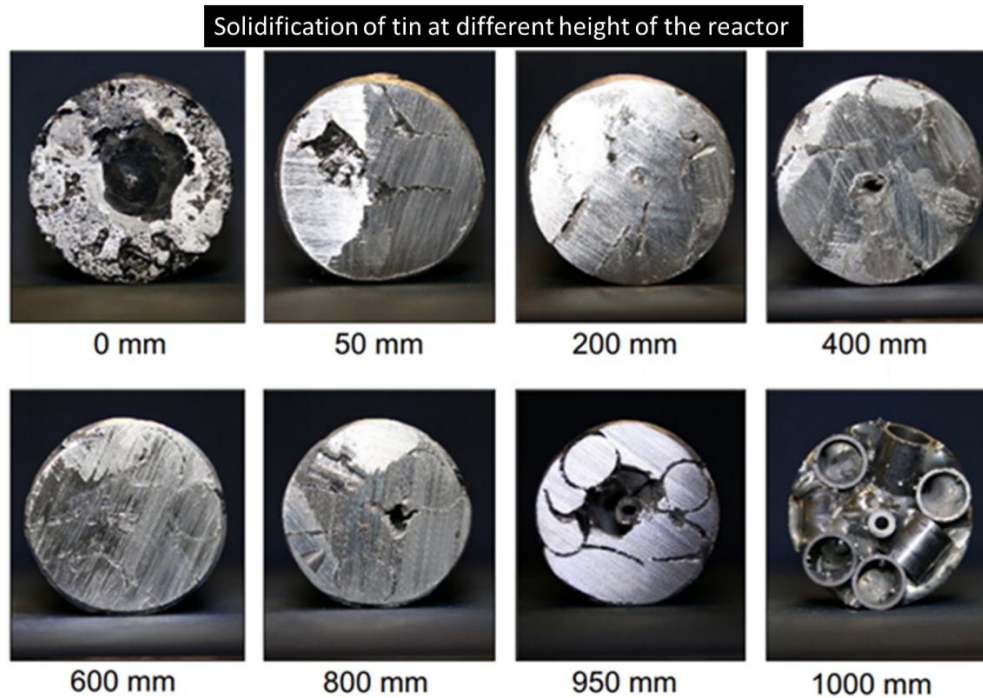


Figure 2.12. The cross section of the reactor, after the test adapted from (Geißler et al., 2015).

For the first time, Ono et al. (Ono et al., 1999) discussed the potential of concentrated solar thermal energy for producing hydrogen for thermal cracking of methane with liquid metals. Solar thermal energy was used to drive the molten metal reactor and then to drive the heat-to-power cycle for the output of mechanical work and/or electricity. The energy generated with the power plant was utilised for the separation of the hydrogen from the unreacted natural gas using a novel membrane. They also studied the first law efficiency of the power plant and concluded that ~35% of the total energy input of the system was lost in the receiver and the molten metal reactor and this was because of the re-radiation from the receiver as the temperature is relatively high (~1000 to 1200°C). Likewise, ~59% of the input energy was implemented in the hydrogen purification unit for the purification of hydrogen. They concluded that the overall thermal performance of the system highly depends on the heat loss from the reactor and receiver to the environment, the extent of the conversion of the natural gas in the reactor, the operating pressure of the membrane and the efficiency of the power generation

cycle. Figure 2.13 presents the schematic diagrams of the conceptual designs for the bubble reactor and the solar thermal process for hydrogen production.

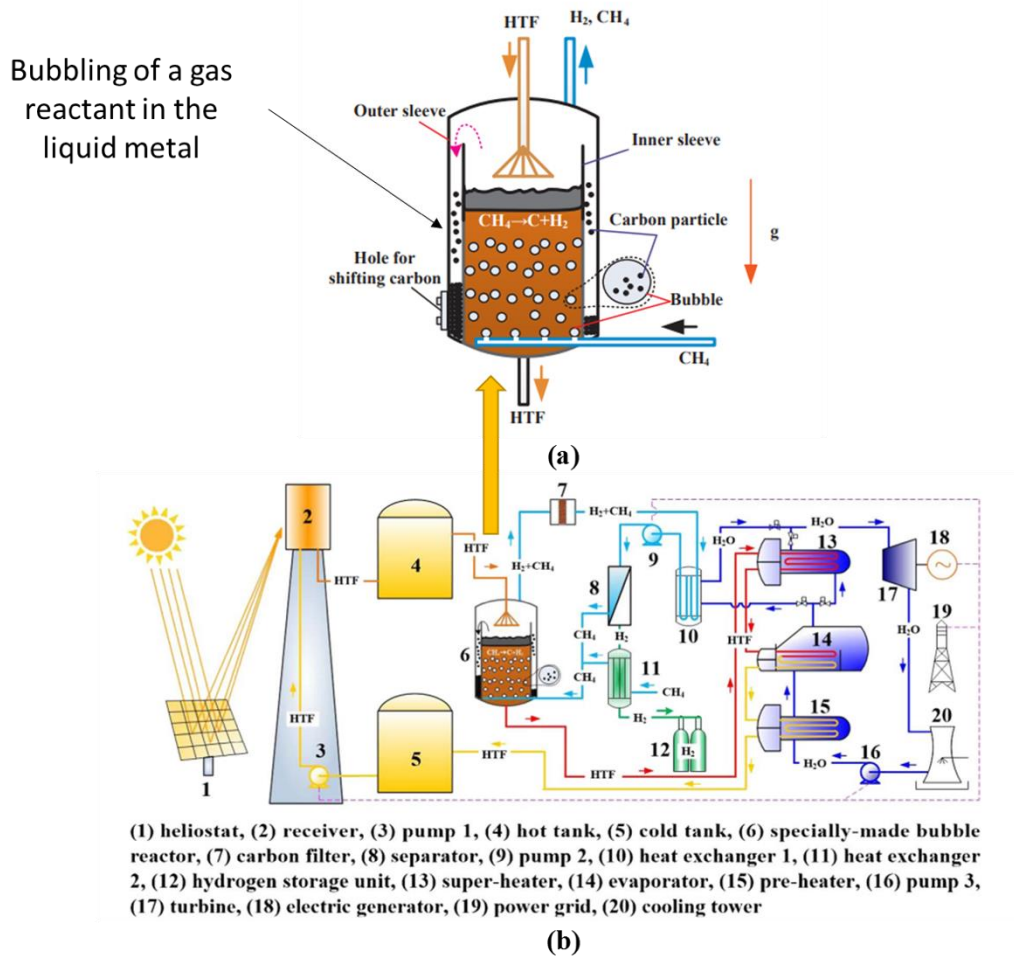


Figure 2.13. Schematic diagram of the co-production of power and hydrogen using concentrated solar thermal energy adapted from (Ono et al., 1999), a) Schematic diagram of the hydrogen reactor, b) Schematic diagram of the process integrated with a concentrated solar thermal process.

A new alternative concept for the pyrolysis of methane has recently been developed at the Institute for Advanced Sustainability Studies. The development was in a collaboration with the Karlsruhe Institute of Technology (KIT) (Abánades et al., 2016). Following the conceptual design of the process, together with material tests, experiments were conducted to produce a CO_2 -free hydrogen from natural gas. They used tin and tin-based alloys in the reactor and reached ~80% conversion of methane to hydrogen. Figure 2.14 presents a schematic diagram

of the process, together with the reactor designed for hydrogen production using molten metal. They used a liquid metal bubble reactor, and a carbon separator to remove any carbon ash from the top of the liquid metal. Since they used a bubbling mechanism, natural gas was used as the main source of the fuel.

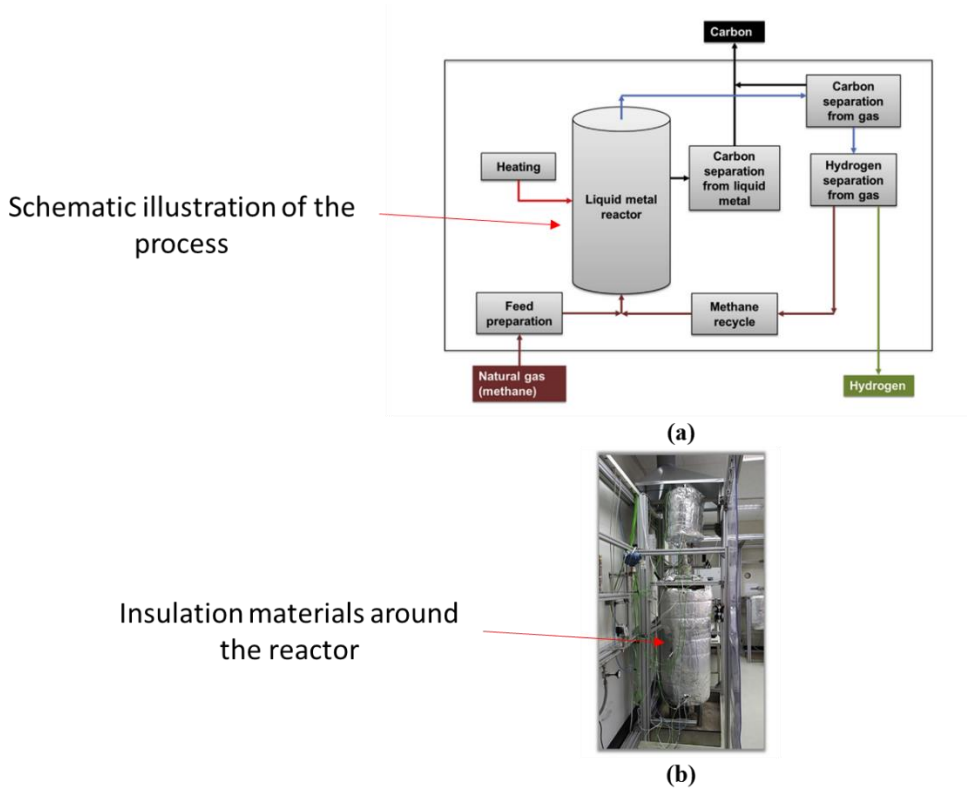


Figure 2.14. Schematic diagram of the process for the production of hydrogen from liquid metals, a) Schematic diagram of the process, b) The hydrogen reactor (Abánades et al., 2016).

During their experiments, however, they noticed that the rate of corrosion is relatively higher than that observed in conventional reactors. They measured the corrosion of the walls of the reactor and understood that the corrosion at high-temperature operation (status B represented in Figure 2.15) is more severe than that for low-temperature operation (status A represented in Figure 2.15). However, high-temperature operation has higher efficiency and conversion extent compared with low-temperature operation. Thus, there is a trade-off between the operating temperature of the process and the corrosion of the molten metal and the conversion of the reaction.

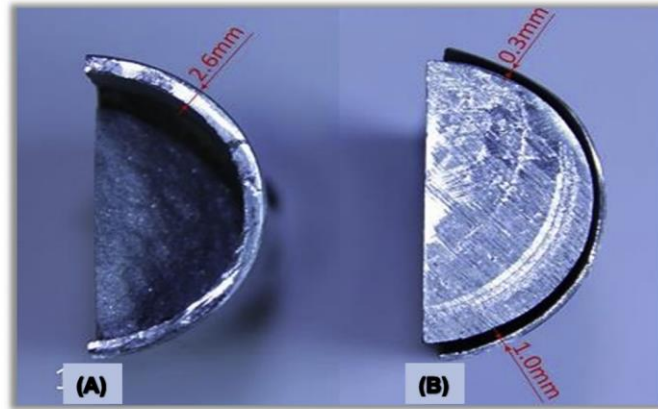


Figure 2.15. Corrosion of liquid tin in a bubble column reactor at a) Low-temperature operation and b) High-temperature operation.

In another study conducted by Tan et al. (Geißler et al., 2016), the production of hydrogen with a gallium/aluminium-based liquid metal was investigated, where the mass percentage of Al was less than 1%. Three different liquid metal alloys at room temperature, including Ga-In, Ga-Sn and Ga-Zn, were examined and compared against pure gallium. The results showed that the production rate of hydrogen with the Ga-In alloy was very much smaller than that recorded for gallium. They also noticed that the presence of gallium has a catalytic effect on the hydrogen production. To optimize the catalytic ability of gallium, they measured the hydrogen production rates at different times of the process and at various temperatures. They found that temperature intensifies the hydrogen production rate and that the gallium remains untouched during the process. They used x-ray diffraction tests to ensure the structure of the gallium and showed that at the end of the experiment, gallium has the same structure, morphology and colour. Figure 2.16a presents the dependence on time of the morphology and chemical composition of different liquid metals. As can be seen, after ~20 minutes of reaction, gallium retains its initial morphology and chemical composition. Figure 2.16b presents the dependence of yield of hydrogen on time for various liquid metals. The highest yield belongs to hydrogen production with a gallium-tin liquid bath, followed by pure gallium. For 20 minutes of the

reaction, the H₂ yield is ~40 ml and ~35 ml for gallium-tin and pure gallium, respectively.

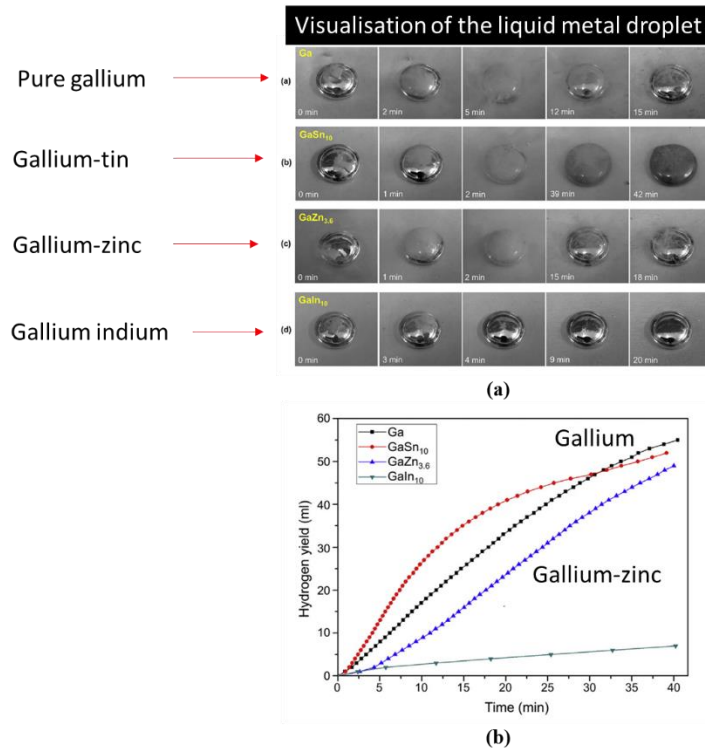


Figure 2.16. Dependence of the morphology of liquid metals and hydrogen yield on time of reaction for various liquid metals adapted from the literature (Geißler et al., 2016), a) Dependence of morphology and chemical composition of liquid metals on the time of the reaction, b) Dependence of hydrogen yield on the time of the reaction.

With the continuous progress in mathematical and modelling sciences, together with advancements in material science, a new process for the gasification of carbonaceous fuel was developed referred to as the Hymelt process, which uses molten iron as the oxygen carrier in a specific type of a furnace (Burke & Gull, 2002). Marathon Ashland Petroleum and Envires LLC re-developed the HyMelt process to produce high-quality syngas with different streams for hydrogen and carbon monoxide (Holcombe & Malone, 2002). The process' principle is based on the release of the energy content of the feedstock, dissolved in the molten iron (Halloran, 2008). There are also several other processes with a similar mechanism but with

different aims, in which, by means of the catalytic effect of molten metal, a carbonaceous material is cracked into a product such as syngas or hydrogen (Bach & Nagel, 1986).

Another process designed for disposing of the petroleum coke is the Corex process, in which the waste materials are poured into the molten slag to produce syngas. The syngas product is then used for iron making processes (Greenwalt, 1997). For most of these processes, the main source of the feedstock is coal, biomass or municipal waste. Steam is also used to promote the mixing, the hydrogen content of the syngas and to control the temperature and the conversion of the reactions. Although this process is plausible for syngas production, the ratio of H₂: CO is limited and the syngas quality cannot reach ~2.

Direct syngas production with molten metals is another pathway for converting feedstock such as coke and biomass to an upgraded fuel such as syngas. For example, in research conducted by Eatwell-Hall et al. (Eatwell-Hall, Sharifi, & Swithenbank, 2010), a liquid metal bath was implemented to gasify the carbon. The gasification occurred in two successive stages: at the first stage, high-temperature steam was fed into the liquid metal phase in a bubbling regime, then a metal oxide formed and, as a result, hydrogen was released. At the second stage, carbon was fed into the molten metal and the metal oxide was reduced, while carbon monoxide and carbon dioxide were released. They fabricated and tested the process. The syngas product was almost pure and did not need to any syngas cleaning process. The syngas product could be used in a fuel cell. Figure 2.17 presents a schematic diagram of the process proposed by Eatwell-Hall for hydrogen production using a tin and iron liquid bath.

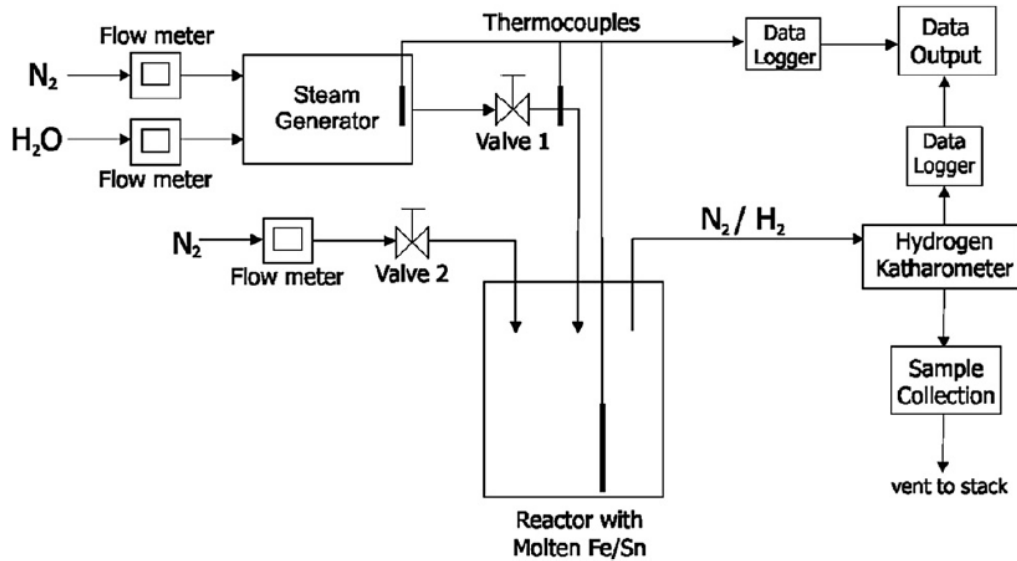


Figure 2.17. Schematic diagram of the process developed by Eatwell-Hall et al. used for hydrogen production from natural gas using an FeO liquid bath, taken from (Eatwell-Hall et al., 2010).

Alberta Innovates Technology Futures (AITF) is another institute where a new liquid metal technology has been developed for hydrogen/syngas production from a carbonaceous fuel. In their commercialisation path, they conducted some bench-scale experiments on methane cracking with liquid metal (Paxman et al., 2014) at 1023 K to 1373 K. They reported that the minimum residence time for methane to be completely converted to hydrogen is highly dependent on the size of the gas bubbles within the molten metal bed. To increase the residence time, they fabricated a ceramic tubular reactor and developed a model to show that the hydrogen yield is a function of the bubble size and the rate of diffusion of the fuel in the liquid metal. Figure 2.18 presents a schematic diagram of the tubular furnace developed for methane cracking with liquid metal. Ceramic material was used, as tin can be contained in ceramic material.

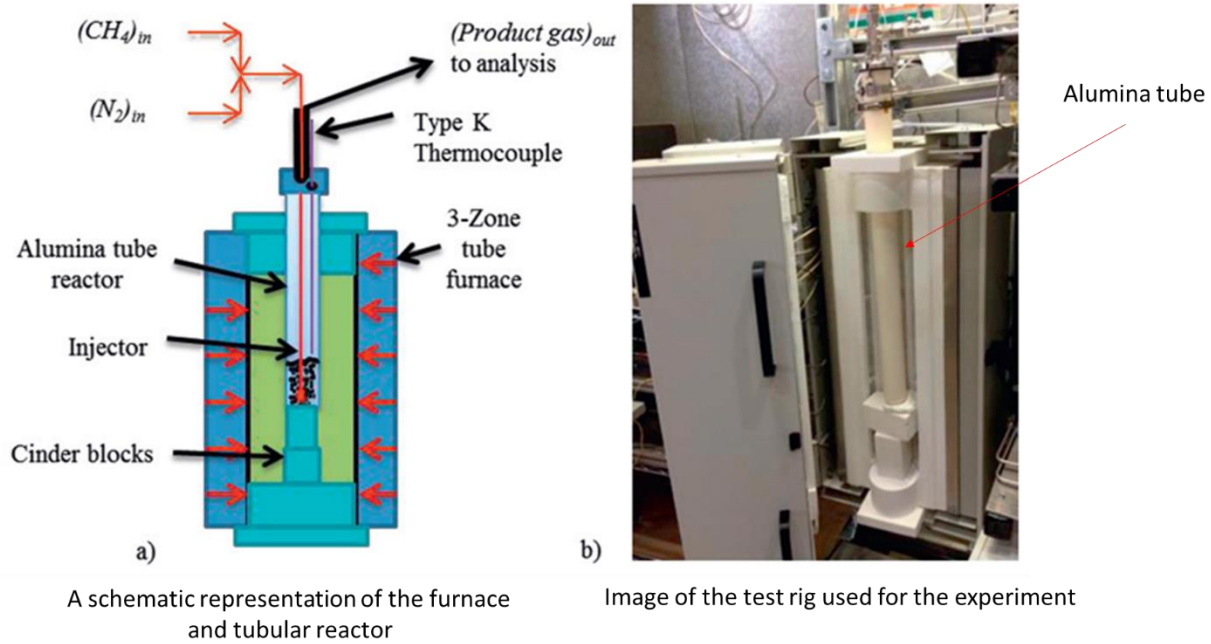


Figure 2.18. A schematic diagram of the reactor developed for hydrogen production from molten tin, adapted from the literature (Paxman et al., 2014), a) Detailed schematic diagram of the reactor, b) Image taken from the tubular reactor for hydrogen production.

The hydromax gasification process is also a relatively new technology, developed for producing hydrogen and syngas with the gasification of carbonaceous feedstock with a liquid bath of Sn and FeO. The system uses the thermal energy of molten iron oxide at high temperatures, e.g. 1250°C, to gasify feedstock into syngas and employs a robust injection system to enrich the hydrogen content of the gaseous product with steam. Around four patents, together with 240 claims of inventions regarding the hydromax process, have been registered. The hydromax process was employed for purifying iron oxide to absorb oxygen, with a carbonaceous material to produce pure iron. However, recently, the application of this process has broadened to include hydrogen and syngas production, though it has only been demonstrated at lab-scale (Energy, 2009). This process has shown some promising results, such as lower N₂ dilution of syngas, higher yield of CO and lower CO₂ production in comparison with current gasification systems (Schenk, 2007). However, it can only be used for molten iron

at high temperatures, such as 1250°C. It is worth mentioning that the containment of molten iron at such high temperatures is technically challenging. Moreover, the molten phase is not pure and has lots of impurity in it, causing a massive reduction in the ratio of H₂: CO. This is because the presence of impurities within the liquid metal results in the occurrence of side reactions, which changes the general kinetics of the gasification. Thus, further investigation is required to develop a new insights into better understanding the kinetics of gasification with molten metals. Figure 2.19 presents a schematic diagram of the hydromax reactor working with an iron oxide/tin alloy for hydrogen production.

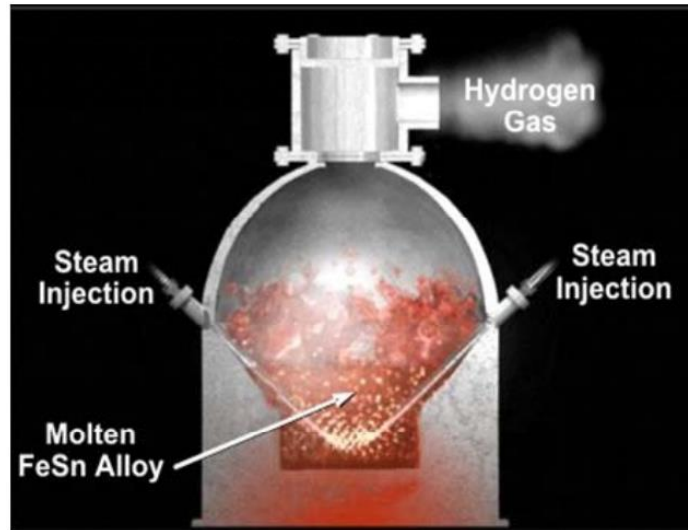


Figure 2.19. A schematic diagram of the hydromax reactor used for hydrogen production, adapted from (Energy, 2009).

2.12. Kinetics of reaction with carbon in liquid metal

The kinetics of reaction between a molten metal oxide and a carbonaceous feedstock is complicated to understand. This is because the reactions occur in three different phase interactions of solid-liquid (feedstock and molten metal oxide), solid-gas (feedstock-gasifying agent and volatile gaseous products), and liquid-gas (molten metal oxide and gasifying agent and gaseous products). The rate of reaction in solid-liquid and solid-gas reactions is generally

slower than that observed for liquid-gas and gas-gas reactions. However, the presence of liquid metal within the reaction container may enhance the reaction rate due to the catalytic effect of the metal. Therefore, it is necessary to investigate the kinetics of gasification reactions with molten metals further, to identify the exact mechanisms involved in the process.

Many experiments have been conducted to better understand the kinetics of reactions in systems containing molten metal reactants. For example, in metal purification processes and steel-making industries, a liquid metal phase referred to as “slag” is in direct contact with solid or gaseous carbonaceous feedstock to reduce the amount of oxygen dissolved in the liquid phase down to a threshold value. This is because the presence of oxygen in the liquid metal can add unfavourable properties, such as brittleness and low thermal conductivity. In such processes, the carbonaceous feedstock is partially/fully oxidised with the oxygen in the slag, resulting in the production of syngas. However, the presence of other impurities such as SiO_2 and some heavy metals may result in the production of syngas with a very low ratio of H_2 : CO . In addition, the reaction rate between slag and feedstock depends on different parameters, such as the temperature, amount of impurity and quantity of oxygen dissolved in the slag.

The mechanism and kinetics of the metal purification process is similar to that which occurs in the gasifier in the CLG process. Many studies have been conducted to understand the mechanism for the reduction of metal oxides with a carbonaceous feedstock. For example, in a study performed by Sato et al. (Sato, Aragane, Kamihira, & Yoshimatso, 1987), a set of experiments was conducted to further understand the mechanism of reduction of iron oxide with a carbonaceous feedstock. They used a mixture of slag and iron oxide to quantify the amount of CO gas produced due to the reduction of iron oxide with graphite. They repeated the experiments at various temperatures ranging between $1320\text{ }^\circ\text{C}$ and $1620\text{ }^\circ\text{C}$ in which iron was kept in liquid state and noticed that the rate of reduction reaction of iron with graphite was proportional to the second power of the concentration of iron (Sato et al., 1987). Seaton et al.

(Seaton, Rodriguez, Gonzalez, & Manrique, 1983) conducted several experiments to assess the reduction of iron pellets in carbon and liquid steel. They demonstrated that the magnitude of heat transfer between iron pellets and molten steel strongly depends on the rate of CO production in the process. They showed that, with an increase in the rate of CO production, the higher heat transfer rate could be seen within the process. Likewise, the produced CO was the product of the reaction between the carbon and the oxygen released from the iron oxide dissolved in the liquid steel (Seaton et al., 1983).

Upadhyaya et al. (Upadhyaya, 1986) assessed the reaction mechanism for the reduction of lead oxide in a dilute liquid mixture of CaO-Al₂O₃-SiO₂ slag using graphite dissolved in iron. They studied the influence of different operating parameters such as the pressure, concentration of carbon and concentration of lead oxide. They noticed that lead oxide is reduced with the reaction between a gas evolved from the lead oxide and the carbon in the system. They also noticed that the ratio of lead oxide to carbon is a determinative parameter influencing the degree of reduction. Likewise, temperature was found to intensify the rate of reduction as well.

With the advent of the thermo-gravimetric analyser (TGA), this technique was used to measure the activation energy of the reactions. However, there are few studies conducted on the kinetics of the reaction of liquid metals, in which the thermo-gravimetric device was used to measure the activation energy. For example, in a study conducted by Monazam et al. (Monazam et al., 2012), the thermo-gravimetric instrument was used to assess the reduction reaction of CuO impregnated in bentonite with natural gas at 1023 K to 1173 K. The experiments were conducted at 20%-100% (by volume) of natural gas. They found that the activation energy of the reduction reaction for copper oxide with natural gas was 37.3 ± 1.3 kJ/mol. They also reported that the copper oxide was not deactivated after 10 successive cycles of the experiments. With another experiment, they confirmed the TGA results using outlet gas measurements. They advised that a CuO/bentonite oxygen carrier is a promising candidate for

CLG/CLC systems. In another study, the activation energy of the reduction reaction of copper oxide with CO gas was measured by Plewa and Skrzypek (Plewa & Skrzypek, 1989). They reported a value of 44.3 ± 1.8 kJ/mol, using experiments conducted with a thermo-gravimetric analyser at 398 K to 473 K. They advised the utilisation of CuO particles for CLC/CLG processes. Figure 2.21 presents a schematic diagram of the thermo-gravimetric device used for the measurement of the activation energy of copper oxide.

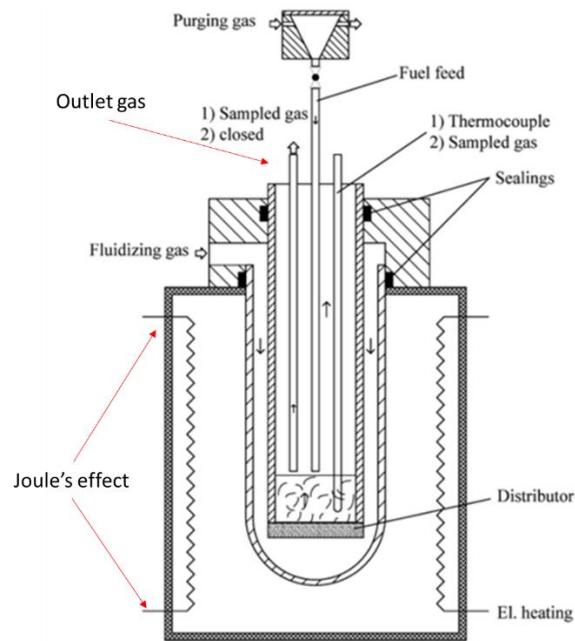


Figure 2.21. Schematic diagram of a thermo-gravimetric test rig used for measuring the reaction kinetics of molten metals with feedstock, adapted from the literature (Monazam et al., 2012).

Faced with this literature review, although the kinetics of reduction of molten metals such as copper, lead, aluminium and iron with carbon has been studied extensively, the lack of a systematic study is seen for other metal oxides, such as bismuth oxide in liquid phase. Having sufficient knowledge of the reaction rate, activation energy and kinetic constants could pave the way for designing an efficient gasification reactor together with optimised operating conditions in liquid chemical looping gasification.

2.13. Summary and discussion of identified gaps

According to the literature review, the following gaps were identified:

- ❖ Combustion of fossil fuels is the main source of energy production in industrial sectors; however, it is not a sustainable source due to the emission of CO₂ and other pollutants such as NO_x. As a result, renewable energy has emerged and new processes such as chemical looping gasification have been developed for producing clean products, such as synthetic gas. A chemical looping gasification system uses metal oxides as the oxygen carrier to provide a plausible rate of heat and mass transfer between the reactors. However, there are challenges associated with the use of solid oxygen carriers, such as agglomeration, sintering and deposition of carbon on the external surface of the oxygen carrier. These challenges deactivate the oxygen carrier over successive operating cycles. Therefore, one potential solution to address these issues is to use a liquid metal oxide instead of solid oxygen carriers. There are a few studies conducted on the application of liquid metals for gasification processes, however, further investigation is still required, as this technology is emerging. Particularly for liquid chemical looping gasification, there is no study to investigate the thermodynamic potential and energetic performance of the process. Hence, the lack of a comprehensive thermodynamic assessment of liquid chemical looping gasification is seen in the literature.

The first objective of this project is to develop a new thermodynamic model to assess the chemical and energetic performance of the liquid chemical looping gasification (LCLG) system.

- ❖ Chemical looping gasification can work with different types of oxygen carriers, including solid and liquid oxygen carriers. For solid oxygen carriers, much effort has been made to identify the parameters associated with solid oxygen carriers influencing the performance of CLG. These parameters include but are not limited to tolerance

against high-temperature operation, sufficient oxygen content, a facile uncoupling feature for releasing the oxygen, a good heat and mass transfer rate, and sufficient rigidity against sintering and agglomeration. However, for a liquid oxygen carrier, there is no systematic study to assess the various liquid metal oxides for potential application in chemical looping gasification systems. Likewise, no systematic approach has been applied to identify the key parameters to select the appropriate liquid oxygen carrier for LCLG. In addition, a detailed assessment of the chemical performance of liquid chemical looping gasification is required to identify the potential oxygen carriers suitable for LCLG for further applications, such as the co-production of heat, power and syngas or biomass gasification.

The second objective of this project is to assess the energetic and chemical performance of the chemical looping gasification process for various liquid metal oxides as the oxygen carrier and to identify some thermodynamic criteria for assessing the suitability of various liquid metal oxides to be used in LCLG.

- ❖ Since liquid chemical looping gasification is a new concept, the potential of this process to be connected to a power block for the co-production of heat, power and syngas needs to be investigated thermodynamically.

The third objective of this project is to assess the potential of the liquid metal oxides identified in the previous tasks for the co-production of syngas, power and heat via a power block.

- ❖ The models developed in the previous objectives are based on pure graphitic carbon. However, renewable resources such as biomass and coal have significant amounts of impurities and ash content. Hence, the performance of the LCLG will be highly influenced by the ash content. For LCLG, the chemical performance of the system has not been assessed thermodynamically for biomass feedstock. Apart from the

thermodynamic point of the view, the detailed kinetics and specifications of the chemical reactions occurring between the liquid metal oxide and a carbonaceous feedstock are yet to be fully understood. Despite the fact that few studies have been conducted to understand the kinetics of the reduction reactions of some liquid metal oxides including copper, iron and alumina with some carbonaceous materials including CH_4 and graphite, the lack of experimental investigation into the reactions of other liquid metal oxides with carbonaceous feedstock can be found in the literature.

The fourth objective of this work is to conduct a set of experiments for assessing the kinetics of the reaction of the liquid metal oxide identified in objective two, not only to validate the thermodynamic models but also to develop a kinetic model for the reduction and oxidation of the liquid metal oxide with a carbon feedstock.

It is worth saying that, in the present work, a thermodynamic assessment followed by an experimental analysis will be conducted to develop and validate the equilibrium model to assess the chemical and thermal performance of a liquid chemical looping process. Hence, design and fabrication of the reactors and the process plant is beyond the scope of the present investigation and will be recommended as a future work.

References

- Abad, A., Adánez, J., García-Labiano, F., Luis, F., Gayán, P., & Celaya, J. (2007). Mapping of the range of operational conditions for Cu-, Fe-, and Ni-based oxygen carriers in chemical-looping combustion. *Chemical Engineering Science*, **62**(1-2), 533-549.
- Abánades, A., Rathnam, R. K., Geißler, T., Heinzl, A., Mehravaran, K., Müller, G., Stoppel, L. (2016). Development of methane decarbonisation based on liquid metal technology for CO₂-free production of hydrogen. *International Journal of Hydrogen Energy*, **41**(19), 8159-8167.
- Abdulally, I., Edberg, C., Andrus, H., Chiu, J., Thibeault, P., & Lani, P. (2011). *ALSTOM's chemical looping combustion prototype for CO₂ capture from existing pulverized coal-fired power plants*. Paper presented at the Proceedings of Department of Energy National Energy Technology Laboratory CO₂ Capture Technology Meeting.
- Adanez, J., Abad, A., Garcia-Labiano, F., Gayan, P., & Luis, F. (2012). Progress in chemical-looping combustion and reforming technologies. *Progress in Energy and Combustion Science*, **38**(2), 215-282.
- Adánez, J., de Diego, L. F., García-Labiano, F., Gayán, P., Abad, A., & Palacios, J. (2004). Selection of oxygen carriers for chemical-looping combustion. *Energy & Fuels*, **18**(2), 371-377.
- Adánez, J., García-Labiano, F., de Diego, L., Gayán, P., Abad, A., & Celaya, J. (2005). Development of oxygen carriers for chemical-looping combustion. *Carbon dioxide capture for storage in deep geologic formations-Results from the CO₂ Capture Project*, **1**, 587-604.
- Adánez, J., García-Labiano, F., de Diego, L. F., Gayán, P., Celaya, J., & Abad, A. (2006). Nickel– copper oxygen carriers to reach zero CO and H₂ emissions in chemical-looping combustion. *Industrial & Engineering Chemistry Research*, **45**(8), 2617-2625.
- Adánez, J., Gayán, P., Celaya, J., de Diego, L. F., García-Labiano, F., & Abad, A. (2006). Chemical looping combustion in a 10-kWth prototype using a CuO/Al₂O₃ oxygen carrier: Effect of operating conditions on methane combustion. *Industrial & Engineering Chemistry Research*, **45**(17), 6075-6080.
- Ahmad, A. A., Zawawi, N. A., Kasim, F. H., Inayat, A., & Khasri, A. (2016). Assessing the gasification performance of biomass: A review on biomass gasification process conditions, optimization and economic evaluation. *Renewable and Sustainable Energy Reviews*, **53**, 1333-1347.
- Bach, R. D., & Nagel, C. J. (1986). Destruction of toxic chemicals. In: Google Patents.

- Brandvoll, O. y., & Bolland, O. (2002). *Inherent CO₂ capture using chemical looping combustion in a natural gas fired power cycle*. Paper presented at the ASME Turbo Expo 2002: Power for Land, Sea, and Air.
- Brown, T., Dennis, J., Scott, S., Davidson, J., & Hayhurst, A. (2010). Gasification and chemical-looping combustion of a lignite char in a fluidized bed of iron oxide. *Energy & fuels*, **24**(5), 3034-3048.
- Burke, P., & Gull, S. (2002). *HIs melt(-The Alternative Ironmaking Technology*. Paper presented at the Proceedings of International Conference on Smelting Reduction for Ironmaking, Jouhari, AK, Galgali, RK, Misra, VN, Eds.
- Cao, Y., & Pan, W.-P. (2006). Investigation of chemical looping combustion by solid fuels. 1. Process analysis. *Energy & Fuels*, **20**(5), 1836-1844.
- Chang, A. C., Chang, H.-F., Lin, F.-J., Lin, K.-H., & Chen, C.-H. (2011). Biomass gasification for hydrogen production. *International Journal of Hydrogen Energy*, **36**(21), 14252-14260.
- Change, I. C. (2007). Mitigation of climate change. *Summary for Policymakers*, **10**(5.4).
- Cho, P., Mattisson, T., & Lyngfelt, A. (2005). Carbon formation on nickel and iron oxide-containing oxygen carriers for chemical-looping combustion. *Industrial & Engineering Chemistry Research*, **44**(4), 668-676.
- Cho, P., Mattisson, T., & Lyngfelt, A. (2006). Defluidization conditions for a fluidized bed of iron oxide-, nickel oxide-, and manganese oxide-containing oxygen carriers for chemical-looping combustion. *Industrial & Engineering Chemistry Research*, **45**(3), 968-977.
- Conti, J., Holtberg, P., Diefenderfer, J., LaRose, A., Turnure, J. T., & Westfall, L. (2016). *International Energy Outlook 2016 With Projections to 2040*. Retrieved from
- Corella, J., Aznar, M. P., Delgado, J., & Aldea, E. (1991). Steam gasification of cellulosic wastes in a fluidized bed with downstream vessels. *Industrial & Engineering Chemistry Research*, **30**(10), 2252-2262.
- Cuadrat, A., Abad, A., Adánez, J., De Diego, L., García-Labiano, F., & Gayán, P. (2012). Behavior of ilmenite as oxygen carrier in chemical-looping combustion. *Fuel Processing Technology*, **94**(1), 101-112.
- Daniel, T. (1931). Production of hydrogen. In: Google Patents.

- De Diego, L. F., García-Labiano, F., Adánez, J., Gayán, P., Abad, A., Corbella, B. M., & Palacios, J. M. a. (2004). Development of Cu-based oxygen carriers for chemical-looping combustion. *Fuel*, **83**(13), 1749-1757.
- De Diego, L. F., Gayán, P., García-Labiano, F., Celaya, J., Abad, A., & Adánez, J. (2005). Impregnated CuO/Al₂O₃ oxygen carriers for chemical-looping combustion: avoiding fluidized bed agglomeration. *Energy & fuels*, **19**(5), 1850-1856.
- de Noronha, R. F., Miranda, M. A., Cavalca, K. L., Memmott, E. A., & Ramesh, K. (2014). 43rd Turbomachinery & 30th Pump Users Symposia (Pump & Turbo 2014) September 23-25, 2014| Houston, TX| pumpturbo. tamu. edu.
- Eatwell-Hall, R., Sharifi, V., & Swithenbank, J. (2010). Hydrogen production from molten metal gasification. *International Journal of Hydrogen Energy*, **35**(24), 13168-13178.
- Energy, D. (2009). HydroMax—Advanced gasification technology. In.
- Gaffney, J. S., & Marley, N. A. (2009). The impacts of combustion emissions on air quality and climate—From coal to biofuels and beyond. *Atmospheric Environment*, **43**(1), 23-36.
- Gao, N., Li, A., Quan, C., & Gao, F. (2008). Hydrogen-rich gas production from biomass steam gasification in an updraft fixed-bed gasifier combined with a porous ceramic reformer. *International Journal of Hydrogen Energy*, **33**(20), 5430-5438.
- Gayán, P., Forero, C. R., Abad, A., de Diego, L. F., García-Labiano, F., & Adánez, J. (2011). Effect of support on the behavior of Cu-based oxygen carriers during long-term CLC operation at temperatures above 1073 K. *Energy & Fuels*, **25**(3), 1316-1326.
- Gayán, P., Luis, F., García-Labiano, F., Adánez, J., Abad, A., & Dueso, C. (2008). Effect of support on reactivity and selectivity of Ni-based oxygen carriers for chemical-looping combustion. *Fuel*, **87**(12), 2641-2650.
- Geißler, T., Abánades, A., Heinzl, A., Mehravaran, K., Müller, G., Rathnam, R., . . . Stückrad, S. (2016). Hydrogen production via methane pyrolysis in a liquid metal bubble column reactor with a packed bed. *Chemical Engineering Journal*, **299**, 192-200.
- Geißler, T., Plevan, M., Abánades, A., Heinzl, A., Mehravaran, K., Rathnam, R., . . . Stückrad, S. (2015). Experimental investigation and thermo-chemical modeling of methane pyrolysis in a liquid metal bubble column reactor with a packed bed. *International Journal of Hydrogen Energy*, **40**(41), 14134-14146.
- Georgakis, C., Chang, C., & Szekely, J. (1979). A changing grain size model for gas—solid reactions. *Chemical Engineering Science*, **34**(8), 1072-1075.

- Greenwalt, R. B. (1997). Method of providing fuel for an iron making process. In: Google Patents.
- Gulevich, A., Martynov, P., Gulevsky, V., & Ulyanov, V. (2008). Technologies for hydrogen production based on direct contact of gaseous hydrocarbons and evaporated water with molten Pb or Pb–Bi. *Energy conversion and management*, **49**(7), 1946-1950.
- Guo, Q., Cheng, Y., Liu, Y., Jia, W., & Ryu, H.-J. (2013). Coal chemical looping gasification for syngas generation using an iron-based oxygen carrier. *Industrial & Engineering Chemistry Research*, **53**(1), 78-86.
- Halloran, J. W. (2008). Extraction of hydrogen from fossil fuels with production of solid carbon materials. *International Journal of Hydrogen Energy*, **33**(9), 2218-2224.
- Hatanaka, T., Matsuda, S., & Hatano, H. (1997). *A new-concept gas-solid combustion system "MERIT" for high combustion efficiency and low emissions*. Paper presented at the Energy Conversion Engineering Conference, 1997. IECEC-97., Proceedings of the 32nd Intersociety.
- He, F., Galinsky, N., & Li, F. (2013). Chemical looping gasification of solid fuels using bimetallic oxygen carrier particles—Feasibility assessment and process simulations. *International Journal of Hydrogen Energy*, **38**(19), 7839-7854.
- Herguido, J., Corella, J., & Gonzalez-Saiz, J. (1992). Steam gasification of lignocellulosic residues in a fluidized bed at a small pilot scale. Effect of the type of feedstock. *Industrial & Engineering Chemistry Research*, **31**(5), 1274-1282.
- Holcombe, T. C., & Malone, D. P. (2002). Two-zone molten metal hydrogen-rich and carbon monoxide-rich gas generation process. In: Google Patents.
- Hossain, M. M., & de Lasa, H. I. (2008). Chemical-looping combustion (CLC) for inherent CO₂ separations—a review. *Chemical Engineering Science*, **63**(18), 4433-4451.
- Hoteit, A., Chandel, M. K., & Delebarre, A. (2009). Nickel-and Copper-Based Oxygen Carriers for Chemical Looping Combustion. *Chemical engineering & technology*, **32**(3), 443-449.
- Huang, Z., Zhang, Y., Fu, J., Yu, L., Chen, M., Liu, S., . . . Zhao, K. (2016). Chemical looping gasification of biomass char using iron ore as an oxygen carrier. *International Journal of Hydrogen Energy*, **41**(40), 17871-17883.
- IEA. (2017). *World Energy Outlook 2017*: Organisation for Economic Co-operation and Development, OECD.
- Irfan, M. F., Usman, M. R., & Kusakabe, K. (2011). Coal gasification in CO₂ atmosphere and its kinetics since 1948: A brief review. *Energy*, **36**(1), 12-40.

- Ishida, M., & Jin, H. (1994). A novel combustor based on chemical-looping reactions and its reaction kinetics. *Journal of Chemical Engineering of Japan*, **27**(3), 296-301.
- Ishida, M., Jin, H., & Okamoto, T. (1998). Kinetic behavior of solid particle in chemical-looping combustion: suppressing carbon deposition in reduction. *Energy & fuels*, **12**(2), 223-229.
- Jafarian, M., Arjomandi, M., & Nathan, G. J. (2014). Influence of the type of oxygen carriers on the performance of a hybrid solar chemical looping combustion system. *Energy & fuels*, **28**(5), 2914-2924.
- Jafarian, M., Arjomandi, M., & Nathan, G. J. (2017). Thermodynamic potential of high temperature chemical looping combustion with molten iron oxide as the oxygen carrier. *Chemical Engineering Research and Design*, **120**, 69-81.
- Jerndal, E., Mattisson, T., & Lyngfelt, A. (2009). Investigation of different NiO/NiAl₂O₄ particles as oxygen carriers for chemical-looping combustion. *Energy & fuels*, **23**(2), 665-676.
- Jin, H., Okamoto, T., & Ishida, M. (1998). Development of a novel chemical-looping combustion: synthesis of a looping material with a double metal oxide of CoO– NiO. *Energy & fuels*, **12**(6), 1272-1277.
- Johansson, E., Lyngfelt, A., Mattisson, T., & Johnsson, F. (2003). Gas leakage measurements in a cold model of an interconnected fluidized bed for chemical-looping combustion. *Powder Technology*, **134**(3), 210-217.
- Johnson, J. (1974). Kinetics of bituminous coal char gasification with gases containing steam and hydrogen. In: ACS Publications.
- Joshi, A., Lou, X., Neuschaefer, C., Chaudry, M., & Quinn, J. (2012). *Development of Computational Approaches for Simulation and Advanced Controls for Hybrid Combustion-Gasification Chemical Looping*. Retrieved from
- Kalinci, Y., Hepbasli, A., & Dincer, I. (2009). Biomass-based hydrogen production: a review and analysis. *International Journal of Hydrogen Energy*, **34**(21), 8799-8817.
- Kern, S., Pfeifer, C., & Hofbauer, H. (2013). Gasification of wood in a dual fluidized bed gasifier: Influence of fuel feeding on process performance. *Chemical Engineering Science*, **90**, 284-298.
- Kim, S. D., Go, K. S., Jeon, Y. W., & Park, C. S. (2010). Chemical-looping steam methane reforming for hydrogen production in a circulating fluidized bed reactor.

- Kirubakaran, V., Sivaramakrishnan, V., Nalini, R., Sekar, T., Premalatha, M., & Subramanian, P. (2009). A review on gasification of biomass. *Renewable and Sustainable Energy Reviews*, **13**(1), 179-186.
- Kolbitsch, P., Pröll, T., Bolhar-Nordenkamp, J., & Hofbauer, H. (2009). Design of a chemical looping combustor using a dual circulating fluidized bed (DCFB) reactor system. *Chemical engineering & technology*, **32**(3), 398-403.
- Kronberger, B., Johansson, E., Löffler, G., Mattisson, T., Lyngfelt, A., & Hofbauer, H. (2004). A two-compartment fluidized bed reactor for CO₂ capture by chemical-looping combustion. *Chemical engineering & technology*, **27**(12), 1318-1326.
- Kronberger, B., Lyngfelt, A., Löffler, G., & Hofbauer, H. (2005). Design and fluid dynamic analysis of a bench-scale combustion system with CO₂ separation– chemical-looping combustion. *Industrial & Engineering Chemistry Research*, **44**(3), 546-556.
- Kumar, A., Jones, D. D., & Hanna, M. A. (2009). Thermochemical biomass gasification: a review of the current status of the technology. *Energies*, **2**(3), 556-581.
- LaMont, D. C., Seaba, J., Latimer, E. G., & Platon, A. (2010). Liquid-phase chemical looping energy generator. In: Google Patents.
- Leion, H., Lyngfelt, A., Johansson, M., Jerndal, E., & Mattisson, T. (2008). The use of ilmenite as an oxygen carrier in chemical-looping combustion. *Chemical engineering research and design*, **86**(9), 1017-1026.
- Leion, H., Mattisson, T., & Lyngfelt, A. (2009). Use of ores and industrial products as oxygen carriers in chemical-looping combustion. *Energy & Fuels*, **23**(4), 2307-2315.
- Li, F., & Fan, L.-S. (2008). Clean coal conversion processes–progress and challenges. *Energy & Environmental Science*, **1**(2), 248-267.
- Li, F., Zeng, L., Velazquez-Vargas, L. G., Yoscovits, Z., & Fan, L. S. (2010). Syngas chemical looping gasification process: Bench-scale studies and reactor simulations. *AIChE Journal*, **56**(8), 2186-2199.
- Lieuwen, T., Yetter, R., & Yang, V. (2009). *Synthesis gas combustion: fundamentals and applications*: CRC Press.
- Liu, G., Liao, Y., Wu, Y., & Ma, X. (2018). Application of calcium ferrites as oxygen carriers for microalgae chemical looping gasification. *Energy conversion and management*, **160**, 262-272. doi:<https://doi.org/10.1016/j.enconman.2018.01.041>
- Luis, F., Garcá, F., Gayán, P., Celaya, J., Palacios, J. M., & Adánez, J. (2007a). Operation of a 10 kWth chemical-looping combustor during 200 h with a CuO–Al₂O₃ oxygen carrier. *Fuel*, **86**(7-8), 1036-1045.

- Luis, F., Garc1, F., Gayán, P., Celaya, J., Palacios, J. M., & Adánez, J. (2007b). Operation of a 10kWth chemical-looping combustor during 200h with a CuO–Al₂O₃ oxygen carrier. *Fuel*, **86**(7), 1036-1045.
- Lyngfelt, A., Kronberger, B., Adanez, J., Morin, J., & Hurst, P. (2004). *The GRACE project. Development of oxygen carrier particles for chemical-looping combustion. Design and operation of a 10KW chemical-looping combustor*: na.
- Lyngfelt, A., Leckner, B., & Mattisson, T. (2001). A fluidized-bed combustion process with inherent CO₂ separation; application of chemical-looping combustion. *Chemical Engineering Science*, **56**(10), 3101-3113.
- Lyngfelt, A., & Thunman, H. (2005a). Construction and 100 h of operational experience of a 10-kW chemical-looping combustor. *Carbon dioxide capture for storage in deep geologic formations-results from the CO₂ capture project*, **1**, 625-645.
- Lyngfelt, A., & Thunman, H. (2005b). Construction and 100 h of operational experience of a 10-kW chemical-looping combustor. *Carbon Dioxide Capture for Storage in Deep Geologic Formations; Results from the CO₂ Capture Project*, **1**, 625-645.
- Martynov, P., Gulevich, A., Orlov, Y. I., & Gulevsky, V. (2005). Water and hydrogen in heavy liquid metal coolant technology. *Progress in Nuclear Energy*, **47**(1-4), 604-615.
- Mattisson, T., Johansson, M., Jerndal, E., & Lyngfelt, A. (2008). The reaction of NiO/NiAl₂O₄ particles with alternating methane and oxygen. *The Canadian Journal of Chemical Engineering*, **86**(4), 756-767.
- Mattisson, T., Johansson, M., & Lyngfelt, A. (2004). Multicycle reduction and oxidation of different types of iron oxide particles application to chemical-looping combustion. *Energy & fuels*, **18**(3), 628-637.
- Mattisson, T., Johansson, M., & Lyngfelt, A. (2006). The use of NiO as an oxygen carrier in chemical-looping combustion. *Fuel*, **85**(5-6), 736-747.
- McGlashan, N. (2008). Chemical-looping combustion—a thermodynamic study. *Proceedings of the Institution of Mechanical Engineers, Part C: Journal of Mechanical Engineering Science*, **222**(6), 1005-1019.
- Monazam, E. R., Siriwardane, R., Breault, R. W., Tian, H., Shadle, L. J., Richards, G., & Carpenter, S. (2012). Kinetics of the reduction of CuO/bentonite by methane (CH₄) during chemical looping combustion. *Energy & Fuels*, **26**(5), 2779-2785.
- Noorman, S., van Sint Annaland, M., & Kuipers, H. (2007). Packed bed reactor technology for chemical-looping combustion. *Industrial & Engineering Chemistry Research*, **46**(12), 4212-4220.

- Noorman, S., van Sint Annaland, M., & Kuipers, J. (2010). Experimental validation of packed bed chemical-looping combustion. *Chemical Engineering Science*, **65**(1), 92-97.
- Ono, H., Yoshida, S., Nezuka, M., Sano, T., Tsuji, M., & Tamaura, Y. (1999). Kinetics and simulation on a high-temperature solar thermochemical energy conversion process on the Boudouard reaction. *Energy & fuels*, **13**(3), 579-584.
- Ortiz, M., Abad, A., Luis, F., García-Labiano, F., Gayán, P., & Adánez, J. (2011). Optimization of hydrogen production by chemical-looping auto-thermal reforming working with Ni-based oxygen-carriers. *International Journal of Hydrogen Energy*, **36**(16), 9663-9672.
- Outlook, A. E. (2007). with Projections to 2030. *US Energy Information Administration*.
- Pan, Y., Velo, E., Roca, X., Manyá, J., & Puigjaner, L. (2000). Fluidized-bed co-gasification of residual biomass/poor coal blends for fuel gas production. *Fuel*, **79**(11), 1317-1326.
- Paxman, D., Trottier, S., Nikoo, M., Secanell, M., & Ordorica-Garcia, G. (2014). Initial experimental and theoretical investigation of solar molten media methane cracking for hydrogen production. *Energy Procedia*, **49**, 2027-2036.
- Plevan, M., Geißler, T., Abánades, A., Mehravaran, K., Rathnam, R., Rubbia, C., . . . Wetzler, T. (2015). Thermal cracking of methane in a liquid metal bubble column reactor: Experiments and kinetic analysis. *International Journal of Hydrogen Energy*, **40**(25), 8020-8033.
- Plewa, J., & Skrzypek, J. (1989). Kinetics of the reduction of copper oxide with carbon monoxide. *Chemical Engineering Science*, **44**(12), 2817-2824.
- Prathap, C., Ray, A., & Ravi, M. (2008). Investigation of nitrogen dilution effects on the laminar burning velocity and flame stability of syngas fuel at atmospheric condition. *Combustion and Flame*, **155**(1-2), 145-160.
- Richter, H. J., & Knoche, K. F. (1983). *Reversibility of combustion processes*. Paper presented at the ACS Symposium series.
- Rostrup-Nielsen, J. R. (2002). Syngas in perspective. *Catalysis today*, **71**(3-4), 243-247.
- Rydén, M., Lyngfelt, A., & Mattisson, T. (2008). Chemical-looping combustion and chemical-looping reforming in a circulating fluidized-bed reactor using Ni-based oxygen carriers. *Energy & Fuels*, **22**(4), 2585-2597.
- Ryu, H., Jo, S.-H., Park, Y. C., Bae, D., & Kim, S. (2010). *Long term operation experience in a 50 kWth chemical looping combustor using natural gas and syngas as fuels*. Paper presented at the 1st International Conference on Chemical Looping.

- Ryu, H.-J., Bae, D.-H., & Jin, G.-T. (2003). Effect of temperature on reduction reactivity of oxygen carrier particles in a fixed bed chemical-looping combustor. *Korean Journal of Chemical Engineering*, **20**(5), 960-966.
- Ryu, H.-J., Jin, G.-T., & Yi, C.-K. (2005). -Demonstration of inherent CO₂ separation and no NO_x emission in a 50kW chemical-looping combustor: Continuous reduction and oxidation experiment. In *Greenhouse Gas Control Technologies 7* (pp. 1907-1910): Elsevier.
- SATO, A., ARAGANE, G., KAMIHIRA, K., & YOSHIMATSU, S. (1987). Reducing rates of molten iron oxide by solid carbon or carbon in molten iron. *Transactions of the Iron and Steel Institute of Japan*, **27**(10), 789-796.
- Schenk, S. (2007). *HydroMax: Breakthrough Molten-Metal Coal Gasification Technology*. Paper presented at the Presentation at the Gasification Technology Conference, San Francisco, CA.
- Schultz, I., & Agar, D. W. (2015). Decarbonisation of fossil energy via methane pyrolysis using two reactor concepts: Fluid wall flow reactor and molten metal capillary reactor. *International Journal of Hydrogen Energy*, **40**(35), 11422-11427.
- Schwebel, G., Wiedenmann, F., & Krumm, W. (2010). *Reduction performance of ilmenite and hematite oxygen carriers in the context of a new CLC reactor concept*. Paper presented at the 1st International Conference on Chemical Looping: An Alternative Concept for Efficient and Clean Use of Fossil Resources.
- Scott, S., Dennis, J., Hayhurst, A., & Brown, T. (2006). In situ gasification of a solid fuel and CO₂ separation using chemical looping. *AIChE Journal*, **52**(9), 3325-3328.
- Serban, M., Lewis, M. A., Marshall, C. L., & Doctor, R. D. (2003). Hydrogen production by direct contact pyrolysis of natural gas. *Energy & Fuels*, **17**(3), 705-713.
- Shen, L., Gao, Y., & Xiao, J. (2008). Simulation of hydrogen production from biomass gasification in interconnected fluidized beds. *Biomass and bioenergy*, **32**(2), 120-127.
- Shen, L., Wu, J., Xiao, J., Song, Q., & Xiao, R. (2009). Chemical-looping combustion of biomass in a 10 kWth reactor with iron oxide as an oxygen carrier. *Energy & fuels*, **23**(5), 2498-2505.
- Son, S. R., & Kim, S. D. (2006). Chemical-looping combustion with NiO and Fe₂O₃ in a thermobalance and circulating fluidized bed reactor with double loops. *Industrial & Engineering Chemistry Research*, **45**(8), 2689-2696.
- Steinberg, M. (1999). Fossil fuel decarbonization technology for mitigating global warming. *International Journal of Hydrogen Energy*, **24**(8), 771-777.

- Szekely, J., Lin, C., & Sohn, H. (1973). A structural model for gas—solid reactions with a moving boundary—V an experimental study of the reduction of porous nickel-oxide pellets with hydrogen. *Chemical Engineering Science*, **28**(11), 1975-1989.
- Turn, S., Kinoshita, C., Zhang, Z., Ishimura, D., & Zhou, J. (1998). An experimental investigation of hydrogen production from biomass gasification. *International Journal of Hydrogen Energy*, **23**(8), 641-648.
- Udomsirichakorn, J., & Salam, P. A. (2014). Review of hydrogen-enriched gas production from steam gasification of biomass: the prospect of CaO-based chemical looping gasification. *Renewable and Sustainable Energy Reviews*, **30**, 565-579.
- Upadhyaya, K. (1986). Kinetics of reduction of lead oxide in liquid slag by carbon in iron. *Metallurgical Transactions B*, **17**(2), 271-279.
- Utigard, T., Sanchez, G., Manriquez, J., Luraschi, A., Diaz, C., Cordero, D., & Almendras, E. (1997). Reduction kinetics of liquid iron oxide-containing slags by carbon monoxide. *Metallurgical and Materials Transactions B*, **28**(5), 821-826.
- Velazquez-Vargas, L. G. (2007). *Development of chemical looping gasification processes for the production of hydrogen from coal*. The Ohio State University,
- Wang, K., Yu, Q., Qin, Q., Hou, L., & Duan, W. (2015). Thermodynamic analysis of syngas generation from biomass using chemical looping gasification method. *International Journal of Hydrogen Energy*.
- Wang, K., Yu, Q., Qin, Q., Hou, L., & Duan, W. (2016). Thermodynamic analysis of syngas generation from biomass using chemical looping gasification method. *International Journal of Hydrogen Energy*, **41**(24), 10346-10353.
- Wolf, J., Anheden, M., & Yan, J. (2001). *Performance analysis of combined cycles with chemical looping combustion for CO₂ capture*. Paper presented at the Proceedings of 18th Pittsburg Coal Conference, December.
- Woolcock, P. J., & Brown, R. C. (2013). A review of cleaning technologies for biomass-derived syngas. *Biomass and bioenergy*, **52**, 54-84.
- Wu, J., Shen, L., Hao, J., & Gu, H. (2010). *Chemical looping combustion of coal in a 1 kWth reactor*. Paper presented at the 1st International Conference on Chemical Looping.

Chapter 3 development of a model for liquid chemical looping gasification

3.1. Chapter overview

In this chapter, a thermodynamic equilibrium model is developed for the chemical looping gasification process with a liquid metal oxide using the thermochemical equilibrium analysis. The model developed in this chapter addresses the first objective of this work. The thermodynamic potential and feasibility of the gasification of a carbonaceous feedstock with a liquid metal is theoretically assessed. In addition, the operating parameters to control the LCLG is identified and a detailed assessment is conducted on the chemical performance of the process. To assess the Gibbs free energy of the potential reactions occurring in the reactors, the Gibbs minimisation method was employed. Enthalpy of reactions together with the composition of components in each phase was estimated using thermochemical equilibrium analysis. A pre-screening on the potential liquid metal oxides revealed that copper oxide can be used for the feasibility study as it has plausible heat and mass transfer properties.

Initially, the phase diagram of copper and oxygen was studied to identify the suitable thermodynamic region for the operation of the CLG. Any regions with two-phase flow and unknown chemical compositions were eliminated. Using the Gibbs minimisation method, potential reactions and components in the air and gasification reactors were identified. Influence of different operating parameters such as the molar ratio of the liquid copper oxide to feedstock, the molar ratio of steam to feedstock, temperature and pressure of the system on the chemical and energetic performance of the system was thermodynamically investigated and discussed. For assessing the chemical performance of the system, the ratio of H₂: CO referred to as “syngas quality” was investigated, while for energetic performance, the enthalpy of reactions together with the exergy efficiency of the process were assessed. The amount of CO₂ and CO production were estimated and the operating regime for the chemical looping

gasification and chemical looping combustion were thermodynamically determined. The conversion extent of the feedstock was calculated at various temperatures and thermodynamic operating conditions. The model was verified using the experimental data available in the literature. Results of this chapter shows that the chemical looping gasification process is thermodynamically feasible and determines the plausible operating conditions for the chemical looping gasification process working with molten copper oxide. This section was published in the journal of Applied Energy (M. Sarafraz, M. Jafarian, M. Arjomandi, & G. Nathan, 2017).

Statement of Authorship

Chapter 3 Development of thermodynamic model for liquid chemical looping gasification process

Title of Paper	Potential use of liquid metal oxides for chemical looping gasification: A thermodynamic assessment
Publication Status	<input checked="" type="checkbox"/> Published <input type="checkbox"/> Accepted for Publication <input type="checkbox"/> Submitted for Publication <input type="checkbox"/> Unpublished and Unsubmitted work written in manuscript style
Publication Details	M.M. Sarafraz, M. Jafarian, M. Arjomandi, G.J. Nathan, Potential use of liquid metal oxides for chemical looping gasification: A thermodynamic assessment, Applied Energy, Volume 195, 1 June 2017, Pages 702-712

Principal Author

Name of Principal Author (Candidate)	Mohammad Mohsen Sarafraz				
Contribution to the Paper	- Research, collecting and analyzing data from different resources, developing thermodynamic models and analyzing the obtained data. - Providing the data, writing of the manuscript and production of original figures. - Correspondence with editor and reviewers including the production of all cover letters and rejoinder				
Overall percentage (%)	80%				
Certification:	This paper reports on original research I conducted during the period of my Higher Degree by Research candidature and is not subject to any obligations or contractual agreements with a third party that would constrain its inclusion in this thesis. I am the primary author of this paper.				
Signature	<table border="1" style="width: 100%;"> <tr> <td style="width: 80%;"></td> <td style="width: 20%;">Date</td> </tr> <tr> <td></td> <td>29/11/18</td> </tr> </table>		Date		29/11/18
	Date				
	29/11/18				

Co-Author Contributions

By signing the Statement of Authorship, each author certifies that:

- i. the candidate's stated contribution to the publication is accurate (as detailed above);
- ii. permission is granted for the candidate to include the publication in the thesis; and
- iii. the sum of all co-author contributions is equal to 100% less the candidate's stated contribution.

Name of Co-Author	Mehdi Jafarian				
Contribution to the Paper	- Supervision of the work, including the production of the manuscript - Participation in the development of the concepts and ideas presented in the manuscript - Evaluation and editing of the manuscript prior to submission				
Signature	<table border="1" style="width: 100%;"> <tr> <td style="width: 80%;"></td> <td style="width: 20%;">Date</td> </tr> <tr> <td></td> <td>29/11/18</td> </tr> </table>		Date		29/11/18
	Date				
	29/11/18				

Name of Co-Author	Maziar Arjomandi				
Contribution to the Paper	- Supervision of the work, including the production of the manuscript - Participation in the development of the concepts and ideas presented in the manuscript - Evaluation and editing of the manuscript prior to submission				
Signature	<table border="1" style="width: 100%;"> <tr> <td style="width: 80%;"></td> <td style="width: 20%;">Date</td> </tr> <tr> <td></td> <td>29/11/18</td> </tr> </table>		Date		29/11/18
	Date				
	29/11/18				

Name of Co-Author	Graham Nathan		
Contribution to the Paper	<ul style="list-style-type: none">- Supervision of the work, including the production of the manuscript- Participation in the development of the concepts and ideas presented in the manuscript- Evaluation and editing of the manuscript prior to submission		
Signature		Date	29/11/18



Potential use of liquid metal oxides for chemical looping gasification: A thermodynamic assessment



M.M. Sarafraz*, M. Jafarian, M. Arjomandi, G.J. Nathan

Centre for Energy Technology, School of Mechanical Engineering, University of Adelaide, SA 5005, Australia

HIGHLIGHTS

- A liquid chemical looping gasification concept for syngas production was introduced.
- Influence of different operating parameters on the syngas production was performed.
- Liquid oxygen carrier/feedstock and steam/feedstock ratios were crucial factors.
- Exergy efficiency of the liquid chemical looping gasification was 67%.
- H₂/CO ratio was as high as 2 suitable for gas to liquid (GTL) processes.

ARTICLE INFO

Article history:

Received 21 November 2016
Received in revised form 20 March 2017
Accepted 22 March 2017
Available online 29 March 2017

Keywords:

Thermochemical cycle
Chemical looping gasification
Liquid copper oxide
Syngas production
Sensitivity analysis

ABSTRACT

A new concept for syngas production is proposed in which a liquid metal oxide (here copper oxide) is implemented as an oxygen carrier for chemical looping gasification. The proposed system consists of two interconnected bubble reactors as the fuel and air reactors, through which a liquid metal oxide is circulated to be successively reduced and oxidised providing the required heat and oxygen for the gasification reaction. The proposed system offers a potential process to avoid challenges such as agglomeration and sintering that are typically associated with the solid metal oxides that have previously been proposed for chemical looping gasification. Thermochemical equilibrium models are presented that show acceptable agreement with the available data. The model is then used to estimate that the carbon conversion of feedstock is up to 84.6% for gasification and 100% for combustion with the proposed concept. In addition, the mole fraction of gaseous copper oxide in the outlet stream from the air reactor is estimated to be 10^{-11} , which implies that no further process is required to separate the evaporated copper oxide from the syngas.

© 2017 Elsevier Ltd. All rights reserved.

1. Introduction

Gasification is a well-established method for the synthesis gas (syngas) production. Syngas is a gas mixture comprises primarily hydrogen, carbon monoxide, and small amount of carbon dioxide and other gaseous products such as CH₄ and N₂, which are produced through the endothermic reaction of a hydrocarbon fuel with a gasifying agent such as steam, and/or CO₂ or air [1]. The state-of-the-art syngas production processes mainly rely on the partial oxidation of the fuel with oxygen from air to provide the heat for the endothermic syngas production reactions [2,3]. However, when air is used as the oxidant, the presence of nitrogen dilutes the syngas, thereby reducing the quality of the syngas product [4]. While nitrogen dilution is acceptable for some processes,

such as power generation plants, it adds significantly to the cost of the downstream processing plant in liquid fuel synthesis plants. Gasification with industrially pure oxygen is one well-established path to avoid the nitrogen dilution [5]. Nevertheless, the requirement for oxygen adds significantly to the cost and energy demand of the plant [6]. Therefore, it is desirable to develop new processes to generate high quality syngas without the need for pure oxygen.

Chemical Looping Gasification (CLG) is a recently developed process with a potential to avoid the dilution of the syngas with N₂ by producing the oxygen from reduction-oxidation (Red-Ox) reactions [7–9]. In CLG, an oxygen carrier (OC), typically a metal oxide in the form of solid particles is employed to partially oxidise the fuel in one reactor, referred to as the fuel reactor, thus avoiding the direct contact between the fuel and nitrogen from the air. The reduced OC particles are then oxidised in another reactor, referred to as the air reactor. The system typically is configured to supply the heat required in the fuel reactor from that released in the air

* Corresponding author.

E-mail address: mohammadmohsen.sarafraz@adelaide.edu.au (M.M. Sarafraz).

Nomenclature

A	constant
C_p	specific molar heat capacity, $\text{kJ kmol}^{-1} \text{ }^\circ\text{C}$
G	Gibbs free energy, kJ
i	component
j	component
L	lagrange multiplier
n	mole fraction
N	number of all component
P	pressure, bar
R	gas constant, $\text{J }^\circ\text{C}^{-1} \text{ mol}^{-1}$
T	temperature, $^\circ\text{C}$
x_o	mole fraction of oxygen in liquid copper oxide

Greek letters

α	constant, see Eq. (1)
β	constant, see Eq. (1)
ζ	constant, see Eq. (1)
α	activity coefficient

ϕ	liquid oxygen carrier to fuel ratio
ψ	steam to fuel ratio
γ	carbon conversion
η	thermal balance ratio
μ	chemical potential
λ_o	air to liquid oxygen carrier ratio

Acronyms

CLC	Chemical Looping Combustion
CLG	Chemical Looping Gasification
CLR	Chemical Looping Reforming
LHV	lower heating value, kJ kmol^{-1}
LOC	Liquid Oxygen Carrier
Gasif.	gasification
LCLC	Liquid Chemical Looping Combustion
LCLG	Liquid Chemical Looping Gasification
Sens.	sensible heat, kJ

reactor. Loop seals are usually employed between the two reactors to mitigate gas leakage between them during the cycling of the OC particles [10]. Notwithstanding the advantages of the solid OC particles, they also introduce some challenges to the system. These include not only agglomeration and sintering [2,11–19], but also the need to separate the OC particles from any carry-over particles from the gasifier and also that to manage the deposition of carbon and ash onto the OC particles, which tends to block their pores [20]. These challenges significantly reduce the effectiveness of the OC particles in transporting oxygen between the reactors [19,21–25], which decreases the efficiency of the process [2]. For example, the gasification of biomass using CLG reported by Acharya et al. [22] only achieved 40% regeneration of the CaO solid particles at a calcination temperature of 800°. A low regeneration efficiency of 50% was also reported by Li et al. [26] with similar values reported elsewhere [2,21,27–30]. Hence, although investigations are in progress to seek suitable techniques to mitigate these disadvantages [2,11–19], it is desirable to identify alternative chemical looping gasification concepts that potentially can bypass them altogether.

The use of a liquid metal oxide as the oxygen carrier for CLG is a potential approach to address the technical challenges associated with the use of solid OC particles. Although it may bring some new challenges. Application of molten metals is a well-known process used for gasifying a carbonaceous feedstock in a heat recovery unit from metal-containing slag at high temperature conditions [31,32]. Molten slag is a mixture of metal oxides and organic materials such as SiO_2 , Al_2O_3 , CaO, FeO and MgO and is a by-product of ironmaking process in a blast furnace [33]. Molten slag leaves a blast furnace at a temperature of up to 1650 $^\circ\text{C}$, hence, its sensible heat can be employed to drive a downstream gasification reaction. In this process, the carbonaceous fuel is partially (or totally) oxidised, typically in the presence of a gasifying agent such as steam and/or CO_2 , by injecting it into a high temperature molten slag. Nevertheless, while it is well known that slags have potential to act as a gasifying medium, no systematic investigation of pure liquid metal oxides and their thermodynamic potential for chemical looping gasification is available.

The process of gasification of carbonaceous feedstock such as coal in molten slag with either steam and/or CO_2 as the gasifying agent has been found to offer some significant advantages and disadvantages over conventional processes. In particular, it offers high rates of heat and mass transfer, which results in good controllabil-

ity in operation and syngas quality. Hence, the ratio of the H_2/CO can be readily adjusted through the ratio of $\text{CO}_2/\text{feedstock}$ or $\text{H}_2\text{O}/\text{feedstock}$, which leads to the high carbon conversion rates and high quality of the syngas product [34–40]. Nevertheless, the use of slags for gasification has been found to suffer from the disadvantage of a low thermal conductivity (1 W/m K for slag versus 120 W/m K for molten copper oxide [41], respectively) due to the presence of minerals. In addition, slag tends to form layers of fused materials of different compositions (e.g. silica layer, minerals and non-metallic compounds,) with relatively low thermal conductivity, which deteriorate the thermal performance of the process [31,32]. However, little attention has been paid to the use of molten metal oxides, which have the potential to retain the good heat transfer characteristics. One aim of the present investigation is therefore to explore this gap.

It has also been shown that molten metals can enhance the rate of reaction because they induce a catalytic effect to the gasification reactions [42–44]. This suggests that it may be possible to achieve relatively low-temperature gasification process if the right type of metal can be identified, which would offer the potential for a low cost process. However, to date no systematic investigation of the potential of different metal/metal oxides has been undertaken to seek to identify metals that could exploit this potential. The present investigation therefore aims to meet this need.

The potential to harness the properties of molten metal oxides as an oxygen carrier in a chemical looping process was recently proposed by Jafarian et al. [10], to reform natural gas using iron/iron oxide. Their proposed system comprises two inter-connected bubbling column reactors to circulate the liquid between the air and fuel reactors. Their thermodynamic analysis shows that the conversion of the natural gas to CO_2 and H_2O depends strongly on the flow rate of circulating liquid oxygen carrier (LOC) between the air and fuel reactors. That is, a higher circulation flow rate of LOC between the reactors than stoichiometric value is required for the complete conversion of the fuel to H_2O and CO_2 , while a lower circulation flow rate than stoichiometric value results in carbon monoxide production. However, no similar assessment of the potential of other metals or fuels has yet been performed.

In the light of above discussion, the primary objective of the present work is to investigate the thermodynamic feasibility of the concept of Liquid Chemical Looping Gasification (LCLG) for the partial oxidation of the fuel to produce syngas. We further aim to assess the influence of different operating parameters on

the quality and quantity of syngas production. Finally, we also aim to assess the potential to implement the chemical path, although the detailed assessment of the technical feasibility of this system is well beyond the scope of the present investigation.

2. Thermodynamics of liquid copper oxide in the LCLG

2.1. Phase diagram

Fig. 1 represents the phase diagram of copper and oxygen as a function of temperature and partial pressure of the dissolved oxygen. In the region above the line A-B-C-D-E, a homogenous liquid slag is formed with a variable mole fraction of oxygen, spanning the range from ~0.01 (at point A) to ~0.5 (at point D). Below this line, the slag comprises both the solid and liquid phases with known composition of copper and oxygen in a two-phase mixture. This regime is inappropriate for the LCLG system because of the technical challenges of operating the reactors in a two-phase regime. In addition, the complex heat and mass transfer between the phases is difficult to predict. In contrast, the region above the line A-B-C-D-E is technically and thermodynamically preferred for the LCLG process. Therefore, LCLG regime is assessed in this region.

2.2. Assumptions

The simulation and model used here rely on the following assumptions:

1. The reactions are at an equilibrium.
2. Heat losses from the fuel and air reactors are neglected.
3. A system is available to transfer the LOC between air and fuel reactors fluid-mechanically) with negligible energy requirement.
4. No solidification occurs in the system and conditions are sufficiently far from any solid-liquid two-phase regions.
5. Any impurities in the fuel have a negligible influence on the reactions and only carbon reacts in the gasifier.
6. An ash separator is available to completely separate the ash from the LOC.
7. The residence time is sufficient for the reactions to reach completion so that no carbon enters the air reactor.
8. Heat loss is negligible from all pipes, tanks and units.
9. The total exergy of the fuel is equivalent to that of syngas product and that carried by the vitiated air.

2.3. HSC and R-Gibbs aspen plus models

Graphite was selected as a surrogate for the carbonaceous fuel here. This is because carbon is the primary component of coal and biomass, while being simpler to analyse. As can be seen from the phase diagram (shown in Fig. 1), the $\text{Cu}_2\text{O}(\text{l})$, above the line A-b-C-D-E, comprises a mixture of $\text{Cu}(\text{l})$, $\text{Cu}_2\text{O}(\text{l})$ and/or $\text{CuO}(\text{l})$, depending on the mole fraction of oxygen in the system. Therefore, these components are selected for the liquid phase reactions. The reducing agents considered are C, H_2 , CO and CH_4 . The three gaseous species can be produced through reactions such as methane reforming, the Boudouard reaction and the water-gas shift reaction. Furthermore, CO can also be produced through incomplete oxidation of C with molten copper oxide, while H_2 can be also produced through reduction of water by the molten copper oxide. The selection of these components was then cross-checked using HSC Chemistry software at the relevant conditions. This revealed that the concentration of other hydrocarbons is of the order of 10^{-6} , which justifies neglecting them.

In the absence of kinetic data of the gasification with copper oxide, thermodynamic assessments have been undertaken to identify plausible chemical pathways. It is assumed that the molten phase of copper oxide (shown as $\text{CuO}(\delta)$) comprises the components of $\text{CuO}(\text{l})$, $\text{Cu}_2\text{O}(\text{l})$ and pure $\text{Cu}(\text{l})$, which react with the graphite in accordance with Eqs. (1) and (2). In the next step, molten copper is assumed to react with the carbon monoxide product in

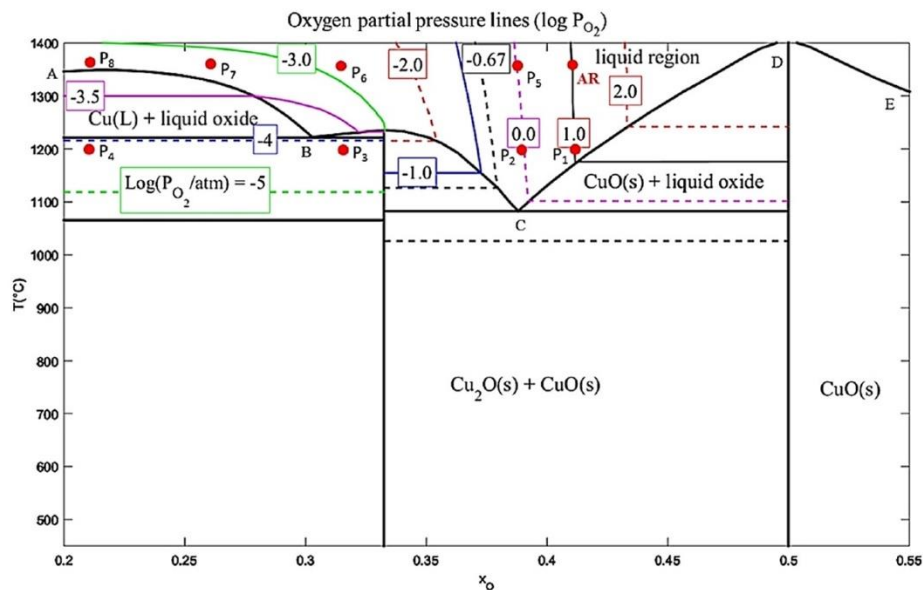
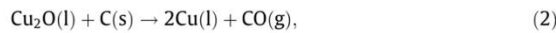
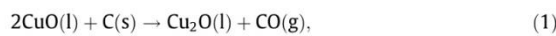


Fig. 1. Phase diagram for Cu-O system, adapted from elsewhere [45,46]. The homogenous molten metal oxide above line A-B-C-D-E is considered the most suitable region for the gasification process. AR is a typical condition for the air reactor. While P_5 to P_8 are possible conditions for the fuel reactor.

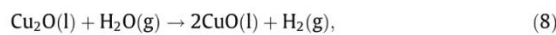
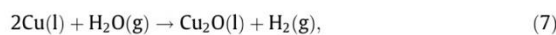
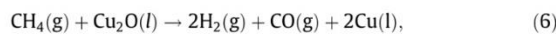
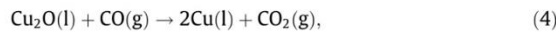
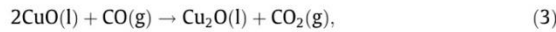
accordance with Eqs. (3) and (4). The reaction of graphite with steam forms methane (Eq. (10)), which reacts with the molten copper according to Eqs. (5) and (6). Importantly, the Gibbs free energy for the reaction between CuO and steam is positive so that it will not proceed (Eqs. (7) and (8)). Instead, the Boudouard reaction, water-gas and water-gas shift reactions, shown in from Eqs. (10)–(12), occur simultaneously with the other reactions in the fuel reactor. Likewise, Eqs. (13) and (14) occur in the air reactor, where molten copper reacts with the oxygen in the air to complete the Red-Ox thermochemical cycle. That is four groups of reactions occur in the different stages of the process.

2.3.1. Reduction reactor

- Reactions between liquid and solid phases [47]



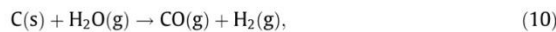
- Reactions between liquid and gas phases [48,49]



- Reactions between solid and gas phases
Methane formation [50,51]



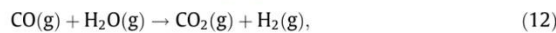
Primary water gas reaction [52]



Boudouard reaction [53,54]



- Reactions within gas phase
Water-gas shift reaction [55]



Oxidation reactor

- Reactions between liquid and gas phases



To assess the aforementioned reactions, thermochemical equilibrium analysis and Gibbs minimization methods are applied using HSC chemistry software. The model was solved for 1 kmol for each of the reactants graphite and steam under the reference condition described in Table 1. A sensitivity analysis was then performed for different operating temperatures and pressures and the ratio of the flow rates of LOC and steam to fuel, which are defined in Section 4.

3. Concept of liquid chemical looping gasification (LCLG)

Fig. 2 presents a schematic diagram of the Liquid Chemical Looping Gasification (LCLG) process assessed here. A plausible configuration with which to implement the process comprises two interconnected bubble reactors proposed by Jafarian et al. [10]. The fuel reactor is proposed to reduce the LOC and produce syngas, while the air reactor is proposed to oxidise the LOC and produce high temperature vitiated air. The bubbling medium is chosen because such systems are known to generate high rates of heat and mass transfer and can also generate circulation via the density difference between two reactors [56–62].

A disk separator utilising the density difference between the ash and slag [63,64] has been identified as a plausible means for this process [10]. However, further work is required to evaluate the technical and economic feasibility of this or other devices.

4. Methodology

The enthalpy of reaction as a function of temperature was estimated using HSC chemistry software based on the phase diagram of the copper-oxygen binary system and the results were compared with data from the literature [45,46]. Thermochemical equilibrium analysis was used to simulate the gasification process. Two additional equations were used to relate the fraction of oxygen in the liquid copper oxide (x_o) to the composition of liquid copper oxide [47] as follows:

$$n_{\text{CuO}} = \frac{3x_o - 1}{1 - x_o}, \quad (15)$$

And

$$n_{\text{Cu}_2\text{O}} = \frac{1 - 2x_o}{1 - x_o}, \quad (16)$$

The fraction of exergy of the syngas product to that of the inlet fuel $\chi_{\text{Ex,syngas-fuel}}$ is defined as follows:

$$\chi_{\text{Ex,syngas-fuel}} = \frac{\sum_{i=1}^n n_{\text{syngas}} \cdot \text{LHV}_{\text{syngas}}}{n_{\text{graphite}} \cdot \text{LHV}_{\text{graphite}}} \Bigg|_{\text{products}}, \quad (17)$$

Eq. (17) was used to compare the fraction of exergy in the syngas product with that of the original fuel, where n_i is the mole fraction of the products and LHV is the Lower Heating Value of the syngas and fuel. The ratio of the flow rates of LOC and steam to fuel were defined to investigate their influence on the gasification performance [23] as follows:

$$\phi = \frac{\dot{n}_{\text{LOC}}}{\dot{n}_{\text{fuel}}}, \quad (18)$$

$$\psi = \frac{\dot{n}_{\text{steam}}}{\dot{n}_{\text{fuel}}}. \quad (19)$$

Table 1 presents the main operating conditions considered with the model.

A sensitivity analysis was employed to assess the influence of ϕ and ψ on the quality and quantity of the syngas relative to a reference point defined in Table 1. The influence of ϕ and ψ on the fuel conversion is also assessed using Eq. (20) [23,65] as follows:

$$\chi_c = \frac{n_{\text{Fuel,init}} - n_{\text{Fuel,cons}}}{n_{\text{Fuel,init}}}. \quad (20)$$

The flow rate of air, \dot{n}_{air} relative to that of the LOC within the oxidation reactor was also defined as follows:

Table 1
Reference operating conditions for the reduction and oxidation reactors.

Unit	Air (kmol)	Fuel (kmol)	Steam (kmol)	LOC (mole)			T (°C)	P (bar)
				Cu (l)	CuO (l)	Cu ₂ O (l)		
Air reactor	1	–	–	–	0.508	0.245	1300	10
Fuel reactor	–	1	1	0.05	–	0.21	1300	10

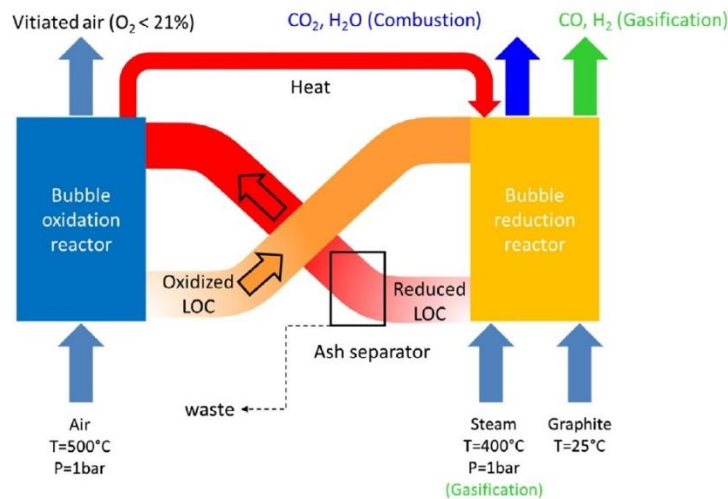


Fig. 2. A schematic diagram of the proposed LCLG configuration.

$$\lambda_0 = \frac{\dot{n}_{air}}{\dot{n}_{LOC}} \quad (21)$$

This parameter characterises the performance of the oxidation reactor and also determines the rate of regeneration of the LOC in the air reactor.

5. Verification of the results

To partially validate the model, the results obtained for the gas production and syngas quality were compared with previous studies on gasification with molten slag reported by Yu et al. [66]. To the best of our knowledge, neither theoretical nor experimental

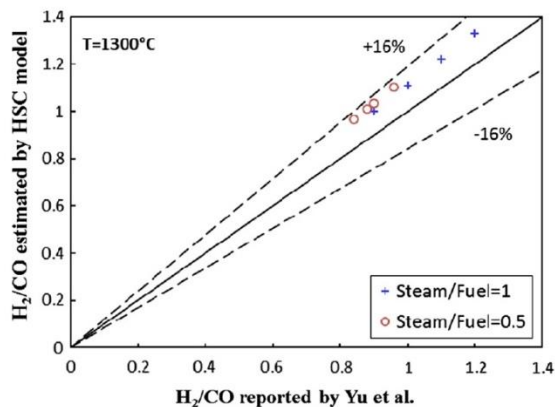


Fig. 3. Comparison between H₂/CO obtained by the HSC model and those of reported in the literature [49].

investigations of gasification using molten metal have been reported previously. Fig. 3 presents the syngas quality (H₂/CO) estimated with the HSC model in comparison with Yu et al. [66] for two different steam to fuel ratios at 1200 °C. As can be seen, the results calculated for syngas quality agree with those of calculated by Yu et al. [66] to within an absolute average deviation of ±16%. This is deemed to be sufficiently reliable for the present assessment of thermodynamic feasibility of the system.

6. Results and discussion

6.1. Gibbs free energy of the reactions

Fig. 4 presents the calculated values of the Gibbs free energy for the reduction reactions as a function of temperature, as simulated with HSC chemistry, referred to as an Ellingham diagram. This

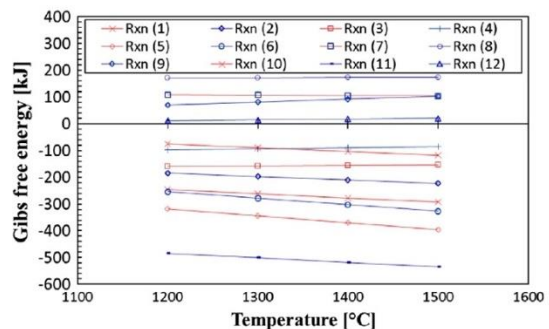


Fig. 4. Dependence of Gibbs free energy for the reduction reactions of liquid copper oxide on temperature.

shows that the value of the Gibbs free energy is negative for all reactions in the gasifier at temperatures ranging from 1200 °C to 1500 °C, implying that the reactions in liquid-gas phases, specifically between CuO (l) and Cu₂O(l) with the fuel, gasifying agent and other compounds are spontaneous.

Fig. 5 presents the calculated values of the Gibbs free energy for the oxidation reactions as a function of temperature. As can be seen, the values of the Gibbs free energy for the oxidation reactions are also negative so that the reactions are also spontaneous. Furthermore, the calculated Gibbs free energy decreases linearly with an increase in the operating temperature of the reactor.

Fig. 6 presents the calculated dependence of the enthalpy of reactions on temperature for the reduction and oxidation reactions together, some of which are exothermic (e. g. the water-gas shift reaction and the catalytic copper oxide reactions with graphite), and some of which are endothermic (e. g. the main Boudouard gasification reaction). The net enthalpy of the reactions in the gasifier and oxidation reactors are endothermic and exothermic, respectively. However, the heat released in the oxidation reactor is sufficient to supply the heat that required for the fuel reactor. Thus, it is thermodynamically possible to avoid the need for any external energy sources to maintain the required heat, provided that the energy is transferred effectively and that the heat losses are sufficiently small.

6.2. Assessment of fuel reactor for the syngas production

Fig. 7 presents the dependence on ϕ of carbon dioxide production with the proposed system for two different operating temperatures of the fuel reactor, namely at 1200 °C and 1350 °C. As shown in Fig. 7, for LOC circulation ratios of less than 8, the oxygen ratio in the fuel reactor is sub-stoichiometric and the proposed system operates in the gasification regime. In this condition, partial oxidation of graphite produces mostly CO instead of CO₂. The presence of steam as the gasifying agent provides the hydrogen for the syngas product. With an increase in the circulation ratio, the stoichiometric ratio increases and the reactions proceed towards complete combustion.

Returning to Fig. 1, we consider four different operating points for each of two given temperatures (P₁-P₄ for 1200 °C and P₅-P₈ for 1350 °C). As can be seen, at 1200 °C, the fuel reactor would need to operate in the two-phase regime at low values of ϕ , which is technically challenging for bubble column reactors. However, at an operating temperature of 1350 °C, the conditions in the fuel reactor are only in the liquid phase for all values of ϕ , which is necessary to enable circulation. Nevertheless, operation at this high-temperature condition is challenging.

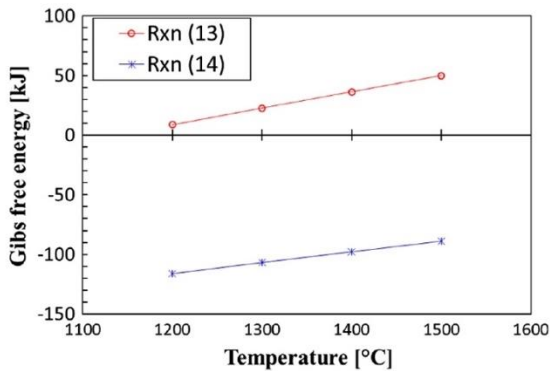


Fig. 5. Dependence of Gibbs free energy on temperature for oxidation reactions of liquid copper oxide.

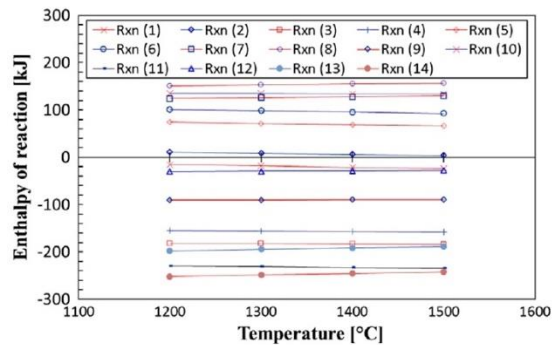


Fig. 6. Dependence of the enthalpy of reaction on temperature for different gasification reactions using liquid copper oxide.

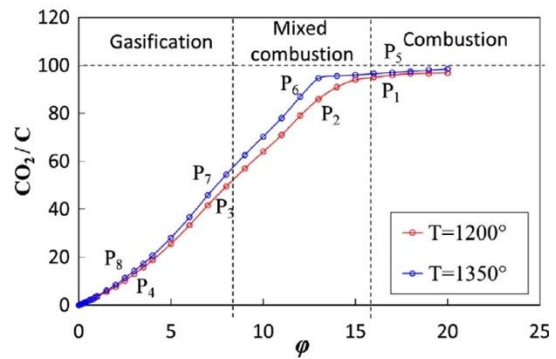


Fig. 7. Dependence on ϕ of CO₂/C for different temperatures of 1200 °C and 1350 °C.

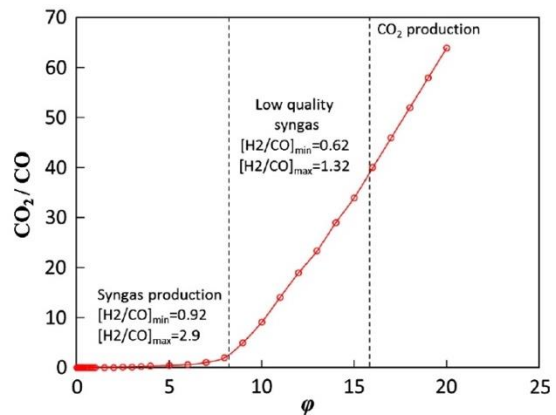


Fig. 8. Dependence on ϕ of CO₂/CO at T = 1350 °C and for $\psi = 1$.

Fig. 8 presents the dependence of CO₂/CO on ϕ . As can be seen, three distinguishable regimes can be seen, namely the gasification, mixed combustion and total combustion regimes. In the gasification regime, (0 < ϕ < 8), the quality of syngas varies from 0.92 to 2.9, while for mixed combustion it is less than 1.32. In addition, CO production from the gasification regime changes slightly with the circulation ratio. However, due to the production of CO₂ in regime 2, the value of CO₂/CO changes considerably. For example,

CO₂/CO = 4 for $\phi = 9$, while it reaches 40 for $\phi = 16$. This reveals that in regime 2, due to the carbon dioxide production, the system works partly in the gasification and partly in the combustion regimes. Therefore, the final product in the mixed combustion regime is CO, H₂ and CO₂. For the total combustion regime, the main products are heat and carbon dioxide, which can be stored and sequestered. Therefore, regime I is appropriate for producing the high-quality syngas. It is noteworthy saying that the quality of syngas can be controlled by ϕ and ψ , which is discussed in more details below.

6.3. Influence of temperature on the syngas quality for different ϕ

Fig. 9 presents the dependence of syngas quality (H₂/CO) on temperature for different values of ϕ . Here, syngas is defined based on its application for a Fischer-Tropsch, (F-T) process, for which the desirable H₂/CO ratio is greater than or equal to 2 [67]. It can be seen that the H₂/CO decreases weakly with an increase in T and strongly with an increase in ϕ . For instance, H₂/CO = 1 for $\phi = 0.01$, $\psi = 1$ and T = 1200 °C. However, for $\phi = 5$, and other conditions being the same, the syngas quality is 0.5. The decrease in H₂/CO with an increase in operating temperature is due to the increase in production of CO. An increase in temperature from 1200 °C to 1400 °C decreases the syngas quality from 0.9 to 0.86. It can also be seen that a value of H₂/CO = 2 can be achieved for sufficiently low ϕ in the range of 0.01–0.1 and for specific values of ψ .

6.4. Influence of temperature on the syngas quality for different ψ

Fig. 10 presents the predicted influence of operating temperature on the syngas quality for different values of ψ . As shown, with an increase in ψ , the syngas quality increases. For example, with an increase in ψ from 0.1 to 1, the syngas quality increases from 0.78 to 1. This is because the production of H₂ depends on the availability of steam. In contrast to H₂, production of CO₂ increases weakly with an increase in ψ , since steam promotes the water-gas shift reaction to convert more CO to CO₂. In addition, an increase in temperature was found to decrease the syngas quality slightly because an increase in temperature favours the production of CO. For $0.1 < \psi < 1$, the variation of syngas quality with temperature is insignificant and with an increase in ψ , the syngas quality increases slightly. However, for further increases in ψ beyond unity, the syngas quality increases significantly. In addition, the role of temperature on the decrease of syngas quality is stronger. Therefore, the condition of H₂/CO > 2 can be achieved for $0.01 < \phi < 0.1$ and $\psi > 1$.

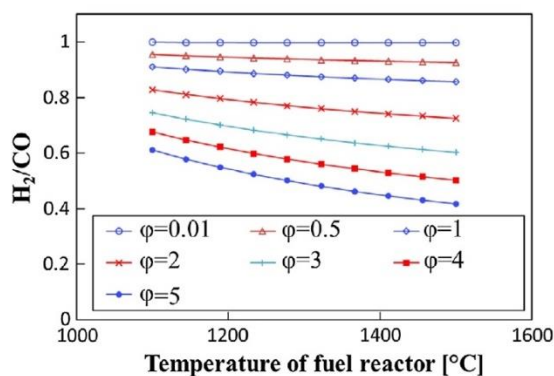


Fig. 9. The influence of temperature on the syngas quality for a range of values of ϕ .

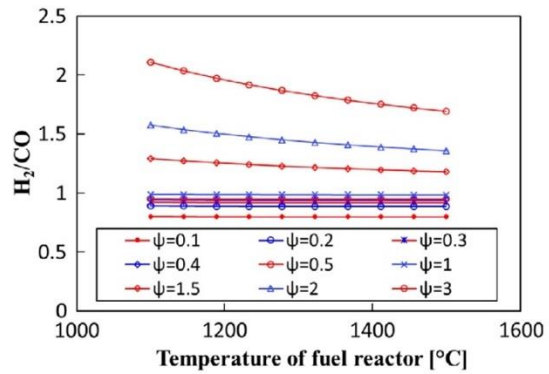


Fig. 10. Influence of temperature on the syngas quality for a range of values of ψ at $\phi = 0.06$. The stoichiometric value for ψ is 1 (blue line with “x” marker).

6.5. Influence of partial pressure of oxygen on syngas quality

The influence of partial pressure of oxygen on the syngas quality produced in the fuel reactor is presented in Fig. 11. As shown, the mole fractions of the CO and H₂ decrease with an increase in partial pressure of oxygen. Syngas quality is also increased by an increase in partial pressure of oxygen, which is due to the decrease in CO production. However, a minimum partial pressure of oxygen is required to avoid solidification of CuO and Cu₂O, that is, to avoid two-phase operation (see Fig. 1), with an anticipated system failure. Given the need for a buffer to avoid solidification, it can be seen that it is difficult to achieve a syngas quality of higher than 0.84, which is well below the target value of 2.

6.6. Oxidation reactor

Fig. 12 presents the dependence of the mole fraction of CuO and Cu₂O on λ_0 at 1350 °C. As can be seen, an increase in λ_0 results in the increase in the number of moles of CuO, while mole fraction of Cu₂O decreases. Since CuO is the target product, a high value of λ_0 is desirable. For $\lambda_0 = 5$, the mole fraction of CuO reaches 0.89. While that of Cu₂O is minimised. For $\lambda_0 \geq 8$, the mole fractions Cu₂O and CuO are constant. For these conditions, the ratio of regeneration, i.e. the value of CuO/Cu₂O = 17:3.

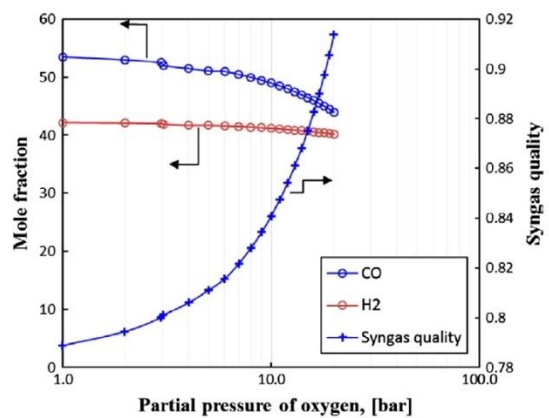


Fig. 11. Dependence of production of H₂ and CO, together with the corresponding syngas quality, on partial pressure of oxygen in the fuel reactor.

6.7. Graphite conversion

Fig. 13 presents the dependence of the calculated conversion of graphite on ϕ for three different operating temperatures. Three regimes can be seen, regime I, ($0 < \phi < 8$) corresponds to LCLG mode, regime II, ($8 < \phi < 13$) corresponds to the mode of mixed combustion and gasification, while regime III ($13 < \phi < 20$) corresponds to complete oxidation of graphite (the LCLC regime). As can be seen, carbon conversion increases with an increase in ϕ , although the rate of increase depends on the partial pressure of oxygen available in the system. For the LCLG mode, carbon conversion is as high as 0.89 (regardless of the optimization of other operating parameters), while carbon conversion is unity in the LCLC mode. These results show that the slope of change for carbon conversion becomes zero for a conversion of 1. However, for the mixed combustion/gasification regime, the slope is higher for the gasification region, meaning that graphite is fully converted in the LCLG regime. This is because the combustion is complete. In addition, an increase in temperature was found to also increase the carbon conversion process slightly.

Fig. 14 presents the calculated graphite conversion with the LCLG model in comparison with those reported in the literature for other gasification process [68–72] at the same temperature. As can be seen, the obtained results agree with previously reported data to within an absolute average difference of 6.5%. The comparison was performed at temperatures ranging from 1000 °C and 1300 °C to show that the fuel conversion for the gasification with molten metal oxides is effectively the same as those reported for other gasification processes and techniques. For example, the difference between the present and previous results are 3.1%, 5.1%, 6.5% and 2.6% for Siriwardane et al. [70], Dennis et al. [72], Li et al. [68] and Yu et al. [69], respectively.

6.8. Exergy analysis

Fig. 15 presents the dependence of fraction of exergy in the syngas product and the hot vitiated air on the circulation ratio. As can be seen, an increase in the syngas quality is associated with an increase in the exergy transported by the syngas. This means that decreasing the circulation ratio causes the system to operate in the liquid chemical looping gasification mode. Conversely, an increase in ϕ promotes a shift toward the chemical looping combustion mode and an increase in the share of the exergy that is removed by the hot gases.

Fig. 16 presents the dependence of exergy fraction of the syngas and hot gases from the air reactor on ϕ for $T = 1350$ °C. As can be

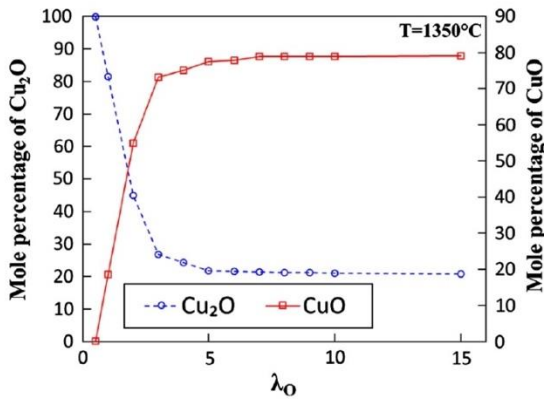


Fig. 12. Dependence on λ_0 of the number of moles of CuO and Cu_2O in the product from the oxidation reactor.

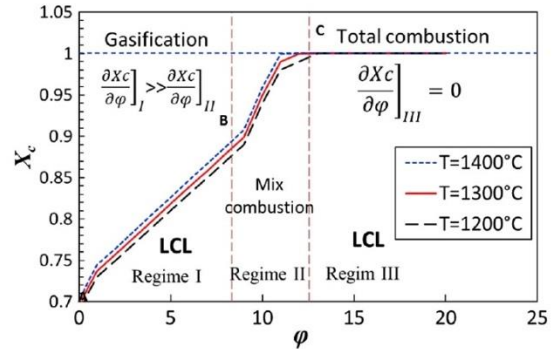


Fig. 13. Dependence of fuel conversion on ϕ for different operating temperatures of the gasifier for the regimes of liquid chemical looping gasification and combustion.

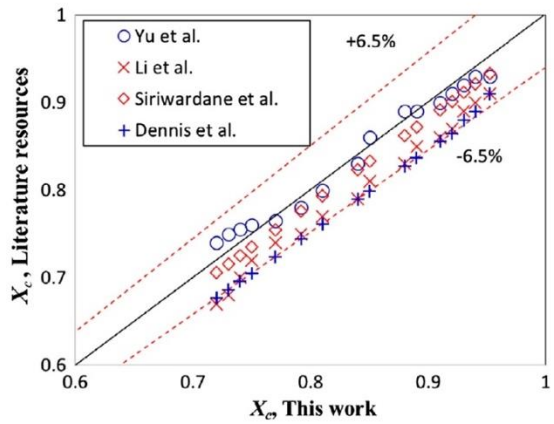


Fig. 14. A comparison between the conversion extent calculated in this study for LCLG and those of reported previously for conventional gasification at 1300 °C.

seen, for $\phi \leq 8$, about 67% of total exergy of fuel is carried by the syngas product, while the remainder is carried by the hot gases the air reactor. However, with an increase in the circulation ratio, the exergy fraction of the syngas decreases. For $\phi = 12$ the amount of exergy is distributed equally to the syngas and hot gases, while for higher values of circulation ratio, the system moves into the chemical looping combustion regime, with majority of the exergy released to the hot gases. For example, at $\phi = 15$, 60% of exergy is partitioned to the hot gas and 40% to the syngas product.

7. Potential benefits and technical challenges

It is important to distinguish between the wider potential of the LCLG concept and the limitations of the system analysed here. The system has been analysed for CuO , in part because of the better availability of thermo-chemical and thermo-chemical data for copper than for other metals. The use of this metal, nevertheless introduces challenges associated with a high operating temperature and corrosiveness. However, the concept offers the potential to bypass some of the key challenges that have plagued chemical looping gasification with solid particles provided that suitable metal/oxide combinations can be identified the possibility of identifying other metal oxides that may achieve comparable benefits at a lower temperature and reasonable pressures. It also offers the potential for hybridization with concentrated solar energy to drive the endothermic reactions.

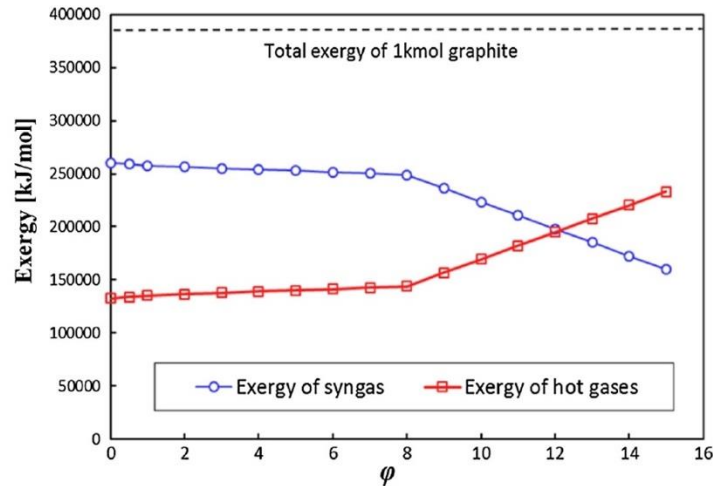


Fig. 15. Dependence on ϕ of exergy in syngas and hot gases ($\text{CO}_2 + \text{H}_2\text{O} + \text{vitiated air}$) at $T = 1350^\circ\text{C}$.

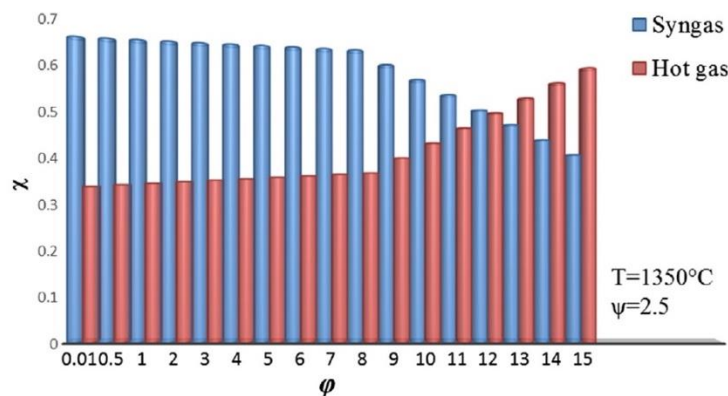


Fig. 16. Dependence on ϕ of exergy fraction of the syngas product at a temperature of 1350°C and for $\psi = 2.5$ and for syngas product and hot gases ($\text{H}_2\text{O} + \text{CO}_2 + \text{vitiated air}$).

The technical challenges associated with the use of CuO for LCLG are as follows:

- (1) A high operating temperature: To the best of our knowledge, no continuous flow reactor has been demonstrated for liquid metal oxides at high temperature and pressure. For copper, a reactor must sustain temperatures higher than 1000°C and a pressure of 10 bar.
- (2) Fluid circulation: A method is required to circulate the molten metal at high temperature. To the best of author's knowledge, no such system is commercially available.
- (3) Heat loss and solidification challenge: Although the process operates with an overall exothermal reaction, heat losses must kept low and managed carefully to avoid solidification. Furthermore, the temperature difference between operation and freezing point should be sufficiently great, which is not the case with copper.
- (4) Robust injection method: It is necessary to avoid local solidification near to the region where the gasifying agent and fuel are injected.

8. Conclusions

The analysis has demonstrated the thermodynamic potential of a new gasification system, in which a liquid metal oxide is employed as the gasification medium. This system offers significant potential benefits if the disadvantages associated with the use of the particular metal oxide chosen here (copper oxide) can be overcome, such as by identification of an alternative metal oxide with a lower operating temperature. The thermodynamic equilibrium analysis of the gasification of carbon using liquid copper oxide has revealed the following:

- Metal oxides (here copper oxide) are a suitable candidate for the gasification process in terms of heat and mass transfer, based on the Gibbs minimization method. From the Ellingham diagram, all potential gasification reactions are feasible, providing that the appropriate pressure and temperature are chosen.
- The gasification process via liquid copper oxide can be achieved isothermally with the same temperature in both reactors, although this requires them to be operated at different

pressures. Furthermore, the process is thermally balanced, meaning that the required heat for the gasification is supplied by the heat released from the oxidation of LOC in the air reactor.

- The pressure was found to have insignificant impact on the syngas production, while it is a controlling parameter of the physical state and stability of the liquid copper oxide. The ratio of LOC to fuel is another important parameter.

The LCLG proposed concept also offers potential to overcome the challenges related to the implementation of the solid oxygen carriers in CLG systems such as sintering, carbon deposition and agglomeration. However, to achieve this, technical challenges of high temperature operation, such as those identified in the discussion, need to be addressed. In addition, new experimental data are required to enable the better development and validation of models.

Acknowledgements

Authors of this work gratefully acknowledge Australian Research Council (ARC) for the financial support through grant DP150102230. The first author of this work acknowledges "Australian Government Research Training Program Scholarship" for the financial supports. Also, Centre for energy technology is gratefully acknowledged for its financial and scientific supports.

References

- [1] Wilhelm D, Simbeck D, Karp A, Dickenson R. Syngas production for gas-to-liquids applications: technologies, issues and outlook. *Fuel Process Technol* 2001;71:139–48.
- [2] Adanez J, Abad A, Garcia-Labiano F, Gayan P, Luis F. Progress in chemical-looping combustion and reforming technologies. *Prog Energy Combust Sci* 2012;38:215–82.
- [3] Martínez JD, Mahkamov K, Andrade RV, Lora EES. Syngas production in downdraft biomass gasifiers and its application using internal combustion engines. *Renewable Energy* 2012;38:1–9.
- [4] Springmann H. High pressure gasification of coal using nitrogen dilution of waste gas from steam generator. US 4019314 A (US patent).
- [5] Doctor R, Molburg J, Thimmapuram P. Oxygen-blown gasification combined cycle: carbon dioxide recovery, transport, and disposal. *Energy Convers Manage* 1997;38:5575–80.
- [6] Simeone E, Siedlecki M, Nacken M, Heidenreich S, De Jong W. High temperature gas filtration with ceramic candles and ashes characterisation during steam-oxygen blown gasification of biomass. *Fuel* 2013;108:99–111.
- [7] Wang P, Means N, Shekhawat D, Berry D, Massoudi M. Chemical-looping combustion and gasification of coals and oxygen carrier development: a brief review. *Energy* 2015;8:10605–35.
- [8] Devi L, Ptasiński KJ, Janssen FJ. A review of the primary measures for tar elimination in biomass gasification processes. *Biomass Bioenergy* 2003;24:125–40.
- [9] Kirubakaran V, Sivaramakrishnan V, Nalini R, Sekar T, Premalatha M, Subramanian P. A review on gasification of biomass. *Renew Sustain Energy Rev* 2009;13:179–86.
- [10] Jafarian M, Arjomandi M, Nathan GJ. Thermodynamic potential of high temperature chemical looping combustion with molten iron oxide as the oxygen carrier. *Chem Eng Res Des* 2017;120:69–81.
- [11] Jafarian M, Arjomandi M, Nathan GJ. A hybrid solar and chemical looping combustion system for solar thermal energy storage. *Appl Energy* 2013;103:671–8.
- [12] Jafarian M, Arjomandi M, Nathan GJ. A hybrid solar chemical looping combustion system with a high solar share. *Appl Energy* 2014;126:69–77.
- [13] Jafarian M, Arjomandi M, Nathan GJ. The energetic performance of a novel hybrid solar thermal & chemical looping combustion plant. *Appl Energy* 2014;132:74–85.
- [14] Tanner J, Bhattacharya S. Kinetics of CO₂ and steam gasification of Victorian brown coal chars. *Chem Eng J* 2016;285:331–40.
- [15] Patra TK, Sheth PN. Biomass gasification models for downdraft gasifier: a state-of-the-art review. *Renew Sustain Energy Rev* 2015;50:583–93.
- [16] Chan FL, Tanksale A. Review of recent developments in Ni-based catalysts for biomass gasification. *Renew Sustain Energy Rev* 2014;38:428–38.
- [17] Ge H, Guo W, Shen L, Song T, Xiao J. Biomass gasification using chemical looping in a 25 kW th reactor with natural hematite as oxygen carrier. *Chem Eng J* 2016;286:174–83.
- [18] Adánez J, Gayán P, Celaya J, de Diego LF, García-Labiano F, Abad A. Chemical looping combustion in a 10 kWth prototype using a CuO/Al₂O₃ oxygen carrier: Effect of operating conditions on methane combustion. *Ind Eng Chem Res* 2006;45:6075–80.
- [19] Li F, Kim HR, Sridhar D, Wang F, Zeng L, Chen J, et al. Syngas chemical looping gasification process: oxygen carrier particle selection and performance. *Energy Fuels* 2009;23:4182–9.
- [20] Liao C, Wu C, Yan Y. The characteristics of inorganic elements in ashes from a 1 MW CFB biomass gasification power generation plant. *Fuel Process Technol* 2007;88:149–56.
- [21] Fan L, Li F, Ramkumar S. Utilization of chemical looping strategy in coal gasification processes. *Particuology* 2008;6:131–42.
- [22] Acharya B, Dutta A, Basu P. Chemical-looping gasification of biomass for hydrogen-enriched gas production with in-process carbon dioxide capture. *Energy Fuels* 2009;23:5077–83.
- [23] Anheden M, Svedberg G. Exergy analysis of chemical-looping combustion systems. *Energy Convers Manage* 1998;39:1967–80.
- [24] Zevenhoven-Onderwater M, Backman R, Skrifvars B-J, Hupa M. The ash chemistry in fluidised bed gasification of biomass fuels. Part I: Predicting the chemistry of melting ashes and ash-bed material interaction. *Fuel* 2001;80:1489–502.
- [25] Florin N. Calcium looping technologies for gasification and reforming. *Calc. Chem. Loop. Technol. Power Gener. Carbon Dioxide (CO₂) Capture* 2015:139–52.
- [26] Li F, Zeng L, Velazquez-Vargas LG, Yoscovits Z, Fan LS. Syngas chemical looping gasification process: bench-scale studies and reactor simulations. *AIChE J* 2010;56:2186–99.
- [27] Fan L-S. *Chemical looping systems for fossil energy conversions*. John Wiley & Sons; 2011.
- [28] Zafar Q, Mattisson T, Gevert B. Integrated hydrogen and power production with CO₂ capture using chemical-looping reforming redox reactivity of particles of CuO, Mn₂O₃, NiO, and Fe₂O₃ using SiO₂ as a support. *Ind Eng Chem Res* 2005;44:3485–96.
- [29] Tong A, Bayham S, Kathe MV, Zeng L, Luo S, Fan L-S. Iron-based syngas chemical looping process and coal-direct chemical looping process development at Ohio State University. *Appl Energy* 2014;113:1836–45.
- [30] Anthony EJ. Solid looping cycles: a new technology for coal conversion. *Ind Eng Chem Res* 2008;47:1747–54.
- [31] Chen W-H, Lin M-R, Leu T-S, Du S-W. An evaluation of hydrogen production from the perspective of using blast furnace gas and coke oven gas as feedstocks. *Int J Hydrogen Energy* 2011;36:11727–37.
- [32] Suopajarvi H, Pongrácz E, Fabritius T. The potential of using biomass-based reducing agents in the blast furnace: a review of thermochemical conversion technologies and assessments related to sustainability. *Renew Sustain Energy Rev* 2013;25:511–28.
- [33] Bagfi MS, Ito Y, Yamada S, Sano M. Effect of slag composition on the kinetics of the reduction of iron oxide in molten slag by graphite. *ISIJ Int* 1992;32:1280–6.
- [34] Zhao Y, Sun S, Tian H, Qian J, Su F, Ling F. Characteristics of rice husk gasification in an entrained flow reactor. *Biores Technol* 2009;100:6040–4.
- [35] Zhou J, Chen Q, Zhao H, Cao X, Mei Q, Luo Z, et al. Biomass-oxygen gasification in a high-temperature entrained-flow gasifier. *Biotechnol Adv* 2009;27:606–11.
- [36] Ponzio A. Thermally homogenous gasification of biomass/coal/waste for medium or high calorific value syngas production: KTH; 2008.
- [37] Liu J, Yu Q, Peng J, Hu X, Duan W. Thermal energy recovery from high-temperature blast furnace slag particles. *Int Commun Heat Mass Transfer* 2015;69:23–8.
- [38] Barati M, Esfahani S, Utigard T. Energy recovery from high temperature slags. *Energy* 2011;36:5440–9.
- [39] Duan W, Yu Q, Xie H, Qin Q, Zuo Z. Thermodynamic analysis of hydrogen-rich gas generation from coal/steam gasification using blast furnace slag as heat carrier. *Int J Hydrogen Energy* 2014;39:11611–9.
- [40] Duan W, Yu Q, Xie H, Liu J, Wang K, Qin Q, et al. Thermodynamic analysis of synergistic coal gasification using blast furnace slag as heat carrier. *Int J Hydrogen Energy* 2016;41:1502–12.
- [41] Rezaei H, Gupta R, Bryant G, Hart J, Liu G, Bailey C, et al. Thermal conductivity of coal ash and slags and models used. *Fuel* 2000;79:1697–710.
- [42] Sinfelt JH, Carter J, Yates D. Catalytic hydrogenolysis and dehydrogenation over copper-nickel alloys. *J Catal* 1972;24:283–96.
- [43] Rudloff WK, Freeman ES. Catalytic effect of metal oxides on thermal decomposition reactions. II. Catalytic effect of metal oxides on the thermal decomposition of potassium chlorate and potassium perchlorate as detected by thermal analysis methods. *J Phys Chem* 1970;74:3317–24.
- [44] Harlé V, Vrinat M, Scharff J, Durand B, Deloume J. Catalysis assisted characterizations of nanosized TiO₂-Al₂O₃ mixtures obtained in molten alkali metal nitrates: effect of the metal precursor. *Appl Catal A* 2000;196:261–9.
- [45] Barin I. *Thermochemical data of pure substances*. Wiley-VCH; 1997. *Thermochemical Data of Pure Substances*.
- [46] Shishin D, Deckerov SA. Critical assessment and thermodynamic modeling of the Cu–O and Cu–O–S systems. *Calphad* 2012;38:59–70.
- [47] Kosenko A, Emel'chenko G. Equilibrium phase relationships in the system Cu–O under high oxygen pressure. *J Phase Equil* 2001;22:12–9.
- [48] McKee D. The copper-catalyzed oxidation of graphite. *Carbon* 1970;8:131IN3137–6IN8139.
- [49] Jernigan G, Somorjai G. Carbon monoxide oxidation over three different oxidation states of copper: metallic copper, copper (I) oxide, and copper (II) oxide—a surface science and kinetic study. *J Catal* 1994;147:567–77.

- [50] Forghani A, Jafarian M, Pendleton P, Lewis D. Mathematical modelling of a hydrocracking reactor for triglyceride conversion to biofuel: model establishment and validation. *Int J Energy Res* 2014;38:1624–34.
- [51] Ding Y, Alpay E. Adsorption-enhanced steam–methane reforming. *Chem Eng Sci* 2000;55:3929–40.
- [52] Grenoble D, Estadt M, Ollis D. The chemistry and catalysis of the water gas shift reaction: 1. The kinetics over supported metal catalysts. *J Catal* 1981;67:90–102.
- [53] Jafarian S, Haseli P, Karimi G. Performance analysis of a solid oxide fuel cell with reformed natural gas fuel. *Int J Energy Res* 2010;34:946–61.
- [54] Calo J, Perkins M. A heterogeneous surface model for the “steady-state” kinetics of the Boudouard reaction. *Carbon* 1987;25:395–407.
- [55] Newsome DS. The water–gas shift reaction. *Catal Rev Sci Eng* 1980;21:275–318.
- [56] Sarafraz M, Hormozi F. Scale formation and subcooled flow boiling heat transfer of CuO–water nanofluid inside the vertical annulus. *Exp Thermal Fluid Sci* 2014;52:205–14.
- [57] Sarafraz M, Hormozi F. Convective boiling and particulate fouling of stabilized CuO–ethylene glycol nanofluids inside the annular heat exchanger. *Int Commun Heat Mass Transfer* 2014;53:116–23.
- [58] Sarafraz M, Hormozi F. Nucleate pool boiling heat transfer characteristics of dilute Al₂O₃–ethyleneglycol nanofluids. *Int Commun Heat Mass Transfer* 2014;58:96–104.
- [59] Sarafraz M, Kiani T, Hormozi F. Critical heat flux and pool boiling heat transfer analysis of synthesized zirconia aqueous nano-fluids. *Int Commun Heat Mass Transfer* 2016;70:75–83.
- [60] Sarafraz MM. Nucleate pool boiling of aqueous solution of citric acid on a smoothed horizontal cylinder. *Heat Mass Transf* 2012;48:611–9.
- [61] Sarafraz M, Hormozi F, Peyghambarzadeh S. Pool boiling heat transfer to aqueous alumina nano-fluids on the plain and concentric circular micro-structured (CCM) surfaces. *Exp Thermal Fluid Sci* 2016;72:125–39.
- [62] Sarafraz M, Hormozi F, Silakhori M, Peyghambarzadeh S. On the fouling formation of functionalized and non-functionalized carbon nanotube nano-fluids under pool boiling condition. *Appl Therm Eng* 2016;95:433–44.
- [63] Coats HM. Ash-separator. *Google Patents*; 1907.
- [64] John Y. Multiple element vortical whirl ash separator. *Google Patents*; 1952.
- [65] Wen C-Y, Lee ES. Coal conversion technology. *NASA STI/Recon Technical Report A* 1979;79:53776.
- [66] Duan W, Yu Q, Xie H, Liu J, Wang K, Qin Q, et al. Thermodynamic analysis of synergistic coal gasification using blast furnace slag as heat carrier. *Int J Hydrogen Energy* 2016;41:1502–12.
- [67] Yun Y, Chung SW, Yoo YD. Syngas quality in gasification of high moisture municipal solid wastes. *Prepr Pap-Am Chem Soc, Div Fuel Chem* 2003;48:823.
- [68] Li P, Lei W, Wu B, Yu Q. CO₂ gasification rate analysis of coal in molten blast furnace slag—for heat recovery from molten slag by using a chemical reaction. *Int J Hydrogen Energy* 2015;40:1607–15.
- [69] Duan W, Yu Q, Liu J, Hou L, Xie H, Wang K, et al. Characterizations of the hot blast furnace slag on coal gasification reaction. *Appl Therm Eng* 2016;98:936–43.
- [70] Siriwardane R, Riley J, Tian H, Richards G. Chemical looping coal gasification with calcium ferrite and barium ferrite via solid–solid reactions. *Appl Energy* 2016;165:952–66.
- [71] Boyd RM, Fischer DD, Humphrey AE, King SB, Whitman DL. Method for in situ coal gasification operations. *Google Patents*; 1981.
- [72] Dennis JS, Scott SA. In situ gasification of a lignite coal and CO₂ separation using chemical looping with a Cu-based oxygen carrier. *Fuel* 2010;89:1623–40.

Chapter 4 Performance assessment of various oxygen carriers for chemical looping gasification process

4.1. Chapter overview

In this chapter, an investigation is conducted on the chemical and energetic performance of a chemical looping gasification process. According to the results discussed in the previous chapter, liquid chemical looping gasification can have different operating modes including gasification, mixed gasification with combustion and combustion. The operating mode is highly dependent on the type of the oxygen carrier. For example, for some oxygen carriers due to the high oxygen content, system operates as the chemical looping combustion, while for some oxygen carriers such as antimony oxide, the process is more efficient to operate as chemical looping gasification. Hence, a thermodynamic assessment was conducted on the chemical looping process to compare the performance of the process working with various metal oxides. Results presented in this chapter can contribute to the second objective of the thesis aiming to identify suitable oxygen carrier for the LCLG process.

To achieve this, a pre-screening analysis was performed on 41 various metal oxides based on the melting temperature, content of oxygen and the Gibbs free energy of their reduction and oxidation reactions. To calculate the Gibbs free energy, the Gibbs minimisation method was employed and the reactions in the gasification and combustion regimes were identified. By assessing the Gibbs free energy of reaction, some metal oxides were eliminated since their Gibbs free energy was positive and their reduction-oxidation reactions were unlikely to happen spontaneously.

For the rest of metal oxides, enthalpy of reaction, the molar ratio of H_2 : CO and CO_2/CO at different temperatures were analysed and the operating regimes for the gasification and combustion processes were identified. Methane formation was also investigated which directly influences the quality of syngas.

Considering the above selection procedure, metal oxides including copper, lead, antimony and bismuth were introduced, which are thermodynamically plausible for the LCLG process as the suitable oxygen carrier. This chapter was published in International Journal of Hydrogen Energy (M. Sarafraz, M. Jafarian, M. Arjomandi, & G. J. Nathan, 2017).

Statement of Authorship

Title of Paper	The relative performance of alternative oxygen carriers for liquid chemical looping combustion and gasification
Publication Status	<input checked="" type="checkbox"/> Published <input type="checkbox"/> Accepted for Publication <input type="checkbox"/> Submitted for Publication <input type="checkbox"/> Unpublished and Unsubmitted work written in manuscript style
Publication Details	M.M. Sarafraz, Mehdi Jafarian, Maziar Arjomandi, Graham J. Nathan, The relative performance of alternative oxygen carriers for liquid chemical looping combustion and gasification, International Journal of Hydrogen Energy, Volume 42, Issue 26, 29 June 2017, Pages 16396-16407.

Principal Author

Name of Principal Author (Candidate)	Mohammad Mohsen Sarafraz
Contribution to the Paper	<ul style="list-style-type: none"> - Research, collecting and analyzing data from different resources, developing thermodynamic models and analyzing the obtained data. - Providing the data, writing of the manuscript and production of original figures. - Correspondence with editor and reviewers including the production of all cover letters and rejoinder
Overall percentage (%)	80%
Certification:	This paper reports on original research I conducted during the period of my Higher Degree by Research candidature and is not subject to any obligations or contractual agreements with a third party that would constrain its inclusion in this thesis. I am the primary author of this paper.
Signature	Date 29/11/18

Co-Author Contributions

By signing the Statement of Authorship, each author certifies that:

- iv. the candidate's stated contribution to the publication is accurate (as detailed above);
- v. permission is granted for the candidate to include the publication in the thesis; and
- vi. the sum of all co-author contributions is equal to 100% less the candidate's stated contribution.

Name of Co-Author	Mehdi Jafarian
Contribution to the Paper	<ul style="list-style-type: none"> - Supervision of the work, including the production of the manuscript - Participation in the development of the concepts and ideas presented in the manuscript - Evaluation and editing of the manuscript prior to submission
Signature	Date 29/11/18

Name of Co-Author	Maziar Arjomandi
Contribution to the Paper	<ul style="list-style-type: none"> - Supervision of the work, including the production of the manuscript - Participation in the development of the concepts and ideas presented in the manuscript - Evaluation and editing of the manuscript prior to submission
Signature	Date 29/11/18

Name of Co-Author	Graham Nathan		
Contribution to the Paper	<ul style="list-style-type: none">- Supervision of the work, including the production of the manuscript- Participation in the development of the concepts and ideas presented in the manuscript- Evaluation and editing of the manuscript prior to submission		
Signature		Date	29/11/18

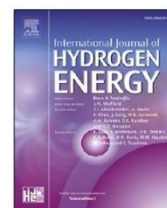


ELSEVIER

Available online at www.sciencedirect.com

ScienceDirect

journal homepage: www.elsevier.com/locate/he



The relative performance of alternative oxygen carriers for liquid chemical looping combustion and gasification



M.M. Sarafraz*, Mehdi Jafarian, Maziar Arjomandi, Graham J. Nathan

Centre for Energy Technology, School of Mechanical Engineering, The University of Adelaide, SA, 5005, Australia

ARTICLE INFO

Article history:

Received 3 March 2017

Received in revised form

1 May 2017

Accepted 15 May 2017

Available online 7 June 2017

Keywords:

Chemical looping combustion
Chemical looping gasification
Energetic analysis
Thermodynamic equilibrium analysis
Syngas production

ABSTRACT

The relative performance of different potential liquid oxygen carriers within a novel system that can be configured for either chemical looping gasification or combustion is assessed. The parameters considered here are the melting temperature, the Gibbs free energy, reaction enthalpy, exergy and energy flows, syngas quality and temperature difference between the two reactors. Results show that lead, copper and antimony oxides are meritorious candidates for the proposed systems. Antimony oxide was found to offer strong potential for high quality syngas production because it has a reasonable oxygen mass ratio for gasification. A sufficiently low operating temperature to be compatible with concentrated solar thermal energy and a propensity to generate methane. In contrast, copper and lead oxides offer greater potential for liquid chemical looping combustion because they have higher oxygen mass ratio and a higher operating temperature, which enables better efficiency from a power plant. For all three metal oxides, the production of methane via the undesirable methanation reaction is less than 2% of the product gases for all operating temperatures and an order of magnitude lower for lead.

© 2017 Hydrogen Energy Publications LLC. Published by Elsevier Ltd. All rights reserved.

Introduction

Liquid Chemical Looping Gasification (LCLG) and liquid Chemical Looping Combustion (LCLC) are two recently proposed technologies to produce synthesis gas (syngas) and to provide integrated CO₂ capture from the combustion of a hydrocarbon fuel, respectively [1–3]. Chemical looping process using solid particles can also be used to produce hydrogen [4–8]. All chemical looping systems operate based via the indirect transfer of oxygen from the air to the fuel by means of a Oxygen Carrier (OC) that is cycled between two reactors, typically termed the air and fuel reactors [9]. However, for a

LCLC system, the amount of oxygen transferred between the reduction and oxidation reactors with the LOC is significantly greater than the stoichiometric ratio, while for a LCLG system, it is sub-stoichiometric. Since the potential use of a liquid as the oxygen carrier has only recently begun to be explored, a wide range of potential LOC materials are yet to be assessed. The overall objective of the present investigation is therefore to assess the relative performance of different potential LOCs for applications in combustion or gasification.

Solid-phase CLG and CLC systems employ solid particles as the oxygen carrier. Although this has the advantage of enabling detailed control of the properties of the OC materials, it also introduces the challenges of attrition, agglomeration

* Corresponding author.

E-mail address: mohammadmohsen.sarafraz@adelaide.edu.au (M.M. Sarafraz).

<http://dx.doi.org/10.1016/j.ijhydene.2017.05.116>

0360-3199/© 2017 Hydrogen Energy Publications LLC. Published by Elsevier Ltd. All rights reserved.

and sintering, particularly at the elevated temperatures, which leads to a limited operating life of the particles [10–16]. In addition, the operating temperatures and pressures of these processes are also limited, which results in a decrease in the exergetic efficiency relative to conventional combustion and gasification processes. These limitations have driven the exploration of alternative approaches, such as the use of a liquid OC [17].

Liquid metal oxides have potential to be used as the OC for gasification process or hydrogen production [18–20]. For example, syngas is produced using liquid slag during the heat recovery process from high-temperature blast furnaces using liquid slag [21–24]. In this process, a carbonaceous fuel is oxidised (partially or totally) by injecting it into a high temperature molten slag. Extensive studies on this process [18,25–29] reveal that it suffers from a low efficiency because of the low thermal conductivity of the slag (1 W/m.K for slag versus 120 W/m.K for molten copper oxide [30], respectively), which is lowered by the presence of minerals. In addition, slag tends to form layers of fused materials of different composition (e.g. silica layer, minerals and non-metallic compounds) with relatively low thermal conductivity, which inhibit the thermal performance of the process [21,22]. However, pure liquid metals have a high thermal conductivity and can offer better chemical and thermal performance [31–34] than molten slag. It has also been shown that the presence of molten metals can enhance the rate of reaction, the thermal performance [32,35–40] and the chemical conversion of the reaction because they catalyse system [41–43].

Recently, Jafarian et al. [17] proposed one potential configuration in which to use a liquid metal oxides could be used as the oxygen carrier with the view to addressing the aforementioned challenges. They evaluated the thermodynamic potential of their cycle using molten iron oxide as a plausible oxygen carrier. This LOC offers the potential to achieve a high operating temperature of 1350 °C, although it suffers the disadvantage of a relatively high solidification temperature. They showed that the proposed system has significant potential to address major limitations of both solid-phase CLC systems and a liquid CLC system proposed by Lamond et al. [44,45] and McGlashan et al. [46–48], which are temperature limited. Jafarian et al. [17] also showed that it is also possible to configure the liquid chemical looping process to operate in either the CLC or CLG modes by controlling the stoichiometry of the reactor, which can be achieved by varying the relative molar flow rate of the LOC. However, no previous investigation has been reported of the potential for alternative types of liquid oxygen carrier for either CLC or CLG.

Although the influence of the type of solid oxygen carrier particles on the performance of chemical looping combustion has been assessed [49,50], to the best of authors' knowledge, no previous assessment has been reported of the relative performance of alternative LOCs for combustion or gasification. Indeed, no criteria have been proposed with which to compare their performance. For this reason, the first aim of this work is to develop a set of thermodynamic criteria with which to assess the relative merit of alternative liquid oxygen carriers for chemical looping. The second is to assess the energetic performance of a particular configuration of reactors for liquid phase CLC and CLG.

Methodology

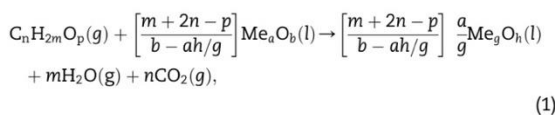
Fig. 1 presents a schematic representation of a potential system for liquid chemical looping combustion or gasification systems, as proposed by Jafarian et al. [17]. The main components of this system are two interconnected bubble column reactors, referred to as the fuel and air reactors. The former is used to reduce the LOC, by the oxidation of the fuel to produce syngas, while the latter is used to oxidize the LOC using oxygen from the air. During operation, the LOC is proposed to be circulated continuously between the reactors. The system is analysed here using graphite as a surrogate for a range of potential carbon containing feedstock together with steam as the gasifying agent. The assumed product of gasification is syngas whose dominant components are CO and H₂. Fig. 1 also proposes an ash separator, which is reasonably assumed to be developable because of the significant difference in density between the molten metal oxides and fused ash [51,52]. The process of oxidation causes the reduced and vitiated air (O₂ < 21%) to leave the oxidation reactor at an elevated temperature.

For the present analysis, it is assumed that the whole process is isothermal. This assumption is reasonable because the oxidation reaction, which is exothermic, can be used to supply the heat required for gasification, which is endothermic, via circulation of the LOC between the reactors. Furthermore, the circulation of heat between the reactors can be controlled via the flow rate of LOC and the partial pressure of oxygen. Isothermal operation also allows solidification to be avoided, which is necessary for reliable operation and is desirable to minimise the energy and exergy losses associated with heating and cooling of the reactants and products. Setting the circulation ratio between the reactors to be sub-stoichiometric will cause the system to operate in the gasification regime, while setting it to be at or above stoichiometric causes the system to operate in the combustion regime.

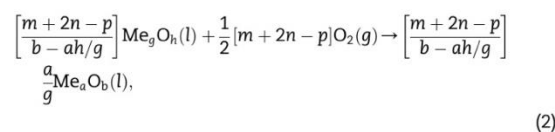
To assess the proposed system thermodynamically the Gibbs minimization method was employed to estimate the Gibbs free energy, enthalpy of reaction and oxygen content ratios. The total or partial oxidation of fuel and feedstock (C_nH_{2m}O_p) with metal oxides shown as Me_aO_b, was calculated as follows:

Combustion mode

In the fuel reactor:



In the air reactor:



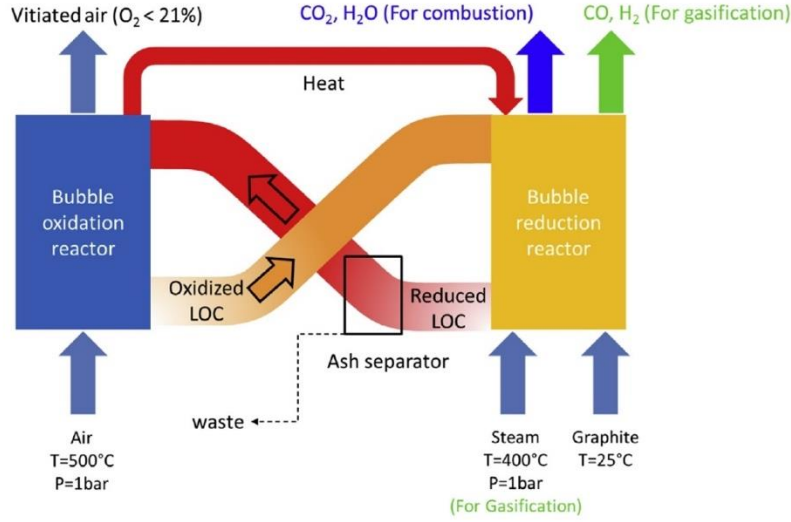
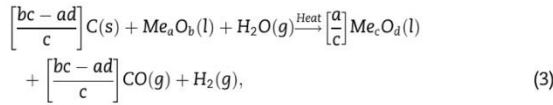


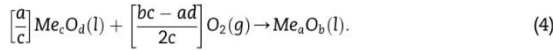
Fig. 1 – A schematic diagram of the liquid CLG/CLC configuration assessed here, for the case of graphite as a surrogate for solid fuels adapted from Ref. [17]. The dominant products are CO and H₂, for gasification or CO₂ and H₂O for combustion.

Gasification mode

In the gasification reactor:



In the air reactor:



The enthalpy of reaction was estimated using Eq. (5). The oxidation of the reduced liquid metal oxide within the air reactor is always exothermic, while the partial combustion of the fuel inside the fuel reactor can be either endothermic or exothermic, depending on the type of fuel, LOC and the operating temperature of the system. Hence:

$$\Delta M_{red,r} = \sum_{prod} \Delta M_i^f(T) - \sum_{react} \Delta M_i^f(T). \quad (5)$$

In this equation, M was assessed for either the Gibbs free energy or enthalpy, while $\Delta M_i^f(T)$ is the change of this parameter for component i at the temperature T. The mole fraction of each of the components in the product gas was obtained using the following equation [53,54]:

$$\gamma_i = \frac{y_i}{\sum_{j=1}^n y_j}. \quad (6)$$

Here, i is a component in the gas product such as CO or CO₂, y_i is the mole fraction of CO or CO₂ depending on whether it is operated in the gasification or combustion mode, respectively.

Eq. (7) was used to assess the ratio of the heat of reaction in the fuel reactor to that transported by the LOC. This parameter was used to assess the condition in which the system can

maintain isothermal operation. It determines the amount of LOC required to minimise the temperature difference between reactors for isothermal operation, as follows:

$$\Delta T = \frac{\Delta H_{red}}{n_{LOC,ox} \cdot C_{p,LOC,ox}}. \quad (7)$$

Here, ΔT is temperature difference between reactors, ΔH_{red} is the enthalpy of reduction [kJ/mol] within the gasifier (or fuel reactor) for the case of gasification (or combustion), while $C_{p,LOC,ox}$ [kJ/mol. °C] is the average of specific heat of the oxidised LOC. Note that the change of $C_{p,LOC,oxidised}$ with temperature is negligible since the process is near to isothermal.

Eq. (8) was used to assess the fraction of exergy carried by the syngas for the gasification system:

$$\chi_{syngas} = \frac{\dot{n}_{syngas} \cdot LHV_{syngas}}{\dot{n}_{fuel} \cdot LHV_{fuel}}. \quad (8)$$

Here, χ_{syngas} is the exergy of the syngas, \dot{n} is the molar flow rate of the syngas and LHV is the molar low heating value of the syngas and fuel [kJ/mol]. The exergy balance of the system can be calculated using Eq. (9) as follows:

$$\chi_{Total} = \dot{n}_{fuel} \cdot LHV_{fuel} = \chi_{syngas} + \chi_{hot\ gas} + \Delta\chi. \quad (9)$$

Here $\Delta\chi$, is the summation of exergy generation and exergy destruction, which is caused by the reactions and losses and is assumed to negligible here in the absence of detailed system information. The oxygen mass ratio, OMR, is defined as the ratio of the mass of reduced LOC to oxidised LOC and characterises the capacity of a given metal oxide to transport oxygen in a Red-Ox cycle [8]:

$$OMR = \frac{b \times MW_{oxygen}}{a \times MW_{metal} + b \times MW_{oxygen}}. \quad (10)$$

Here MW_i is the molecular weight of the compound, while a and b are the number of atoms of metal and oxygen,

respectively. For the thermodynamic equilibrium analysis, the set of reference conditions shown in Table 1 was defined for the fuel reactor of the liquid CLG and liquid CLC systems. These conditions were chosen based on the stoichiometric value of oxygen in fuel or gasification reactors.

To assess the influence of operating parameters, the molar ratios of LOC to fuel (φ) and molar ratio of steam to fuel (ψ) were defined as follows:

$$\varphi = \frac{\dot{n}_{LOC}}{\dot{n}_{Feedstock}} \quad (11)$$

and

$$\psi = \frac{\dot{n}_{Steam}}{\dot{n}_{Feedstock}} \quad (12)$$

where, \dot{n}_i is the molar flow rate of liquid oxygen carrier.

The state of a liquid oxygen carrier depends on the temperature, mole fraction and partial pressure of oxygen. That is, the LOC will remain in the liquid phase and will keep its phase and structure indefinitely, if the temperature and partial pressure of oxygen is kept within a specific range. For example, within the range $1250 \text{ }^\circ\text{C} < T < 1350 \text{ }^\circ\text{C}$ and $-1 < \log P_{O_2} < 1$, liquid copper oxide is in form of Cu_2O and CuO , whose relative mole fraction can be calculated from the phase diagram [17,55]. Nevertheless, mixing the type of liquid oxygen carrier can potentially create unstable phases of oxygen carrier. Therefore, only pure metal oxides were considered for the present thermodynamic assessment of the proposed system, using experimental data reported in the literature.

The criteria that were chosen to select the metal oxides for the present investigation are as follows:

- (1) The metal oxide should be in the liquid phase over as wide a range of oxygen content as possible and be operable at, or near to, a constant temperature. This is to minimise exergy loss in cycling between reactors.
- (2) The solidification temperature should be as far below the operating temperature as possible, which we have nominally chosen to be at least $100 \text{ }^\circ\text{C}$, to enable solidification to be avoided without excessive technical difficulty.

Table 1 – Reference conditions for thermodynamic equilibrium analysis of the metal oxides in the fuel reactor.

Operating condition	Lead oxide	Copper oxide	Antimony oxide
Temperature ($^\circ\text{C}$)	900	1350	1000
Pressure (bar)	5	10	5
Gasification			
LOC/feedstock (φ) ^a	0.2	0.45	0.25
Steam/feedstock (ψ)	1	1	1
Combustion			
LOC/Fuel ratio (φ) ^b	1	1	1
Steam/Fuel ratio (ψ)	1	1	1

^a Less than stoichiometric value of oxygen.
^b 4 times higher than stoichiometric value.

- (3) The operating temperature should desirably be below $1000 \text{ }^\circ\text{C}$ to keep the system within the temperature range for which metals can be used for containment, although we also assess the broader range of $800\text{--}1300 \text{ }^\circ\text{C}$ to maximise relevance to other potential applications, including for concentrated solar thermal energy.

Results and discussion

Melting temperature

Table 2 presents the melting temperature for the 41 metals and metal oxides investigated here. As can be seen, the oxides of copper, antimony, lead and rhodium are potentially suitable for the liquid CLC and liquid CLG regimes. For example, copper oxide has three states of oxidation including Cu , CuO

Table 2 – Melting point of the metal and metal oxides considered in this study.

Materials	Melting point ($^\circ\text{C}$)	Reference
Co	1495	[56]
CoO	1933	[57]
Co_3O_4	895	[58]
Cu	1085	[59,60]
Cu_2O	1230	[59,60]
CuO	1325.6	[61]
Cd	321.3	[62]
CdO	1559	[62]
Fe	1539	[63,64]
Fe_2O_3	1566	[64]
Fe_3O_4	1597	[63]
FeO	1377	[57]
Ni	1455	[65]
NiO	1955	[65]
Mn	1246	[66]
MnO	1945	[66]
MnO_2	535	[66]
Mn_2O_3	940	[66]
Sb	630.6	
Sb_2O_3	656	[66]
Sb_2O_4	540	[66]
Sb_2O_5	380	[66]
Pb	327.5	
PbO	888	[66]
Pb_3O_4	500	[66]
PbO_2	290	[66]
Sn	231.9	
SnO	1080	[66]
SnO_2	1630	[66]
V	1910	
VO	1789	[66]
V_2O_3	1940	[66]
VO_2	1967	[66]
V_2O_5	690	[66]
Cr	1907	
CrO_3	197	[66]
Cr_2O_3	2435	[66]
CrO	300	[66]
Rh	1963	
Rh_2O_3	1100	[66]
RhO_2	1050	[66]

and Cu_2O , with similar melting temperatures of 1085 °C, 1230 °C and 1325.6 °C, respectively. In contrast, chrome does not meet the criteria because its oxides have very different melting temperature i.e. 197–2435 °C. In addition, it is possible that a solid-phase oxidation state of chrome will form, since Cr_2O_3 has a much higher melting temperature (2435 °C) than the target operating temperature of ~1300 °C. This risks significant operational challenges, such as blockages and degraded performance. From this approach, eleven metals were selected for further investigation.

Fig. 2 presents schematically the distribution of melting temperature and OMR for the oxides of eleven metals. As can be seen, the oxides of Cr, Mn, V, Ag, Fe and Cd do not meet the second and third criteria, because the difference between melting temperatures of their oxidation states is too great as noted above. These metals were therefore eliminated from the selection process. However, Cu, Pb, Rh and Sb oxides do satisfy the aforementioned criteria. All oxidation states of Pb have melting temperature lower than 900 °C, while for copper oxide, it ranges between 1085 °C and 1300 °C. Similarly, for Sb the melting temperature of the oxide is in range 380 °C–650 °C, while for rhodium oxide, the range is 1050 °C–1100 °C. Therefore, these four metal oxides were selected for further assessments.

Gibbs free energy

Fig. 3 (a and b) presents the dependence on temperature of the Gibbs free energy of the oxidation and reduction reactions for different metal oxides (Sb, Pb, Cu, and Rh) reduced with pure graphite, as derived with Eqs. (1)–(4). It can be seen that the Gibbs free energy for the reduction and oxidation of antimony with graphite and air, respectively is negative. In addition, it has a negative slope, so that ΔG becomes increasingly negative with an increase in the operating temperature. This implies that the reaction is spontaneous. Its oxidation reaction also has negative values, although its slope is positive. For

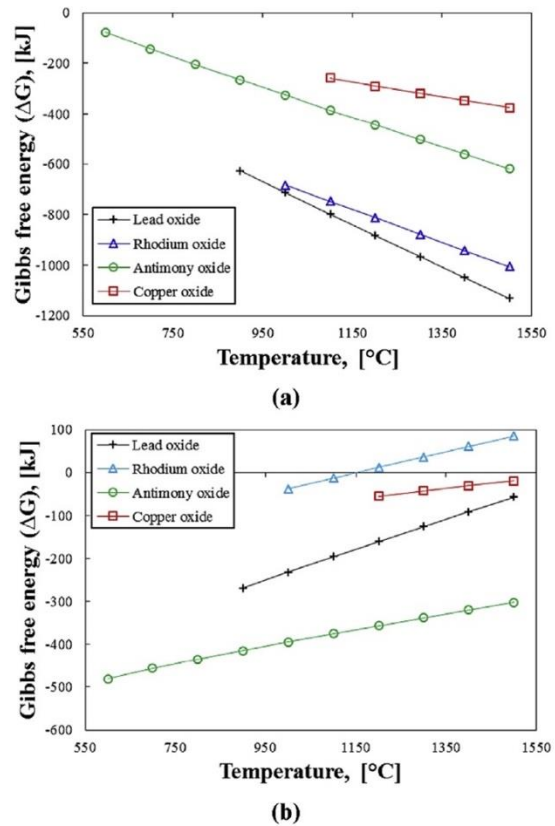


Fig. 3 – Dependence on temperature of the Gibbs free energy of the reduction and oxidation reactions for three metal oxides. a) Reduction reaction, b) Oxidation reaction.

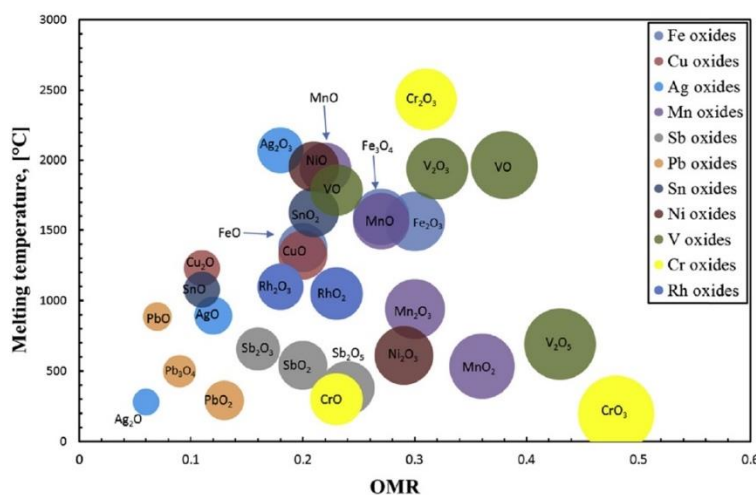


Fig. 2 – Comparison of the melting temperature as a function of the oxygen mass ratio of the oxidative states of eleven metal oxides. Each sphere is centred on the data point, while its area is proportional to oxygen mass ratio.

both lead and copper oxides, ΔG is also negative for the reduction with graphite and the oxidation with air, although the oxidation has a positive slope with temperature. However, for rhodium oxide, $\Delta G > 0$, meaning that this reaction is not likely to occur at temperatures within the range 1100°C–1500 °C. Therefore, rhodium is unsuitable for the liquid CLG and liquid CLC systems. In addition, rhodium is both radioactive and a scarce element, which are further disadvantages. However, both lead and antimony oxides exhibit favourable Gibbs free energy in the liquid phase, although over different ranges of operating temperature. Antimony oxide stays in the liquid phase over the temperature range of 600 °C < T < 1500 °C, while copper oxide has a smaller range of 1100 °C < T < 1500 °C and lead ranges from 900 °C to 1500 °C. It is readily apparent that a wider range of operating temperature offers greater flexibility. In addition, as is shown below, the production of CO₂ is also temperature-dependent and its rate decreases with an increase in the operating temperature (see Section *Mole fractions of syngas and hot gas*).

Enthalpy of reactions

Fig. 4(a–c) presents the calculated dependence on temperature of the enthalpy of reduction and oxidation for the metal oxides Pb, Cu and Sb in both the gasification and combustion regimes assuming that the reactions proceed to equilibrium. It can be seen that all metals exhibit the same general trend in which $\Delta H_{red} > 0$ and decreases with temperature, while $\Delta H_{ox} < 0$ and increases with temperature. The net enthalpy of reaction is greatest for antimony, slightly less for lead and significantly less for copper. In contrast, for the oxidation reaction, the reaction enthalpy of lead is slightly greater than antimony, whilst for copper it is again the least. Of the three metals, copper exhibits the most dependence on temperature, which occurs over the range 1100°C–1300 °C. This change in the slope is due to the chemical conversion of CuO to Cu₂O. Where the enthalpy of reaction is sufficiently negative to overcome heat losses from the reactor, there is no risk of solidification of liquid LOC. On the other hand, where the enthalpy is positive, there is potential to employ concentrated solar thermal energy to supply the required heat. However, the detailed assessment of these options is beyond the scope of the present investigation.

Energetic analysis of reactors

Fig. 5 presents the calculated dependence on temperature of the ratio of the enthalpy of oxidation with air to that of reduction ($\frac{\Delta H_{ox}}{\Delta H_{red}}$) for the case of graphite. As can be seen, $\frac{\Delta H_{ox}}{\Delta H_{red}} > 1$ for all three metal oxides, showing that the overall process is exothermic and can be self-sustaining. However, the ratio is greatest for lead oxide, reaching a value as high as 1.85 at 1000 °C. The ratio for copper is slightly lower at 1.7 for 1300 °C and lowest for antimony (1.48 at 1000 °C).

Fig. 6 presents the dependence of ΔT on the ϕ for copper, lead and antimony oxides. As can be seen, for lead oxide, a

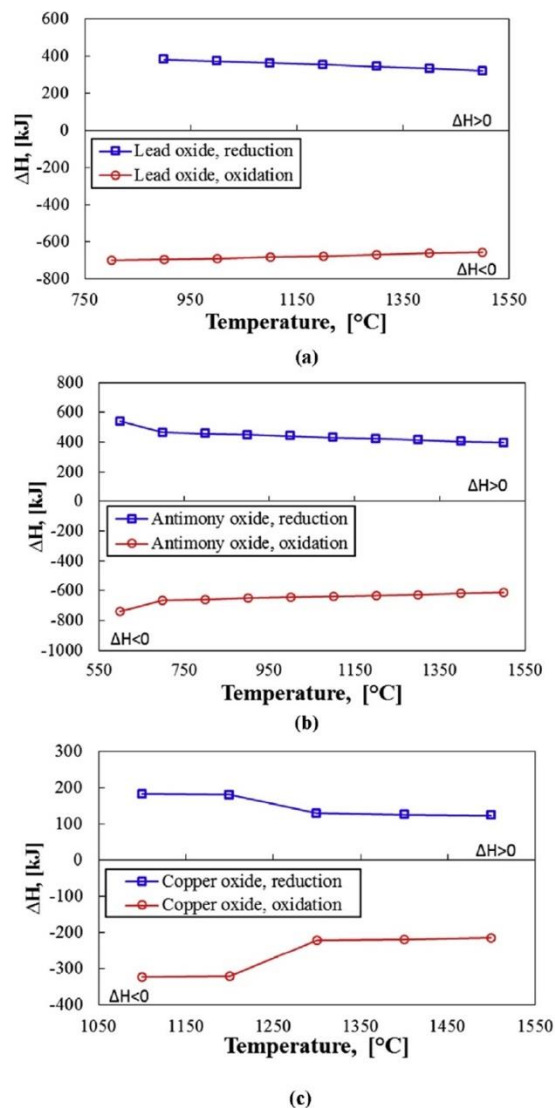


Fig. 4 – Dependence of the enthalpy of the reduction and oxidation reactions on temperature for a) lead oxide b) antimony oxide c) copper oxide.

minimum of 168 mol of LOC per moles of feedstock is required for a 10 °C temperature difference between reactors, while for copper and antimony oxides, these values are 193 and 268, respectively. For a 50 °C temperature difference between the reactors, the required LOC/feedstock molar ratio is 35, 38 and 52, respectively while for a 100 °C temperature difference, the ratio is 17, 19 and 26, respectively. Based on this criterion, antimony oxide provides a lower temperature difference for higher LOC/fuel molar ratios, meaning that this oxide can provide sufficient oxygen for complete combustion also.

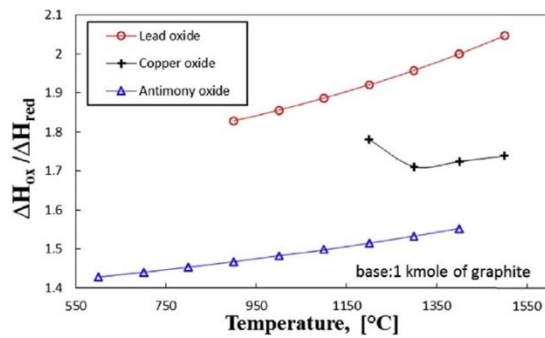


Fig. 5 – Dependence on temperature of the calculated $\frac{\Delta H_{ox}}{\Delta H_{red}}$ for three liquid metal oxides.

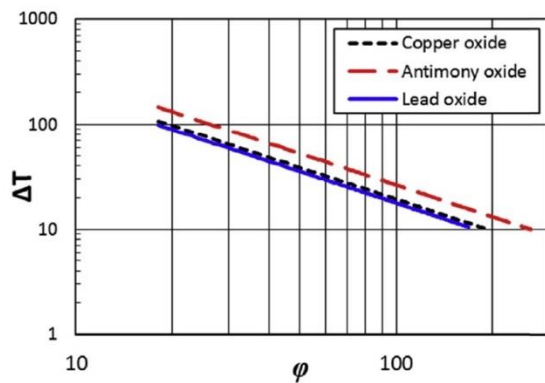
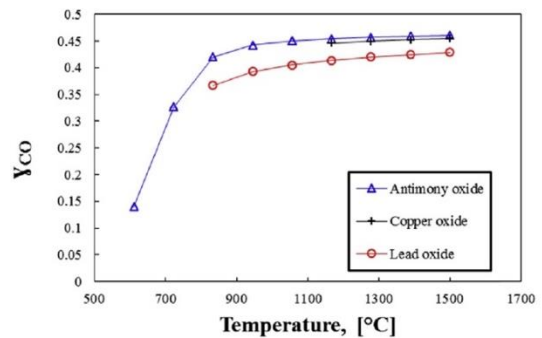


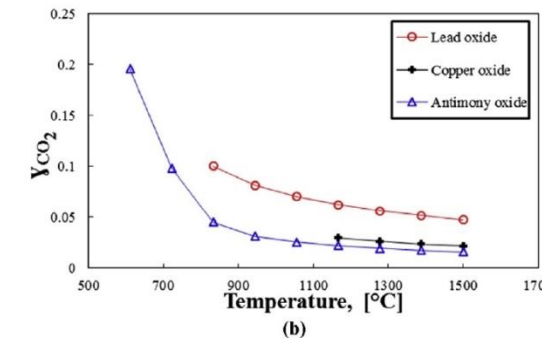
Fig. 6 – Dependence of temperature difference (ΔT) between reactors on the molar ratio of liquid oxygen carrier to fuel (ϕ) for different metal oxides at the reference conditions given in Table 1.

Mole fractions of syngas and hot gas

Fig. 7(a–b) presents the calculated dependence on reactor temperature of the calculated mole fractions of CO and CO₂ in the product gases from the liquid CLG system for lead, copper and antimony oxides as the LOC. As can be seen, for all three metal oxides, the mole fraction of CO in the outlet stream of the fuel reactor increases with an increase in temperature, while that of CO₂ decreases. The trend is clearest for antimony oxide, for which the mole fraction of CO increases asymptotically with temperature to approach a constant value, although the asymptotic value is not quite reached over this temperature range (see Fig. 7a). The data for copper oxide is similar to that for antimony oxide, but is only possible for a narrower range of operating temperature. However, it is significantly lower for lead oxide. The inverse results can be seen for CO₂ (Fig. 7b), in that a relatively high production of CO is associated with a relatively low production of CO₂. For gasification, it is desirable to maximise the production of CO and minimize that of CO₂. In addition, it is also desirable to operate at as low a temperature as possible. On this basis,



(a)



(b)

Fig. 7 – Dependence of the mole fractions of CO and CO₂ in the product gas on the temperature of the reduction reactor for three metal oxides reduced by graphite in a liquid CLG system, a) CO mole fraction, b) CO₂ mole fraction.

antimony oxide is the preferred LOC since it results in a mole fraction of CO of 0.45, and allows operation at temperatures below 1000 °C with very little trade off in performance. On the other hand, while copper has only slightly poorer performance in terms of product gas composition, it requires operation at temperatures of at least 1200 °C to retain some buffer, which constitutes a significant disadvantage. Also poor is the performance of lead oxide. While it exhibits a temperature range that is almost as wide as that of antimony, it yields a significantly lower production of CO and higher production of CO₂. More specifically, antimony generates the lowest amount of CO₂ at the reference operating conditions with a mole fraction of 0.04, followed by copper and lead oxides, for which it is 0.06 and 0.11, respectively (See Fig. 7b).

Fig. 8(a–b) presents the dependence on temperature of the calculated mole fractions of CO and CO₂ for the same three metal oxides in a liquid CLC system. Unlike liquid CLG, the mole fraction of CO₂ is at least an order of magnitude higher than that of CO. Although the conversion to CO₂ decreases with an increase in temperature for antimony and copper oxides, complete conversion is achieved independent of temperature for lead oxide. This shows that, for temperatures greater than 850 °C, lead is preferable over the other two metal oxides at higher temperatures from the point of view of complete combustion. Importantly, while antimony approaches the complete combustion for temperatures ~600 °C,

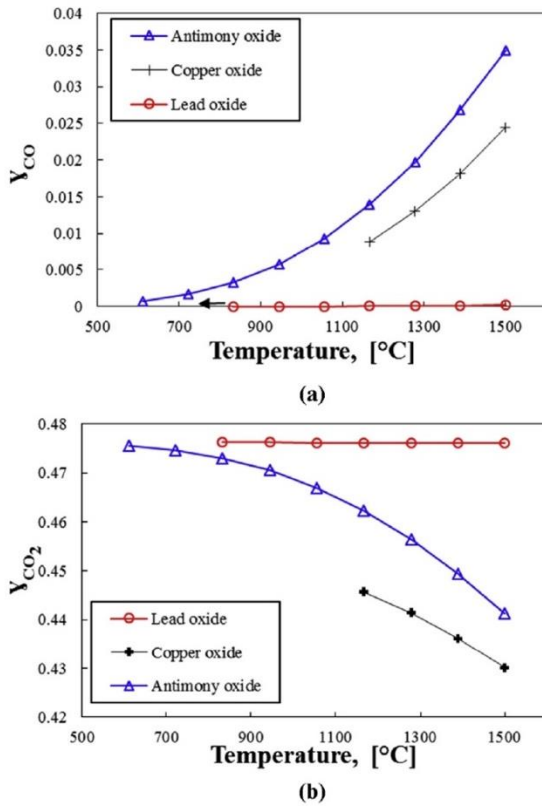


Fig. 8 – Dependence on temperature of the mole fractions in the product gas for three metal oxides reduced by graphite in a liquid CLC system, for a) CO, b) CO₂.

the lowest concentration of CO is 2000 ppm at 1300 °C, so that further treatment may be necessary, which would add to cost. Moreover, temperature has a direct influence on of the extent of the reduction reaction, while the quantity of oxygen

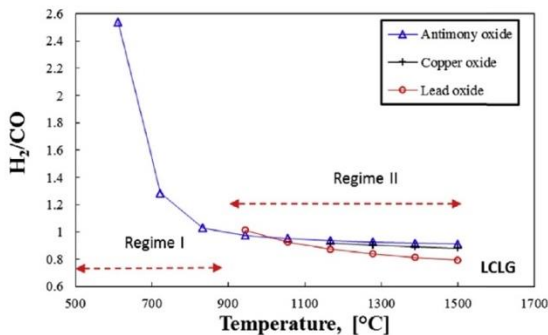


Fig. 9 – Dependence of predicted syngas quality (H_2/CO) on temperature for different metal oxides in LCLG at the reference condition given in Table 1. In regime 1, the system operates as CLG to produce a high quality of syngas. In regime 2, the system operates in the mixed combustion or complete combustion modes.

released with lead oxide is limited. As a result, increasing the temperature has no effect on the mole fractions of CO or CO₂. Therefore, lead oxide is the preferred LOC and can be used over the temperature range 900°C–1500 °C.

Syngas quality

Fig. 9 presents the calculated dependence of syngas quality on temperature for the liquid CLG system with three different metal oxides. As can be seen, the ratio of H_2/CO , which is often referred to as syngas quality, decreases with an increase in temperature [67]. Significantly, this decrease is non-linear for antimony oxide, and is nearly linear within the range of temperatures for copper and lead oxides. For antimony oxide, the trend can be divided into two regimes. In regime I, the rate of decrease in syngas quality is considerably higher than regime II. This is because for temperatures below 900 °C, the Boudouard reaction proceeds to produce more CO. However, for temperatures higher than 900 °C, the Boudouard reaction is suppressed. As a result, CO production is suppressed in this regime, which reduces the syngas quality. Significantly, at the reference operating condition, antimony oxide produces the highest syngas quality of the three metals. In addition, it is the only metal oxide that enables the target quality of 2.1 for the Fischer–Tropsch process to be reached, since both lead and copper oxides operate in regime 2 throughout the temperature range. Importantly, operation at low temperatures causes the production of both methane and tar for conventional gasification. However, for gasification with liquid antimony oxide, methanation is avoided for temperatures in the range 800–1000 °C.

Fig. 10 presents the dependence of syngas quality on ϕ for three metal oxides at the reference conditions. As can be seen, for the case where $\phi < 1$ (regime I), the quality of the syngas product is higher than in regime 2, for which $\phi > 1$. In regime I, due to the gasification process, a mixture of CO and H_2 with an insignificant amount of CO₂ is produced (for all metal oxides ranged from 0.2% to 8%). For example, for $\phi = 0.05$, the value of $H_2/CO = 1.09$ (with 0.02 CO₂) for antimony oxide, while it is

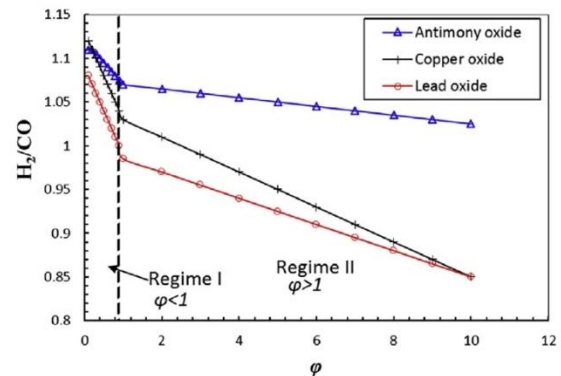


Fig. 10 – Dependence of syngas quality (H_2/CO) on the ratio of liquid oxygen carrier to fuel, ϕ for three metal oxides and for steam/fuel ratio, ψ of unity. All other conditions are as per Table 1.

1.07 (with 0.06 CO₂) and 1.04 (with 0.05 CO₂) for copper and lead oxides, respectively. Likewise, with an increase in φ , the syngas quality decreases for all three metal oxides. However, for $\varphi > 2$, the mode of the system changes to mixed combustion so that more carbon dioxide is produced, which decreases the syngas quality.

Fig. 11 presents the dependence of syngas quality on ψ for the three metal oxides at the reference conditions. Also shown is the target syngas quality of 2.1 that is suitable for Fischer–Tropsch synthesis and for alcohol production process. As can be seen, antimony oxide requires less steam in comparison with copper or lead oxide. For example, for the case with 1 kmol of feedstock introduced to the gasifier, 2.6 kmol of steam is required for antimony oxide to achieve H₂/CO = 2, while the equivalent ratio is 3.2 and 4 for copper and lead oxide, respectively. It can also be seen that there is an optimal value of ψ , although the peak value of ψ is also greatest for antimony. That is, antimony oxide offers the highest syngas quality and requires the lowest amount of steam, followed by copper and lead oxides at similar operating conditions.

Exergy analysis for gasification using liquid metal oxides

Fig. 12 presents the dependence on temperature of the exergy efficiency of syngas production for the three metal oxides, each calculated with Eq. (8) for the values of φ and ψ corresponding to a value of H₂/CO = 1. As can be seen, gasification with antimony oxide produces the highest quality of syngas, together with slightly higher exergy efficiency than copper oxide. However, for lead oxide, gasification can be performed at lower temperatures, which increases the possibility of side production of methane and tar (900 °C versus 1300 °C). At 1300 °C, for antimony oxide, approximately, 68% of the exergy is partitioned in the syngas, while for copper oxide; about 50% of the exergy is partitioned in the syngas (LHV based). For lead oxide, about 61% of the exergy is partitioned in the syngas and the rest is in the vitiated air. For the system operated with copper oxide, some of the exergy from the air reactor could potentially be recovered (e.g. by preheating reactants or by use

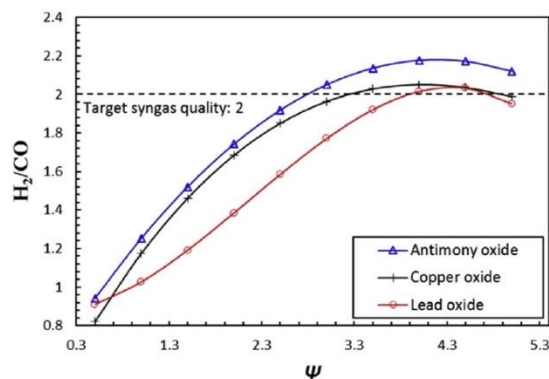


Fig. 11 – Dependence of syngas quality (H₂/CO) on the molar ratio of steam to fuel (ψ) for three metal oxides at the reference conditions.

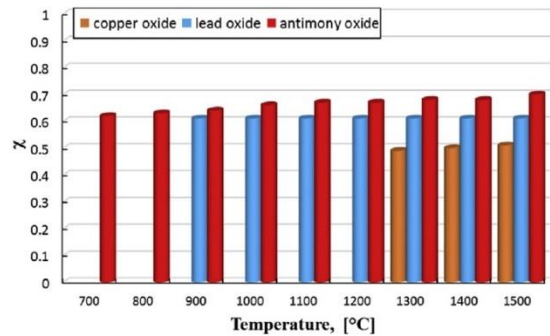


Fig. 12 – Dependence of the exergy efficiency (χ) on temperature for the production of syngas from the gasification of graphite for three metal oxides for the reference conditions given in Table 1 and for H₂/CO = 1.

of a power plant), but this is beyond the scope of the present investigation.

Methane formation

Fig. 13 presents the dependence of mole fraction of CH₄ on temperature for gasification with three molten metals at the reference condition given in Table 1. As can be seen, the methane mole fraction decreases with an increase in temperature for all the molten metals. Likewise, for all three molten metals, the mole fraction of CH₄ is less than 2% of product gases meaning that the gasification with molten metals can be performed without significant methane formation. For example, lead and copper oxides, both have the least methane formation during gasification, while for antimony oxide at 600–700 °C, mole fraction of methane in product is about 1.7%. For copper and antimony oxides, the mole fraction of methane is approximately zero at 1500 °C. While for lead oxide this occurs at 900 °C. Therefore, the LCLG concept has great potential to eliminate undesirable production of methane or at least achieve low values of significantly

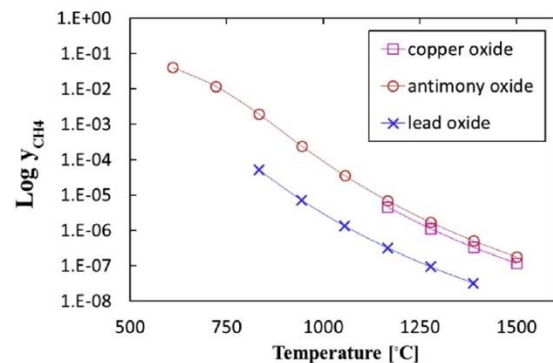


Fig. 13 – Dependence of the mole fraction of methane on temperature in gasification with three different molten metals.

less than 2% of product gases, and an order of magnitude for lead.

Technical challenges

To allow the potential advantages (identified above) to be harnessed the following technical challenges would need to be addressed:

- 1) A continuous flow reactor for high temperature molten metal: To the best of our knowledge, no continuous flow reactor has been demonstrated for liquid metal oxides at high temperatures. For copper, a reactor must sustain temperatures higher than 1000 °C, while for lead and antimony oxides, the reactor should be operable at 900 °C and 650 °C, respectively.
- 2) Fluid circulation: A method is required to circulate the molten metal at high temperatures. To the best of author's knowledge, no such system is commercially available. However, some manufacturers¹ claim that their pumps can circulate molten metal oxides at temperatures of up to 900 °C.
- 3) Heat loss and solidification: Although the process operates with an overall exothermic reaction, heat loss must be kept low and managed carefully to avoid solidification. Furthermore, the operating conditions should be sufficiently far above solidification to avoid freezing, which may be challenging to achieve for copper but is likely to be more achievable for lead and antimony oxides.
- 4) Pressure drop across the reactors: The relatively high values of density and viscosity of liquid metal oxides will result in a relatively high pressure drop from circulating fluid in the reactors. Further work will be required to assess the trade-off between pressure drop, which depends on the height of the liquid head, design of the reactor, and parameters such as conversion extent and flow rate. Similarly, the influence of gas holdup will need to be evaluated for the metal oxides.
- 5) Sparging technology: For good heat and mass transfer, gases should be injected uniformly into the reactors. In addition, the spargers must be carefully designed to avoid local solidification of liquid metals. However, it is reasonable to expect that these could be adapted from commercially available systems used to inject carbon-containing gas into molten slag for reduction or heat recovery in blast furnaces [68,69] or methane into molten copper oxide for copper purification [70]. Therefore, a robust injection system should be designed for the system.
- 6) Ash separation: A system will be required to remove ash for any application of the system with a realistic fuel-a challenge that was avoided for the present assessment graphite as a surrogate fuel. Nevertheless, it is reasonable to expect that these could be adapted from previous experiments by Plevan et al. [71] and Eatwell-Hall et al. [72] who demonstrated that ash can be separated from the molten metal due to density difference.

¹ HITEMP company, for more info see <http://hitemp.com/molten-metal-pump/>.

- 7) Lifetime of oxygen carrier: Further research is needed to assess the influence of followings on the lifetime of a liquid oxygen carrier: a) solidification or crystallization of LOC [6,73,74] within the gasifier, b) the reaction with either air or impurities in the feedstock such as sulphur or heavy metals, or c) reaction with refractory materials and d) sintering and deactivation [6,73,74]. However, this is beyond the scope of the present work.

Conclusions

A comparative study of the relative performance of 41 oxides of 11 metals as potential oxygen carriers for liquid chemical looping gasification or combustion has revealed the following conclusions:

- A critical ratio of the moles of liquid oxygen carrier to fuel has been identified, below which the system operates in the gasification regime and above which it operates in the combustion regime. This critical value is 0.18, 0.24 and 0.08 for the metals of antimony, copper and lead as the LOCs, respectively.
- The LOC with the greatest overall thermodynamic potential for operation in the gasification regime was found to be antimony oxide. This was calculated to yield the highest quality of syngas (up to 2.12) for all of the metals assessed here and requires the lowest flow rate of steam for gasification. In addition, it offers potential to operate at temperatures as low as 600 °C, which is the lowest of these metal oxides.
- The LOC with the greatest overall thermodynamic potential for operation in the combustion regime was found to be lead oxide. This was found to enable the most complete combustion, which is also independent from the operating temperatures greater than 900 °C to prevent solidification.
- Gasification with three molten metals investigated in this work showed that methane formation is kept to a value of less than 2% of the products over the entire operating regime. Antimony and lead oxides offer a process with exergy efficiency of 68% and 50% (at the reference condition for $H_2/CO = 1$), respectively with methane production of less than 2% of gas products for temperatures of between 700 and 900 °C.

Acknowledgement

Authors of this work gratefully acknowledge Australian Research Council (ARC) for the financial support through grant DP150102230. The first author of this work acknowledges "Australian Government Research Training Program Scholarship" for the financial supports.

Nomenclature

C_p	Heat capacity, kJ/kg
H	Enthalpy, kJ
M	Enthalpy or Gibbs free energy, kJ (See Eq. (5))

T Temperature, °C or K
 y Mole fraction of component

Superscripts and subscripts

i component
 f formation

Greek letters

Δ difference
 χ Temperature difference between reactors, °C or K
 γ Production extent (mole fraction of components)

Abbreviations

g Gas
 LCLC Liquid chemical looping combustion
 LCLG Liquid chemical looping gasification
 LOC Liquid oxygen carrier
 Me Metal oxide
 Oxid Oxidation
 Prod product
 Reac Reactant
 Red Reduction
 Redox Reduction-Oxidation
 S Solid

REFERENCES

- [1] Wang K, Yu Q, Qin Q, Hou L, Duan W. Thermodynamic analysis of syngas generation from biomass using chemical looping gasification method. *Int J Hydrogen Energy* 2016;41:10346–53.
- [2] Gnanapragasam N, Reddy B, Rosen M. Hydrogen production from coal using coal direct chemical looping and syngas chemical looping combustion systems: assessment of system operation and resource requirements. *Int J hydrogen energy* 2009;34:2606–15.
- [3] Huang Z, Zhang Y, Fu J, Yu L, Chen M, Liu S, et al. Chemical looping gasification of biomass char using iron ore as an oxygen carrier. *Int J Hydrogen Energy* 2016;41:17871–83.
- [4] Wang Y, Hua X, Zhao C, Fu T, Li W, Wang W. Step-wise reduction kinetics of Fe₂O₃ by CO/CO₂ mixtures for chemical looping hydrogen generation. *Int J Hydrogen Energy* 2017;42:5667–75.
- [5] Heng L, Zhang H, Xiao R. Hydrogen production from heavy fraction of bio-oil using iron-based chemical looping process: thermodynamic simulation and performance analysis. *Int J Hydrogen Energy* 2016;41:17771–83.
- [6] Zeng D-W, Xiao R, Zeng J-M, Zhang H-Y. Liquid foam assisted sol-gel synthesis of iron oxides for hydrogen storage via chemical looping. *Int J Hydrogen Energy* 2016;41:13923–33.
- [7] Zeng D-W, Xiao R, Huang Z-c, Zeng J-M, Zhang H-Y. Continuous hydrogen production from non-aqueous phase bio-oil via chemical looping redox cycles. *Int J Hydrogen Energy* 2016;41:6676–84.
- [8] Ismail M, Liu W, Dunstan MT, Scott SA. Development and performance of iron based oxygen carriers containing calcium ferrites for chemical looping combustion and production of hydrogen. *Int J Hydrogen Energy* 2016;41:4073–84.
- [9] Gopaul SG, Dutta A, Clemmer R. Chemical looping gasification for hydrogen production: a comparison of two unique processes simulated using ASPEN plus. *Int J Hydrogen Energy* 2014;39:5804–17.
- [10] Adanez J, Abad A, Garcia-Labiano F, Gayan P, Luis F. Progress in chemical-looping combustion and reforming technologies. *Prog Energy Combust Sci* 2012;38:215–82.
- [11] Kenarsari SD, Yang D, Jiang G, Zhang S, Wang J, Russell AG, et al. Review of recent advances in carbon dioxide separation and capture. *Rsc Adv* 2013;3:22739–73.
- [12] Lyngfelt A, Kronberger B, Adanez J, Morin J, Hurst P. The GRACE project. Development of oxygen carrier particles for chemical-looping combustion. Design and operation 10KW chemical-looping combustor: na. 2004.
- [13] Leion H, Lyngfelt A, Johansson M, Jerndal E, Mattisson T. The use of ilmenite as an oxygen carrier in chemical-looping combustion. *Chem Eng Res Des* 2008;86:1017–26.
- [14] Linderholm C, Mattisson T, Lyngfelt A. Long-term integrity testing of spray-dried particles in a 10-kW chemical-looping combustor using natural gas as fuel. *Fuel* 2009;88:2083–96.
- [15] Johansson M, Mattisson T, Lyngfelt A. Use of NiO/NiAl₂O₄ particles in a 10 kW chemical-looping combustor. *Ind Eng Chem Res* 2006;45:5911–9.
- [16] Forero C, Gayán P, García-Labiano F, De Diego L, Abad A, Adánez J. High temperature behaviour of a CuO/ γ -Al₂O₃ oxygen carrier for chemical-looping combustion. *Int J Greenh Gas Control* 2011;5:659–67.
- [17] Jafarian M, Arjomandi M, Nathan GJ. Thermodynamic potential of high temperature chemical looping combustion with molten iron oxide as the oxygen carrier. *Chem Eng Res Des* 2017;120:69–81.
- [18] Luo S, Zhou Y, Yi C. Hydrogen-rich gas production from biomass catalytic gasification using hot blast furnace slag as heat carrier and catalyst in moving-bed reactor. *Int J hydrogen energy* 2012;37:15081–5.
- [19] Ghandehariun S, Rosen M, Naterer G, Wang Z. Comparison of molten salt heat recovery options in the Cu–Cl cycle of hydrogen production. *Int J hydrogen energy* 2011;36:11328–37.
- [20] Liao C-H, Horng R-F. Investigation on the hydrogen production by methanol steam reforming with engine exhaust heat recovery strategy. *Int J Hydrogen Energy* 2016;41:4957–68.
- [21] Chen W-H, Lin M-R, Leu T-S, Du S-W. An evaluation of hydrogen production from the perspective of using blast furnace gas and coke oven gas as feedstocks. *Int J hydrogen energy* 2011;36:11727–37.
- [22] Suopajarvi H, Pongrácz E, Fabritius T. The potential of using biomass-based reducing agents in the blast furnace: a review of thermochemical conversion technologies and assessments related to sustainability. *Renew Sustain Energy Rev* 2013;25:511–28.
- [23] Li P. Thermodynamic analysis of waste heat recovery of molten blast furnace slag. *Int J Hydrog Energy* 2017;42(15):9688–95.
- [24] Sun Y, Zhang Z, Liu L, Wang X. Integration of biomass/steam gasification with heat recovery from hot slags: thermodynamic characteristics. *Int J Hydrogen Energy* 2016;41:5916–26.
- [25] Liu J, Yu Q, Peng J, Hu X, Duan W. Thermal energy recovery from high-temperature blast furnace slag particles. *Int Commun Heat Mass Transf* 2015;69:23–8.
- [26] Barati M, Esfahani S, Utigard T. Energy recovery from high temperature slags. *Energy* 2011;36:5440–9.
- [27] Duan W, Yu Q, Xie H, Qin Q, Zuo Z. Thermodynamic analysis of hydrogen-rich gas generation from coal/steam gasification using blast furnace slag as heat carrier. *Int J hydrogen energy* 2014;39:11611–9.
- [28] Duan W, Yu Q, Xie H, Liu J, Wang K, Qin Q, et al. Thermodynamic analysis of synergistic coal gasification using blast furnace slag as heat carrier. *Int J Hydrogen Energy* 2016;41(3):1502–12.
- [29] Li P, Lei W, Wu B, Yu Q. CO₂ gasification rate analysis of coal in molten blast furnace slag—for heat recovery from molten

- slag by using a chemical reaction. *Int J Hydrogen Energy* 2015;40:1607–15.
- [30] Rezaei H, Gupta R, Bryant G, Hart J, Liu G, Bailey C, et al. Thermal conductivity of coal ash and slags and models used. *Fuel* 2000;79:1697–710.
- [31] Sarafraz M, Peyghambarzadeh S, Fazel SA, Vaeli N. Nucleate pool boiling heat transfer of binary nano mixtures under atmospheric pressure around a smooth horizontal cylinder. *Period Polytech Chem Eng* 2013;57:71.
- [32] Sarafraz M, Peyghambarzadeh S, Vaeli N. Subcooled flow boiling heat transfer of ethanol aqueous solutions in vertical annulus space. *Chem Ind Chem Eng Q* 2012;18:315–27.
- [33] Sarafraz MM. Nucleate pool boiling of aqueous solution of citric acid on a smoothed horizontal cylinder. *Heat Mass Transf* 2012;48:611–9.
- [34] Sarafraz M, Peyghambarzadeh S, Alavifazel S. Enhancement of nucleate pool boiling heat transfer to dilute binary mixtures using endothermic chemical reactions around the smoothed horizontal cylinder. *Heat Mass Transf* 2012;48:1755–65.
- [35] Sarafraz M, Hormozi F, Peyghambarzadeh S. Pool boiling heat transfer to aqueous alumina nano-fluids on the plain and concentric circular micro-structured (CCM) surfaces. *Exp Therm Fluid Sci* 2016;72:125–39.
- [36] Sarafraz M, Kiani T, Hormozi F. Critical heat flux and pool boiling heat transfer analysis of synthesized zirconia aqueous nano-fluids. *Int Commun Heat Mass Transf* 2016;70:75–83.
- [37] Sarafraz M, Hormozi F, Peyghambarzadeh S. Thermal performance and efficiency of a thermosyphon heat pipe working with a biologically ecofriendly nanofluid. *Int Commun Heat Mass Transf* 2014;57:297–303.
- [38] Sarafraz M, Hormozi F, Nikkhal V. Thermal performance of a counter-current double pipe heat exchanger working with COOH-CNT/water nanofluids. *Exp Therm Fluid Sci* 2016;78:41–9.
- [39] Sarafraz M, Hormozi F. Experimental investigation on the pool boiling heat transfer to aqueous multi-walled carbon nanotube nanofluids on the micro-finned surfaces. *Int J Therm Sci* 2016;100:255–66.
- [40] Sarafraz M, Hormozi F. Comparatively experimental study on the boiling thermal performance of metal oxide and multi-walled carbon nanotube nanofluids. *Powder Technol* 2016;287:412–30.
- [41] Sinfelt JH, Carter J, Yates D. Catalytic hydrogenolysis and dehydrogenation over copper-nickel alloys. *J Catal* 1972;24:283–96.
- [42] Rudloff WK, Freeman ES. Catalytic effect of metal oxides on thermal decomposition reactions. II. Catalytic effect of metal oxides on the thermal decomposition of potassium chlorate and potassium perchlorate as detected by thermal analysis methods. *J Phys Chem* 1970;74:3317–24.
- [43] Harlé V, Vrinat M, Scharff J, Durand B, Deloume J. Catalysis assisted characterizations of nanosized TiO₂-Al₂O₃ mixtures obtained in molten alkali metal nitrates: effect of the metal precursor. *Appl Catal A General* 2000;196:261–9.
- [44] LaMont DC, Seaba J, Latimer EG, Platon A. Liquid-phase chemical looping energy generator. *Google Patents*; 2011.
- [45] LaMont DC, Seaba J, Latimer EG, Platon A. Liquid-phase chemical looping energy generator. *Google Patents*; 2010.
- [46] McGlashan N. Chemical-looping combustion—a thermodynamic study. *Proc Inst Mech Eng Part C J Mech Eng Sci* 2008;222:1005–19.
- [47] McGlashan NR, Childs PR, Heyes AL, Marquis AJ. Producing hydrogen and power using chemical looping combustion and water-gas shift. *J Eng Gas Turbines Power* 2010;132:031401.
- [48] McGlashan NR, Childs PR, Heyes AL. Chemical looping combustion using the direct combustion of liquid metal in a gas turbine based cycle. *J Eng Gas Turbines Power* 2011;133:031701.
- [49] Cho P, Mattisson T, Lyngfelt A. Comparison of iron-, nickel-, copper- and manganese-based oxygen carriers for chemical-looping combustion. *Fuel* 2004;83:1215–25.
- [50] Wang K, Yu Q, Qin Q. The thermodynamic method for selecting oxygen carriers used for chemical looping air separation. *J Therm Anal Calorim* 2013;112:747–53.
- [51] Coats HM. Ash-separator. *Google Patents*; 1907.
- [52] John Y. Multiple element vortical whirl ash separator. *Google Patents*; 1952.
- [53] Jerndal E, Mattisson T, Lyngfelt A. Thermal analysis of chemical-looping combustion. *Chem Eng Res Des* 2006;84:795–806.
- [54] Lyngfelt A, Leckner B, Mattisson T. A fluidized-bed combustion process with inherent CO₂ separation; application of chemical-looping combustion. *Chem Eng Sci* 2001;56:3101–13.
- [55] Sarafraz M, Jafarian M, Arjomandi M, Nathan G. Potential use of liquid metal oxides for chemical looping gasification: a thermodynamic assessment. *Appl Energy* 2017;195:702–12.
- [56] Enghag P. Encyclopedia of the elements: technical data-history-processing-applications. John Wiley & Sons; 2008.
- [57] Patnaik P. Handbook of inorganic chemicals. New York: McGraw-Hill; 2003.
- [58] Feher F, Brauer G. Handbook of preparative inorganic chemistry. New York: Academic Press; 1963. p. 341.
- [59] Smith WF, Hashemi J. Foundations of materials science and engineering. McGraw-Hill; 2011.
- [60] File END, part B, version V. National nuclear data center. Brookhaven National Lab; 1990.
- [61] Chadwick SS. Ullmann's encyclopedia of industrial chemistry. *Ref Serv Rev* 1988;16:31–4.
- [62] Morrow H. Cadmium and cadmium alloys. *Kirk-Othmer Encyclopedia of Chemical Technology*; 2001.
- [63] Price GD. Mineral physics: treatise on geophysics. Elsevier; 2010.
- [64] Hay J, Pharr G. ASM handbook: mechanical testing and evaluation. *ASM Int* 2000;8:232.
- [65] Cotton FA, Wilkinson G, Murillo CA, Bochmann M, Grimes R. Advanced inorganic chemistry. Wiley New York; 1999.
- [66] Barin I. Thermochemical data of pure substances, thermochemical data of pure substances. Wiley-VCH; 1997.
- [67] Yun Y, Chung SW, Yoo YD. Syngas quality in gasification of high moisture municipal solid wastes. *Prepr Pap Am Chem Soc Div Fuel Chem* 2003;48:823.
- [68] Kasai E, Kitajima T, Akiyama T, Yagi J, Saito F. Rate of methane-steam reforming reaction on the surface of molten BF slag-for heat recovery from molten slag by using a chemical reaction. *ISIJ Int* 1997;37:1031–6.
- [69] Nick PA, Hunnicutt H, Peters RR, Anderson EA, Dolbear GE. Process for pyrolytic heat recovery enhanced with gasification of organic material. *Google Patents*; 2008.
- [70] Davis Jr. John H, Klein L. Gaseous reduction of oxygen-containing copper. *Google Patents*; 1961.
- [71] Plevan M, Geißler T, Abánades A, Mehravaran K, Rathnam R, Rubbia C, et al. Thermal cracking of methane in a liquid metal bubble column reactor: experiments and kinetic analysis. *Int J Hydrogen Energy* 2015;40:8020–33.
- [72] Eatwell-Hall R, Sharifi V, Swithenbank J. Hydrogen production from molten metal gasification. *Int J hydrogen energy* 2010;35:13168–78.
- [73] Zeng D-W, Xiao R, Zhang S, Zhang H-Y. Bio-oil heavy fraction for hydrogen production by iron-based oxygen carrier redox cycle. *Fuel Process Technol* 2015;139:1–7.
- [74] Dumitrescu L, Sundman B. A thermodynamic reassessment of the Si- Al- O- N system. *J Eur Ceram Soc* 1995;15:239–47.

Chapter 5 Co-production of syngas and power with liquid chemical looping gasification process

5.1. Chapter overview

In this chapter, the co-production of power and syngas with a chemical looping gasification process is thermodynamically modelled. The results and discussion in this chapter contributes to the second and third objectives of the present work by assessing the thermodynamic potential of the LCLG for the co-production of power and syngas. From the previous assessments in chapter 4, lead oxide showed a potential for the gasification and syngas production with H_2 : $CO \sim 2$ and also it showed that around $\sim 60\%$ of exergy can be partitioned in the syngas while still 40% of exergy is partitioned in the vitiated air and hot gases that can be used for further energy production in a power block. Therefore, a thermodynamic assessment was conducted on the integration of chemical looping gasification with a supercritical steam turbine cycle.

To identify the operating regime, the stability diagram together with phase diagram of the lead-oxygen system was studied and plausible thermodynamic region for the process was obtained. Energy and mass balances were coupled to obtain the total energy required for the system. Chemical composition of syngas was also determined using the Gibbs minimisation method via HSC chemistry software package. Aspen plus software package was used to model the power block.




To control the quality of syngas, two different gasifying agents were blended and employed namely steam (to drive the water gas shift reaction) and CO_2 (to drive the main gasification reactions including Boudouard). Influence of different operating parameters such as molar ratios of steam to feedstock, carbon dioxide to feedstock and liquid lead oxide to feedstock on the thermal energy of the process, quality and yield of syngas was thermodynamically investigated. Influence of operating parameters on the first law thermodynamic efficiency of the power block was also investigated and discussed. Results showed that the first law

efficiency of the power block can be as high as 35% which is within the range of the state-of-the-art power blocks. Moreover, a syngas with $H_2: CO$ ratio > 2 at $900^\circ C$ can be produced. The process showed a potential to be hybridised with concentrated solar thermal energy. The detailed assessment of the present work have been published in International Journal of Hydrogen Energy (Sarafraz, Jafarian, Arjomandi, & Nathan, 2018).

Statement of Authorship

Title of Paper	Potential of molten lead oxide for liquid chemical looping gasification (LCLG): A thermochemical analysis
Publication Status	<input checked="" type="checkbox"/> Published <input type="checkbox"/> Accepted for Publication <input type="checkbox"/> Submitted for Publication <input type="checkbox"/> Unpublished and Unsubmitted work written in manuscript style
Publication Details	M.M. Sarafraz, M. Jafarian, M. Arjomandi, G.J. Nathan, Potential of molten lead oxide for liquid chemical looping gasification (LCLG): A thermochemical analysis, International Journal of Hydrogen Energy, Volume 43, Issue 9, 1 March 2018, Pages 4195-4210




Principal Author




Name of Principal Author (Candidate)	Mohammad Mohsen Sarafraz				
Contribution to the Paper	<ul style="list-style-type: none"> - Research, collecting and analyzing data from different resources, developing thermodynamic models and analyzing the obtained data. - Providing the data, writing of the manuscript and production of original figures. - Correspondence with editor and reviewers including the production of all cover letters and rejoinder 				
Overall percentage (%)	80%				
Certification:	This paper reports on original research I conducted during the period of my Higher Degree by Research candidature and is not subject to any obligations or contractual agreements with a third party that would constrain its inclusion in this thesis. I am the primary author of this paper.				
Signature	<table border="1" style="width: 100%;"> <tr> <td style="width: 80%;"></td> <td style="width: 20%;">Date</td> </tr> <tr> <td style="text-align: center;"></td> <td style="text-align: center;">29/11/18</td> </tr> </table>		Date		29/11/18
	Date				
	29/11/18				

Co-Author Contributions

By signing the Statement of Authorship, each author certifies that:

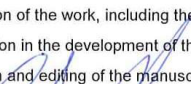
- vii. the candidate's stated contribution to the publication is accurate (as detailed above);
- viii. permission is granted for the candidate to include the publication in the thesis; and
- ix. the sum of all co-author contributions is equal to 100% less the candidate's stated contribution.

Name of Co-Author	Mehdi Jafarian				
Contribution to the Paper	<ul style="list-style-type: none"> - Supervision of the work, including the production of the manuscript - Participation in the development of the concepts and ideas presented in the manuscript - Evaluation and editing of the manuscript prior to submission 				
Signature	<table border="1" style="width: 100%;"> <tr> <td style="width: 80%;"></td> <td style="width: 20%;">Date</td> </tr> <tr> <td style="text-align: center;"></td> <td style="text-align: center;">29/11/18</td> </tr> </table>		Date		29/11/18
	Date				
	29/11/18				

Name of Co-Author	Maziar Arjomandi				
Contribution to the Paper	<ul style="list-style-type: none"> - Supervision of the work, including the production of the manuscript - Participation in the development of the concepts and ideas presented in the manuscript - Evaluation and editing of the manuscript prior to submission 				
Signature	<table border="1" style="width: 100%;"> <tr> <td style="width: 80%;"></td> <td style="width: 20%;">Date</td> </tr> <tr> <td style="text-align: center;"></td> <td style="text-align: center;">29/11/18</td> </tr> </table>		Date		29/11/18
	Date				
	29/11/18				

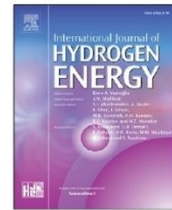
Chapter 5 Co-production of syngas and power with liquid chemical looping gasification process

Chapter 5 Co-production of syngas and power with liquid chemical looping gasification process

Name of Co-Author	Graham Nathan
Contribution to the Paper	<ul style="list-style-type: none">- Supervision of the work, including the production of the manuscript- Participation in the development of the concepts and ideas presented in the manuscript- Evaluation and editing of the manuscript prior to submission
Signature	
	Date 29/11/18

Available online at www.sciencedirect.com

ScienceDirect

journal homepage: www.elsevier.com/locate/he

Potential of molten lead oxide for liquid chemical looping gasification (LCLG): A thermochemical analysis

M.M. Sarafraz^{*}, M. Jafarian, M. Arjomandi, G.J. Nathan

Centre for Energy Technology, School of Mechanical Engineering, University of Adelaide, SA 5005, Australia

ARTICLE INFO

Article history:

Received 27 May 2017

Received in revised form

20 November 2017

Accepted 6 January 2018

Available online 4 February 2018

Keywords:

Liquid chemical looping gasification

Molten lead

Nitrogen dilution

Power block

Syngas production

ABSTRACT

Molten lead oxide is revealed to have favourable thermodynamic performance for gasification in a new process employing chemical looping of a molten liquid metal oxide. In this process, the feedstock is partially oxidized with molten lead oxide in the fuel reactor, while the reduced molten lead is oxidized in the air reactor. As with other chemical looping processes, this avoids direct contact between air and fuel, which prevents the undesirable dilution of the gaseous product with nitrogen. The Gibbs minimization method was employed together with thermo-chemical equilibrium analysis to assess the feasibility of the gasification process using graphite as a surrogate for more realistic, but complex carbonaceous fuels, together with steam and/or carbon dioxide as the gasifying agent. It was found that both the reduction and oxidation reactions of molten lead oxide with carbonaceous fuel are spontaneous. Likewise, the ratio of H₂:CO can be as high as 2.5, while the carbon conversion can reach 94% based on the thermochemical analysis. An energetic performance analysis was also employed for the case of a supercritical steam turbine cycle to extract work from the hot gaseous co-products. On this basis, the first law efficiency of the power cycle was estimated to be up to 33.8%, while the syngas co-product stream for applications such as Fischer-Tropsch synthesis has a chemical exergy efficiency of 41%.

© 2018 Hydrogen Energy Publications LLC. Published by Elsevier Ltd. All rights reserved.

Introduction

Previous assessments of Chemical Looping Combustion (CLC) and Chemical Looping Gasification (CLG), an emerging processes under development (to produce energy and syngas, respectively) via reduction and oxidation of an oxygen carrier, have mostly been limited to materials in the solid state [1–3]. The driver for CLG is the potential to avoid direct contact between air and feedstock, whilst also providing the required heat for the gasification reactions, while the use of solid

particles offers potential to develop novel materials with desirable properties. The process is performed in two interconnected reactors. The oxygen carrier is reduced in the reduction reactor and then transferred to the oxidation reactor, where it is oxidized with air [4,5]. The potential advantages of CLG include the possibility of producing high-quality syngas (i.e. a high ratio of H₂ to CO) and to avoid nitrogen dilution without the need for expensive oxygen plant [5,6]. However, its main disadvantages particularly for the case in which solid materials are used is high-temperature operation for the oxygen carrier and the challenge of cycling

^{*} Corresponding author.

E-mail address: mohammadmohsen.sarafraz@adelaide.edu.au (M.M. Sarafraz).

<https://doi.org/10.1016/j.ijhydene.2018.01.035>

0360-3199/© 2018 Hydrogen Energy Publications LLC. Published by Elsevier Ltd. All rights reserved.

oxygen carriers for many cycles. The overall objective of the present paper is to assess the thermodynamic potential of a novel alternative configuration of CLG in which a liquid metal oxide (here lead oxide II) is employed to deliver net advantage over previously proposed cycles.

High-temperature operation of CLC and CLG systems with solid particles as the oxygen carrier causes morphological changes to the particles, such as sintering and agglomeration, which reduces their life [7,8]. This challenge is particularly significant in the gasification reactor because the oxygen-starved atmosphere generates unreacted carbon, which readily deposits onto the particles [9]. These carbon deposits then react with air in the oxidation reactor to generate wasted heat and carbon dioxide, significantly reducing the effectiveness of the oxygen transport and the efficiency of the process [5]. For example, the gasification of biomass using CLG reported by Acharya et al. [10] only achieved 40% regeneration of the CaO solid particles at a calcination temperature of 800 °C. A low regeneration efficiency of 50% was also reported by Li et al. [11], with similar values reported elsewhere [5,12–16]. It is also desirable to identify alternative approaches for chemical looping gasification that might bypass them altogether.

The use of a liquid metal oxide as the oxygen carrier for CLG offers potential to avoid the aforementioned technical challenges associated with the use of solid OC particles, but although brings alternative challenges such as the risk of solidification and the challenge of containment. However, before beginning to assess these other challenges and potential solutions, it is first necessary to assess the thermodynamic potential of the LCLG concept to identify whether the magnitude of the potential benefit is sufficient to justify the additional investment that would be needed to overcome the challenges. Hence, the objective of the present investigation is to meet this need.

Molten metal oxides are known for their high thermal performance and also they are known to be effective for gasifying carbonaceous feedstock from previous works with high temperature metal-containing slags in blast furnaces [17,18,34–38]. Molten slag is a by-product of the refining of metals such as iron and comprises a mixture of metal oxides such as SiO₂, Al₂O₃, CaO, FeO and MgO [19]. Molten slag typically leaves a blast furnace at temperatures of up to 1650 °C, so that it carries sufficient sensible heat resource to contribute to gasification. In the commercial application of this process, a carbonaceous fuel is partially oxidized, typically in the presence of a gasifying agent such as steam and/or CO₂, by injecting it into the high temperature molten slag. However, no systematic investigation is available of the gasification of solid feedstock with pure liquid metal oxides or of their thermodynamic potential for chemical looping gasification.

The potential to harness the properties of molten iron/iron oxide to reform natural gas in a chemical looping process was recently proposed by Jafarian et al. [20]. Their proposed system comprises two inter-connected bubbling column reactors to circulate the liquid hydro-dynamically. Their thermodynamic analysis shows that the extent of conversion of the natural gas to CO₂ and H₂O depends strongly on the molar flow rate of the liquid oxygen carrier (LOC) between the air and fuel reactors. A molar flow rate of LOC between the reactors greater than the stoichiometric value is required for the

complete conversion of the fuel to H₂O and CO₂, while a flow rate lower than this results in carbon monoxide production. However, no similar assessment of the potential of other metals or fuels has been performed previously.

The process of gasification of carbon-containing feedstock with different molten metal oxides was recently investigated by Sarafraz et al. [21,22]. They showed that the production of high-quality syngas with the chemical looping of molten metals such as molten copper, lead and antimony oxides is thermodynamically realistic. They showed that both the ratios of LOC to fuel and that of the gasifying agent to fuel influence the ratio of H₂ to CO in the syngas product. However, the maximum value for H₂:CO achieved with that particular process is 2.05, while its operating temperature of 1350 °C is technically challenging to achieve. Furthermore, all of the reactions in that process are exothermic, which makes it difficult to employ solar thermal energy to drive the reaction. Hence, it is desirable to explore the use of other materials to seek to identify any that can offer a higher quality of syngas, a lower operating temperature, and/or the potential to introduce solar energy into an endothermic reaction.

The present investigation aims to assess the thermodynamic potential of a LCLG cycle that employs molten lead as the oxygen carrier, graphite as a surrogate for the carbonaceous feedstock and steam and/or CO₂ as the gasifying agent. It aims to assess the influence of different operating parameters such as temperature, ratio of LOC/fuel, steam/fuel and CO₂/fuel on the quality of syngas product. It also aims to assess the energetic performance of a system in which the thermal energy from the hot gases is recovered using a supercritical steam power cycle.

Conceptual design and modelling

Fig. 1 presents a schematic diagram of the key components of a plausible configuration of the LCLG system for the gasification of a solid carbonaceous feedstock. Here we have chosen graphite as a surrogate for more realistic carbon-containing fuels since its properties are well understood. Steam and CO₂ were both considered as alternative or blended gasifying agents with a view to identifying a mechanism to control the ratio of H₂:CO via the main gasification, Boudouard and water gas shift reactions.

The cycle was assessed assuming a plausible configuration of interconnected bubble column reactors for the fuel and air reactors (see Fig. 1), in which a gasifying agent is bubbled through the molten metal oxide, while air is bubbled through the molten metal in the air reactor. Bubble reactors are chosen here because they are known to provide high rates of heat and mass transfer. Impurities in the fuel and gasifying agent are assumed to be separable from the liquid metal, such as by means of a disk-shaped centrifugal ash separator as proposed previously [23]. Molten lead oxide has been selected as the oxygen carrier because the temperature required for its oxidation and reduction reactions lies between 888 °C and 1000 °C. This range of temperature is within the range of many industrial processes. In addition, the oxidation reaction of molten lead oxide with air is exothermic while the reduction reaction of molten lead oxide with carbon is endothermic.

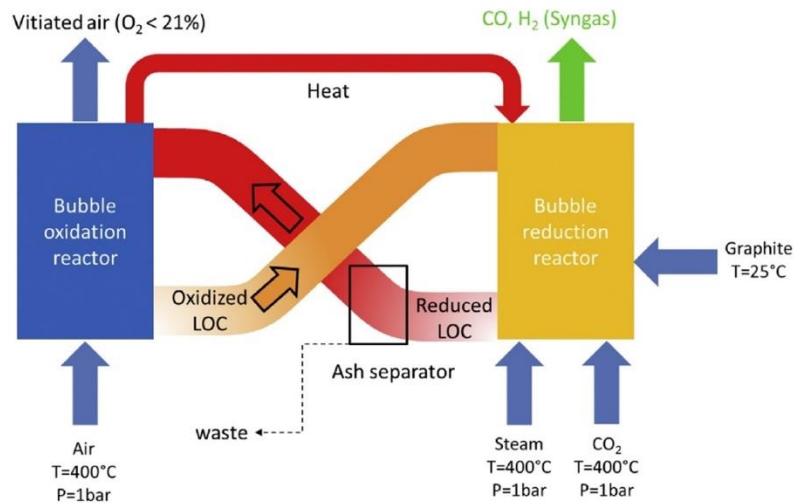


Fig. 1 – A Schematic diagram of the proposed liquid chemical looping gasification system operated with molten lead oxide.

Accordingly, the bubble reduction reactor can also be hybridised with solar thermal energy to allow the possibility for some of the heat required for the gasification from the solar energy. However, this assessment is beyond the scope of the present work.

As can be seen from Fig. 1, the LOC is circulated between the two reactors, which together provide the required heat and oxygen for the gasification reactions. For the present thermodynamic assessment, the following assumptions have been made:

1. The residence time within the reactors is sufficient for the reactions to reach equilibrium so that the Gibbs minimization method can be applied to estimate the equilibrium compositions in the gas and liquid phases.
2. Heat losses from the fuel and air reactors are negligible.
3. A system is available to transfer the LOC between the air and fuel reactors (e.g. fluid-mechanically) with a negligible energy penalty.
4. No solidification occurs in the system, i.e. the conditions are sufficiently far from any solid-liquid two-phase regime.
5. Any impurities in the fuel have a negligible influence on the reactions, so that the only elements involved in the reactions are carbon, hydrogen, oxygen and lead.
6. The sensible heat transferred via the circulation of the LOC, together with the internal transport of heat, is sufficient to satisfy all requirements for heat.
7. Steam and CO₂ enter the fuel reactor at a temperature and a pressure of 400 °C and 1 bar, respectively, while the solid fuel is fed into the reactor at 25 °C and 1 bar. The outlet temperatures from the fuel and air reactors are the same as those of the corresponding reactor.

For the proposed concept, separate water gas shift reactor is avoided and steam is directly injected into the reactor. The reason for the direct injection of steam to the reactor is:

- 1) It proceeds the water gas shift reaction and increases the syngas quality with more hydrogen production.
- 2) It also avoids using a separate water gas shift reactor, which is favourable as it increases the economic viability and reduces the energy required for the start-up.
- 3) Following the concept of interconnected bubble column reactors, proposed by Jafarian et al. [20], the injection of the steam into the fuel reactor, together with the fuel, can induce further lift within the reactor, which in turn can lead to an efficient circulation of the LOC between the air and the fuel reactors.
- 4) Injection of steam into the fuel reactor can also lead to the enhancement in mass and heat transfer within the fuel reactor through increasing of mixing.

Fig. 2 presents the phase diagram of lead oxide as a function of oxygen mass fraction and for various values of temperature. As can be seen, the region confined by the red rectangle comprises liquids in the form of PbO and Pb [24]. Therefore, this regime is suitable for operating the LCLG process. In other regions of the phase diagram, lead oxide comprises either a two-phase (solid-liquid) slag or solid-phase material (e.g. T = 888 °C), which are unsuitable for LCLG and do not offer high rates of heat and mass transfer.

Fig. 3 presents the dependence on temperature of the partial pressure of gas-phase oxygen in a molten system of Pb-O-C-N-H. As can be seen, for operating temperatures in the range 888 °C < T < 1200 °C, PbO (s) can be in form of stable PbO (l) or Pb (l) or a mixture of PbO (l) and Pb (l). In addition, Table 1 shows the potential reactions in the fuel and air reactors. As can be seen, the reduction reaction for molten lead oxide with carbon has a very large equilibrium constant meaning that the forward reaction proceeds towards completion. Thus, the molten lead oxide from the fuel reactor is predominantly in form of Pb (l). Similarly, the equilibrium constant for the oxidation reaction of Pb (l) with air is also large, so that the

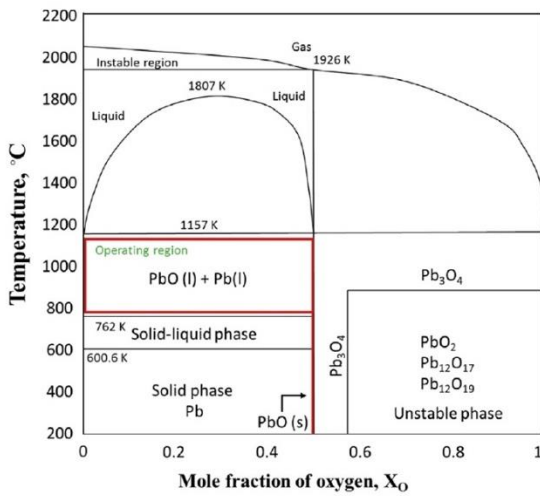


Fig. 2 – The dependence of the state of various lead oxide compounds on temperature and mole fraction of oxygen reproduced from previous work [25,26].

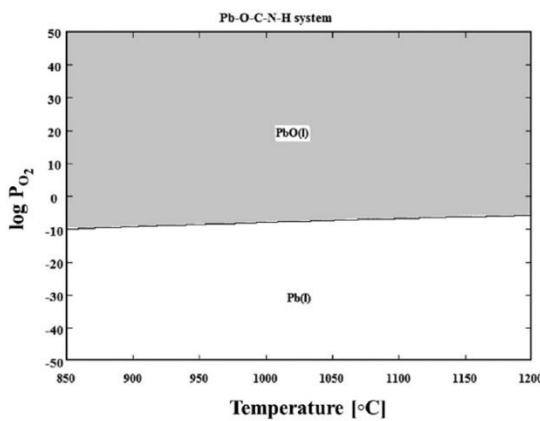


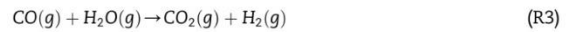
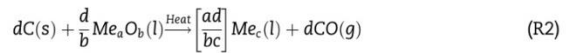
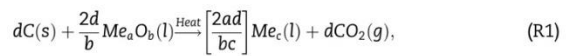
Fig. 3 – Phase stability diagram of molten lead and lead oxide showing the dependence on temperature of the oxygen partial pressure.

molten lead at the outlet of the air reactor is predominantly in form of PbO (l).

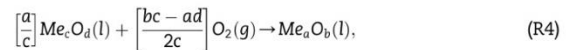
Methodology

The reduction of the oxygen carrier Me_aO_b to Me_cO_d with $C_nH_{2m}O_p$ (as the fuel) within the fuel reactors and its re-oxidation with O_2 from the air in the air reactor is described as follows:

- In the fuel reactor (the general reaction):



- In the air reactor (the general reaction):



The mole fraction of oxygen available in the molten lead (X_o) determines the final composition of the mixture. Since, $n_{PbO(l)} = n_{PbO(l)} + n_{Pb(l)}$. An atom balances with the assumption that $n_{PbO(l)} = 1$ result in the following equations:

$$n_{Pb} = \frac{2X_o - 1}{X_o}, \quad (1)$$

$$n_{PbO} = \frac{1 - X_o}{X_o}, \quad (2)$$

where,

$$X_o = \frac{n_o}{n_{Pb} + n_o}. \quad (3)$$

Here, X_o is the mole fraction of oxygen in molten lead oxide, while n_o and n_{Pb} are the number of moles of oxygen and Pb in

Table 1 – Reactions occurring in the fuel and air reactors.

No.	Reaction	Equilibrium constant (K)			Enthalpy (kJ/mol)		
		900 °C	1000 °C	1100 °C	900 °C	1000 °C	1100 °C
Main reactions in the fuel reactor							
R(5)	$PbO(l) + C(s) \rightleftharpoons Pb(l) + CO(g)$	1.05E+5	1.94E+5	3.21E+5	77.028	74.54	72.04
R(6)	$PbO(l) + CO(g) \rightleftharpoons Pb(l) + CO_2(g)$	2.93E+3	1.39E+3	7.29E+2	-91.81	-93.2	-94.56
R(7)	$PbO(l) + H_2(g) \rightleftharpoons Pb(l) + H_2O(g)$	3.81E+3	2.35E+3	1.53E+3	58.67	61	63.26
R(8)	$C(s) + O_2(g) \rightleftharpoons CO_2(g)$	4.31E+17	1.79E+16	1.18E+15	-394.9	-395.1	-395.3
R(9)	$CO_2(g) + C(s) \rightleftharpoons 2CO(g)$	3.59E+1	1.39E+2	4.4E+2	168.8	167.7	166.6
R(10)	$C(s) + H_2O(g) \rightleftharpoons H_2(g) + CO(g)$	135.7	135.54	135.31	2.76E+1	8.23E+1	2.1E+2
R(11)	$CO(g) + H_2O(g) \rightleftharpoons H_2(g) + CO_2(g)$	7.68E-1	5.9E-1	4.74E-1	-33.13	-32.196	-31.3
Main reaction in the air reactor							
R(12)	$Pb(l) + 0.5O_2(g) \rightleftharpoons PbO(l)$	1.39E+9	6.6E+8	5.03E+7	-380.17	-376.5	-372.8

molten lead, respectively. For example, for $X_o = 0.5$, PbO (δ) is in form of PbO (l). In addition, from the reactions presented in Table 2, for the fuel and air reactor, the fraction of PbO (l) and Pb (l) can be obtained for any temperatures and partial pressure of oxygen.

To assess the partial pressure of oxygen in molten lead oxide inside the air reactor, following equation was used:

$$P_{\text{air reactor, inlet}} = \frac{y_{\text{O}_2, \text{equilibrium}} \times 101325}{0.21} \quad (4)$$

Here $y_{\text{O}_2, \text{equilibrium}}$ is the mole fraction of the oxygen in the outlet of the air reactor, which is in equilibrium with the mole fraction of oxygen in molten lead oxide and can be obtained from Fig. 3. So that the inlet air to the air reactor can be obtained.

The enthalpy and the net Gibbs free energy change of the reaction can be calculated as follows:

$$\Delta M_{\text{red,r}} = \sum_{\text{prod}} \Delta M_i^f(T) - \sum_{\text{react}} \Delta M_i^f(T). \quad (5)$$

In this equation, M denotes either the Gibbs free energy or enthalpy of formation of component i , while $\Delta M_i^f(T)$ represents either the Gibbs free energy of formation or the change in enthalpy of formation of the component i at a given temperature T . Furthermore, the subscripts “red”, “prod” and “react” denote “reduction”, “products” and “reactants”, respectively. As a measure of the thermodynamics potential of the reaction, the Gibbs free energy is the primary criterion chosen to assess the potential of the LOC for the reaction with graphite and air. It is calculated using the data obtained Barin [27]. The mole fraction of the products was estimated using the Gibbs minimization method and thermochemical analysis.

The influence of various operating parameters on the chemical and energetic performance of the LCLG system was assessed with a sensitivity analysis of thermochemical potential following earlier work [28,29] (using HSC chemistry and an Aspen Plus R-Gibbs reactor). In previous works, for this purpose, ϕ is defined as the ratio of inlet moles of molten lead oxide to those of carbon feedstock at the inlet to the fuel reactor:

$$\phi_{\text{LOC}} = \frac{\dot{n}_{\text{LOC}}}{\dot{n}_{\text{fuel}}}. \quad (6)$$

Here, \dot{n} is the molar flow of the liquid oxygen carrier (LOC) and carbonaceous fuel introduced to the fuel reactor. For the CLG configuration, steam is proposed to be used as the gasifying agent to maximise the hydrogen production and increase the $\text{H}_2:\text{CO}$ ratio. For this gasifying agent, the flow rate of steam fed to the fuel reactor is:

$$\phi_{\text{steam}} = \frac{\dot{n}_{\text{steam}}}{\dot{n}_{\text{fuel}}}. \quad (7)$$

Here also, \dot{n}_{steam} and \dot{n}_{fuel} are the molar flow rates of the steam and fuel introduced to the fuel reactor, respectively. Similarly:

$$\phi_{\text{CO}_2} = \frac{\dot{n}_{\text{CO}_2}}{\dot{n}_{\text{fuel}}}. \quad (8)$$

where \dot{n}_{CO_2} is the molar flow rate of CO_2 . In LCLG system, to assess the portion of exergy transported by syngas, the following equation was used:

$$\chi = \frac{\dot{n}_{\text{syngas}} \cdot \text{LHV}_{\text{syngas}}}{\dot{n}_{\text{fuel}} \cdot \text{LHV}_{\text{fuel}}}. \quad (9)$$

where, \dot{n}_{syngas} is the molar flow of the outlet syngas from the fuel reactor and LHV is the lower heating value of the syngas, which depends on the $\text{H}_2:\text{CO}$ ratio. The exergy of the syngas can be calculated with Eq. (10).

$$\text{Ex}_{\text{Chem}} = \dot{n}_{\text{syngas}} \cdot \text{LHV}_{\text{syngas}}. \quad (10)$$

The net work from the power block comprising a steam turbine less that consumed by the pumps and other auxiliaries is presented in Eq. (11):

$$W_{\text{net}} = \sum_{\text{produced}} W - \sum_{\text{consumed}} W = \sum W_{\text{ST}} - \sum W_{\text{pump}}. \quad (11)$$

Here W_{ST} is the total work produced by the steam turbine, W_{pump} is the total work consumed by the pump to produce the required pressure. Both parameters were obtained using an Aspen plus process simulator. The mechanical and thermodynamic efficiencies of the turbine and pump were assumed to be 0.9 and 0.92, respectively following previous work [30]. The first law efficiency of the power block (η) can be defined as the ratio of the work produced from the system to the total input energy, as is given in Eq. (12):

$$\eta = \frac{W_{\text{net}}}{\dot{n}_{\text{fuel}} \cdot \text{LHV}_{\text{fuel}}}. \quad (12)$$

To assess the fuel conversion following equation is used:

$$X = \frac{\dot{n}_{\text{fuel, initial}} - \dot{n}_{\text{fuel, remaining}}}{\dot{n}_{\text{fuel, initial}}}. \quad (13)$$

Here $\dot{n}_{\text{fuel, initial}}$ is the amount of fuel introduced to the gasifier and $\dot{n}_{\text{fuel, remaining}}$ is the amount of the unreacted fuel during the gasification. In addition, the carbon conversion depends on both the reaction kinetics and the rates of mass and heat transfer within the reactors, which are characterised by the residence time and depend on the configuration of the reactors. However, an assessment of the role of these parameters is beyond the scope of the present work.

To assess the net enthalpy of reaction of system, an energy balance over the fuel and the air reactors were done considering the enthalpies of inlet air and fuel streams, liquid metal oxide, and outlet streams, which are expressed as:

Table 2 – Operating conditions of the fuel reactor for the molten lead LCLG system.

Parameter	T(°C), (Fuel and air reactors)	Log P _{O₂}		ϕ _{LOC} (mol/mol)	ϕ _{steam} (mol/mol)	ϕ _{CO₂} (mol/mol)
		Air reactor (bar)	Fuel reactor (bar)			
Reference condition	900	−0.301	−0.301	1	1	1
Range (min–max)	800–1000	Variable from −50 to +50		0.05–1.5	0.5–3	0–1.6

$$\Delta H_{\text{air reactor}} = \sum_{\text{outlet}} H - \sum_{\text{inlet}} H \quad (14)$$

and

$$\Delta H_{\text{fuel reactor}} = \sum_{\text{outlet}} H - \sum_{\text{inlet}} H \quad (15)$$

and

$$Q = \Delta H_{\text{LCLG}} = \Delta H_{\text{air reactor}} - \Delta H_{\text{fuel reactor}} = \sum_{\text{prod.}} H - \sum_{\text{react.}} H \quad (16)$$

Here

$$\sum_{\text{prod.}} H = \sum n_i \cdot \Delta H_i \quad (17)$$

and

$$\sum_{\text{react.}} H = \sum n_i \cdot \Delta H_i \quad (18)$$

here n_i is the mole fraction of each component and ΔH_i is the enthalpy of each component. Prod and react are acronyms for products and reactants, respectively. Depending on the sign of the net enthalpy of the system, Q is the required heat to be supplied to the LCLG (when total energy balance of the system is positive) or released heat from the LCLG (when total energy balance of the system is negative). Table 2 presents the list of both reference operating conditions and the range of their possible values.

Results and discussion

Gibbs free energy and enthalpy of the reactions

Fig. 4 presents the dependence on temperature of the enthalpy of reaction and the Gibbs free energy of the gasification and oxidation reactions for graphite in the molten lead medium. As can be seen, the Gibbs free energy is negative for both the reduction and oxidation reactions, meaning that they are spontaneous and feasible. For example, at 800 °C, the Gibbs free energy of reduction is -250 kJ, while for oxidation it

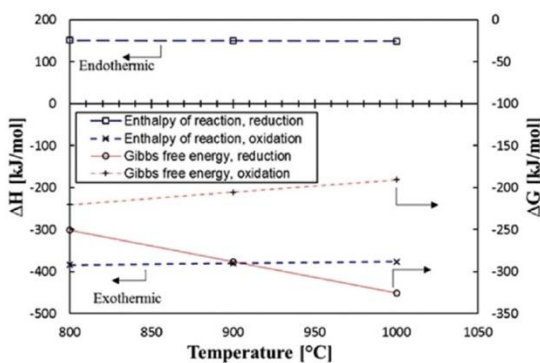


Fig. 4 – The calculated dependence on temperature of the enthalpy of reaction and the Gibbs free energy of the reduction and oxidation reactions for molten lead in the fuel and air reactors.

is approximately -221 kJ. At the same temperature, $\Delta H_{\text{ox}} > \Delta H_{\text{red}}$ and the reduction reaction is endothermic. It can also be seen that the enthalpy of reduction reaction decreases with an increase in temperature, although not by much. For instance, at 800 °C, $\Delta H_{\text{red}} = 150.8$ kJ, while it is 148 kJ at 1000 °C. The oxidation reaction is exothermic, i.e. $\Delta H_{\text{ox}} < 0$, and the temperature has only a slight impact on ΔH_{ox} so that ΔH_{ox} increases slightly with an increase in the operating temperature of the air reactor.

Fig. 5 presents the estimated dependence on temperature of the mole fraction of products for $\phi_{\text{LOC}} = 1$, $\phi_{\text{steam}} = 2$, $\phi_{\text{CO}_2} = 1$. As can be seen, the estimated mole fractions of steam and CO₂ are relatively insensitive to variations in temperature. For example, with an increase in the temperature of the fuel reactor from 900 to 1150 °C, the mole fraction of CO₂ in the product decreased by ~2% from ~20% to ~18%, while mole fraction of CO is ~17% and remain constant. This is because the equilibrium constant for reaction 6 is sufficiently small for any CO₂ produced to be consumed by reaction R (11). Furthermore, reaction 6 proceeds in the reverse direction. However, the magnitude of equilibrium constant for reactions R (5), R (8) and R (12) is quite large ($K \gg -10^4$) so that these reactions can be expected to proceed to completion resulting in only small changes in the mole fraction of CO₂. The same trend is also seen for CO, which is produced with reaction R (5) and is consumed by reaction R (9) which proceeds in the reverse direction. It can also be seen that the products with the greatest mole fractions are steam and CO₂, which yield 37% and 24.6% at 900 °C and 38.7% and 22.8% at 1150 °C. This is because there is excess oxygen at the reference condition, which causes the system to operate in the combustion mode. Nevertheless, the syngas quality is still 1.16 if the excess steam is removed from the products (by condensation), with the resulting mole fractions of CO₂, H₂, CO and CH₄ being 39%, 32.8%, 28.2% and 0.00001%.

Fig. 6 presents the calculated dependence on temperature of $\frac{\Delta H_{\text{ox}}}{\Delta H_{\text{red}}}$ for the conditions given in Table 2 for 1 kmol of carbon and steam. As can be seen, $\frac{\Delta H_{\text{ox}}}{\Delta H_{\text{red}}}$ is highest at 800 °C and decreases with an increase in the temperature. However, this change is less than 1%, which means that the net $\frac{\Delta H_{\text{ox}}}{\Delta H_{\text{red}}}$ is very

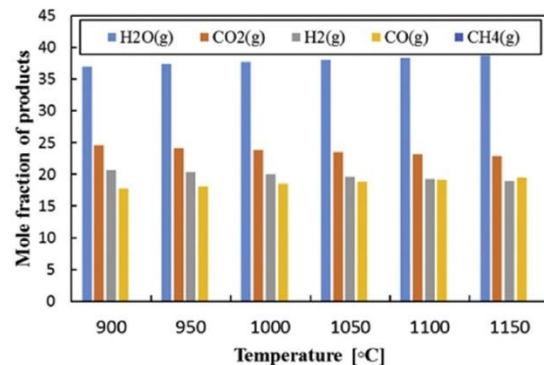


Fig. 5 – The calculated dependence on temperature of the mole fraction of products from the fuel reactor for the reference condition given in Table 2.

insensitive to operating temperature. Furthermore, the released heat from the oxidation reactor is 2.5 times larger than that required by the reduction reactor. That is, the process is strongly exothermic, with a net excess energy available for other applications that is insensitive to temperature, making it a relatively stable system and suggesting that there is a little to be gained thermodynamically from operating at temperatures above $\sim 900^\circ\text{C}$. Note that, some of the released heat in the air reactor is transported with vitiated air, which can be sent to a power block to generate work. Enthalpy of formation of the components is a function of temperature. In Fig. 6, the enthalpy for the oxidation and reduction reactions based on 1 mol of fuel has been obtained. Although dependency is not significant, results show that with an increase in the temperature of the reactors, the ratio of $\Delta H_{ox}/\Delta H_{red}$ decreases. This is because dependency of the enthalpy of formation for reduction reaction is stronger than that of oxidation reaction; thereby an increase in temperature reduces the $\Delta H_{ox}/\Delta H_{red}$ ratio.

Fig. 7 presents the dependence on temperature of the calculated net enthalpy of the system (Eq. (13)) on ϕ_{LOC} . Other operating conditions are as per Table 2. Where $\Delta H_{LCLG} < 0$, the heat released from the air reactor exceeds that required by the fuel reactor. Where $\Delta H_{LCLG} = 0$, they are exactly matched, while where $\Delta H_{LCLG} > 0$, the net process is endothermic. As can be seen, ΔH_{LCLG} decreases with an increase in ϕ_{LOC} , implying that the system becomes more exothermic with an increased role of combustion relative to gasification. Furthermore, the net enthalpy of the system increases slightly with an increase in the temperature of the reactor, making the system more endothermic. That is, an increase in temperature favours gasification over combustion.

Fig. 8 presents the dependence of total enthalpy of the system (Eq. (16)) on ϕ_{steam} for a range of alternative temperatures. Other conditions are as per Table 2. As can be seen, the total enthalpy of the system decreases with an increase in ϕ_{steam} . This is because this increase results in an increase in the proportion of excess steam which results in enthalpy being removed from the system.

Fig. 9 presents the dependence of the total system enthalpy on ϕ_{CO_2} for a range of constant temperatures. As can be seen,

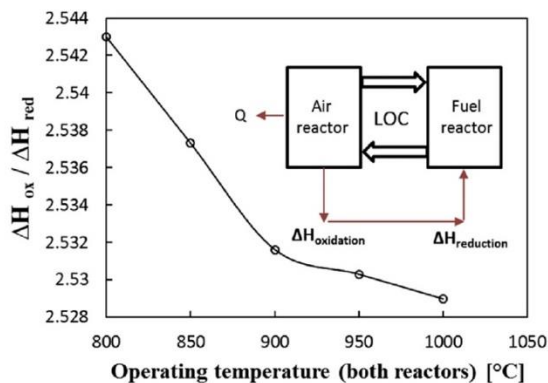


Fig. 6 – Calculated dependence on temperature of ratio of enthalpy of reaction of oxidation reactor to that required in the fuel reactor ($\frac{\Delta H_{ox}}{\Delta H_{red}}$). Conditions are as per Table 2.

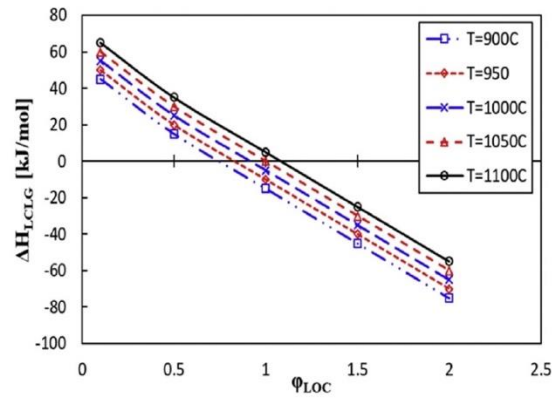


Fig. 7 – Calculated dependence of the net enthalpy of the system on the liquid oxygen carrier to fuel ratio for a range of alternative temperatures. Other operating conditions are as per Table 2.

there are two regimes. In one regime, the total enthalpy of the system decreases strongly with an increase in ϕ_{CO_2} for $0 < \phi_{CO_2} < 0.05$. This is because, in this range, CO_2 changes the equilibrium such that reaction 11 proceeds in the forward direction resulting in an increase in the enthalpy stored in the syngas ($\sim 26\%$ at 900°C). In another regime, for $\phi_{CO_2} > 0.05$, the decrease is weak. This is because the excess CO_2 removes smaller amount of enthalpy from the reactor (e.g. $\sim 4.9\%$ at 900°C). Overall, at lower values of ϕ_{LOC} such as $0.01 < \phi_{LOC} < 0.7$ and $0 < \phi_{steam} < 3$, the main portion of enthalpy is stored in syngas rather than exhausted gas or vitiated air.

Influence of temperature on mole fraction of gaseous products

Fig. 10 presents the calculated dependence on temperature of the mole fraction of the various components of the gaseous products at the reference conditions given in Table 2. It can be

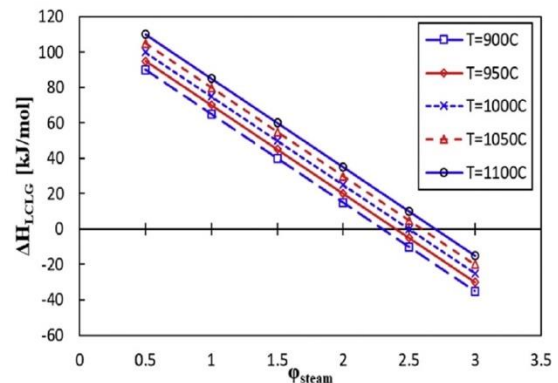


Fig. 8 – Calculated dependence of the net enthalpy of the system on the steam/fuel molar ratio for a range of alternative temperatures. Other operating conditions are as per Table 2.

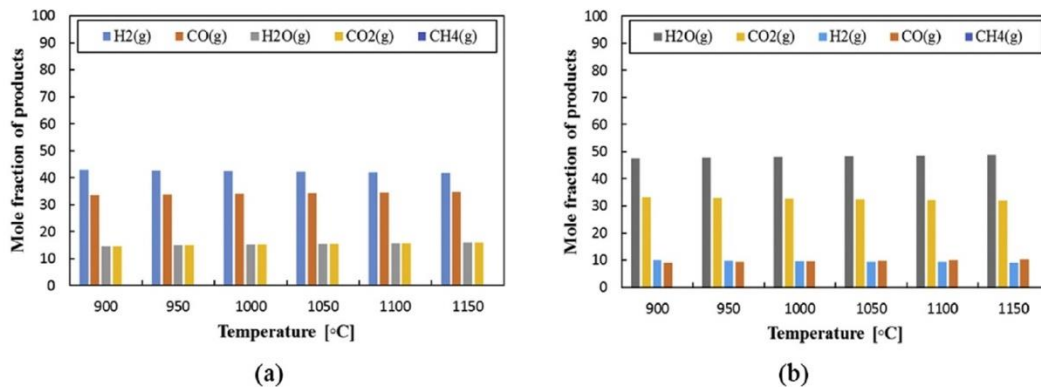


Fig. 12 – Calculated dependence of mole fraction of products on temperature for liquid oxygen carrier to fuel ratios of, a) 0.5 and b) 1.5.

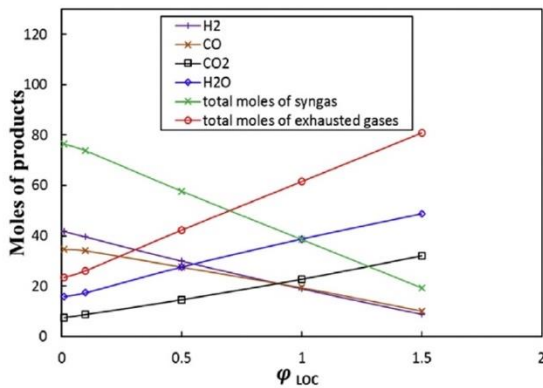


Fig. 13 – Calculated dependence of moles of products on liquid oxygen carrier to fuel ratio at 1000 °C.

increase in ϕ_{steam} . For example, the syngas quality is increased from 0.76 to 2.3 by an increase in ϕ_{steam} from 0.5 to 3 at a temperature range of 850–1000 °C. This further highlights the benefit of operation at the low temperature of the molten regime. Likewise, temperature has a very weak influence on the syngas quality particularly for $0.5 < \phi_{steam} < 2$, for an increase in temperature from 850 °C to 1000 °C. However, a significant amount of excess steam is required to achieve the high quality syngas at the expense of mass and enthalpy loss due to the excess steam at the outlet.

Fig. 15 presents the dependence on temperature of mole fraction products for different molar ratios of steam to fuel for 100 mol of carbon. Other conditions are as per Table 2 and $\phi_{LOC} = 0.01$. As can be seen, more hydrogen is produced with an increase in ϕ_{steam} up to $\phi_{steam} = 1$, beyond which it is decreased slightly. However, excess steam is purged out of the reactor. Therefore, there is a need to employ a condenser to recover the mass and enthalpy loss in form of water and heat, respectively. It is worth saying that portion of enthalpy is also transported and stored in the syngas. As can be seen, for $\phi_{steam} = 0.5$, the mole fraction of hydrogen is ~40%, followed by ~58% of CO, while CO₂ and H₂O are both less than 1%.

However, for $\phi_{steam} = 3$, the mole fraction of hydrogen and CO in the presence of excess steam is 33% and 10%, which can be reach to ~56.1% and ~23.4%, respectively if excess steam is condensed and taken out of the system.

Fig. 16 presents the dependence of moles of products on steam to fuel ratio at 1000 °C. The other conditions are as per Table 2. As can be seen, with an increase in ϕ_{steam} , the mole fraction of H₂, CO and the total mole fraction of the syngas decreases. However, the total moles of the exhausted gases increase. This is because the presence of steam proceeds the water gas shift reaction and more CO₂ is produced.

Importantly, the quality of syngas (H₂:CO ratio) > 1 at $\phi_{steam} > 1$, while the total moles of the syngas decreases. For example, at $\phi_{steam} = 3$, the moles of the syngas is 45 and H₂:CO~2, while total moles of the exhausted gases is 55.

Influence of the ratio of CO₂ to fuel on syngas quality

The effect of blending CO₂ with steam as the gasifying agent is presented in Fig. 17. As can be seen, an increase in the fraction

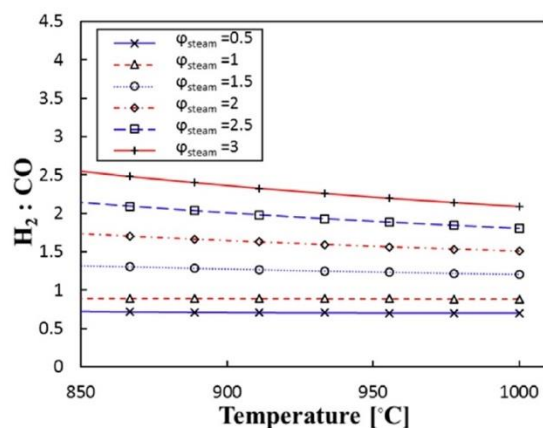


Fig. 14 – Calculated dependence on temperature of H₂:CO (syngas quality) for various ratios of steam to fuel. Other conditions are as per Table 2.

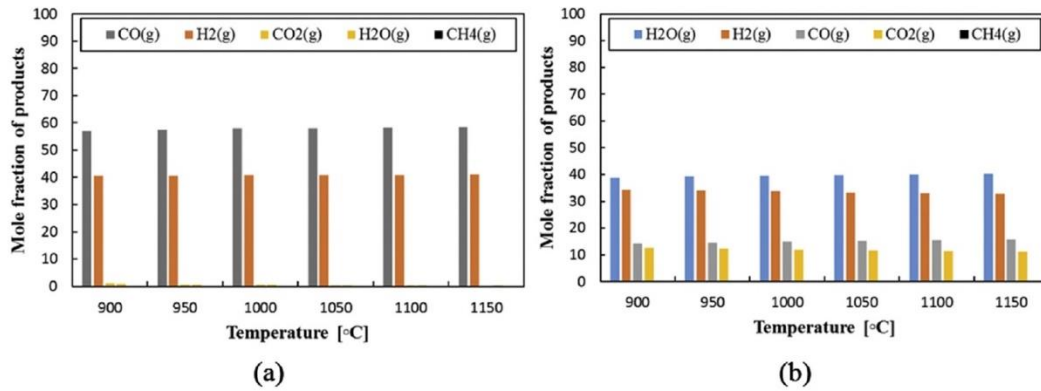


Fig. 15 – Calculated dependence of mole fraction of products on temperature for a ratio of steam to fuel, a) 0.5 b) 3.

of CO_2 as the gasifying agent decreases the syngas quality. This can be attributed to the role of the equilibrium water-gas shift reaction. Increasing the mole fraction of CO_2 inside the fuel reactor. Overall, the second gasifying agent (here CO_2) offers potential to help to accurately manage the syngas quality, although the influence of CO_2 is generally to lower the syngas quality, which is not desirable for applications such as FTS.

Fig. 18 presents the dependence on temperature of mole fraction of products for different molar ratios of CO_2 to fuel. As can be seen, for $\varphi_{\text{CO}_2} = 1.5$, the mole fractions of CO and H_2 are almost the same at ~ 31 and $\sim 30\%$ respectively. However, for $\varphi_{\text{CO}_2} = 0.05$, the mole fraction of H_2 is insignificantly higher at $\sim 42\%$, while that of CO is $\sim 32\%$. The mole fractions of H_2O and CO_2 are significantly lower at $\sim 15\%$ and $\sim 7\%$, respectively. Furthermore, for $\varphi_{\text{CO}_2} > 0.05$, the water gas shift reaction is suppressed, which decreases the syngas quality. However, as it was shown from the enthalpy balance, this results in a greater loss of enthalpy through the CO_2 product. Therefore, a value of $\varphi_{\text{CO}_2} = 0.05$, has a good balance of $\text{H}_2:\text{CO}$ ratio and total product.

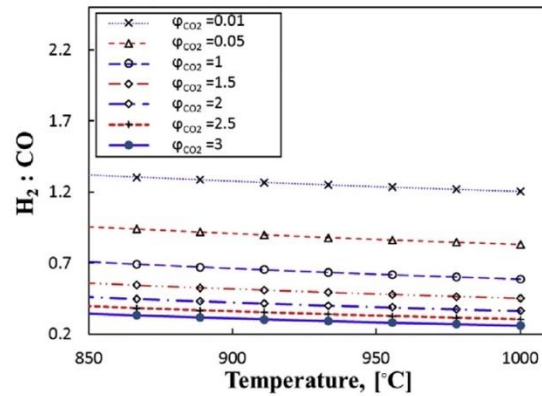


Fig. 17 – Calculated dependence of $\text{H}_2:\text{CO}$ ratio (syngas quality) on the temperature for various ratios of CO_2 to fuel. Other conditions are as per Table 2.

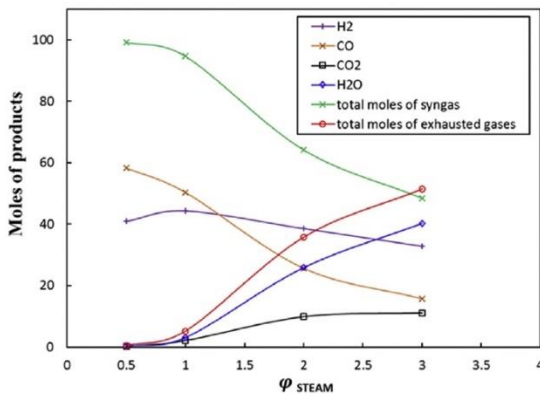


Fig. 16 – Calculated dependence of moles of products on steam to fuel ratio at 1000°C .

Influence of the operating parameters on fuel conversion

Fig. 19 presents the calculated dependence of fuel conversion on different operating parameters at 1000°C and 1 bar for the fuel reactor. Here the parameter M can be ϕ_{LOC} , ϕ_{steam} or ϕ_{CO_2} . It can be seen that from these parameters, the proposed LCLG is most sensitive to ϕ_{LOC} . That is, with an increase in ϕ_{LOC} , not only does the fuel conversion increase but the system also changes from the gasification mode to the mixed and complete combustion modes. In the transition regime (mixed combustion-gasification regime), the system simultaneously produces the CO, H_2 and CO_2 in various ratios that depend on the operating conditions. That is, the fraction of CO_2 can be less than, equivalent to or greater than that of CO. It is also notable that the fuel conversion increases linearly with an increase in ϕ_{steam} , albeit with a slope that is lower than that for ϕ_{LOC} . Furthermore, this LCLG process is least sensitive to ϕ_{CO_2} , but displays similar trends to the other parameters.

Overall, three different regimes were identified for the fuel conversion, which are as follows:

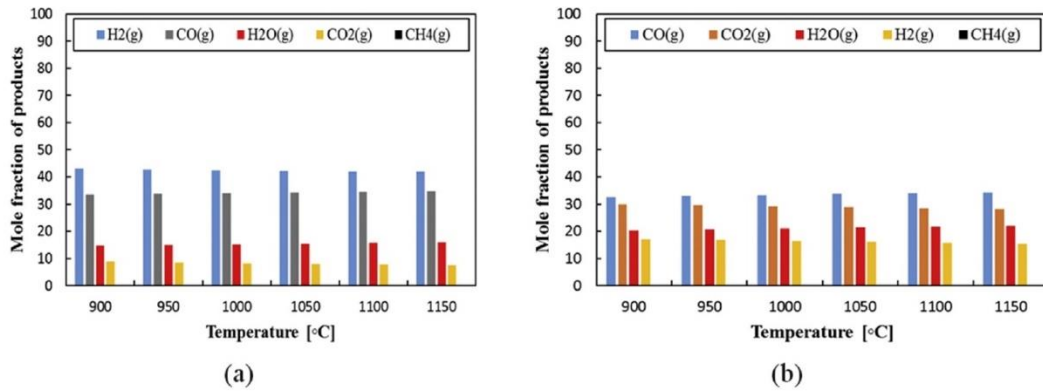


Fig. 18 – Calculated dependence of mole fraction of products on temperature for two different values of CO_2 to fuel ratios, a) CO_2 to fuel ratio = 0.05 b) CO_2 to fuel ratio = 1.5.

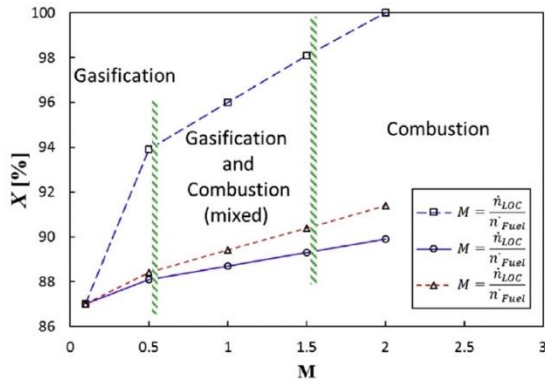


Fig. 19 – Calculated dependence of fuel conversion on different operating parameters including liquid oxygen carrier to fuel ratio, steam to fuel ratio and CO_2 to fuel ratio at $T = 1000\text{ °C}$ and $P = 1\text{ bar}$.

- Gasification regime, for which the main products are CO and H_2 , while $X < 88\%$,
- Mixed gasification-combustion regime, for which $88\% < X < 98\%$ and,
- Combustion for which $X > 98\%$.

Exergy partitioning

Fig. 20 presents the calculated dependence on temperature of net exergy in syngas for various values of ϕ_{LOC} . As can be seen, the net exergy partitioned in the syngas increases with an increase in the temperature, although only slightly. However, it decreases with an increase in ϕ_{LOC} , because the operating mode of the system changes to the chemical looping combustion regime. This decreases the quality of syngas and increases the exergy portioned in the vitiated air. That is, the operating conditions can be chosen to partition the exergy into the syngas or the hot vitiated air preferentially.

Fig. 21 presents the calculated dependence (on a LHV basis) of chemical exergy of the syngas on different operating parameters including ϕ_{LOC} , ϕ_{steam} and ϕ_{CO_2} at 900 °C and 1 bar . As can be seen, the quality of the syngas product and its exergy is maximised (to exceed 287 MJ/kmol) for $0.01 < \phi_{LOC} < 0.7$, $0 < \phi_{steam} < 3$ and $0.01 < \phi_{CO_2} < 0.06$. This regime, however, has the lowest potential to generate work from the hot vitiated air. On the other hand, the production of work with vitiated air is maximised for the regime $\phi_{LOC} > 1$, $\phi_{steam} < 1.7$ and $\phi_{CO_2} > 0.1$.

Power generation plant

Fig. 22 presents a schematic diagram of the supercritical steam power plant that was evaluated here to estimate the power generation potential from the outlet streams of the LCLG system. Flow rates, temperatures and pressures of the streams are given in Table 3. Water at 25 °C and 1 bar is fed

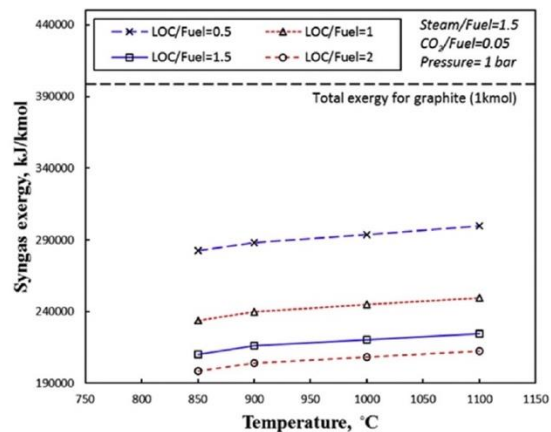


Fig. 20 – Calculated dependence on temperature of net exergy of the syngas product for various molar ratios of liquid oxygen carrier to fuel. The molar ratio of steam to fuel ratio is 1.5 and of CO_2 to fuel is 0.05. Other conditions are as per Table 2.

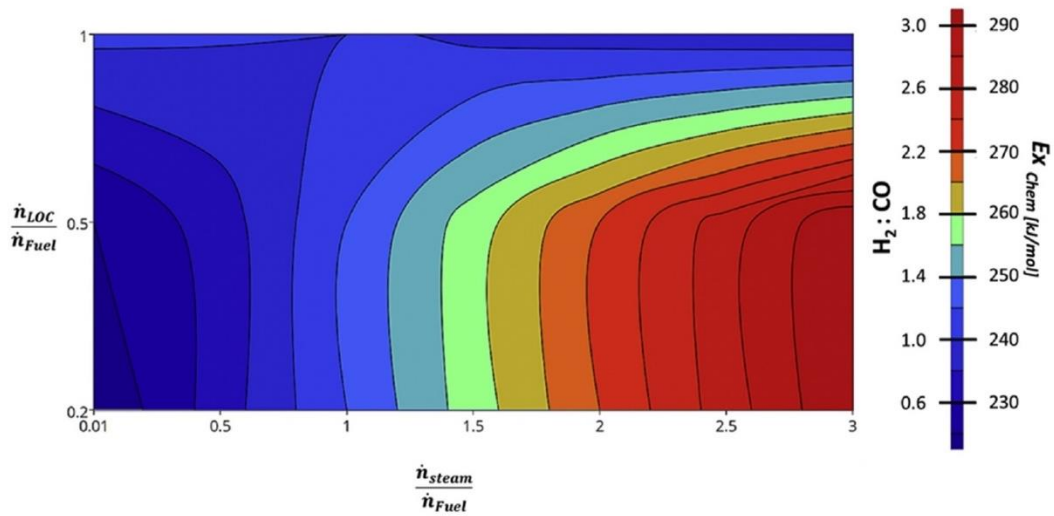


Fig. 21 – Calculated dependence of chemical exergy (MJ/kmol) of the syngas product on steam to fuel and liquid oxygen carrier to fuel ratios at $T = 900\text{ }^{\circ}\text{C}$ and at $\varphi_{\text{CO}_2} = 0.05$. The other conditions are as per Table 2.

into the pumps to produce high pressure water (streams 3 and 4), which are then fed to two shell and tube heat exchangers. In addition, the outlet streams from the air and fuel reactors (streams 11 and 12) are sent to heat exchangers to recover heat as steam (streams 5 and 6). The steam is then fed to two multi-stage steam turbines to generate work. The outlet from the turbines (Streams 7 and 8) is condensed in two condensers and recirculated. The details of the heat exchanger selected for the process are given in Table 3. The cold outlet stream of the heat exchanger (stream 13) is a cooled syngas, which is fed

to a gas to liquid process or Fischer-Tropsch unit to produce liquid fuels. A three-stage steam turbine was selected for the power block with inlet temperature to turbine of $511\text{--}600\text{ }^{\circ}\text{C}$ depending on the operating temperature of reactors in LCLG system. The steam turbine inlet temperature was chosen to be $600\text{ }^{\circ}\text{C}$, the temperature of stages 1 and 2 and 3 are $428\text{ }^{\circ}\text{C}$, $265\text{ }^{\circ}\text{C}$ and $143\text{ }^{\circ}\text{C}$, respectively and the pressure ratio for each stage is kept constant at 0.255. In addition, the heat loss from the coolers at each stage was 10.4% and the total efficiency of the turbine was 72% (see Table 4).

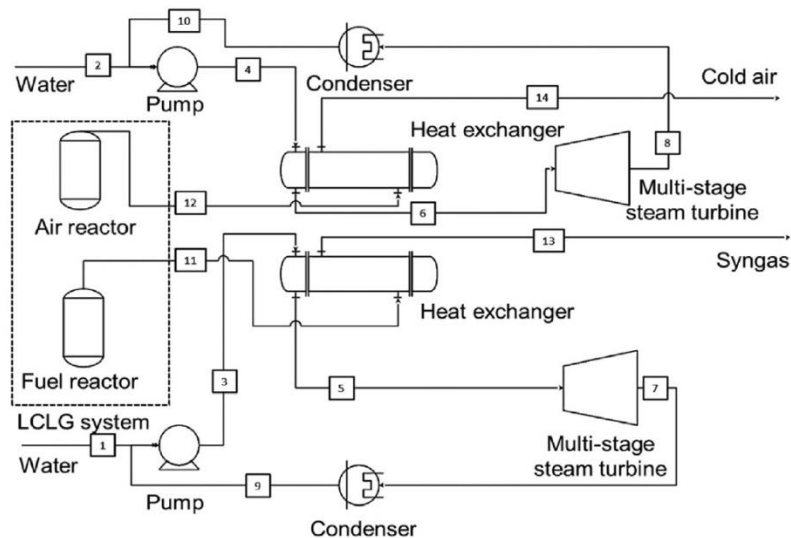


Fig. 22 – A schematic diagram of the proposed supercritical steam power plant connected to the outlet streams of the proposed LCLG system.

Table 3 – Flow rates and operating conditions of the streams in the proposed supercritical steam power plant.^b

Parameter ^a	1, 10	2, 9	3 ^c	4 ^c	5 ^d	6 ^d	7	8	11	12	13 ^e	14
T (°C) [21]	25	25	26.2	25.6	511–600	511–600	100	100	1000	1000	91.2	78.1
P(bar)	1	1	230	230	230	230	1	1	1	1	1	1
Flow rate ^a (kmol/hr) [31]	24590	16374	24590	16374	24590	16374	24590	16374	52158	34541	52158	34541
Enthalpy (MJ/hr)	-7.03	-4.681	-7.02	-4.67	-5.45	-4.67	-5.88	-3.91	-2.13	1.13	-3.7	0.07
Air ^a (kmol/hr)	0	0	0	0	0	0	0	0	0	34541	0	34541
Water ^a (kmol/hr)	24590	16374	24590	16374	24590	16374	24590	16374	0	0	0	0
CO ^a (kmol/hr)	0	0	0	0	0	0	0	0	34424	0	34424	0
H ₂ ^a (kmol/hr)	0	0	0	0	0	0	0	0	17733	0	17733	0

^a Temperature, pressure and flow rates are as per the conditions presented in Sarafraz et al.' work [21] and Taimoor et al.'s work [31] respectively. Uniquac was used as the thermodynamic model for liquid phase and for the gas phase modified Peng-Robinson equation of state was employed.

^b Obtained from the HSC chemistry simulations [39].

^c With the consideration of temperature rise and entropy generation in pumps.

^d Temperature of streams 5 and 6 depends on the operating temperature of the air and fuel reactors.

^e For H₂:CO-0.5.

First law efficiency

Fig. 23 presents the calculated dependence of the first law efficiency, Carnot efficiency and the net work on the operating temperature of the reactors. As can be seen, the output from the power plant increases with temperature. This is because the inlet temperature of the steam turbine depends strongly on the operating temperature of the LCLG reactors. At higher operating temperatures of the LCLG system, more thermal energy in form of enthalpy is transferred to power block by exhausted gases. This results in the increase in steam turbine temperature, which causes more work generation in the power block. For instance, when reactors operate at 900 °C, the inlet temperature of the steam turbine is 511 °C, while when the temperature of reactors is 1250 °C the inlet temperature of turbine is 645 °C. Thus, when reactors operate at 900 °C, the first law efficiency of power block is 26.1%, which can be increased up to 33.8% at operating temperature of reactors of 1250 °C. However, as discussed in the previous sections, higher temperatures decrease the quality of syngas and mole fraction of gaseous products. Therefore, there is a trade-off between the quality and quantity of produced syngas and the quantity of the produced work in the power plant. Moreover, the work generated with power cycle strongly depends on the circulation of LOC between reactors.

Exergy partitioning in LCLG

Fig. 24 represents the dependence of exergy efficiency of the LCLG system on ϕ_{LOC} . As can be seen, the exergy of fuel is partitioned between the syngas (As a chemical exergy) and power plant (as the generated work). With an increase in ϕ the exergy partitioned in the syngas decreases, while exergy transferred to work from the power plant increases. For

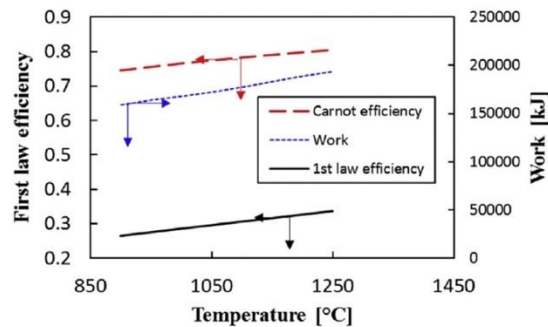


Fig. 23 – Calculated dependence of first law efficiency, Carnot efficiency generated work from the power plant on temperature of reactors for $\phi_{LOC} = 1.5$.

$0.01 < \phi_{LOC} < 0.5$, up to ~60% of total exergy is partitioned in syngas. However, for $\phi_{LOC} > 0.5$, exergy partitioned in syngas decreases, while more exergy is transferred to work. For example, for $\phi_{LOC} = 1$, the exergy efficiency of the power block can be as high as 56%, while it is 59%, when $\phi_{LOC} = 1.5$. So, for the case that high-quality syngas is targeted (e.g. H₂:CO = 2.05), work generation with power plant decreases. This is because at higher ϕ_{LOC} , more heat is exchanged between reactors and amount of exergy partitioned in vitiated air increases, however, at lower ϕ_{LOC} , oxygen is limited in the fuel reactor, which is more favourable for gasification reactions to proceed. Thus, the chemical exergy partitioned in the syngas product increases.

Table 4 – Specifications of the heat exchangers designed^a for the power plant.

Total Size (m)	Type	Mount	Number (bundle)	Surface area per unit, (m ²)	Shell number per unit	Shell side	Tube side	Fouling (m ² . K/W)	Tube material	Shell material
5.9	BEM	Horizontal	10	105141	40	Air/syngas	Water, (230 bar)	0.005	Carbon steel	Stainless steel

^a Designed with HTRI and Aspen heat exchanger design.

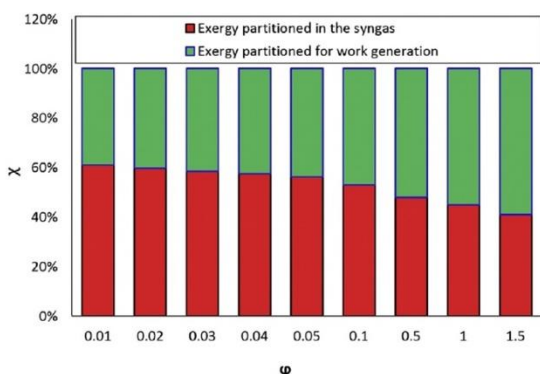


Fig. 24 – Dependence of exergy efficiency on molar ratio of LOC to fuel (ϕ_{LOC}) for the LCLG system excluded the power block.

Advantages and technical challenges

The proposed concept working with molten lead offers the potential to bypass some of the key challenges that have plagued chemical looping gasification with solid particles. It also offers the potential for hybridization with concentrated solar energy to drive the endothermic reactions. However, the use of molten lead introduces challenges associated with the solidification and high operating temperature operation. There are also some technical challenges, which need further investigations that come as follows:

- 1) A High operating temperature: To the best of our knowledge, no continuous flow reactor has been demonstrated for liquid metal oxides at high temperature. For lead oxide, a reactor must sustain temperatures higher than 900 °C.
- 2) Fluid circulation: A method is required to circulate the molten metal at high temperature. To the best of author's knowledge, no such system is commercially available.
- 3) Heat loss and solidification: For the proposed system, reactors, pipes and other units need to be designed to minimise heat losses and avoid solidification. Furthermore, the temperature difference between operating and freezing points should be sufficiently great, which is difficult to achieve with lead oxide.
- 4) Robust injection method: It is necessary to avoid local solidification near to the region where the gasifying agent and fuel are injected.
- 5) Pressure drop across the reactors: The relatively high values of density and viscosity of liquid metal oxides will result in a relatively high pressure drop from circulating fluid in the reactors. Further work will be required to assess the trade-off between pressure drop, which depends on the height of the liquid head, design of the reactor, and parameters such as conversion extent and flow rate. Similarly, the influence of gas holdup will need to be evaluated for the metal oxides.

- 6) Ash separation: In the present work, the assessment of the proposed system was performed for graphite as a surrogate for any carbonaceous fuel. In case of a fuel with impurity, it is expected that the impurities together with unreacted fuel form an ash layer. Experimental studies of Plevan et al. [32] and Eatwell-Hall et al. [33], demonstrated that ash can be separated from the molten metal due to density difference. Nevertheless, further experimental investigation is still required and a robust method for the separation of ash from the liquid metal oxides needs to be developed.

Conclusions

Significant thermodynamic potential was found for a new concept for the gasification of a solid fuel (assessed here for graphite as a surrogate) using molten lead in a chemical looping gasification with blended gasification agents of steam and/or CO₂. This system showed potential for the gasification of the carbon-containing feedstock and following conclusions were made:

- For the proposed system, the total enthalpy of the system can be positive (endothermic), zero (auto-thermal) and negative (exothermic) depending on ϕ_{LOC} , ϕ_{steam} and ϕ_{CO_2} . Furthermore, the system can be self-sustaining if the rate of circulation of molten lead oxide between reactors is sufficient. For molten lead oxide, the system is self-sustained if $\phi_{LOC} = 0.7$ and $\phi_{steam} = 2.5$, system is self-sustained.
- The molar ratios of LOC to fuel (ϕ_{LOC}), steam to fuel (ϕ_{steam}) and CO₂ to fuel (ϕ_{CO_2}) in the gasifier can be used to control the quality of syngas from the fuel reactor. Further flexibility is plausible from the blending of CO₂ as a secondary gasifying agent with steam to promote the water gas shift reactions and increase the quality of syngas. For example, for $0.01 < \phi_{LOC} < 0.7$, $0 < \phi_{steam} < 3$ and $0.01 < \phi_{CO_2} < 0.05$, a syngas quality of up to 2.8 can be achieved. However, this also introduces an enthalpy loss due to the excess steam and CO₂. While some enthalpy can be recovered from the steam. However, the recovery process from steam has low efficiency.
- The system offers potential for the power generation by connecting the LCLG system to a supercritical steam power cycle. The maximum first law efficiency and chemical exergy efficiency of the power cycle was 33.8% and 41%, respectively at 1250 °C and for $\phi_{LOC} = 1.5$.

Acknowledgement

Authors of this work gratefully acknowledge Australian Research Council (ARC) for the financial support through grant DP150102230. The first author of this work acknowledges "Australian Government Research Training Program Scholarship" for the financial supports.

Nomenclature

Ex_{chem}	Exergy, MJ/kmol
G	The Gibbs free energy, kJ
H	Enthalpy, kJ/mol
T	Temperature, °C
P	Pressure, bar
Q	Heat, kJ
W	Work, kJ
\dot{n}	Molar flow rate
X	Fuel conversion

Greek letters

φ	Operating parameter, see methodology section
Δ	Difference
η	First law efficiency
χ	Exergy efficiency

Subscripts

ox	Oxidation
red	Reduction
ST	Steam turbine

Abbreviations

AR	Air Reactor
Eq.	Equation
FR	Fuel reactor
LOC	Liquid oxygen carrier
LHV	Lower heating value, kJ/kmol or kJ/kg
ST	Steam turbine

REFERENCES

- García-Díez E, García-Labiano F, de Diego L, Abad A, Gayán P, Adánez J. Autothermal chemical looping reforming process of different fossil liquid fuels. *Int J Hydrogen Energy* 2017;42:13633–40.
- Ortiz M, Abad A, Luis F, García-Labiano F, Gayán P, Adánez J. Optimization of hydrogen production by chemical-looping auto-thermal reforming working with Ni-based oxygen-carriers. *Int J Hydrogen Energy* 2011;36:9663–72.
- Ortiz M, Luis F, Abad A, García-Labiano F, Gayán P, Adánez J. Hydrogen production by auto-thermal chemical-looping reforming in a pressurized fluidized bed reactor using Ni-based oxygen carriers. *Int J Hydrogen Energy* 2010;35:151–60.
- Pans MA, Abad A, Luis F, García-Labiano F, Gayán P, Adánez J. Optimization of H₂ production with CO₂ capture by steam reforming of methane integrated with a chemical-looping combustion system. *Int J Hydrogen Energy* 2013;38:11878–92.
- Adanez J, Abad A, Garcia-Labiano F, Gayan P, Luis F. Progress in chemical-looping combustion and reforming technologies. *Prog Energy Combust Sci* 2012;38:215–82.
- Kenarsari SD, Yang D, Jiang G, Zhang S, Wang J, Russell AG, et al. Review of recent advances in carbon dioxide separation and capture. *RSC Adv* 2013;3:22739–73.
- Qin L, Cheng Z, Guo M, Fan JA, Fan L-S. Morphology evolution and nanostructure of chemical looping transition metal oxide materials upon redox processes. *Acta Mater* 2017;124:568–78.
- San Pio M, Roghair I, Gallucci F, van Sint Annaland M. Investigation on the decrease in the reduction rate of oxygen carriers for chemical looping combustion. *Powder Technol* 2016;301:429–39.
- Liao C, Wu C, Yan Y. The characteristics of inorganic elements in ashes from a 1 MW CFB biomass gasification power generation plant. *Fuel Process Technol* 2007;88:149–56.
- Acharya B, Dutta A, Basu P. Chemical-looping gasification of biomass for hydrogen-enriched gas production with in-process carbon dioxide capture. *Energy Fuels* 2009;23:5077–83.
- Li F, Zeng L, Velazquez-Vargas LG, Yoscovits Z, Fan LS. Syngas chemical looping gasification process: bench-scale studies and reactor simulations. *AIChE J* 2010;56:2186–99.
- Fan L-S. *Chemical looping systems for fossil energy conversions*. John Wiley & Sons; 2011.
- Zafar Q, Mattisson T, Gevert B. Integrated hydrogen and power production with CO₂ capture using chemical-looping reforming redox reactivity of particles of CuO, Mn₂O₃, NiO, and Fe₂O₃ using SiO₂ as a support. *Ind Eng Chem Res* 2005;44:3485–96.
- Fan L, Li F, Ramkumar S. Utilization of chemical looping strategy in coal gasification processes. *Particuology* 2008;6:131–42.
- Tong A, Bayham S, Kathe MV, Zeng L, Luo S, Fan L-S. Iron-based syngas chemical looping process and coal-direct chemical looping process development at Ohio State University. *Appl Energy* 2014;113:1836–45.
- Anthony EJ. Solid looping cycles: a new technology for coal conversion. *Ind Eng Chem Res* 2008;47:1747–54.
- Chen W-H, Lin M-R, Leu T-S, Du S-W. An evaluation of hydrogen production from the perspective of using blast furnace gas and coke oven gas as feedstocks. *Int J Hydrogen Energy* 2011;36:11727–37.
- Suopajarvi H, Pongrácz E, Fabritius T. The potential of using biomass-based reducing agents in the blast furnace: a review of thermochemical conversion technologies and assessments related to sustainability. *Renew Sustain Energy Rev* 2013;25:511–28.
- Bafghi MS, Ito Y, Yamada S, Sano M. Effect of slag composition on the kinetics of the reduction of iron oxide in molten slag by graphite. *ISIJ Int* 1992;32:1280–6.
- Jafarian M, Arjomandi M, Nathan GJ. Thermodynamic potential of high temperature chemical looping combustion with molten iron oxide as the oxygen carrier. *Chem Eng Res Des* 2017;120:69–81.
- Sarafraz M, Jafarian M, Arjomandi M, Nathan G. Potential use of liquid metal oxides for chemical looping gasification: a thermodynamic assessment. *Appl Energy* 2017;195:702–12.
- Sarafraz M, Jafarian M, Arjomandi M, Nathan GJ. The relative performance of alternative oxygen carriers for liquid chemical looping combustion and gasification. *Int J Hydrogen Energy* 2017;42(26):16396–407.
- Coats HM. *Ash-separator*. Google patents; 1907.
- Wriedt H. The O–Pb (Oxygen-Lead) system. *J Phase Equil* 1988;9:106–27.
- Risold D, Nagata J-I, Suzuki R. Thermodynamic description of the Pb–O system. *J Phase Equil* 1998;19:213–33.
- Jak E, Degterov S, Hayes PC, Pelton AD. Thermodynamic optimisation of the systems Cao–Pb–O and Pbo–CaO–SiO₂. *Can Metall Q* 1998;37(1):41–7.
- Barin I. *Thermochemical data of pure substances*, thermochemical data of pure substances. Wiley-VCH; 1997.
- Melgar A, Perez JF, Laget H, Horillo A. Thermochemical equilibrium modelling of a gasifying process. *Energy Convers Manag* 2007;48:59–67.
- Li F, Zeng L, Fan L-S. Biomass direct chemical looping process: process simulation. *Fuel* 2010;89:3773–84.

- [30] Jafarian M, Arjomandi M, Nathan GJ. The energetic performance of a novel hybrid solar thermal & chemical looping combustion plant. *Appl Energy* 2014;132:74–85.
- [31] Taimoor AA, Muhammad A, Saleem W. Humidified exhaust recirculation for efficient combined cycle gas turbines. *Energy* 2016;106:356–66.
- [32] Plevan M, Geißler T, Abánades A, Mehravaran K, Rathnam R, Rubbia C, et al. Thermal cracking of methane in a liquid metal bubble column reactor: experiments and kinetic analysis. *Int J Hydrogen Energy* 2015;40:8020–33.
- [33] Eatwell-Hall R, Sharifi V, Swithenbank J. Hydrogen production from molten metal gasification. *Int J Hydrogen Energy* 2010;35:13168–78.
- [34] Sarafraz MM, Hormozi F. Comparatively experimental study on the boiling thermal performance of metal oxide and multi-walled carbon nanotube nanofluids. *Powder Technol* 2016;287:412–30.
- [35] Sarafraz MM, Arya A, Hormozi F, Nikkhah V. On the convective thermal performance of a CPU cooler working with liquid gallium and CuO/water nanofluid: a comparative study. *Appl Therm Eng* 2017;112:1373–81.
- [36] Kamalgharibi M, Hormozi F, Zamzamian SAH, Sarafraz MM. Experimental studies on the stability of CuO nanoparticles dispersed in different base fluids: influence of stirring, sonication and surface active agents. *Heat Mass Tran* 2016;52(1):55–62.
- [37] Salari E, Peyghambarzadeh SM, Sarafraz MM, Hormozi F. Boiling thermal performance of TiO₂ aqueous nanofluids as a coolant on a disc copper block. *Period Polytech Chem Eng* 2016;60(2):106.
- [38] Sarafraz MM, Nikkhah V, Nakhjavani M, Arya A. Fouling formation and thermal performance of aqueous carbon nanotube nanofluid in a heat sink with rectangular parallel microchannel. *Appl Therm Eng* 2017;123:29–39.
- [39] Roine A. HSC Chemistry 7.0 User's guide-chemical reaction and equilibrium software with extensive thermochemical database and flowsheet simulation [computer program]. Outotec; 2009. Retrieved from www.hsc-chemistry.com.

Chapter 6 Syngas production from biomass using liquid chemical looping gasification

6.1. Chapter overview

Biomass is a renewable source of energy with relatively sufficient lower heat value normally ranged (but not limited to) between $\sim 8\text{MJ/kg}$ and 22 MJ/kg . Gasification of biomass is CO_2 neutral since biomass in principle is a solid formed from solar energy stored in form of water and hydrocarbon. By combusting a biomass, CO_2 is released to environment. The previous assessments of the liquid chemical looping gasification systems (chapters 3-5) were based on a pure graphitic carbon as a feedstock. Hence, the LHV of fuel was ~ 1.5 to 2 times larger than a typical biomass. Therefore, the performance of the liquid chemical looping gasification needs to be assessed for gasifying a biomass as well.

The thermodynamic model developed in chapters 3 and 4 was improved in Aspen and HSC chemistry software packages so that the model can be applied to biomass gasification. Results represented in this chapter can contribute to the second and third objective of the project aiming at assessing the thermodynamic potential of liquid chemical looping gasification process for the biomass gasification.

Based on the previous assessments conducted in chapters 4 and 5, bismuth oxide shows a plausible thermodynamic potential for the liquid chemical looping gasification process with similar properties to lead oxide. It also has good heat and mass transfer characteristics in liquid phase, while it does not have any containment issue with refractory materials such as alumina. Four types of feedstock were analysed including almond hull, lignite, carbon and natural gas for the simulations. Thermodynamic operating regime was identified and the chemical performance of the process for all the fuels were assessed. For bismuth oxide, thermodynamic calculations showed that steam in values more than the stoichiometric value can fortify the quality of syngas to more than 4, meaning that the produced syngas can have wide applications

in fuel cells and energy production sector, since a large portion of exergy is partitioned in syngas. Also, depending on the content of hydrogen and carbon in feedstock, the composition of the syngas product varies and the net thermal energy demand of the system greatly changes. Comparing with other gasification systems, despite the excess steam requirements, the LCLG is thermodynamically plausible to produce syngas at high H₂: CO ratios. The economic viability of the process can be enhanced by using a robust and efficient condenser to recover the thermal energy from the outlet of the gasifier. The results of the work have been published in International Journal of Hydrogen Energy as follows:

M. M. Sarafraz, M. Jafarian, M. Arjomandi, G. J. Nathan, The thermo-chemical potential liquid chemical looping gasification with bismuth oxide, International Journal of Hydrogen Energy, 44, (2019) 8038-8050 (Sarafraz, Jafarian, Arjomandi, & Nathan, 2019b).

Statement of Authorship

Title of Paper	The thermo-chemical potential liquid chemical looping gasification with bismuth oxide
Publication Status	<input checked="" type="checkbox"/> Published <input type="checkbox"/> Accepted for Publication <input type="checkbox"/> Submitted for Publication <input type="checkbox"/> Unpublished and Unsubmitted work written in manuscript style
Publication Details	M. M. Sarafraz, M. Jafarian, M. Arjomandi, G. J. Nathan, The thermo-chemical potential liquid chemical looping gasification with bismuth oxide, International Journal of Hydrogen Energy, 44, (2019) 8038-8050

Principal Author

Name of Principal Author (Candidate)	Mohammad Mohsen Sarafraz				
Contribution to the Paper	- Research, collecting and analyzing data from different resources, developing thermodynamic models and analyzing the obtained data. - Providing the data, writing of the manuscript and production of original figures. - Correspondence with editor and reviewers including the production of all cover letters and rejoinder				
Overall percentage (%)	80%				
Certification:	This paper reports on original research I conducted during the period of my Higher Degree by Research candidature and is not subject to any obligations or contractual agreements with a third party that would constrain its inclusion in this thesis. I am the primary author of this paper.				
Signature	<table border="1" style="width: 100%;"> <tr> <td style="width: 80%;"></td> <td style="width: 20%;">Date</td> </tr> <tr> <td></td> <td>29, 11, 18</td> </tr> </table>		Date		29, 11, 18
	Date				
	29, 11, 18				

Co-Author Contributions

By signing the Statement of Authorship, each author certifies that:

- x. the candidate's stated contribution to the publication is accurate (as detailed above);
- xi. permission is granted for the candidate to include the publication in the thesis; and
- xii. the sum of all co-author contributions is equal to 100% less the candidate's stated contribution.

Name of Co-Author	Mehdi Jafarian				
Contribution to the Paper	- Supervision of the work, including the production of the manuscript - Participation in the development of the concepts and ideas presented in the manuscript - Evaluation and editing of the manuscript prior to submission				
Signature	<table border="1" style="width: 100%;"> <tr> <td style="width: 80%;"></td> <td style="width: 20%;">Date</td> </tr> <tr> <td></td> <td>29, 11, 18</td> </tr> </table>		Date		29, 11, 18
	Date				
	29, 11, 18				

Name of Co-Author	Maziar Arjomandi
-------------------	------------------

Chapter 6 Plausible application of bismuth oxide liquid chemical looping gasification towards the production of high-quality syngas

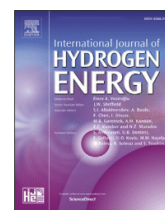
Chapter 6 Plausible application of bismuth oxide liquid chemical looping gasification towards the production of high-quality syngas

Contribution to the Paper	- Supervision of the work, including the production of the manuscript - Participation in the development of the concepts and ideas presented in the manuscript - Evaluation and editing of the manuscript prior to submission		
Signature		Date	29/11/18

Name of Co-Author	Graham Nathan		
Contribution to the Paper	- Supervision of the work, including the production of the manuscript - Participation in the development of the concepts and ideas presented in the manuscript - Evaluation and editing of the manuscript prior to submission		
Signature		Date	29/11/18

Available online at www.sciencedirect.com

ScienceDirect

journal homepage: www.elsevier.com/locate/he

The thermo-chemical potential liquid chemical looping gasification with bismuth oxide

M.M. Sarafraz^{*}, M. Jafarian, M. Arjomandi, G.J. Nathan

Centre for Energy Technology, School of Mechanical Engineering, University of Adelaide, SA 5005, Australia

ARTICLE INFO

Article history:

Received 12 December 2018

Received in revised form

7 February 2019

Accepted 9 February 2019

Available online 5 March 2019

Keywords:

Thermodynamic analysis

Liquid chemical looping gasification

Molten bismuth oxide

High-quality syngas

Thermo-chemical performance

ABSTRACT

The thermodynamic potential of a chemical looping gasification with liquid bismuth oxide for the production of syngas was assessed using thermo-chemical analysis. In the proposed process, the feedstock is partially oxidised by the molten bismuth in the gasification reactor and then oxidised with air in the air reactor. The motivation for this process is its potential to avoid both the technical challenges associated with the use of solid oxygen carriers in conventional chemical looping gasification systems (e.g. agglomeration and sintering of solid-state oxygen carrier) and the challenge of dilution of syngas with nitrogen that occurs in conventional air gasification systems. This revealed thermochemical potential to achieve a higher quality of syngas for a given amount of steam than has been reported previously for other gasification systems at a moderate temperature of 850 °C. Plausible approaches to address the research challenges that need to be overcome to implement the method are also identified, justifying further development of the technology.

© 2019 Hydrogen Energy Publications LLC. Published by Elsevier Ltd. All rights reserved.

Introduction

Gasification is a well-established method for the production of synthetic gas (referred to as syngas), which comprises primarily hydrogen and carbon monoxide with some CO₂, CH₄ and N₂ that can be either major or minor components depending on whether or not the gasification is performed with air. The production of syngas occurs via an endothermic process in which several reactions take place between a carbonaceous feedstock and a gasifying agent, which can be steam or CO₂ [1–3]. In most of the conventional gasification routes, an air blower or an air separation unit is used to supply the required oxygen for the partial oxidation of the fuel that provides heat for the endothermic gasification reactions. This, in turn, dilutes the syngas product with nitrogen [4,5].

Although for some processes, e.g. power blocks, the presence of nitrogen in the synthetic gas is acceptable, for liquid fuel synthesis, it is undesirable because it increases the cost of the downstream processing units. An air separation unit (ASU) is a well-established route to produce relatively high-quality syngas without nitrogen, although it adds to the final cost of the syngas [6]. Hence, considerable effort has been devoted to identify methods that avoid the need for an air separation unit for the syngas production. One plausible solution is to utilise the concentrated solar thermal energy (CST) to provide endothermic energy for the gasification process. However, while a range of technologies have been proposed to utilise CST for gasification, the technology is still pre-commercial [7,8], so that there is an ongoing need to identify alternative methods to produce syngas with high ratios of H₂: CO without nitrogen dilution and without the need for an ASU.

^{*} Corresponding author.

E-mail address: mohammadmohsen.sarafraz@adelaide.edu.au (M.M. Sarafraz).

<https://doi.org/10.1016/j.ijhydene.2019.02.081>

0360-3199/© 2019 Hydrogen Energy Publications LLC. Published by Elsevier Ltd. All rights reserved.

Previous assessments of Chemical Looping Gasification (CLG), an emerging process under development to produce syngas with redox reactions, has been undertaken with solid oxygen carriers (OC). This process is subjected to constraints in the composition of the solid oxygen carrier such as agglomeration and sintering at high temperatures, e.g. 1000 °C [9–15]. The extension of the process to CLG introduces to these already significant challenges, the additional ones of carbon deposition [2,16–24] and the need to separate the OC particles from any carry-over particles from the gasifier [25]. Additionally, these challenges decrease the reactivity of OC over the time [24,26–30], degrading the performance of the reactors [2]. For example, Acharya et al. [27] measured a ~40% reduction in the regeneration of oxygen carriers with successive cycling due to agglomeration, sintering and carbon deposition in a CLG process. Similarly, Li et al. [31] recorded an efficiency of a CLG as low as 50%, which was attributed to the challenges associated with the use of solid calcium oxide particles. Similar reports can be found elsewhere [2,12,26,32–34]. Liu et al. [35] conducted a set of experiments to evaluate the chemical performance of some calcium ferrites such as CaFe_2O_4 and $\text{Ca}_2\text{Fe}_2\text{O}_5$ in a CLG system using a fixed-bed reactor and thermo-gravimetric analyser. They demonstrated that calcium ferrites have lower oxidisability than Fe_2O_3 , require higher reduction temperature, while producing lower amount of CO_2 and higher amount of CO. The selectivity of calcium ferrites was also demonstrated using a fixed-bed tests. By injecting steam as the gasifying agent, the efficiency was enhanced from 82.95% (with Fe_2O_3) to 92.49% (with $\text{Ca}_2\text{Fe}_2\text{O}_5$) at 850 °C. They reported that the ferrite particles form an obvious agglomeration with a small number of pores, which might influence the reactivity over several cycles of experiments. Hematite oxygen carrier was also assessed in a CLG system at 900 °C for gasifying a sewage sludge as a feedstock. It was found that the quality of syngas can be as high as 0.55. Also, the presence of calcium and aluminium decreased the amount of agglomeration and sintering of the oxygen carrier [36]. It was also identified that the temperature must be kept as low as possible to minimise the reduction of hematite and the agglomeration. Hu et al. [37] conduct some pre-treatments on iron oxide as the oxygen carrier in a quartz reactor and found that microwave pre-treatment is a crucial step to CLG chemical performance. However, the higher power or the longer time in the process of microwave pre-treatment could not exhibit a better effect on CLG. They identified that microwave at 750 W and 60 s can be the optimal microwave pre-treatment power and time respectively to obtain a great reducibility of oxygen carrier, high chemical conversion efficiency, large product yield and reasonable lower heating value. This could minimise the rate of agglomeration and carbon deposition within the oxygen carrier.

In light of the above literature, extensive effort has been invested to seek to identify practical approaches to mitigate these disadvantages [2,16–24]. One proposal is the potential to use a liquid metal oxide instead of a solid one, which was introduced by Jafarian et al. [38] and Sarafraz et al. [39]. It has been proved that metal oxides and liquid metals can provide a plausible medium for heat and mass transfer at low, medium and high temperature conditions [78–89].

Sarafraz et al. [39] showed that it is thermodynamically plausible to produce a syngas with a molar ratio of H_2 : CO -2 via CLG of a liquid metal oxide. This composition is well-suited to application in Fischer-Tropsch and fuel cells. Nevertheless, the operating temperature was 1350 °C required for the reduction and/or oxidation of Cu/CuO , which brings other challenges of a relatively high risk of solidification and the challenge of containment, which require further investigation to resolve. In addition, this temperature is technically challenging to be supplied with a concentrating solar thermal system. To reduce these risks, lead, antimony and bismuth oxides were subsequently identified as thermodynamically plausible alternative candidates for liquid chemical looping gasification [40]. Their further investigation revealed lead oxide, as also being thermodynamically feasible to co-produce syngas and power [41]. However, more detailed assessment with bismuth and antimony oxides are yet to be undertaken. For this reason, the overall objective of the present investigation is to assess the thermodynamic potential of liquid bismuth oxide as an oxygen carrier for liquid chemical looping gasification with the view to lower the operating temperature to <1000 °C and to assess the influence of the type of the feedstock on the quality of the syngas. This offers a potential for utilizing a concentrated solar thermal energy system to maintain the temperature of the reactors. Also, the molar ratio of H_2 : CO > 2 was targeted to enhance the exergy partitioned in the syngas, while also improving the application of the produced syngas in Fischer-Tropsch and fuel cells. Likewise, bismuth oxide seems plausible to be used with refractories and its eutectics is currently used for cooling applications in nuclear reactors [42,43]. To the best of author's knowledge, there is no study in which the thermodynamic potential of a liquid metal such as bismuth oxide for producing a high-quality syngas with a liquid chemical looping gasification process is investigated. In particular, we also aim to assess the potential influence of different operating conditions such as temperature of reactor, the molar ratio of LOC to feedstock, the molar ratio of steam to feedstock and the type of feedstock on the quality of syngas.

Thermodynamic cycle and process concept

Fig. 1(a and b) present both the phase stability and thermodynamic phase diagram of the bismuth-oxygen system as a function of temperature and the partial pressure of the oxygen. As can be seen from Fig. 1a, three regions can be identified, namely pure Bi_2O_3 , pure Bi and a mixture of $\text{Bi}_2\text{O}_3/\text{Bi}$. These are coloured in blue, green and yellow, respectively in Fig. 1a. Each component can be found in the solid or liquid state and the boundary between solid and liquid phases is shown with a vertical dashed line (the melting temperature line).

Two potential operating points have been identified with which to assess the operation of the air and the fuel reactors. At operating point A, bismuth oxide is above its melting temperature and in the liquid state, while at operating point B, the material is in form of pure liquid bismuth. Both of these points are plausible for the LCLG, because the LOC remains in the liquid phase at all points between them and because the operating temperature of 850 °C is technically achievable with

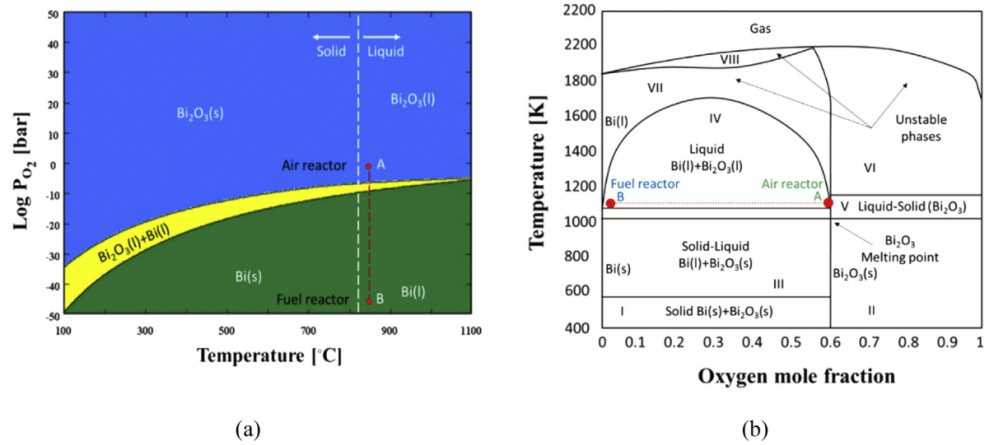


Fig. 1 – The operating conditions of the air and the fuel reactors of the proposed liquid chemical looping gasification in bismuth and its oxides shown on phase diagrams (a) partial pressure of oxygen as a function of temperature adapted from previous works [44,45], and b) temperature as a function of oxygen mole fraction adapted from the previous works [44,45].

the concentrated solar thermal energy and well within the operating range of high temperature steels.

Fig. 1b presents the thermodynamic phase diagram of the bismuth-oxygen binary mixture as a function of the partial pressure of oxygen. Eight different regions can be identified. In regions, I-II, the bismuth-oxygen thermodynamic system is in the solid state, which is unsuitable for the LCLG cycle. In regions III and V, the thermodynamic system is in the solid-liquid (two-phase) state, which is also undesirable for LCLG. Regions VI and VII are also not appropriate for the operation because bismuth-oxygen system is unstable in these regions. The two suitable operating points from Fig. 1a can be seen to lie in region III, which is thermodynamically favourable for LCLG. This region is in liquid state and comprises a mixture of bismuth oxide and pure bismuth. The temperature range between 850 °C and 1300 °C can potentially be explored in the future with the view to use CST to supply the required thermal energy. However, this is beyond the scope of the present investigation.

Fig. 2 presents a schematic diagram of the proposed LCLG process with molten bismuth oxide as the LOC. A plausible configuration for implementing the proposed process comprises two interconnected bubble reactors as proposed by Jafarian et al. [46]. In this proposed cycle, the gasification (fuel) reactor is used to reduce the LOC with a feedstock. Also, a gasifying agent is introduced into the fuel reactor not only to maintain the heat and mixing required for the gasification, but to enrich the gaseous products by adding hydrogen to syngas, while the air reactor is proposed to oxidise the LOC, resulting in the production of a high-temperature vitiated air. A plausible method to circulate the fluid through the two reactors is via bubbling, which can sufficient heat and mass transfer together with an efficient mixing and plausible contact between the gas-solid, gas-gas and gas-liquid phases [47–49]. Moreover, bubbling can generate a lift, which can be used to circulate a liquid [50,51]. To separate any ash, a disk ash separator has been identified as a plausible tool [46] due to the density difference between ash and liquid metal [52,53]. On this basis, the

forementioned cycle was chosen with which to assess the thermo-chemical performance for a series of different operating conditions. However, the technical and economic feasibility is beyond the scope of the present investigation.

Table 1 presents the operating conditions of each stream and reactors chosen for the thermodynamic assessment. Importantly, all streams and reactors are at atmospheric pressure, which greatly facilitates the technical feasibility of the process. The partial pressure of oxygen is altered by the addition of air or an oxygen carrier to the respective reactors.

The following assumptions were made to simplify the model: (1) it is assumed that the residence time is sufficient for the reactions to reach the equilibrium. This allows one to use the Gibbs minimisation modelling; (2) any heat losses to the

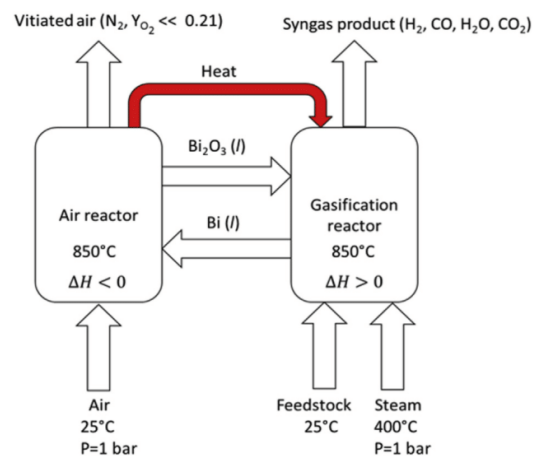


Fig. 2 – A schematic representation of the bismuth liquid chemical looping gasification system chosen for the present study.

Table 1 – Thermodynamic properties of the streams and reactor chosen for the assessment.

Stream/reactor	Temperature	Pressure (absolute)	Chemical components
Inlet streams			
Steam	400 °C	1 atm	H ₂ O
Feed	25 °C	1 atm	C
Air	25 °C	1 atm	O ₂ /N ₂
Outlet streams			
Vitiated air	850 °C	1 atm	N ₂ and O ₂ ^a
Product	850 °C	1 atm	H ₂ , CO, H ₂ O, CO ₂ , CH ₄ , N ₂ ^b
Reactors			
Fuel reactor	850 °C	1 atm	Bi, Bi ₂ O ₃ , C, H ₂ O
Air reactor	850 °C	1 atm	Bi, Bi ₂ O ₃ , O ₂ , N ₂

^a Trace.
^b Generated for the case of biomass feedstock but in negligibly small quantities.

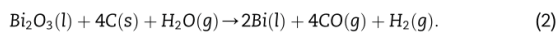
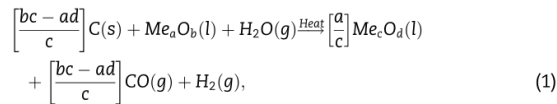
environment are negligible; (3) the circulation of LOC between the reactors is thermodynamically feasible and the energy required for the circulation is negligible; (4) the oxygen carrier does not solidify anywhere within the system since the operating temperature is sufficiently high; (5) Impurities inside the feedstock have no influence on the kinetics of the reactions; (6) The efficiency of the ash separator is 100% and ash is completely removed from the system; (7) no reactions occur between the walls of the reactor, pipes and devices.

Other details of the model, together with its validation, have been reported previously [39,54].

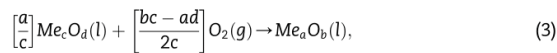
Methodology

The generalised reactions for the reduction (1) and the oxidation (3) of Me_aO_b to Me_cO_d with C_nH_{2m}O_p (as the fuel) and air are shown below for the gasification and the oxidation, respectively:

In the reduction (fuel) reactor:



In the oxidation (air) reactor:



The enthalpy and the net Gibbs free energy change of the reaction can be calculated as follows:

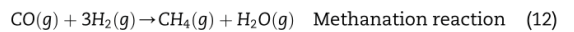
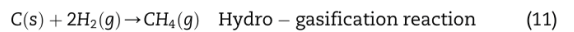
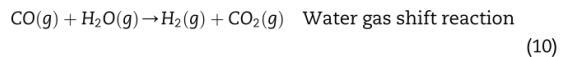
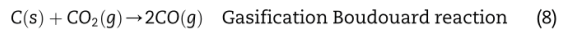
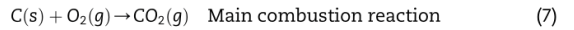
$$\Delta M_{red,r} = \sum_{prod} \Delta M_i^f(T) - \sum_{reac} \Delta M_i^f(T) \quad (5)$$

$$\Delta G_{red,r} = \sum_{prod} \Delta G_i^f(T) - \sum_{reac} \Delta G_i^f(T) \quad (6)$$

In Eq. (5), M is the Gibbs free energy and in Eq. (6), M is the enthalpy of reaction for the component i at a given

temperature. To identify whether or not these reactions occur spontaneously, their Gibbs free energy was calculated for any potential reactions. This approach was also utilised to identify any potential components that can be produced in the gasifier and in the air reactor [55–57]. A thermodynamic assessment for the operating temperature and an energetic performance of the process was conducted using thermochemical equilibrium analysis and thermochemical modelling [49,55,58–60]. The HSC chemistry and the Aspen plus software packages were employed for the energy and mass balance models following previous works [61,62].

In addition, the following reactions contribute to the gasification:



Molten bismuth and its primary oxide form a mixture, whose oxidative state is typically described by the notation Bi₂O₃(δ), where $n_{Bi_2O_3}(\delta) = n_{Bi_2O_3}(l) + n_{Bi}(l)$. A simple atom balance on the number of atoms of the bismuth oxide and bismuth considering $n_{Bi_2O_3}(\delta) = 1$, yields the following equations:

$$n_{Bi} = \frac{2x_o - 1}{x_o}, \quad (13)$$

$$n_{Bi_2O_3} = \frac{1 - x_o}{x_o}, \quad (14)$$

where,

$$x_o = \frac{n_o}{n_{Bi} + n_o}. \quad (15)$$

Here, x_o is the fraction of oxygen in the liquid bismuth oxide, n_o and n_{Bi} are the number of moles of oxygen and Bi in

the molten phase, respectively. The molar ratio of liquid oxygen carrier to fuel is defined from their molar flow rates as follows:

$$\phi_{\text{LOC}} = \frac{\dot{n}_{\text{LOC}}}{\dot{n}_{\text{feed}}} \quad (16)$$

Here, \dot{n} is the molar flow rate of the LOC and feedstock. For the present assessment, steam is used as the gasifying agent to maximise the molar ratio of H_2 : CO so that ϕ_{steam} is defined as:

$$\phi_{\text{steam}} = \frac{\dot{n}_{\text{steam}}}{\dot{n}_{\text{feedstock}}} \quad (17)$$

The molar ratio of the liquid oxygen carrier and of steam to their respective stoichiometric values are also referred to as the equivalence ratio of LOC and steam, and are defined as follows:

$$\phi_{\text{LOC}}^* = \frac{\phi_{\text{LOC}}}{\phi_{\text{LOC,stoich}}} \quad (18)$$

and

$$\phi_{\text{steam}}^* = \frac{\phi_{\text{steam}}}{\phi_{\text{steam,stoich}}} \quad (19)$$

Here, $\phi_{\text{LOC,stoich}}$ and $\phi_{\text{steam,stoich}}$ are the stoichiometric ratios of liquid oxygen carrier to fuel and steam to fuel, respectively. The extent of carbon conversion was assessed with the following equation:

$$X_c = \frac{\dot{n}_{\text{carbon, in}} - \dot{n}_{\text{carbon, out}}}{\dot{n}_{\text{carbon, in}}} \times 100 \quad (20)$$

The exergy efficiency is defined here as the ratio of exergy partitioned in the syngas to the total exergy of the inlet feedstock [63] as follows:

$$\chi = \frac{\dot{n}_{\text{syngas}} \cdot \text{LHV}_{\text{syngas}}}{\dot{n}_{\text{feed}} \cdot \text{LHV}_{\text{feed}}} \quad (21)$$

To assess the net enthalpy of reaction, an energy balance over the fuel and the air reactors was performed as follows:

$$\Delta H_{\text{AR}} = \sum_{\text{AR,out}} H - \sum_{\text{AR,in}} H \quad (22)$$

and

$$\Delta H_{\text{FR}} = \sum_{\text{FR,out}} H - \sum_{\text{FR,in}} H \quad (23)$$

and

$$Q = \Delta H_{\text{LCLG}} = \Delta H_{\text{AR}} - \Delta H_{\text{FR}} = \sum_{\text{prod.}} H - \sum_{\text{react.}} H \quad (24)$$

Here:

$$\sum_{\text{prod.}} H = \sum n_i \cdot \Delta H_i, \quad (25)$$

and

$$\sum_{\text{react.}} H = \sum n_i \cdot \Delta H_i. \quad (26)$$

Here n_i and ΔH_i are the number of moles the enthalpy of component i . The subscripts “prod” and “react” are abbreviations for “products” and “reactants”, respectively. Furthermore, Q is the net heat required for the LCLG process such that $Q < 0$ indicates an exothermic process, while $Q > 0$ shows an endothermic one. The operating conditions and the associated range of variations employed for the assessment are given in Table 2.

Results and discussion

The Gibbs free energy and enthalpy of the reaction

Fig. 3 presents the calculated dependence on temperature of the Gibbs free energy of the oxidation and the reduction (redox) reactions. As can be seen, the value of the Gibbs free energy is negative for both of these processes implying that both reactions are spontaneous and feasible over the range of temperatures assessed. It can also be seen that the Gibbs free energy for the reduction reaction decreases with an increase in the operating temperature of the reactors, so that the reaction is spontaneous at high temperatures. For example, $\Delta G_{\text{red}} = -400$ kJ at 817 °C, while $\Delta G_{\text{red}} = -520$ kJ at 1000 °C. In contrast, the value of ΔG of the oxidation reaction increases with an increase in the temperature. For example, ΔG is ~ -310 kJ at 817 °C while ΔG is ~ -230 kJ at 1000 °C. Nevertheless, the Gibbs free energy is plausibly low to drive the reactions within the temperature range of 817 °C–1200 °C.

Fig. 4 presents the calculated dependence on temperature of the enthalpy of reaction for the oxidation and the reduction reactions. As can be seen, the reduction reaction is endothermic ($\Delta H > 0$), while the oxidation reaction is exothermic ($\Delta H < 0$), consistent with the previous work [64]. Also, ΔH decreases slightly with an increase in the temperature from 310 kJ/mol at 817 °C to 290 kJ/mol at 1200 °C. In contrast, for the oxidation reaction, ΔH increases only slightly with an increase in temperature from approximately -550 kJ at 817 °C to approximately -500 kJ/mol at $T = 1000$ °C. Therefore, the thermal energy released in the oxidation reactor can potentially be transferred to the fuel reactor using the LOC, which will decrease the thermal load of the fuel reactor.

Table 2 – The reference conditions and the operating range of the parameters used in the modelling.

Parameter	T(°C) (Fuel and air reactors)	P _{O₂} (atm)	ϕ_{LOC} (mol/mol)	ϕ_{steam} (mol/mol)	Stoichiometric value	
					ϕ_{LOC} (mol/mol)	ϕ_{steam} (mol/mol)
Reference condition	900	0.21	1	1	0.25	0.25
Range (min-max)	817–1000	0–0.21	0.05–1.5	0.1–4		

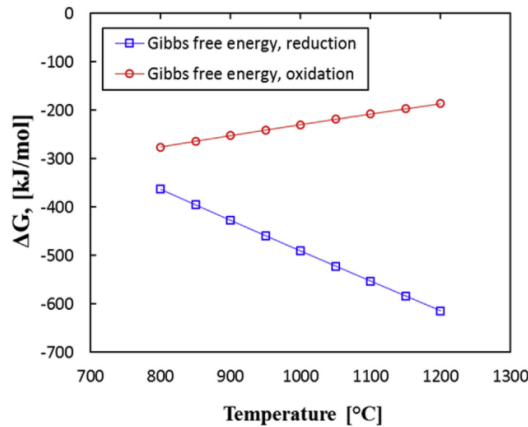


Fig. 3 – Calculated dependence of the Gibbs free energy on temperature for the redox reactions for the conditions shown in Tables 1 and 2.

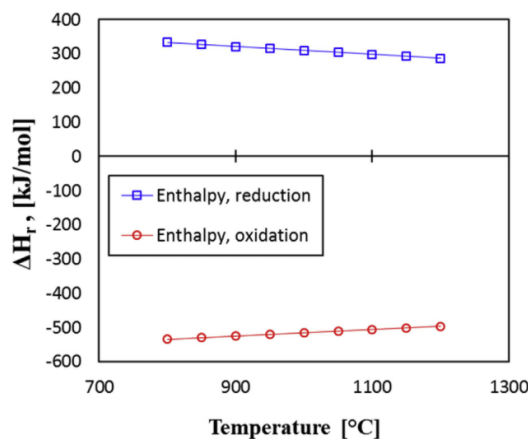


Fig. 4 – The calculated dependence of enthalpy of reaction on the temperature of the reduction and oxidation reactions.

Thermochemical equilibrium analysis

Fig. 5 presents the dependence on temperature of the molar composition of the gaseous products from the fuel reactor at the reference conditions (Table 1). Here, graphite is chosen as a surrogate for more complex fuels and to allow a direct comparison with the previous assessments by Sarafraz et al. using copper [39], lead and antimony oxides [54]. The reference (stoichiometric) molar ratio of steam to graphite is 0.25, which has been chosen to allow operation in the mixed gasification and combustion regime following Sarafraz et al. [54]. As can be seen, the molar percentages of CO increases with an increase in the temperature of the fuel reactor. This can be attributed to the Boudouard reaction, which is intensified with an increase in temperature. Also, the reverse water-gas shift reaction can proceed at high temperatures producing more

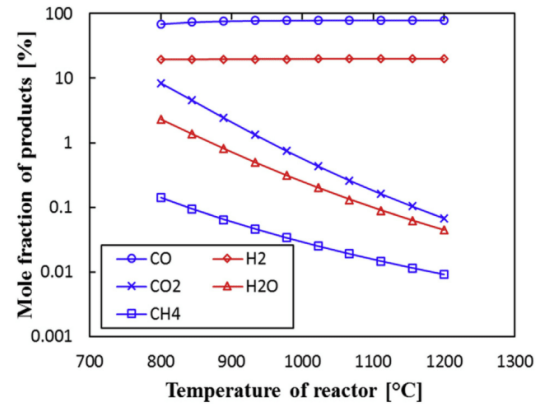


Fig. 5 – The calculated dependence of the mole fraction of products on the temperature of the gasification reactor for different components at stoichiometric value of steam and LOC. Conditions are as per Tables 1 and 2.

CO. For example, the mole percentage of CO is 68.4% at $T = 850$ °C and it is 78% at 1200 °C. The molar percentage of hydrogen is 20%, independent from the temperature of the reactor. It is worth noting that for the reference conditions, the quality of the syngas product is as low as ~ 0.25 for the stoichiometric value of the steam. However, the molar ratio of H₂: CO depends strongly on the value of ϕ_{LOC} and ϕ_{steam} as will be discussed in the following sections. Significantly, at $T > 817$ °C, the mole fraction of CH₄ is negligible throughout the investigated range of $T > 817$ °C, which is in accordance with our previous work [54].

Influence of the molar ratio of liquid oxygen carrier to feedstock

Fig. 6 presents the calculated dependence of H₂: CO on temperature for various ϕ_{LOC} and for $\phi_{steam} = 0.25$. Other operating conditions are as per Table 1. This shows that the molar ratio of H₂: CO decreases weakly with an increase in the operating temperature for low values of $\phi_{LOC} < 0.1$. However, the dependence on temperature increases with ϕ_{LOC} . Also, the molar ratio of H₂: CO decreases with an increase in ϕ_{LOC} . For example, at 1000 °C, the value of H₂: CO halves (from 1.1 to 0.58) as ϕ_{LOC} is increased from 0.01 to 0.7. Importantly, with an increase in the operating temperature of reactor, the H₂: CO ratio decreases non-linearly for all values of ϕ_{LOC} . Notably, higher temperatures reverse the water-gas shift reaction, which can consume more H₂ to decrease the quality of the syngas product. The water-gas shift reaction plausibly proceeds at lower temperature range. Hence, the ratio of H₂: CO is the highest for temperatures ranging from 817 °C to 900 °C.

Influence of the molar ratio of steam to feedstock

Fig. 7 presents the calculated dependence on temperature of the molar ratio of H₂: CO for various values of ϕ_{steam} and for $\phi_{LOC} = 0.25$ (the stoichiometric value) at $T = 1000$ °C. As can be seen, an increase in ϕ_{steam} increases the H₂: CO ratio. This can

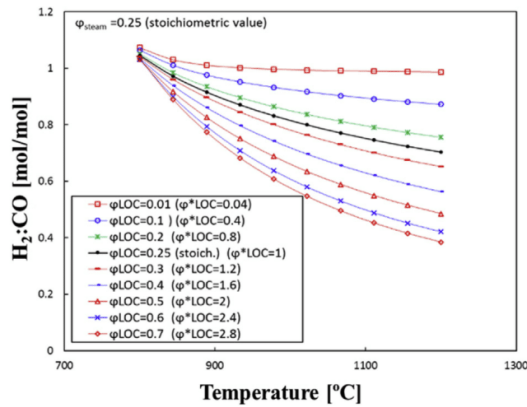


Fig. 6 – The calculated dependence on temperature of the molar ratio of H_2 : CO for various molar ratios of liquid oxygen carrier to fuel (ϕ_{LOC}^*) and for a fixed $\phi_{steam}^* = 0.25$ ($\phi_{steam}^* = 1$).

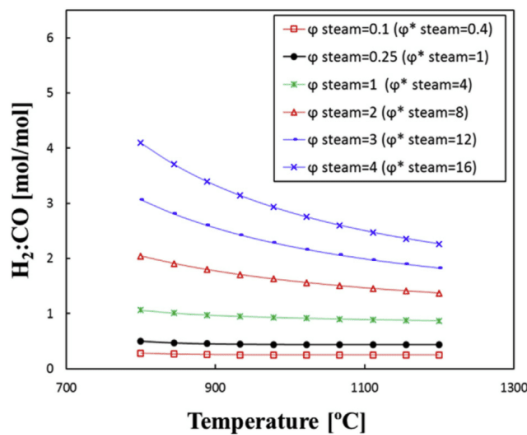


Fig. 7 – Dependence of calculated H_2 : CO ratio on temperature for various molar ratio of steam to fuel (ϕ_{steam}^*).

be attributed to the increased availability of hydrogen with the increase in the partial pressure of steam. It should be noted that a value of $\phi_{steam}^* = 8$ is required to achieve a syngas quality of ~ 3 , which implies the need for 700% excess steam and would be associated with a significant loss of enthalpy through the sensible and latent heat loss associated with the unreacted steam. Nevertheless, all of these reactions are achieved with temperatures as low as 817 °C, which are compatible with the operating temperature supplied by concentrated solar thermal energy. Likewise, this temperature is relatively low for other gasification processes. It is worth noting that the quality of syngas decreases with an increase in temperature. This is attributed to the increased significance of the Boudouard reaction together with the reverse water gas shift reaction, which produce CO, as noted above with reference to Fig. 5.

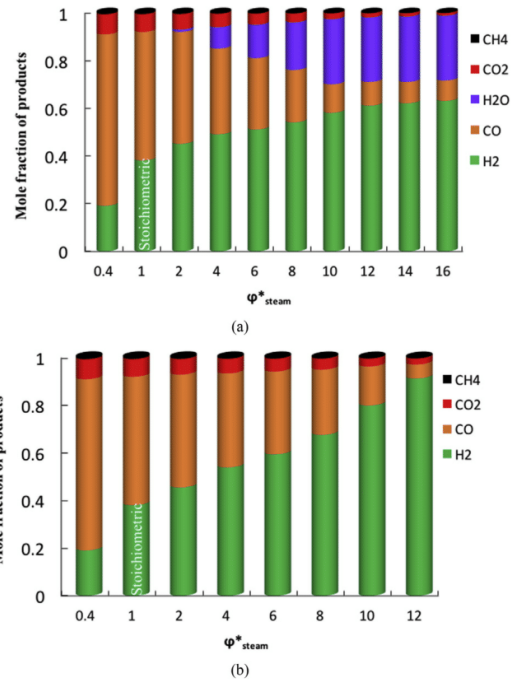


Fig. 8 – The calculated dependence of mole fraction of products on equivalence ratio of steam to fuel (ϕ_{steam}^*) at 850 °C, a) wet basis, b) dry basis.

Fig. 8(a and b) present the calculated dependence of mole fraction of products on ϕ_{steam}^* at 850 °C for the wet and dry syngas product. For $\phi_{steam}^* < 1$, CO is the main product of the system, followed by hydrogen. For example, for $\phi_{steam}^* = 0.4$, the mole fraction of CO is ~ 0.72 and that of H_2 is ~ 0.19 . For $\phi_{steam}^* = 1$ where steam is close to the stoichiometric value, the mole fractions of CO and H_2 are ~ 0.54 and ~ 0.38 , respectively. However, for large values of ϕ_{steam}^* , H_2 becomes the dominant product, with unconverted H_2O and CO as the secondary products. For example, for $\phi_{steam}^* = 16$, the mole fraction of H_2 is ~ 0.63 in wet syngas, which can be increased to 86.4% in dry syngas by condensing the unreacted steam. It is worth mentioning that condensing a gaseous mixture of non-condensable gases and a condensable gas is not efficient [65,66]. Therefore, the implementation of this condition would require the development of new technology to both condense the unconverted steam and recover the heat.

Energy balance of the process

Fig. 9 presents the dependence of the net thermal energy requirement for the LCLG process on ϕ_{LOC}^* and ϕ_{steam}^* for a temperature of 1000 °C, based on the input conditions shown in Table 1. As can be seen, the system can be configured to operate in either a gasification mode, with a net endothermic requirement, or in a mixed combustion mode with a net exothermic output, depending on the value of ϕ_{LOC}^* . That is because the net oxygen availability within

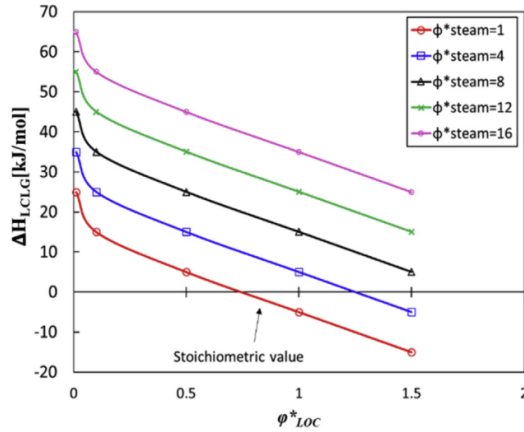


Fig. 9 – Dependence of the net thermal energy requirement of the system on both the stoichiometric molar ratio of liquid oxygen carrier to fuel and on the stoichiometric steam to fuel ratios (ϕ^*_{LOC} and ϕ^*_{steam}) for a temperature of 1000 °C.

the fuel reactor increases with an increase in ϕ^*_{LOC} , which leads to the complete oxidation of the fuel auto-thermal/combustion reactions. For example, for $\phi^*_{steam} = 1$ and $\phi^*_{LOC} = 1$, the net thermal energy requirement of the system is +25 kJ/mol, while it is -15 kJ/mol for $\phi^*_{LOC} = 1.5$. Likewise, the availability of steam increases with an increase in ϕ^*_{steam} to promote the hydro-gasification reaction, and also increases the requirement for excess (unreacted) steam, thereby increasing the net thermal energy requirement. This is in accordance with the results published previously in the literature [40,41].

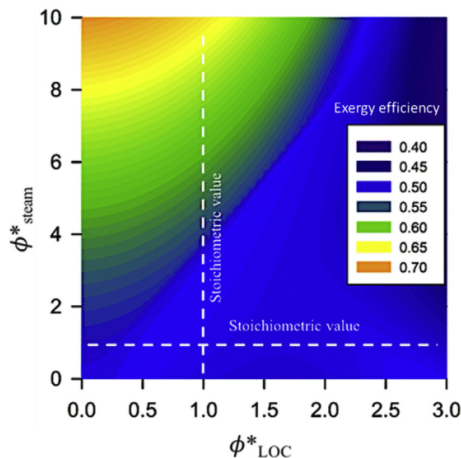


Fig. 10 – Dependence of the exergy efficiency of syngas production with LCLG, as defined by Eq. (21), on both the stoichiometric molar ratio of liquid oxygen carrier to fuel and on the stoichiometric steam to fuel ratios (ϕ^*_{LOC} and ϕ^*_{steam}) at 1000 °C.

Fig. 10 presents the dependence of the ratio of the exergy partitioned in the syngas to that of the total exergy of feedstock on ϕ^*_{LOC} and ϕ^*_{steam} at 1000 °C, as derived from Eq. (21). It can be seen that the net exergy efficiency depends strongly and inversely on ϕ^*_{LOC} and weakly on ϕ^*_{steam} . This is because an increase in ϕ^*_{LOC} changes the working mode from gasification to that of mixed gasification-combustion and combustion regions. In the gasification and mixed gasification-combustion regimes, the exergy partitioned in the syngas is higher than that for the combustion regime. Hence, with an increase in ϕ^*_{LOC} , the exergy partitioned in syngas reduces. For example, for $\phi^*_{LOC} = 0.5$, the exergy efficiency is ~70%, decreasing by ~65% for $\phi^*_{LOC} \sim 1$, while at $\phi^*_{LOC} = 3$, the exergy efficiency reaches ~40%. Hence, in the complete combustion regime, the exergy partitioned in the syngas approaches zero, while the majority of exergy is partitioned as a sensible heat in the form of H₂O or CO₂ in the vitiated air. To maximise the utilisation of exergy, the air reactor can be incorporated with a power block system (e.g. a combined cycle or gas turbine) to produce power, as assessed by Sarafraz et al. [41].

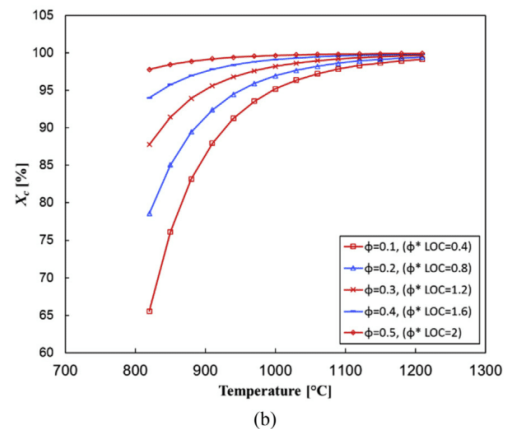
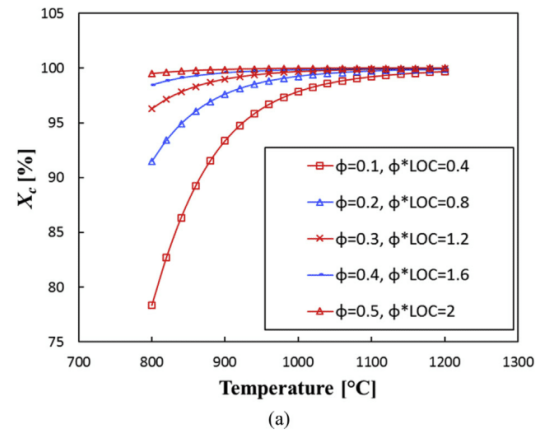


Fig. 11 – The calculated dependence on temperature of fuel conversion for various stoichiometric molar ratio of liquid oxygen carrier to fuel ratios (ϕ^*_{LOC}), a) $\phi^*_{steam} = 1$, b) $\phi^*_{steam} = 16$.

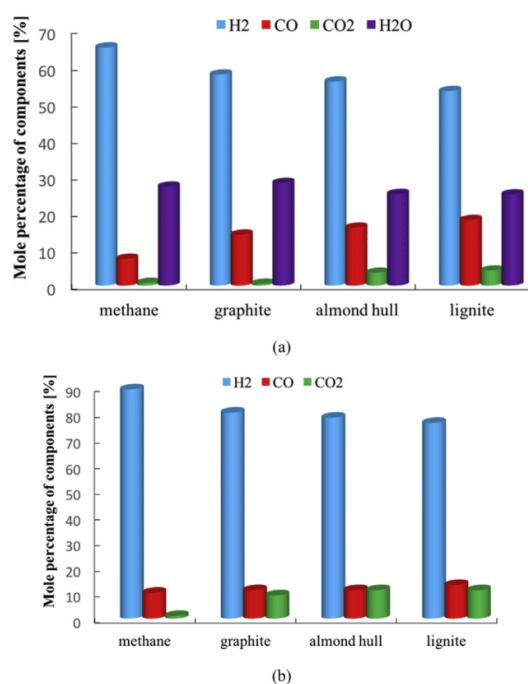


Fig. 12 – Dependence of the mole fraction of the gaseous products on the type of the feedstock shown, a) wet, b) dry. Conditions as per Table 1.

Carbon conversion

Fig. 11 (parts a and b) present the calculated dependence of carbon conversion of the feedstock on temperature for various values of ϕ_{LOC} and for two different ϕ_{steam}^* . As can be seen in Fig. 11a, X_c increases nonlinearly with an increase in either temperature or ϕ_{LOC} . For example, $X_c = 97\%$ can be achieved for either $\phi_{LOC}^* = 1.2$ and $850\text{ }^\circ\text{C}$ or at $\phi_{LOC}^* = 0.8$ and $950\text{ }^\circ\text{C}$.

This shows that there is something of a trade-off between the carbon conversion and both the exergy efficiency of syngas production (see Fig. 10), together with the net thermal energy requirement (Fig. 9). That is, for the case of $\phi_{steam}^* = 1.0$, a high carbon conversion is associated with the transition from the gasification to the combustion regime, which leads to the production of CO_2 and water. Fig. 11b presents the calculated dependence of X_c on temperature for various values of ϕ_{LOC} and at $\phi_{steam}^* = 16$. Once again, X_c increases with an increase in either temperature or ϕ_{LOC} and exhibits the same trade-off between the carbon conversion and the exergy

efficiency. For example, the high carbon conversion for $\phi_{steam}^* = 16$ is also associated with the transition from the gasification to the combustion regime and the production of CO_2 and water. Therefore, ϕ_{LOC} is a key parameter determining the operating regime, carbon conversion and the exergy of the syngas, while ϕ_{steam}^* only influences the exergy of the syngas by increasing the hydrogen content of the syngas product.

Influence of feedstock composition

Fig. 12 presents the calculated mole percentage of the main gaseous components of the syngas generated at $850\text{ }^\circ\text{C}$ from the selected feedstock with various carbon-hydrogen-oxygen compositions, whose proximate and ultimate analysis are reported in Table 2. The concentration of nitrogen is omitted, because it is less than 0.1% even for biomass. The values of ϕ_{LOC}^* and ϕ_{steam}^* are 0.4 and 12, respectively. Other conditions are as per Table 1. As can be seen, the largest mole fraction of hydrogen is produced from the reforming of natural gas (89%), followed by the gasification of graphite (80%), almond hulls (78%) and lignite (76%). The mole fraction of CO in the product is similar for all feedstock although it is slightly higher for lignite at 13%, than for the other feedstock (11%). This is consistent with the higher mole fraction of hydrogen in almond hull than in lignite (see Table 3). However, lignite has a higher mole fraction of carbon than does almond hull. Hence, the gasification of lignite produces more CO_2 and CO than does that of almond hull.

Advantages and disadvantages of the LCLG

Table 4 compares the LCLG operating characteristics with some other current technologies revealing the advantages and disadvantages of the LCLG. It can be seen that the LCLG process offers the following thermodynamic advantages relative to the other previously reported systems operated at the same temperature of $850\text{ }^\circ\text{C}$, with similar feedstock and similar amount of steam.

The identified disadvantages of the LCLG are mostly associated with the fabrication and operation of LCLG, and are as follows:

- 1) An increase in the syngas quality (H_2 : CO ratio) from 2.3 to 3.4 and a decrease in CO_2 production from 15% to ~2.1% relative to dual fluidised bed systems [69,72,73], a decrease in the syngas quality (H_2 : CO ratio) from 5 to 3.4 and a significant decrease in CO_2 production from 33% to 2.1% relative to circulating fluidised bed [70] and an increase in the syngas quality (H_2 : CO ratio) from 0.8 to 3.4 and a

Table 3 – Proximate and ultimate analysis of two different biomass feedstock assessed below [67].

No #	Feedstock	Proximate analysis			Ultimate analysis					
		Moisture content	Ash	Volatile matter	Fixed carbon	C	H	N	S	O
1	Almond hull ^a	8.18	5.67	67.22	18.93	42.7	5.48	1.06	0.04	36.82
2	Lignite [68]	1.2	14.8	41	43	49.8	3.3	1	0.5	27.7

^a https://www.nrel.gov/tredc/biomass_resource.html.

Table 4 – A comparison between the calculated operating characteristics of the LCLG process and other published steam gasification technologies.

Parameter	LCLG	Dual fluidised bed [69]	Circulating fluidised bed [70]	Downdraft gasifier [71]
Feedstock	Almond hull	Wood	Coal	Wood
Temperature (°C)	850	850	850	850
Pressure (bar)	1	1 ^a	1	1
$n_{\text{steam}}/n_{\text{carbon}}$ (mol/mol)	4	5.2	5	0.6–1.2
H ₂ : CO ratio (mol/mol)	3.4	2.3	~5	0.8
Steam in the product (vol. %)	34.19	35.76	51.2	Not reported
CO ₂ production (%)	~2.1	~15	~33	~30
Nitrogen dilution	–	–	+	+

^a Assumed value, actual value is not reported.

decrease in CO₂ from 30% to 2.1% relative to down-draft gasifiers [74]

- 2) Lack of a commercially-available system for injecting steam and feedstock into the gasifier; this system is not yet available, so would need to be developed.
- 3) Material constraints and containment issues to prevent corrosion of reactors and associated components (e.g. pipes), although, silicon carbide has already been identified as a potential containment materials for bismuth [75].
- 4) Circulation of liquid bismuth oxide between reactors: No complete system is commercially available, although there are some high-temperature pumps available [76,77].
- 5) Prevention of solidification of the liquid bismuth oxide within any piping and reactors: No complete system is commercially available. A trace heating may be required.
- 6) To achieve high-quality syngas, excess steam need to be injected to the gasifier. Hence, there is a large heat, exergy loss and steam loss (e.g. ~34.2% at 850 °C and $\phi_{\text{steam}} \sim 4$) through the excess steam leaving the gasifier. Thus, there is a need to develop an efficient but robust condenser not only to separate the excess steam from syngas product but to recover the heat to the process again to increase its thermal efficiency.

Conclusions

In conclusion, liquid chemical looping gasification with molten bismuth has been found to offer significant thermodynamic advantages over other published systems operating with similar feedstock at equivalent temperature and excess steam. These are high ratio of H₂: CO, lower production of CO₂ and the potential for the hybridisation of the process with solar thermal energy. However, several challenges need to be overcome to access the advantages of the system. The most significant challenges are the lack of an established method with which to circulate the molten metal and the absence of a proven method with which to contain the material. Nevertheless, plausible approaches with which to overcome these challenges have been identified to foster further research on this topic.

The thermodynamic analysis quantified the dependence of the molar ratio of H₂: CO in the gaseous products on the molar ratio of liquid oxygen carrier to feedstock (ϕ_{LOC}) and steam to feedstock (ϕ_{steam}). This found that the relatively

low values of ϕ_{LOC} and high values of ϕ_{steam} are thermodynamically favoured to yield high-quality syngas production. Furthermore, while the production of high-quality syngas requires excess steam consumption (e.g. a H₂: CO of 3–4 requires ~600%–800% excess steam), the amount is less than those of reported for some gasification processes under similar operating conditions.

Of the type of feedstock assessed, CH₄ showed the potential to produce the highest-quality of syngas with H₂: CO is 7 (wet basis), followed by graphite, almond hull and lignite for which the molar ratios are 4, 3 and 2.6, respectively for $\phi_{\text{LOC}}^* = 0.4$ and $\phi_{\text{steam}}^* = 16$. Also, a thermodynamic assessment of the carbon conversion of graphite revealed that the fuel conversion can be higher than 0.9 for $\phi_{\text{LOC}} > 0.2$ and $T > 850$ °C.

Finally, the trade-off between carbon conversion and both the exergy efficiency of syngas production and the net thermal energy requirement for the LCLG was calculated. Thus, to achieve the complete conversion of carbon under the range of conditions assessed here, the system must be operated in the combustion mode rather than the gasification model.

Acknowledgement

The authors gratefully acknowledge the Australian Research Council (ARC) for its financial support through grant DP150102230 and the Australian Renewable Energy Agency (ARENA) for its support through the Australian Solar Thermal Research Initiative (ASTRI). The first author of this work acknowledges the “Australian Government Research Training Program Scholarship” for its financial supports.

Nomenclature

A	Area, m ²
Ex _{chem}	Exergy, MJ/kmol
g	Gas
G	The Gibbs free energy, kJ
H	Enthalpy, kJ/mol
l	Liquid
n	Number of moles, mol
P	Pressure, bar
Q	Heat, kJ
s	Solid

T	Temperature, °C
W	Work, kJ
\dot{n}	Molar flow rate
x_o	Mole fraction of oxygen
X_c	Feedstock conversion

Greek letters

φ	Operating parameter, see methodology section
Δ	Difference
χ	Exergy efficiency

Subscripts

c	Carbon
ox	Oxidation
red	Reduction

Abbreviations

AR	Air Reactor
Eq	Equation
FR	Fuel reactor
LOC	Liquid oxygen carrier
LHV	Lower heating value, kJ/kmol or kJ/kg
Me	Metal oxide
Prod	Products
Reac	Reactant
Red	reduction

REFERENCES

- [1] Wilhelm D, Simbeck D, Karp A, Dickenson R. Syngas production for gas-to-liquids applications: technologies, issues and outlook. *Fuel Process Technol* 2001;71:139–48.
- [2] Adanez J, Abad A, Garcia-Labiano F, Gayan P, Luis F. Progress in chemical-looping combustion and reforming technologies. *Prog Energy Combust Sci* 2012;38:215–82.
- [3] Martínez JD, Mahkamov K, Andrade RV, Lora EES. Syngas production in downdraft biomass gasifiers and its application using internal combustion engines. *Renew Energy* 2012;38:1–9.
- [4] H. Springmann, High pressure gasification of coal using nitrogen dilution of waste gas from steam generator, in, Google Patents, 1977.
- [5] Lu Z, Jafarian M, Arjomandi M, Nathan GJ. Particle-Scale investigation of heat transfer in radiation-driven char gasification. *Chem Eng Technol* 2016;39:1903–11.
- [6] Doctor R, Molburg J, Thimmapuram P. Oxygen-blown gasification combined cycle: carbon dioxide recovery, transport, and disposal. *Energy Convers Manag* 1997;38:S575–80.
- [7] Piatkowski N, Steinfeld A. Solar-driven coal gasification in a thermally irradiated packed-bed reactor. *Energy Fuels* 2008;22:2043–52.
- [8] Simeone E, Siedlecki M, Nacken M, Heidenreich S, De Jong W. High temperature gas filtration with ceramic candles and ashes characterisation during steam–oxygen blown gasification of biomass. *Fuel* 2013;108:99–111.
- [9] Wang J, Zhao H. Evaluation of CaO-decorated Fe₂O₃/Al₂O₃ as an oxygen carrier for in-situ gasification chemical looping combustion of plastic wastes. *Fuel* 2016;165:235–43.
- [10] Penthor S, Mayer K, Kern S, Kitzler H, Wöss D, Pröll T, Hofbauer H. Chemical-looping combustion of raw syngas from biomass steam gasification—Coupled operation of two dual fluidized bed pilot plants. *Fuel* 2014;127:178–85.
- [11] Jerndal E, Mattisson T, Lyngfelt A. Thermal analysis of chemical-looping combustion. *Chem Eng Res Des* 2006;84:795–806.
- [12] Zafar Q, Mattisson T, Gevert B. Integrated hydrogen and power production with CO₂ capture using chemical-looping reforming redox reactivity of particles of CuO, Mn₂O₃, NiO, and Fe₂O₃ using SiO₂ as a support. *Ind Eng Chem Res* 2005;44:3485–96.
- [13] Brandvoll Oy, Bolland O. Inherent CO₂ capture using chemical looping combustion in a natural gas fired power cycle. In: ASME turbo expo 2002: power for land, sea, and air. American Society of Mechanical Engineers; 2002. p. 493–9.
- [14] Huang Z, Zhang Y, Fu J, Yu L, Chen M, Liu S, He F, Chen D, Wei G, Zhao K. Chemical looping gasification of biomass char using iron ore as an oxygen carrier. *Int J Hydrog Energy* 2016;41:17871–83.
- [15] Gopaul SG, Dutta A, Clemmer R. Chemical looping gasification for hydrogen production: a comparison of two unique processes simulated using ASPEN Plus. *Int J Hydrog Energy* 2014;39:5804–17.
- [16] Jafarian M, Arjomandi M, Nathan GJ. A hybrid solar and chemical looping combustion system for solar thermal energy storage. *Appl Energy* 2013;103:671–8.
- [17] Jafarian M, Arjomandi M, Nathan GJ. A hybrid solar chemical looping combustion system with a high solar share. *Appl Energy* 2014;126:69–77.
- [18] Jafarian M, Arjomandi M, Nathan GJ. The energetic performance of a novel hybrid solar thermal & chemical looping combustion plant. *Appl Energy* 2014;132:74–85.
- [19] Tanner J, Bhattacharya S. Kinetics of CO₂ and steam gasification of Victorian brown coal chars. *Chem Eng J* 2016;285:331–40.
- [20] Patra TK, Sheth PN. Biomass gasification models for downdraft gasifier: a state-of-the-art review. *Renew Sustain Energy Rev* 2015;50:583–93.
- [21] Chan FL, Tanksale A. Review of recent developments in Ni-based catalysts for biomass gasification. *Renew Sustain Energy Rev* 2014;38:428–38.
- [22] Ge H, Guo W, Shen L, Song T, Xiao J. Biomass gasification using chemical looping in a 25kW th reactor with natural hematite as oxygen carrier. *Chem Eng J* 2016;286:174–83.
- [23] Adanez J, Gayan P, Celaya J, de Diego LF, Garcia-Labiano F, Abad A. Chemical looping combustion in a 10 kWth prototype using a CuO/Al₂O₃ oxygen carrier: effect of operating conditions on methane combustion. *Ind Eng Chem Res* 2006;45:6075–80.
- [24] Li F, Kim HR, Sridhar D, Wang F, Zeng L, Chen J, Fan L-S. Syngas chemical looping gasification process: oxygen carrier particle selection and performance. *Energy Fuels* 2009;23:4182–9.
- [25] Liao C, Wu C, Yan Y. The characteristics of inorganic elements in ashes from a 1 MW CFB biomass gasification power generation plant. *Fuel Process Technol* 2007;88:149–56.
- [26] Fan L, Li F, Ramkumar S. Utilization of chemical looping strategy in coal gasification processes. *Particuology* 2008;6:131–42.
- [27] Acharya B, Dutta A, Basu P. Chemical-looping gasification of biomass for hydrogen-enriched gas production with in-process carbon dioxide capture. *Energy Fuels* 2009;23:5077–83.
- [28] Anheden M, Svedberg G. Exergy analysis of chemical-looping combustion systems. *Energy Convers Manag* 1998;39:1967–80.

- [29] Zevenhoven-Onderwater M, Backman R, Skrifvars B-J, Hupa M. The ash chemistry in fluidised bed gasification of biomass fuels. Part I: predicting the chemistry of melting ashes and ash-bed material interaction. *Fuel* 2001;80:1489–502.
- [30] Florin N. Calcium looping technologies for gasification and reforming, calcium and chemical looping technology for power generation and carbon dioxide (CO₂) capture. 2015.
- [31] Li F, Zeng L, Velazquez-Vargas LG, Yoscovits Z, Fan L.S. Syngas chemical looping gasification process: bench-scale studies and reactor simulations. *AIChE J* 2010;56:2186–99.
- [32] Fan L-S. *Chemical looping systems for fossil energy conversions*. John Wiley & Sons; 2011.
- [33] Tong A, Bayham S, Kathe MV, Zeng L, Luo S, Fan L-S. Iron-based syngas chemical looping process and coal-direct chemical looping process development at Ohio State University. *Appl Energy* 2014;113:1836–45.
- [34] Anthony EJ. Solid looping cycles: a new technology for coal conversion. *Ind Eng Chem Res* 2008;47:1747–54.
- [35] Liu G, Liao Y, Wu Y, Ma X. Application of calcium ferrites as oxygen carriers for microalgae chemical looping gasification. *Energy Convers Manag* 2018;160:262–72.
- [36] Huang Z, Xu G, Deng Z, Zhao K, He F, Chen D, Wei G, Zheng A, Zhao Z, Li H. Investigation on gasification performance of sewage sludge using chemical looping gasification with iron ore oxygen carrier. *Int J Hydrog Energy* 2017;42:25474–91.
- [37] Hu Z, Ma X, Jiang E. The effect of microwave pretreatment on chemical looping gasification of microalgae for syngas production. *Energy Convers Manag* 2017;143:513–21.
- [38] Jafarian M, Arjomandi M, Nathan GJ. Thermodynamic potential of high temperature chemical looping combustion with molten iron oxide as the oxygen carrier. *Chem Eng Res Des* 2017;120:69–81.
- [39] Sarafraz M, Jafarian M, Arjomandi M, Nathan G. Potential use of liquid metal oxides for chemical looping gasification: a thermodynamic assessment. *Appl Energy* 2017;195:702–12.
- [40] Sarafraz M, Jafarian M, Arjomandi M, Nathan GJ. The relative performance of alternative oxygen carriers for liquid chemical looping combustion and gasification. *Int J Hydrog Energy* 2017;42:16396–407.
- [41] Sarafraz M, Jafarian M, Arjomandi M, Nathan G. Potential of molten lead oxide for liquid chemical looping gasification (LCLG): a thermochemical analysis. *Int J Hydrog Energy* 2018;43:4195–210.
- [42] Gromov B, Belomitcev YS, Yefimov E, Leonchuk M, Martinov P, Orlov YI, Pankratov D, Pashkin YG, Toshinsky G, Chekunov V. Use of lead-bismuth coolant in nuclear reactors and accelerator-driven systems. *Nucl Eng Des* 1997;173:207–17.
- [43] Weeks J. *Lead, bismuth, tin, and their alloys as nuclear coolants*. Upton, NY: Brookhaven National Lab.; 1971.
- [44] Risold D, Hallstedt B, Gauckler L, Lukas H, Fries S. The bismuth-oxygen system. *J Phase Equil* 1995;16:223.
- [45] Hallstedt B, Risold D, Gauckler LJ. Thermodynamic evaluation of the Bi-Cu-O system. *J Am Ceram Soc* 1996;79:353–8.
- [46] Mehdi Jafarian MA, Nathan Graham. Thermodynamic potential of molten copper oxide for high temperature solar energy storage and oxygen production. *Applied Energy*; 2017. Under-review.
- [47] Michaelides E. *Particles, bubbles & drops: their motion, heat and mass transfer*. World Scientific; 2006.
- [48] Yin J, Kang X, Qin C, Feng B, Veeraragavan A, Saulov D. Modeling of CaCO₃ decomposition under CO₂/H₂O atmosphere in calcium looping processes. *Fuel Process Technol* 2014;125:125–38.
- [49] Adiya ZIS, Dupont V, Mahmud T. Chemical equilibrium analysis of hydrogen production from shale gas using sorption enhanced chemical looping steam reforming. *Fuel Process Technol* 2017;159:128–44.
- [50] Drandev S, Penev KI, Karamanev D. Study of the hydrodynamics and mass transfer in a rectangular air-lift bioreactor. *Chem Eng Sci* 2016;146:180–8.
- [51] Hosseini NS, Shang H, Ross GM, Scott JA. Comparative analysis of top-lit bubble column and gas-lift bioreactors for microalgae-sourced biodiesel production. *Energy Convers Manag* 2016;130:230–9.
- [52] H.M. Coats, Ash-separator, in, *Google Patents*, 1907.
- [53] Y. John, Multiple element vortical whirl ash separator, in, *Google Patents*, 1952.
- [54] Sarafraz MM, Jafarian M, Arjomandi M, Nathan GJ. The relative performance of alternative oxygen carriers for liquid chemical looping combustion and gasification. *Int J Hydrog Energy* 2017;42(26):16396–407.
- [55] Wang K, Yu Q, Qin Q, Hou L, Duan W. Thermodynamic analysis of syngas generation from biomass using chemical looping gasification method. *Int J Hydrog Energy* 2016;41:10346–53.
- [56] Freitas AC, Guirardello R. Comparison of several glycerol reforming methods for hydrogen and syngas production using Gibbs energy minimization. *Int J Hydrog Energy* 2014;39:17969–84.
- [57] Demidov D, Mishin I, Mikhailov M. Gibbs free energy minimization as a way to optimize the combined steam and carbon dioxide reforming of methane. *Int J Hydrog Energy* 2011;36:5941–50.
- [58] Sefidari H, Lindblom B, Wiinikka H, Nordin L-O, Lennartsson A, Mouzon J, Bhuiyan IU, Öhman M. The effect of disintegrated iron-ore pellet dust on deposit formation in a pilot-scale pulverized coal combustion furnace. Part II: thermochemical equilibrium calculations and viscosity estimations. *Fuel Processing Technology*; 2018.
- [59] Yakaboylu O, Harinck J, Smit K, De Jong W. Testing the constrained equilibrium method for the modeling of supercritical water gasification of biomass. *Fuel Process Technol* 2015;138:74–85.
- [60] Moradian F, Tchoffer PA, Davidsson KO, Pettersson A, Backman R. Thermodynamic equilibrium prediction of bed agglomeration tendency in dual fluidized-bed gasification of forest residues. *Fuel Process Technol* 2016;154:82–90.
- [61] Melgar A, Perez JF, Laget H, Horillo A. Thermochemical equilibrium modelling of a gasifying process. *Energy Convers Manag* 2007;48:59–67.
- [62] Li F, Zeng L, Fan L-S. Biomass direct chemical looping process: process simulation. *Fuel* 2010;89:3773–84.
- [63] Seyitoglu S, Dincer I, Kilicarslan A. Energy and exergy analyses of hydrogen production by coal gasification. *Int J Hydrog Energy* 2017;42:2592–600.
- [64] Mattisson T, Johansson M, Lyngfelt A. Multicycle reduction and oxidation of different types of iron oxide particles application to chemical-looping combustion. *Energy Fuels* 2004;18:628–37.
- [65] Al-Diwany H, Rose J. Free convection film condensation of steam in the presence of non-condensing gases. *Int J Heat Mass Transf* 1973;16:1359–69.
- [66] Kroger DG, Rohsenow WM. Condensation heat transfer in the presence of a non-condensable gas. *Int J Heat Mass Transf* 1968;11:15–26.
- [67] Zhai Y, Peng C, Xu B, Wang T, Li C, Zeng G, Zhu Y. Hydrothermal carbonisation of sewage sludge for char production with different waste biomass: effects of reaction temperature and energy recycling. *Energy* 2017;127:167–74.

- [68] Nikkhah K, Bakhshi N, MacDonald D. Co-pyrolysis of various biomass materials and coals in a quartz semi-batch reactor. *Energy Biomass Wastes* 1993;16: 857–857.
- [69] Kern S, Pfeifer C, Hofbauer H. Gasification of wood in a dual fluidized bed gasifier: influence of fuel feeding on process performance. *Chem Eng Sci* 2013;90:284–98.
- [70] Gokon N, Izawa T, Abe T, Kodama T. Steam gasification of coal cokes in an internally circulating fluidized bed of thermal storage material for solar thermochemical processes. *Int J Hydrog Energy* 2014;39:11082–93.
- [71] Lv P, Yuan Z, Ma L, Wu C, Chen Y, Zhu J. Hydrogen-rich gas production from biomass air and oxygen/steam gasification in a downdraft gasifier. *Renew Energy* 2007;32:2173–85.
- [72] Pfeifer C, Koppatz S, Hofbauer H. Steam gasification of various feedstocks at a dual fluidised bed gasifier: impacts of operation conditions and bed materials. *Biomass Convers Biorefinery* 2011;1:39–53.
- [73] Corella J, Toledo JM, Molina G. A review on dual fluidized-bed biomass gasifiers. *Ind Eng Chem Res* 2007;46:6831–9.
- [74] Xiao R, Zhang M, Jin B, Huang Y, Zhou H. High-temperature air/steam-blown gasification of coal in a pressurized spout-fluid bed. *Energy Fuels* 2006;20:715–20.
- [75] Nikolopoulos P, Los SAP, Angelopoulos G, Naoumidis A, Grübmeier H. Wettability and interfacial energies in SiC-liquid metal systems. *J Mater Sci* 1992;27:139–45.
- [76] E. Pavlov, D. Ivanov, P. Gasanov, A. Gulayev, Method and apparatus for moving molten metal, in, Google Patents, 2018.
- [77] Hvasta M, Nollet W, Anderson M. Designing moving magnet pumps for high-temperature, liquid-metal systems. *Nucl Eng Des* 2018;327:228–37.
- [78] Sarafraz MM, Hormozi F, Kamalgharibi M. Sedimentation and convective boiling heat transfer of CuO-water/ethylene glycol nanofluids. *Heat Mass Transf* 2014;50(9):1237–49.
- [79] Sarafraz MM, Peyghambarzadeh SM. Nucleate pool boiling heat transfer to Al₂O₃-water and TiO₂-water nanofluids on horizontal smooth tubes with dissimilar homogeneous materials. *Chem Biochem Eng Q* 2012;26(3):199–206.
- [80] Sarafraz MM, Hormozi F, Silakhori M, Peyghambarzadeh SM. On the fouling formation of functionalized and non-functionalized carbon nanotube nano-fluids under pool boiling condition. *Appl Therm Eng* 2016;95:433–44.
- [81] Sarafraz MM, Peyghambarzadeh S, Alavi Fazel S, Vaeli N. Nucleate pool boiling heat transfer of binary nano mixtures under atmospheric pressure around a smooth horizontal cylinder, *Periodica Polytechnica. Chem Eng* 2013;57(1-2):71–7.
- [82] Sarafraz MM, Nikkhah V, Madani SA, Jafarian M, Hormozi F. Low-frequency vibration for fouling mitigation and intensification of thermal performance of a plate heat exchanger working with CuO/water nanofluid. *Appl Therm Eng* 2017;121:388–99.
- [83] Sarafraz MM, Hormozi F, Peyghambarzadeh SM, Vaeli N. Upward Flow Boiling to DI-Water and CuO Nanofluids Inside the Concentric Annuli. *J Appl Fluid Mech* 2015;8(4):p651–9.
- [84] Sarafraz MM, Arya A, Nikkhah V, Hormozi F. Thermal performance and viscosity of biologically produced silver/coconut oil Nanofluids. *Chem Biochem Eng Q* 2017;30(4):489–500.
- [85] Sarafraz MM, Arjomandi M. Demonstration of plausible application of gallium nano-suspension in microchannel solar thermal receiver: experimental assessment of thermo-hydraulic performance of microchannel. *Int Commun Heat Mass Transf* 2018;94:39–46.
- [86] Sarafraz MM, Arjomandi M. Thermal performance analysis of a microchannel heat sink cooling with Copper Oxide-Indium (CuO/In) nano-suspensions at high-temperatures. *Appl Therm Eng* 2018;137:700–9.
- [87] Sarafraz MM, Arya H, Arjomandi M. Thermal and hydraulic analysis of a rectangular microchannel with gallium-copper oxide nano-suspension. *J Mol Liq* 2018;263:382–9.
- [88] Sarafraz MM, Hart J, Shrestha E, Arya H, Arjomandi M. Experimental thermal energy assessment of a liquid metal eutectic in a microchannel heat exchanger equipped with a (10 Hz/50 Hz) resonator. *Appl Therm Eng* 2019;148:578–90.
- [89] Sarafraz MM, Jafarian M, Arjomandi M, Nathan GJ. Experimental investigation of the reduction of liquid bismuth oxide with graphite. *Fuel Process Technol* 2019;188:110–7.

Chapter 7 Experimental investigation of the reduction of liquid bismuth oxide with graphite

7.1. Chapter overview

This chapter contributes to the fourth objective of the thesis. An experimental investigation is conducted on the gasification of graphitic carbon with liquid bismuth oxide. To conduct the experiments, a thermo-gravimetric analyser (manufactured by Netzsch Co.) was utilised. The experiments were conducted at different temperatures, different heating rates and different molar ratios of bismuth oxide to carbon. Reactions occur in an alumina crucible at high temperatures up to 900°C.

Initially, the reduction and oxidation of bismuth oxide were experimentally demonstrated. Then, the various molar ratios of bismuth oxide to carbon were tested and mass change over the time was measured. The activation energy and reaction constant of the reduction reaction and oxidation reaction were measured using Kissinger method and a Kinetic model was developed based on the Arrhenius equation. Then, the characterization tests including x ray diffraction (XRD) and scanning electron microscopy (SEM) tests were conducted to characterise the samples before and after the gasification reaction. The obtained results with the experiments were compared to those of calculated with thermodynamic models developed in the previous objectives. Results of this work showed the potential of bismuth oxide to gasify the graphitic carbon. Also, the containment of liquid bismuth oxide in a refractory-made crucible was demonstrated.

Results showed that the reduction and oxidation of bismuth oxide in an alumina crucible at temperatures around 900°C was technically feasible for over five operating cycles. The activation energy for the reduction was larger than that of measured for the oxidation, which was in accordance with the nature of endothermic and exothermic reactions and is in-line with

the findings reported in the literature. It was identified that the chemical conversion of carbon in the presence of bismuth oxide can reach ~85%, while can also drive the combustion reaction to the completion. Results of the present work was published in Fuel Processing Technology as follows:

M. M. Sarafraz, M. Jafarian, M. Arjomandi, G. J. Nathan, Experimental investigation of the reduction of liquid bismuth oxide with graphite, Fuel Processing Technology, 188, (2019) 110-117 (Sarafraz, Jafarian, Arjomandi, & Nathan, 2019a).

Statement of Authorship

Title of Paper	Experimental investigation of the reduction of liquid bismuth oxide with graphite
Publication Status	<input checked="" type="checkbox"/> Published <input type="checkbox"/> Accepted for Publication <input type="checkbox"/> Submitted for Publication <input type="checkbox"/> Unpublished and Unsubmitted work written in manuscript style
Publication Details	M. M. Sarafraz, M. Jafarian, M. Arjomandi, G. J. Nathan, Experimental investigation of the reduction of liquid bismuth oxide with graphite, Fuel Processing Technology, 188, (2019) 110-117.

Principal Author

Name of Principal Author (Candidate)	Mohammad Mohsen Sarafraz
Contribution to the Paper	- Running the experiments, post-processing the data, estimating the reaction parameters, - Providing the data, writing of the manuscript and production of original figures. - Correspondence with editor and reviewers including the production of all cover letters and rejoinder
Overall percentage (%)	80%
Certification:	This paper reports on original research I conducted during the period of my Higher Degree by Research candidature and is not subject to any obligations or contractual agreements with a third party that would constrain its inclusion in this thesis. I am the primary author of this paper.
Signature	<div style="display: flex; justify-content: space-between;"> _____ Date </div> <div style="text-align: right; margin-top: 5px;">29/11/18</div>

Co-Author Contributions

By signing the Statement of Authorship, each author certifies that:

- xiii. the candidate's stated contribution to the publication is accurate (as detailed above);
- xiv. permission is granted for the candidate to include the publication in the thesis; and
- xv. the sum of all co-author contributions is equal to 100% less the candidate's stated contribution.

Name of Co-Author	Mehdi Jafarian
Contribution to the Paper	- Supervision of the work, including the production of the manuscript - Participation in the development of the concepts and ideas presented in the manuscript - Evaluation and editing of the manuscript prior to submission
Signature	<div style="display: flex; justify-content: space-between;"> _____ Date </div> <div style="text-align: right; margin-top: 5px;">29/11/18</div>

Name of Co-Author	Maziar Arjomandi
Contribution to the Paper	- Supervision of the work, including the production of the manuscript - Participation in the development of the concepts and ideas presented in the manuscript - Evaluation and editing of the manuscript prior to submission
Signature	<div style="display: flex; justify-content: space-between;"> _____ Date </div> <div style="text-align: right; margin-top: 5px;">29/11/18</div>

Chapter 7 Reduction of carbon feedstock with liquid bismuth oxide: A proof of the concept for liquid chemical looping gasification

Name of Co-Author	Graham Nathan		
Contribution to the Paper	- Supervision of the work, including the production of the manuscript - Participation in the development of the concepts and ideas presented in the manuscript - Evaluation and editing of the manuscript prior to submission		
Signature		Date	29/11/18



Contents lists available at ScienceDirect

Fuel Processing Technology

journal homepage: www.elsevier.com/locate/fuproc

Research article

Experimental investigation of the reduction of liquid bismuth oxide with graphite

M.M. Sarafraz*, M. Jafarian, M. Arjomandi, G.J. Nathan

Centre for Energy Technology, School of Mechanical Engineering, the University of Adelaide, Australia

ARTICLE INFO

Keywords:

Thermo-gravimetric analysis
Bismuth oxide
Liquid oxygen carrier
Kissinger method
Liquid bismuth containment

ABSTRACT

We report an experimental demonstration of the chemical reactions for the chemical looping gasification process using molten bismuth oxide as the oxygen carrier. Cycling of the material without noticeable degradation was shown using a thermo-gravimetric analyser (TGA) furnace through both the reduction of bismuth oxide with carbon and its oxidation with air. The potential for any contamination of liquid bismuth oxide with the alumina container and of any agglomeration was assessed experimentally using x-ray diffraction (XRD) test. A kinetic model was also developed using Kissinger method to estimate the activation energy and the pre-exponential factor for the reduction and the oxidation reactions. It was found that the reduction and oxidation of bismuth and its oxide is feasible at temperatures of approximately 900 °C with the activation energies of 229.4 kJ/mol and 173.6 kJ/mol for the reduction and oxidation reactions, respectively at chemical conversion of 0.7. The chemical conversion of carbon in the presence of bismuth oxide was measured to reach 85% for the partial oxidation of carbon and to reach completion for the complete oxidation of bismuth. Furthermore, no containment challenges for liquid bismuth were identified in the alumina crucible at 900 °C. Hence, the proposed system offers potential to avoid the challenges of sintering and agglomeration that are associated with chemical looping systems using a solid oxygen carrier.

1. Introduction

Gasification is a well-established method. Liquid chemical looping gasification (LCLG) is a newly proposed method, which to produce syngas from a carbonaceous feedstock such as coal and biomass [1–3]. In the conventional chemical looping gasification processes, an air and a gasification reactor are used with a solid oxygen carrier to provide oxygen for the gasification reaction. In the gasifier, the solid oxygen carrier, which is typically a metal oxide particle with chemical looping oxygen uncoupling (CLOU), is reduced to release oxygen from the particle and partially oxidise the carbonaceous feedstock. The oxygen uncoupling phenomenon occurs under a specific temperature and pressure and for some specific metal oxides such as iron or copper oxides. A gasifying agent can also be used to maintain the required temperature and to increase the concentration of hydrogen in the gaseous product. The steam is often used as the gasifying agent and the fluidising medium within the reactor.

The gaseous product from the gasifier is typically referred to as “synthetic gas”, which is abbreviated as “syngas”. This comprises a mixture of carbon monoxide, hydrogen and smaller quantities of methane and carbon dioxide. The production of syngas through chemical

looping gasification is a plausible path to mitigate the challenges associated with the nitrogen dilution, which is typical of the conventional air blown gasification processes. However, the lifetime of the solid state oxygen carrier in the chemical looping gasification systems highly depends on the rate of sintering and agglomeration of particles [4,5], leading to diminishing of the capacity of the solid oxygen carriers in transferring oxygen between the oxidation and reduction reactors of the CLG systems. While also, the deposition of the carbon within the porous structure of the oxygen carrier particles decreases both the efficiency of CLG system for carbon capture and the surface active sites of the oxygen carrier particles for the reduction and oxidation reactions. [6,7]. One potential option to bypass these challenges is to use a liquid metal oxide instead of a solid oxygen carrier in chemical looping gasification systems. Metal oxides offer a great potential for heat and mass transfer [49,50,51,52,53,54] in comparison with conventional heat transfer medium [55,56,57]. The concept was firstly proposed by McGlashan et al. [8,9] in chemical looping combustion systems. Recently, Sarafraz et al. [1,2] and Jafarian et al. [10] have proposed the use of a liquid metal oxides in chemical looping gasification and reforming systems.

In our previous publications, for the liquid chemical looping gasification process (LCLG) a bubbling media has been proposed for the air

* Corresponding author.

E-mail address: mohammadmohsen.sarafraz@adelaide.edu.au (M.M. Sarafraz).<https://doi.org/10.1016/j.fuproc.2019.02.015>

Received 21 November 2018; Received in revised form 27 January 2019; Accepted 12 February 2019

Available online 18 February 2019

0378-3820/ © 2019 Elsevier B.V. All rights reserved.

Chapter 7 Reduction of carbon feedstock with liquid bismuth oxide: A proof of the concept for liquid chemical looping gasification

M.M. Sarafraz, et al.

Fuel Processing Technology 188 (2019) 110–117

and the gasification reactors as the medium to transport the heat and/or oxygen required to drive the reactions [1–3]. This approach typically yields higher rates of heat and mass transfer than for the solid reactants [11]. It is worth noting that; advantageously, the LCLG concept eliminates some of the technical challenges associated with the use of solid-state oxygen carriers. Furthermore, the demonstration of chemical potential is a necessary step in the development of the process. Nevertheless, it is premature to address economic potential at present, since this requires a system to be available with which to calculate both performance and cost. Before the techno-economic potential of the concept can be properly evaluated, it is necessary to develop technology to overcome the following additional challenges:

- (1) **Feeding:** Technology needs to be developed with which to inject both steam and the carbonaceous feedstock into the molten metal bath, because no such system is commercially available, although tuyeres have been developed to inject gases into molten metals during purification of metals [12],
- (2) **Containment:** Further work is required to identify materials that are suitable to contain the molten bismuth safely during long-term cycling although, silicon carbide was found to be chemically stable during the present short-term trials and has already been identified as the potential material for containers [13],
- (3) **Circulation:** Technology is also needed to circulate the liquid bismuth and its oxide between reactors. No complete system is commercially available, although some high-temperature pumps are available [14,15],
- (4) **Solidification:** Technology is also needed to prevent solidification of the liquid bismuth oxide within the chemical looping system. No complete system is commercially available, although trace heating has been developed for molten salt systems [16].

Apart from the potentials and disadvantages of the proposed system, the proposed process needs to be verified experimentally, since limited experimental measurements are available of the kinetics of these reactions. The first attempt to gasify a carbonaceous fuel with a molten metal was performed by Tyrer et al. [17] and a very low conversion of reactants together with the solidification of the molten metal was reported. Also, the kinetics of the reaction was not assessed. Since then, Steinberg et al. [18] used liquid tin to decompose natural gas into hydrogen and CO at temperatures between ~500 and 900 °C. They also found that the composition of carbon monoxide depends strongly on the amount of oxygen dissolved in the tin liquid bath. However, the mechanisms and the kinetics of the reactions remain to be investigated. Martynov et al. [19] and Gulevich et al. [20] developed a bubble reactor to produce hydrogen via a liquid metal alloy (of lead and bismuth) into which natural gas was injected. They demonstrated the feasibility of hydrogen production from methane cracking, but the kinetics and mechanisms involved in this process are yet to be reported. Later, Paxman et al. [21] reported the thermochemical equilibrium of the decomposition of carbonaceous feedstock in a bubble column reactor at various designs and operating conditions and found that the reactor temperature changes the performance of the system significantly, which they attributed it to changes in the activation energy of the reaction. However, the detailed influence of the temperature on the kinetics of the reaction remains to be reported. Schultz et al. [22] assessed a capillary reactor to use a liquid metal for the decomposition of natural gas and demonstrated that at 1100 °C, methane conversion can reach ~32%. Interestingly, after 5 h of operation, neither carbon deposition nor agglomeration was seen on the walls and within the liquid phase.

The aforementioned literature further motivated many investigators to conduct research on the plausible application of liquid metal for the gasification [22–25]. For example, Serban et al. [23] conducted some experiments using a stainless steel-made micro-reactor filled with liquid tin, liquid lead and a combination of tin/packed bed material. They

used natural gas as a fuel and chose bubbling regime for mixing the natural gas in the liquid bath. They reported a ~57% conversion of methane to hydrogen at temperature ~750 °C. They utilised SiC-made packed bed material and noticed that tin can be contained with SiC as well. Plevan et al. [24] performed some experiments in a larger stainless steel reactor but with the same experimental conditions to those of conducted by Serban et al. [23]. They reached ~18% conversion at 900 °C. For the similar experiments with liquid tin, Geibler et al. [25] reported a conversion of 30% without significant carbon deposition within the reactor. They used a tubular quartz-made reactor and the experiments were performed to investigate the methane pyrolysis with liquid tin in the reactor. The reactor was filled with tin and some cylindrical quartz rings were used as a packed bed to increase the contact of gas and liquid. Tests were performed at different temperatures ranged between 930 °C and 1175 °C. Methane was bubbled within the column and the ratio of methane to liquid tin was also adjusted using dilution of inlet gas with nitrogen. It was found that with an increase in the flow rate of methane, the yield of hydrogen increased. Likewise, an increase in the temperature of liquid metal resulted in an increase in the hydrogen yield as well. Interestingly, the hydrogen yield reached ~78% at 1175 °C. The liquid phase was analysed and it was found that only 1.5% of liquid metal can be converted to other tin-related products such as SnC alloy. Also, carbon formed a flake-shaped ash on the surface of tin and some agglomerated particles with the mean size of 40 nm to 100 nm was observed during the experiments. They reported that the presence of ash changes the rate of reaction significantly, however, no detailed study was conducted to understand the mechanism and kinetics of the reactions in liquid metal bubble column.

Apart from equilibrium modelling [26–30] and experimental tests [31–33], a lot of information is available on the kinetics of the reduction of metal oxides with a carbonaceous feedstock from previous work on metal refining. Sato et al. [34] showed that the rate of reduction reaction of iron oxide with graphite at temperatures above the melting temperature of iron oxide (1320–1620 °C) is proportional to the second power of the concentration of iron oxide [34]. Seaton et al. [35] demonstrated that the rate of heat transfer between iron pellets and molten steel increases with the rate of CO production in the process. This was attributed to the first-order influence of temperature on the activation energy and other kinetic parameters. Similarly, Upadhyaya et al. [36] found that the kinetics of the reduction of lead oxide in a dilute liquid mixture of CaO-Al₂O₃-SiO₂ slag using graphite dissolved in iron is driven by the evolved gases and scales with the ratio of lead oxide to carbon. However, a general kinetic model was not developed for the reduction reaction of lead oxide with graphite.

Thermo-gravimetric analysis (TGA) has also been used to accurately measure the activation energy of the reduction of molten metals with carbon. For example, Monazam et al. [37] used TGA to show that the reduction of CuO impregnated in bentonite with natural gas within the range of 1023 K to 1173 K has an activation energy of 37.3 ± 1.3 kJ/mol. They also reported that copper oxide was not deactivated after 10 successive cycles of the experiments. With another experiment, they confirmed the results with the measurement of the outlet gases and concluded that the CuO/bentonite oxygen carrier is a promising candidate for the CLG/CLC systems. In another study, the activation energy of reduction reaction of copper oxide with CO gas was measured by Plewa and Skrzypek [38]. They reported the value of 44.3 ± 1.8 kJ/mol using TGA measurements at 398 K to 473 K.

In our previous assessments, bismuth oxide has been identified as the suitable liquid oxygen carrier for the LCLG [2]. Therefore, a systematic experimental study need to be conducted to further understand the chemical performance, kinetic of the reaction and its containment. Bismuth oxide with melting temperature of ~830 °C is a plausible liquid oxygen for the LCLG system. However, to the best of authors' knowledge, no experimental study has been conducted to assess the potential of reduction of molten bismuth and its oxide with a carbonaceous fuel. Hence, the first aim of this work is to experimentally demonstrate the

Table 1
Experimental conditions used in the thermo-gravimetric analysis measurements.

Parameter	Value and/or description	Remarks
Oxygen carrier	Bismuth/Bismuth oxide	Nominal diameter: 50 μm , melting temperature of bismuth oxide: 1123 K
Reductant	Graphitic carbon	Carbon nominal particle size: 50 μm Bismuth nominal particle size: 50 μm
Temperature	298 K–1173 K	Melting temperature of bismuth oxide: 1123 K Experiments were conducted at various heating rate
Pressure	1 bar	–
Time	0–85 min	–
Crucible	Alumina cylinder 40 cc with PT lid and protector	No reaction between bismuth oxide and the alumina crucible was observed.
Heating rate	5 K/min–35 K/min	–
Shielding gas	Nitrogen (purity 99.99%)	Used to control the atmosphere and to cool the balance.
Shielding gas flow rate	20 ml/min	–
Carrier gases	Reduction: Nitrogen @ 120 ml/min Oxidation: Air @ 120 ml/min	–

reduction of bismuth oxide with a carbonaceous feedstock. The paper also aims to develop a first-order kinetic model for the reduction of bismuth oxide with carbon through measurement of the activation energy and pre-exponential factors.

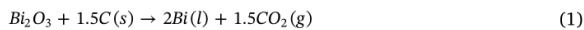
2. Experimental

2.1. Experimental instruments

The reduction and oxidation experiments were performed in a high-temperature thermo-gravimetric analyser (TGA) manufactured by Netzsch (STA 449F1). The shielding gas for the device was nitrogen, while the carrier gas for the reduction and oxidation stages were nitrogen and air for reduction and oxidation reactions, respectively. The temperature, residual mass and the gas flow rate were processed with Proteus TGA-MS software using a transient module. Table 1 represents the experimental conditions used in the present work.

2.2. Chemical reactions

The reduction reaction occurs in the gasifier according to the following chemical equation:



and



Both reactions are endothermic and spontaneous at a temperature range of 473–1573 K. However, thermodynamic assessments show that Reaction 1 proceeds when the oxygen released from the bismuth oxide is sufficient for the complete combustion of carbon, while reaction 2 proceeds with sub-stoichiometric values of oxygen. Hence, the molar ratio of Bi_2O_3 to carbon determines which reaction is dominant.

The oxidation reaction of Bi with oxygen is described as follows:



This equation is exothermic and spontaneous in the temperature range $298\text{ K} < T < 1573\text{ K}$.

The oxygen uncoupling feature of the bismuth oxide is shown with the following equation:



2.3. Data reduction and uncertainty analysis

The extent of chemical conversion was determined with the following equation:

$$\alpha = \frac{m(t) - m_i}{m_i - m_e} \quad (5)$$

Here, m is the mass of sample at time t , i and f are the ‘initial’ and ‘final’ mass of the sample, respectively, α is the conversion of the sample at time t , which was measured with TGA. The rate of a reaction was estimated with the following equation:

$$-r_A = K_T \cdot C_A^n \cdot C_{B\dots} \quad (6)$$

Here, K_T is the constant of the reaction, and C is the concentration of the species participating in the reaction. The rate of a reaction is defined by the Arrhenius equation as follows:

$$K_T = A \cdot e^{\frac{-E_a}{RT}} \quad (7)$$

Here, E_a is the activation energy, R is the universal gas constant (8.314 J/mol·K) and A is the pre-exponential factor. To obtain the activation energy and the pre-exponential factor, Kissinger [39] proposed the following equation:

$$\ln\left(\frac{B}{T^2}\right) = \ln\left(\frac{A \cdot R}{E_a}\right) - \frac{E_a}{RT} \quad (8)$$

where B is the heating rate (K/min), T is the peak temperature of the Derivative Thermo-Gravimetric curve (DTG), E_a is the activation energy, kJ/mol, A is the pre-exponential factor and R is universal gas constant (J/mol·K). Eq. (2) implies that E_a is the slope of the line obtained from plotting $\ln(B/T^2)$ versus $1/T$, while the intercept of this line represents the pre-exponential factor (A). The molar ratio of liquid oxygen carrier to fuel is defined from their molar flow rates as follows:

$$\varphi_{LOC} = \frac{\dot{n}_{LOC}}{\dot{n}_{feed}} \quad (9)$$

Here, \dot{n} is the molar flow rate of the LOC and feedstock (graphitic carbon). φ is used to show the amount of liquid oxygen carrier in the reaction, which also describes the amount of oxygen available in the system.

Table 2 presents the uncertainty of these experiments, which were estimated from the correlation introduced by Kline-McClintock [40] was used. It can be seen that the uncertainty of the measured values of

Table 2

The uncertainty of the present measurements, as obtained with the method of Kline-McClintock [40].

Parameter	Value	SI unit	Range
Temperature	$\pm 0.1\%$	K	313–1173
Sample mass	± 1	mg	0.1–5
Time	$\pm 1/60$	min	1–85
Gas flow rate	$\pm 1\%$ of reading value	ml/min	120
Heating rate	$\pm 0.1\%$	K/min	5–35
Activation energy	$\pm 1.6\%$	kJ/mol	–
Pre-exponential	$\pm 3.1\%$	–	–
Residual mass	$\pm 0.03\%$	mg	–

activation energy and pre-exponential factor is $\pm 6.1\%$ and $\pm 5.8\%$, respectively.

2.4. Experimental procedure

The measurements in the TGA were performed with alumina crucibles (40 ml, cylindrical, purchased from Netzsch CO.) Before each experiment, the crucibles were washed with methanol to remove any impurities and then exposed to 800 °C for 120 min to remove any moisture. Bismuth, bismuth oxide and carbon particles were purchased from Chem-supply with a purity of 99.9% and used as purchased. The reduction tests were conducted at a series of heating rates from 5 to 35 K/min in steps of 5 K/min as shown in Table 2. Nitrogen with a purity of 99.99% at a flow rate of 20 ml/min of nitrogen was employed as the shielding gas around the TGA balance, preventing any ingress of reactive gases such as air, and also to protect the balance from any thermal shock. The flow rate for the carrier gas was 120 ml/min. Nitrogen was also used as the carrier gas for the reduction reaction, while air was used for the oxidation reaction at a flow rate of 120 ml/min. The reference TGA measurements were also conducted for samples of pure carbon, pure bismuth oxide and a mixture of bismuth oxide and carbon. The reduction and the oxidation reactions were assessed in the nitrogen and the air environments at heating rates of 5–35 K/min and for the conditions shown in Table 3.

A Shimadzu XRD-7000 x-ray diffractometer was employed to assess the composition and structure of the solid phase materials before and after the experiments. The XRD experiments were used to identify any potential side-reactions between the crucible and the carbonaceous feedstock, the crucible and the liquid bismuth oxide or the crucible with the gaseous products. The XRD tests were conducted under irradiation of Cu-K α lamp and the operating potential is +25.1 kV, at current value of 10 mA and the scanning rate 1°/min.

A scanning Electron Microscopy (SEM) was employed to assess any changes in morphology or physical structure of the samples before and after the thermo-gravimetric tests, e.g. agglomeration and penetration of carbon inside the solidified bismuth oxide. Before each SEM test, the samples were prepared by coating them on a disk with mean diameter of 2 mm. This was sufficient to achieve high-quality clear images with low noise.

3. Results and discussion

3.1. Thermo-gravimetric analysis

3.1.1. Reduction reaction

Fig. 1 presents the dependence on time of the residual mass for reduction (samples S2 and S3) and oxidation (samples S4 and S5). The drying process can be identified for the carbon-containing samples S2 and S4 as a small but discernible mass loss in the temperature range $T < 300$ °C, which is too low for carbon to undergo any reaction. This small mass change is consistent with the low moisture content of the

carbon particles and can be attributed to the porous structure of the carbon, which causes it to adsorb moisture from atmosphere. This contrasts the trace for bismuth oxide, whose structure has sufficiently low porosity for any weight change to be negligible in this temperature range.

No reduction in mass with heating was observed for sample S1, which is consistent with the absence of oxygen, and hence of any reaction. In contrast, the oxidation of carbon in the presence of air for sample S4 results in the strong reduction nearly to zero. The reduction of bismuth oxide, sample S3 results in a gradual reduction of mass by up to $\sim 10.7\%$ due to the release of oxygen content of the sample at temperatures $> \sim 850$ °C which is above the melting temperature of the bismuth oxide (830 °C). The equilibrium value of the residual mass of bismuth after reduction at a temperature of 900 °C was estimated to be $\sim 88\%$ using HSC Chemistry 7.0 Software. This value is in a good agreement with 89.96%, which was obtained experimentally with the TGA. This measurement also provides further support for the validity of previous models developed for the reduction of bismuth oxide and other liquid metal oxides with carbon [3].

The weight loss of the blend of carbon and bismuth oxide, sample S2, is consistent with the fact that carbon further reduces the bismuth oxide and this results in more release of oxygen from bismuth oxide (according to Eq. (4)). The released oxygen reacts with carbon, which further decreased the mass of the sample resulting in a $\sim 16\%$ decrease in the mass of the sample (in comparison with 10.7% mass reduction of sample S3).

As can be seen from Fig. 1, the reduction reaction with carbon can be achieved with complete conversion at $T = 900$ °C providing that the φ value is sufficiently high (e.g. $\varphi = 2$). This is compatible with tower technologies under development for concentrated solar thermal energy, which have achieved 1000 °C in pilot-scale trials [4]. In contrast, no tower-based concentrating technology has yet been demonstrated to achieve temperatures of > 1200 °C that are required for a conventional chemical looping process to achieve the highest carbon conversion [41]. Interestingly, for the proposed process, complete conversion of carbon can occur at $T = 900$ °C providing that the φ value is sufficiently high (e.g. $\varphi = 2$).

3.1.2. Oxidation reaction

Fig. 2 presents the dependence of the residual mass of the bismuth samples on time since the start of the heating during the reduction-oxidation reactions. As can be seen, for each cycle of reduction-oxidation, the residual mass for the reduction reaction is 10.04% (i.e. a loss), which is recovered identically during the oxidation. The extent of conversion was also cross-checked after each redox cycle by removing the sample and characterising it with XRD to ensure that no residual carbon was presented in the bismuth. The identical quantity of carbon was then added to the sample before repeating the cycle. No significant change in mass of the bismuth oxide was detected after five successive cycles, which implies no significant loss of bismuth by evaporation. This is consistent with the low vapour pressure of bismuth oxide ($\sim 2.04 \times 10^{-8}$ MPa at ~ 800 – 900 °C) [42]. This demonstrates the chemical feasibility of the cyclical reduction of bismuth oxide with carbon and the oxidation of bismuth with air and hence also for the LCLG process. For many chemical looping process with solid oxygen carriers, such as copper and iron oxides [43], the residual mass decreases after several cycles of operation due to the evaporation of the metal. The reactivity of some oxygen carriers also decreases with cycling [44]. In contrast, both the reactivity and residual mass for bismuth oxide were unchanged, even after five successive cycles of operation.

3.2. Carbon conversion

Fig. 3 presents the dependence of carbon conversion on time of the reaction for various molar ratios of bismuth oxide to carbon. The tests were conducted in a non-isothermal condition (heating rate: 35 K/min,

Table 3
Specifications of the samples used in the thermo-gravimetric tests.

Sample	Mass of carbon	Mass of bismuth oxide	Mass of bismuth	Environment
S1 ^a (carbon)	0.38	–	–	Nitrogen
S2 (Bi ₂ O ₃ + C), gasification	0.38	5	–	Nitrogen
S3 (Bi ₂ O ₃)	–	5	–	Nitrogen
S4 ^b (carbon)	0.38	–	–	Air
S5 (bismuth), oxidation	4.48	–	–	Air

^a N₂ shielding gas was fed to the system at 20 ml/min.

^b N₂ shielding gas was fed to the system at 10 ml/min.

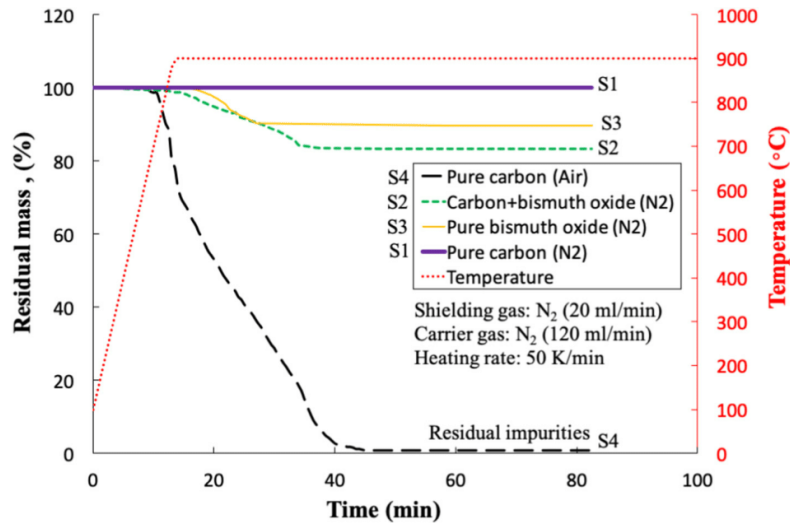


Fig. 1. Time history of the residual mass of the samples during heating for carbon, bismuth oxide and the combination of both in either nitrogen or air environments as per Table 3 at heating rate of 50 K/min.

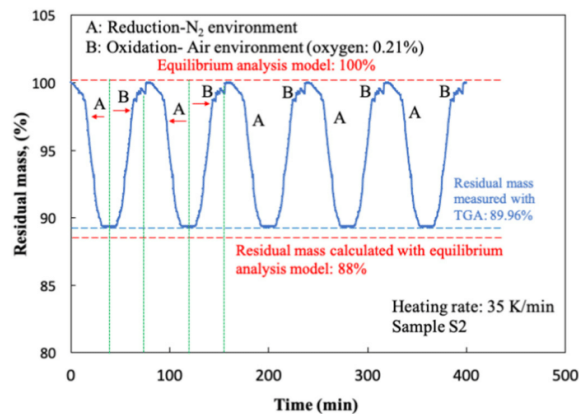


Fig. 2. Reduction and oxidation of sample S2 with nitrogen and air after 5 successive cycles. Carbon with mass of 0.38 mg was added to the sample after each cycle is completed.

time span: 45 min), followed by an isothermal test at 1173 K for 35 min both in N₂ environment. The carbon conversion extent slightly changes in drying region and anomalously increases due to the partial and/or complete oxidation of carbon with the released oxygen from bismuth oxide particles. For example, at $\varphi = 2.0$, the carbon conversion increases from 7% at $t = 16$ min, to $\sim 100\%$ at $t = 37$ min and remains constant since the remaining residue only consists of very small quantity of impurities together with pure bismuth. Fig. 3 also shows that the extent of conversion increases with an increase in the molar ratio of bismuth to carbon. For sub-stoichiometric values of φ , insufficient oxygen is available for the complete oxidation of carbon, which results in the formation of carbon monoxide and the presence of unreacted carbon remains in the system. For example, for $\varphi = 0.25$, only 68% of the total carbon has reacted after 60 min of run time, while for $\varphi = 0.5$ and $\varphi = 1$, the carbon conversion extent has reached 74% and 90%, respectively. This is in accordance with the previous results published in the literature [2]. Furthermore, for $\varphi = 1.5$ –2.0, the carbon conversion extent reaches 100%. However, for φ values smaller than 1.0, the oxidation of carbon is only partial. Therefore, there is a trade-off

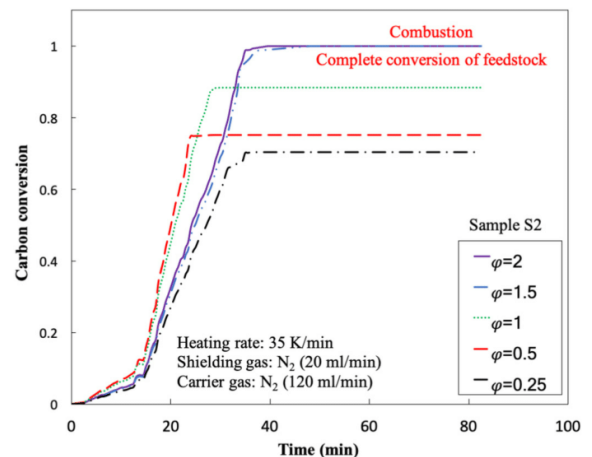


Fig. 3. Dependence of carbon conversion on time of the reaction for various molar ratios of bismuth oxide to carbon (sample S2) at heating rate of 35 K/min.

between the amount of the unreacted carbon and the value of φ in the system.

3.3. Characterization of samples

Fig. 4 presents the XRD spectra for bismuth oxide and carbon (sample S2) before and after the TGA measurements at $\varphi = 1$. As can be seen, the XRD spectra of sample S2 recorded before the reduction contains the characteristic peaks of bismuth oxide at 27.5°, 33.2°, 33.4° [45] and those at 26°, 45°, 46° and 53° and 55° for graphitic carbon [46]. In contrast, the spectra recorded after the reduction reaction contain the characteristic peaks of pure bismuth [47] at 26°, 27°, 37.5°, 40°, 47.5°, 50°, 53° and 56° together with peaks of unreacted carbon including 26°, 45°, 46° and 53° and 55°. Importantly, no characteristic peak associated with alumina (from the crucible) can be seen in the XRD spectrum. Nevertheless, some residual oxygen peaks are evident, which shows that oxygen has not been fully consumed in this reaction.

Chapter 7 Reduction of carbon feedstock with liquid bismuth oxide: A proof of the concept for liquid chemical looping gasification

M.M. Sarafraz, et al.

Fuel Processing Technology 188 (2019) 110–117

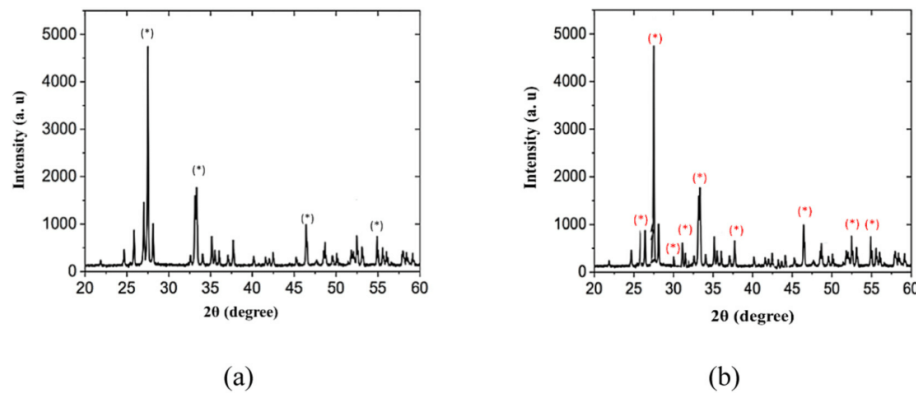


Fig. 4. The XRD spectra obtained for sample S2 (bismuth oxide and carbon) under the reduction reaction a) before the TGA test, b) after the TGA test under the heating rate of 35 K/min.

This suggests that some aspects of the reaction are diffusion controlled. Further evidence for this can be found from the carbon conversion of the sample being 0.9 for $\varphi = 1.0$ was 0.9, so that some unreacted carbon remains in the residue.

Fig. 5 represents the scanning electron microscopic images taken from the samples before and after the experiments with TGA. As can be seen, the bismuth oxide particles are spherical and uniform in terms of size and morphology (Fig. 5a), however, after the TGA test (Fig. 5b), due to the melting and then the solidification processes, the particles lose their morphology and form an agglomerated clog within the crucible. However, the clog formation does not influence the chemical performance of the sample since the reactions occur in the liquid phase in each cycle.

3.4. Kinetic modelling

Fig. 6 presents the dependence of $\ln(\beta/T^2)$, where β is defined in Eq. (7), on $1000/T$ for the reduction of bismuth oxide with carbon and for the oxidation of bismuth with air. As can be seen, the data has a good fit to a linear dependence between $\ln(\beta/T^2)$ and $1000/T$, the slope of the line which corresponds to the activation energy of the reaction. For example, for the reduction reaction, E/R is 27.625, while it is 21.151 for the oxidation reaction. The R-square for the obtained lines is 0.9953 and 0.9955 for oxidation and reduction reactions showing the high accuracy of the Kissinger method for estimating the activation energy. Hence, the first-order Kissinger kinetic method is suitable for estimating this parameter. It can also be seen that the oxidation reaction has a

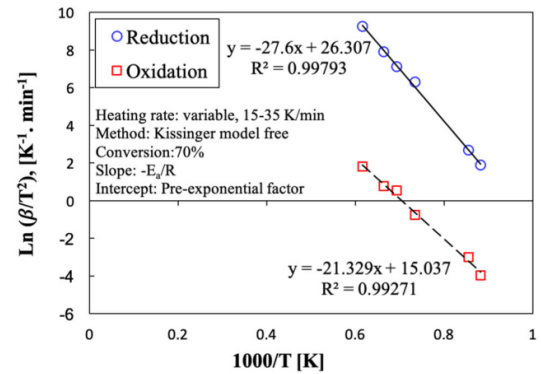


Fig. 6. The measured dependence of parameter “ $\ln(\beta/T^2)$ ” in Eq. (7) on temperature for the reduction and oxidation reactions at a conversion of 0.7 as defined with the Kissinger free kinetic method.

lower activation energy than the reduction reaction, which is consistent with the higher values of the reaction rate in the higher temperature. Also, the oxidation reaction is an aggressive reaction with a relatively low activation energy, resulting in a quick reaction. Notably, the pre-exponential factor for the reduction and oxidation reactions can also be obtained from Eq. (7), which is the intercept of the interpolated line. The technique was applied for various carbon conversion extends and

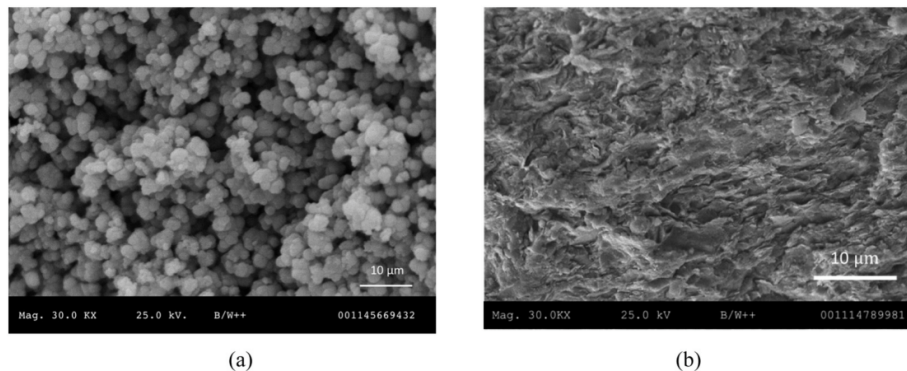


Fig. 5. SEM micro-graphs obtained for sample S2 (bismuth oxide and carbon) under the reduction reaction in TGA, a) before the TGA test, b) after the TGA test at heating rate of 35 K/min.

Table 4

The values of the activation energy and pre-exponential factor for the reduction and oxidation of bismuth oxide with carbon and air, respectively, as derived from the Kissinger method.

Kissinger model	Reduction		Oxidation	
	Carbon conversion	Activation energy (kJ/mol)	Pre-exponential factor	Pre-exponential factor
	0.1	196.4	2.39E+11	138.2
	0.3	201.3	8.92E+11	142.5
	0.5	211.6	3.28E+12	155.6
	0.7	229.4	1.193E+13	173.6
	0.9	237.1	1.04E+13	180.7

are reported in Table 4. Notably, the kinetic parameters were estimated after each cycle and it was found that the kinetic remains the same after successive cycles of reduction and oxidation. The activation energy parameters were within $\pm 1.1\%$ of deviation with each other.

Notably, to independently assess the accuracy of the Kissinger method for estimating the activation energy, this method was also applied to the reduction of iron oxide with carbon. The activation energy derived from this measurement was 355 kJ/mol, which is within $\pm 1.3\%$ of the value published in the literature for the activation energy of the iron oxide-carbon monoxide reduction reaction (360 kJ/mol) [48].

3.5. Containment of bismuth oxide

Fig. 7 presents the images of the surface of the alumina crucibles after successive cycles of reduction of bismuth oxide with carbon and the oxidation of bismuth with air at 900 °C with the TGA. As can be seen, the reduction and oxidation of bismuth oxide after five cycles can occur in an alumina crucible. However, some agglomeration was observed after 2 cycles. Importantly, this was found not to affect the reactivity of the sample, because the sample melts during each cycle, which renders any agglomeration process irrelevant. Similarly, the SEM images taken from the sample after each cycle show that the porosity of bismuth oxide decreases with the number of test cycles. This can be

expected to influence the reactivity of the bismuth oxide over successive cycles. This, in turn, suggests that the device used to generate bismuth oxide will need to be carefully designed to achieve the right and sufficient porosity. These issues can be addressed in the future work.

4. Conclusion

It has been found that it is chemically feasible to employ liquid bismuth oxide as an oxygen carrier for the proposed liquid chemical looping gasification process. The cyclical reduction of bismuth oxide with carbon and oxidation of bismuth with air was measured to be repeatable for five cycles with no detectable difference in the extent of mass change between these cycles. Furthermore, with graphite as the reductant, the alumina crucible was found to provide effective containment in these short-term tests. The extent of carbon conversion was measured to be as high as $\sim 85\%$, while the combustion reactions were found to exhibit complete conversion. In addition, the specific findings are as follows:

- No net loss in mass was detectable over the five successive cycles of oxidation and reduction, demonstrating no significant evaporative loss of bismuth. This is consistent with the low vapour pressure of bismuth.
- No side reactions between the bismuth and the alumina crucible were detected.
- The extent of chemical conversion was found to scale with the residual oxygen molar ratio in the reactor.
- The conversion of bismuth oxide to bismuth by reduction with carbon and of bismuth to bismuth oxide by oxidation with air was confirmed by XRD and SEM measurements.
- Some agglomeration of bismuth oxide particles was observed and the porosity of the samples decreased over the five successive cycles. This did not influence the type of reactions because the LCLG operates in the liquid phase, but can be expected to decrease the reactivity of the bismuth over time. This suggests that further application of the technology may be required a robust method to be developed to control the porosity of the bismuth oxide particles.
- The kinetics of the reaction was measured using the Kissinger method. The activation energy and the pre-exponential factor for

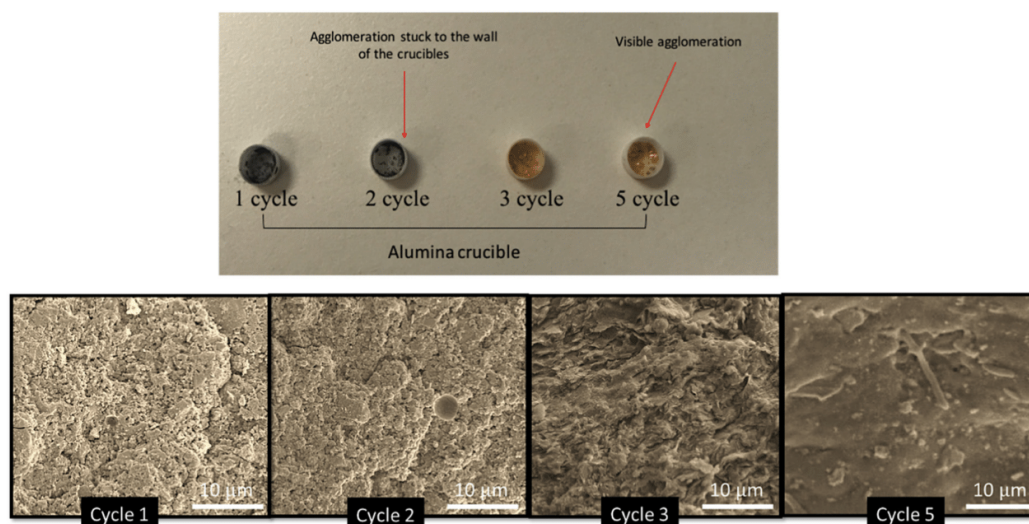


Fig. 7. Photographs (upper images) and micrographs (lower images) of the surface of the alumina crucible after successive cycles of reduction of bismuth oxide with carbon and oxidation with air.

Chapter 7 Reduction of carbon feedstock with liquid bismuth oxide: A proof of the concept for liquid chemical looping gasification

M.M. Sarafraz, et al.

Fuel Processing Technology 188 (2019) 110–117

the reduction and oxidation reactions were found to be ~ 229 kJ/mol and ~ 175.8 kJ/mol, respectively for a conversion extend of 0.7.

Acknowledgement

The authors gratefully acknowledge the Australian Research Council (ARC) for its financial support through grant DP150102230 and the Australian Renewable Energy Agency (ARENA) for its support through the Australian Solar Thermal Research Initiative (ASTRI). The first author of this work acknowledges the “Australian Government Research Training Program Scholarship” for its financial supports.

References

- [1] M. Sarafraz, M. Jafarian, M. Arjomandi, G. Nathan, Potential use of liquid metal oxides for chemical looping gasification: a thermodynamic assessment, *Appl. Energy* 195 (2017) 702–712.
- [2] M. Sarafraz, M. Jafarian, M. Arjomandi, G.J. Nathan, The relative performance of alternative oxygen carriers for liquid chemical looping combustion and gasification, *Int. J. Hydrog. Energy* 42 (2017) 16396–16407.
- [3] M. Sarafraz, M. Jafarian, M. Arjomandi, G. Nathan, Potential of molten lead oxide for liquid chemical looping gasification (LCLG): a thermochemical analysis, *Int. J. Hydrog. Energy* 43 (2018) 4195–4210.
- [4] J. Adanez, A. Abad, F. Garcia-Labiano, P. Gayan, F. Luis, Progress in chemical-looping combustion and reforming technologies, *Prog. Energy Combust. Sci.* 38 (2012) 215–282.
- [5] P. Cho, T. Mattisson, A. Lyngfelt, Comparison of iron-, nickel-, copper- and manganese-based oxygen carriers for chemical-looping combustion, *Fuel* 83 (2004) 1215–1225.
- [6] J.d. Adánez, L.F. de Diego, F. García-Labiano, P. Gayán, A. Abad, J. Palacios, Selection of oxygen carriers for chemical-looping combustion, *Energy Fuel* 18 (2004) 371–377.
- [7] B. Wang, R. Yan, D.H. Lee, D.T. Liang, Y. Zheng, H. Zhao, C. Zheng, Thermodynamic investigation of carbon deposition and sulfur evolution in chemical looping combustion with syngas, *Energy Fuel* 22 (2008) 1012–1020.
- [8] N.R. McGlashan, P.R. Childs, A.L. Heyes, Chemical looping combustion using the direct combustion of liquid metal in a gas turbine based cycle, *J. Eng. Gas Turbines Power* 133 (2011) 031701.
- [9] N. McGlashan, Chemical-looping combustion: a thermodynamic study, *Proc. Inst. Mech. Eng. C J. Mech. Eng. Sci.* 222 (2008) 1005–1019.
- [10] M. Jafarian, M. Arjomandi, G.J. Nathan, Thermodynamic potential of high temperature chemical looping combustion with molten iron oxide as the oxygen carrier, *Chem. Eng. Res. Des.* 120 (2017) 69–81.
- [11] J. Heijnen, K. Van't Riet, Mass transfer, mixing and heat transfer phenomena in low viscosity bubble column reactors, *Chem. Eng. J.* 28 (1984) B21–B42.
- [12] D.B. George, Apparatus and process for the production of fire-refined blister copper, *Google Patents*, 1995.
- [13] P. Nikolopoulos, S.A.P. Los, G. Angelopoulos, A. Naoumidis, H. Grübmeier, Wettability and interfacial energies in SiC-liquid metal systems, *J. Mater. Sci.* 27 (1992) 139–145.
- [14] E. Pavlov, D. Ivanov, P. Gasanov, A. Gulayev, Method and apparatus for moving molten metal, *Google Patents*, 2018.
- [15] M. Hvasta, W. Nollt, M. Anderson, Designing moving magnet pumps for high-temperature, liquid-metal systems, *Nucl. Eng. Des.* 327 (2018) 228–237.
- [16] D. Kearney, U. Herrmann, P. Nava, B. Kelly, R. Mahoney, J. Pacheco, R. Cable, N. Potrovitza, D. Blake, H. Price, Assessment of a molten salt heat transfer fluid in a parabolic trough solar field, *J. Sol. Energy Eng.* 125 (2003) 170–176.
- [17] T. Daniel, Production of hydrogen, *Google Patents*, 1931.
- [18] M. Steinberg, Fossil fuel decarbonization technology for mitigating global warming, *Int. J. Hydrog. Energy* 24 (1999) 771–777.
- [19] P. Martynov, A. Gulevich, Y.I. Orlov, V. Gulevsky, Water and hydrogen in heavy liquid metal coolant technology, *Prog. Nucl. Energy* 47 (2005) 604–615.
- [20] A. Gulevich, P. Martynov, V. Gulevsky, V. Ulyanov, Technologies for hydrogen production based on direct contact of gaseous hydrocarbons and evaporated water with molten Pb or Pb–Bi, *Energy Convers. Manag.* 49 (2008) 1946–1950.
- [21] D. Paxman, S. Trottler, M. Nikoo, M. Secanell, G. Ordorica-Garcia, Initial experimental and theoretical investigation of solar molten media methane cracking for hydrogen production, *Energy Procedia* 49 (2014) 2027–2036.
- [22] I. Schultz, D.W. Agar, Decarbonisation of fossil energy via methane pyrolysis using two reactor concepts: fluid wall flow reactor and molten metal capillary reactor, *Int. J. Hydrog. Energy* 40 (2015) 11422–11427.
- [23] M. Serban, M.A. Lewis, C.L. Marshall, R.D. Doctor, Hydrogen production by direct contact pyrolysis of natural gas, *Energy Fuel* 17 (2003) 705–713.
- [24] M. Plevan, T. Geißler, A. Abánades, K. Mehravarán, R. Rathnam, C. Rubbia, D. Salmieri, L. Stoppel, S. Stückrad, T. Wetzel, Thermal cracking of methane in a liquid metal bubble column reactor: experiments and kinetic analysis, *Int. J. Hydrog. Energy* 40 (2015) 8020–8033.
- [25] T. Geißler, M. Plevan, A. Abánades, A. Heinzl, K. Mehravarán, R. Rathnam, C. Rubbia, D. Salmieri, L. Stoppel, S. Stückrad, Experimental investigation and thermo-chemical modeling of methane pyrolysis in a liquid metal bubble column reactor with a packed bed, *Int. J. Hydrog. Energy* 40 (2015) 14134–14146.
- [26] H. Sefidari, B. Lindblom, H. Wiinikka, L.-O. Nordin, A. Lennartsson, J. Mouzon, I.U. Bhuiyan, M. Öhman, The effect of disintegrated iron-ore pellet dust on deposit formation in a pilot-scale pulverized coal combustion furnace. Part II: thermo-chemical equilibrium calculations and viscosity estimations, *Fuel Process. Technol.* 180 (2018) 189–206.
- [27] O. Yakaboğlu, J. Harinck, K. Smit, W. De Jong, Testing the constrained equilibrium method for the modeling of supercritical water gasification of biomass, *Fuel Process. Technol.* 138 (2015) 74–85.
- [28] F. Moradian, P.A. Tchhoffor, K.O. Davidsson, A. Pettersson, R. Backman, Thermodynamic equilibrium prediction of bed agglomeration tendency in dual fluidized-bed gasification of forest residues, *Fuel Process. Technol.* 154 (2016) 82–90.
- [29] Z.I.S. Adiya, V. Dupont, T. Mahmud, Chemical equilibrium analysis of hydrogen production from shale gas using sorption enhanced chemical looping steam reforming, *Fuel Process. Technol.* 159 (2017) 128–144.
- [30] J. Yin, X. Kang, C. Qin, B. Feng, A. Veeraragavan, D. Saulov, Modeling of CaCO_3 decomposition under $\text{CO}_2/\text{H}_2\text{O}$ atmosphere in calcium looping processes, *Fuel Process. Technol.* 125 (2014) 125–138.
- [31] M. Su, J. Ma, X. Tian, H. Zhao, Reduction kinetics of hematite as oxygen carrier in chemical looping combustion, *Fuel Process. Technol.* 155 (2017) 160–167.
- [32] K. Mondal, H. Lorethova, E. Hippo, T. Wiltowski, S. Lalvani, Reduction of iron oxide in carbon monoxide atmosphere: reaction controlled kinetics, *Fuel Process. Technol.* 86 (2004) 33–47.
- [33] D. Bom, R. Andrews, D. Jacques, J. Anthony, B. Chen, M.S. Meier, J.P. Selegue, Thermogravimetric analysis of the oxidation of multiwalled carbon nanotubes: evidence for the role of defect sites in carbon nanotube chemistry, *Nano Lett.* 2 (2002) 615–619.
- [34] A. Sato, G. Aragane, K. Kamihira, S. Yoshimatsu, Reducing rates of molten iron oxide by solid carbon or carbon in molten iron, *Trans. Iron Steel Inst. Jpn.* 27 (1987) 789–796.
- [35] C.E. Seaton, A.A. Rodriguez, M. González, M. Manrique, The rate of dissolution of reduced iron in molten steel, *Trans. Iron Steel Inst. Jpn.* 23 (1983) 14–20.
- [36] K. Upadhyaya, Kinetics of reduction of lead oxide in liquid slag by carbon in iron, *Metall. Trans. B* 17 (1986) 271–279.
- [37] E.R. Monazam, R. Siriwardane, R.W. Breault, H. Tian, L.J. Shadle, G. Richards, S. Carpenter, Kinetics of the reduction of $\text{CuO}/\text{bentonite}$ by methane (CH_4) during chemical looping combustion, *Energy Fuel* 26 (2012) 2779–2785.
- [38] J. Plewa, J. Skrzypek, Kinetics of the reduction of copper oxide with carbon monoxide, *Chem. Eng. Sci.* 44 (1989) 2817–2824.
- [39] H.E. Kissinger, Reaction kinetics in differential thermal analysis, *Anal. Chem.* 29 (1957) 1702–1706.
- [40] S.A. Kline, F.A. McClintock, Describing uncertainties in single-sample experiments, *Mech. Eng.* 75 (1953) 3–8.
- [41] E.J. Marek, Y. Zheng, S.A. Scott, Enhancement of char gasification in CO_2 during chemical looping combustion, *Chem. Eng. J.* 354 (2018) 137–148.
- [42] G. Moiseev, N. Vatolin, N. Belousova, Thermodynamic investigations in the Bi-O system, *J. Therm. Anal. Calorim.* 61 (2000) 289–303.
- [43] Y. Zhongliang, Y. Yanyan, Y. Song, Z. Qian, Z. Jiantao, F. Yitian, H. Xiaogang, G. Guoqing, Iron-based oxygen carriers in chemical looping conversions: a review, *Carbon Resour. Convers.* 2 (2019) 23–34.
- [44] L.F. De Diego, F. Garcia-Labiano, J. Adánez, P. Gayán, A. Abad, B.M. Corbella, J.M.A. Palacios, Development of Cu-based oxygen carriers for chemical-looping combustion, *Fuel* 83 (2004) 1749–1757.
- [45] L. Leontie, M. Caraman, M. Alexe, C. Harnagea, Structural and optical characteristics of bismuth oxide thin films, *Surf. Sci.* 507 (2002) 480–485.
- [46] Z. Li, C. Lu, Z. Xia, Y. Zhou, Z. Luo, X-ray diffraction patterns of graphite and turbostratic carbon, *Carbon* 45 (2007) 1686–1695.
- [47] H.C. Hoover, *Georgius Agricola De Re Metallica*, Russian version (1950).
- [48] T. Utigard, G. Sanchez, J. Manriquez, A. Luraschi, C. Diaz, D. Cordero, E. Almendras, Reduction kinetics of liquid iron oxide-containing slags by carbon monoxide, *Metall. Mater. Trans. B Process Metall. Mater. Process. Sci.* 28 (1997) 821–826.
- [49] M.M. Sarafraz, F. Hormozi, M. Kamalgharibi, Sedimentation and convective boiling heat transfer of CuO -water/ethylene glycol nanofluids, *Heat Mass Transf.* 50 (2014) 1237–1249.
- [50] M.M. Sarafraz, S. Peyghambarzadeh, S. Alavi Fazel, N. Vaeli, Nucleate pool boiling heat transfer of binary nano mixtures under atmospheric pressure around a smooth horizontal cylinder, *Period. Polytech., Chem. Eng.* 57 (2013) 71–77.
- [51] M.M. Sarafraz, F. Hormozi, M. Silakhori, S.M. Peyghambarzadeh, On the fouling formation of functionalized and non-functionalized carbon nanotube nano-fluids under pool boiling condition, *Appl. Therm. Eng.* 95 (2016) 433–444.
- [52] M.M. Sarafraz, V. Nikkhah, S.A. Madani, M. Jafarian, F. Hormozi, Low-frequency vibration for fouling mitigation and intensification of thermal performance of a plate heat exchanger working with CuO/water nanofluid, *Appl. Therm. Eng.* 121 (2017) 388–399.
- [53] M.M. Sarafraz, F. Hormozi, S.M. Peyghambarzadeh, N. Vaeli, Upward Flow Boiling to DI-Water and CuO Nanofluids Inside the Concentric Annuli, *J. Appl. Fluid Mech.* 8 (2015) 651–659.
- [54] M. Nakhjavani, V. Nikkhah, M.M. Sarafraz, S. Shoja, M. Sarafraz, Green synthesis of silver nanoparticles using green tea leaves: Experimental study on the morphological, rheological and antibacterial behaviour, *Heat Mass Transf.* 53 (2017) 3201–3209.
- [55] M.M. Sarafraz, S.M. Peyghambarzadeh, N. Vaeli, Subcooled flow boiling heat transfer of ethanol aqueous solutions in vertical annulus space, *Chem. Ind. Chem. Eng. Q.* 18 (2012) 315–327.
- [56] M.M. Sarafraz, Nucleate pool boiling of aqueous solution of citric acid on a smoothed horizontal cylinder, *Heat Mass Transf.* 48 (2012) 611–619.
- [57] M.M. Sarafraz, F. Hormozi, Application of thermodynamic models to estimating the convective flow boiling heat transfer coefficient of mixtures, *Exp. Thermal Fluid Sci.* 53 (2014) 70–85.

Chapter 8 Conclusion and future work

In the research conducted for this thesis, a thermodynamic assessment was conducted on the potential application of liquid metal oxides in a chemical looping gasification process for the syngas production. A series of experiments were conducted not only to produce some novel experimental data on the reduction and oxidation of bismuth oxide with carbon and air respectively, but also to validate the thermodynamic models developed in the thesis experimentally. The following sections show the significance of the study and make some suggestions for future research.

8.1. Significance of the present study

In this study, a new configuration for chemical looping gasification of carbonaceous feedstock was introduced, which employs a liquid oxygen carrier between the reactors. The first important contribution of this project is the feasibility study of the chemical looping gasification system, which offers a clean syngas with exergy efficiency ~68% from a graphitic carbon as a surrogate for more realistic fuels. The second significance of the project is that the proposed system can address the challenges associated with the utilisation of solid oxygen carriers in chemical looping systems, which include sintering, agglomeration, particle deactivation and deposition of carbon on the particles (for CLG systems). Likewise, the identification of various metal oxides, which are thermodynamically plausible for a chemical looping gasification system is another significance of the project. Hence, the following conclusions were drawn from different objectives of this research:

- 1) The results of the thermochemical equilibrium analysis showed that the molar ratio of the liquid oxygen carrier to the feedstock and the molar ratio of the gasifying agent (e.g. steam, CO₂ or a blended agent) to the feedstock are key parameters, which can control

the operation of the liquid chemical looping system. If the quantity of the liquid oxygen carrier is sufficient to supply stoichiometric oxygen to the reactor, the system operates as liquid chemical looping combustion, however, if the oxygen is in sub-stoichiometric value, the partial oxidation of the fuel results in gasification of the feedstock, since Boudouard and gasification reactions proceed.

- 2) The presence of steam in the reactor has several benefits: (1) it enriches the hydrogen content in the syngas resulting in the enhancement of the H_2 : CO ratio. Since the application of syngas strongly depends on the syngas quality, CLG can produce syngas with wide applications such as for Fischer-Tropsch processes, fuel cells and combustion applications. (2) Steam enhances the mixing in the reactor and, as a result, high heat and mass transfer is seen in the gasifier, resulting in high rates of conversion of the feedstock to syngas. (3) The presence of steam can maintain the required temperature inside the gasification reactor. Importantly, it adds more control to the water-gas shift reactor in the gasifier, resulting in a better quality of syngas. Hence, for the CLG process, a water-gas shift unit is not required, which reduces the costs and the energy associated with this reactor.
- 3) The chemical looping gasification system prevents direct contact between the feedstock and the air. By separating the air from the feedstock, nitrogen does not appear at the outlet syngas product. Therefore, the produced syngas has higher ratios of H_2 : CO and nitrogen dilution is also addressed.
- 4) Energetic analysis revealed that the amount of exergy partitioned in the syngas varies with the change in the molar ratio of the liquid oxygen carrier to the feedstock and the steam to the feedstock. The higher the ratio of liquid oxygen carrier to feedstock, the less the chemical exergy is partitioned in syngas. However, vitiated air, together with exhaust gases, carry a large portion of exergy as thermal energy. Likewise, the higher,

the molar ratio of steam to feedstock, the larger the portion of exergy partitioned in the syngas. For example, with copper oxide as the liquid oxygen carrier, ~68% of the total exergy is partitioned in syngas, however, for lead, bismuth and antimony oxides, the exergy transported in the syngas was 60.5%, 58% and 49%, respectively.

- 5) The liquid oxygen carrier with the most plausible thermochemical potential for a liquid chemical looping gasification system was antimony oxide. This selection was based on the highest quality of syngas that can be achieved with graphitic carbon as a feedstock. Interestingly, antimony oxide can operate at temperatures around $\sim 600^{\circ}\text{C}$, which offers a potential for hybridisation with solar thermal energy.
- 6) The liquid chemical looping gasification process minimised the production of methane during the process. For example, methane production for gasification with lead and antimony oxides was less than 1%. This results in a higher yield of hydrogen and syngas quality in comparison with other gasification methods, in which the production of methane is $\sim 5\%$ to $\sim 10\%$.
- 7) For the chemical looping gasification process, the total enthalpy of the process can be positive (the CLG process is endothermic), zero (the CLG process is auto-thermal) and negative (the CLG process is exothermic). This strongly depends on the molar ratios of the liquid oxygen carrier to the feedstock and the steam to the feedstock. Hence, the process is self-sustaining if the circulation rate of the oxygen carrier between the reactors is sufficient. For example, for lead oxide, at a molar ratio of liquid oxygen carrier to feedstock of 0.7 and steam to feedstock of 2.5, the process is fully self-sustained if heat loss from the system is neglected.
- 8) The analysis of the energetic performance of the chemical looping gasification showed that the exergy of feedstock can be partitioned either in the syngas or via vitiated air through sensible heat. The CLG process offers potential for the generation of power

that is either mechanical or electrical. A thermodynamic assessment of the potential of co-production of syngas, heat and power, with the LCLG working with liquid lead oxide showed that the maximum first law efficiency and chemical exergy efficiency of the power cycle was 33.8% and 41%, respectively at 1250°C and for a liquid oxygen carrier to feedstock of 1.5 and steam to feedstock of 2.

- 9) Blending various gasifying agents increased control over the operation of LCLG and enhanced the molar ratio of H₂: CO and the amount of lower heating value of the syngas product. For example, for LCLG working with liquid lead oxide, further control of the syngas quality was obtained through the blending of a secondary gasifying agent such as carbon dioxide with steam, which not only enhanced the hydrogen content but increased the level of hydrogen production through the water-gas shift reaction. However, there is some exergy loss due to the sensible heat loss through excess steam and CO₂. Although some of it can be recovered using a robust recovery system, thermal energy recovery from CO₂ and excess steam using current technologies has low efficiency.
- 10) The results of the modelling for the gasification of natural gas and biomass feedstock showed that the low values of the liquid oxygen carrier to the feedstock ratio and high values of the steam to the feedstock ratio are thermodynamically plausible to yield high-quality syngas. However, achieving the syngas with a ratio of H₂: CO ~3 is thermodynamically possible at the cost of excess steam consumption (~600%-800%). Thus, for the gasification of biomass, the ratio of the liquid oxygen carrier the feedstock must be between 0.4 and 1.23, and also the ratio of the steam to the feedstock must be between 1 and 4.
- 11) The effect of the content of feedstock on the quality of syngas was investigated for various types of feedstock and it was found that natural gas has potential for the

production of high-quality syngas when the ration of H₂: CO is ~10, followed by almond hull, lignite and graphite with molar ratios of H₂: CO is ~9.2, 8.7, 6.08, respectively. Importantly, the conversion extent of feedstock can be as high as 90% at T > 850°C. It was also found that there is a trade-off between the extent of the carbon conversion and both the exergy partitioned in the syngas product and the net thermal energy requirement for the LCLG. Thus, to reach complete conversion of the feedstock, the operating mode must necessarily change from a gasification to a combustion mode.

12) The results of the experimental study on the reduction and oxidation of liquid bismuth with graphite and air showed that chemical looping gasification is technically feasible in a refractory-made crucible at a temperature of ~900°C. Kinetic models for the reduction and oxidation reactions were developed using the Kissinger method and the activation energy and the reaction constant were experimentally estimated for both reactions. Characterization of the liquid phase with an x-ray diffraction test (before and after the reduction) experiments showed that there is no reaction between bismuth and the container. Also, the equilibrium models supported the experimental data reasonably well.

8.2. Recommendations for future work

In this thesis, a new system for the production of syngas via liquid metal oxides was developed thermodynamically. Thermodynamic assessments were completed, and the feasibility of the process was assessed thermodynamically and experimentally. Suitable metal oxides for the process were identified and the reactions in the gasifier were analysed experimentally. However, despite the significant knowledge developed in the field, there are some gaps, which need further research, and this is highly recommended since they would pave the way for commercialization of the process. Some suggestions are as follows:

8.2.1. Experimental analysis of the outlet gases

Although in the present research a set of experiments were conducted to assess the activation energy and reaction rate of the reduction and oxidation reactions of liquid bismuth, the main focus was only on the reactions in the liquid phase and the evolved gases were not measured experimentally. Therefore, simultaneous measurements in the liquid and gas phases are still required not only to measure the quality of the syngas, but also to measure the oxygen content in the liquid phase experimentally. The results of these experiments can be compared with the models developed for the liquid and gas phases. Moreover, in the experiments conducted in this research, 45 cc and 70 cc alumina crucibles with ceramic liners were employed in a thermogravimetric analyser. Therefore, it was not possible to measure the outlet gases online. Notably, the duration of the experiments was limited to 250 minutes, for five successive cycles; therefore, the lifetime of such crucibles over the long period of operation at high temperatures is unknown. In addition, materials such as alumina are quite expensive to be used for the fabrication of a reactor; therefore, a study should be conducted on the containment of liquid metal oxides at various temperatures to identify other plausible materials for the fabrication of the reactor. In addition, whilst the catalytic effect of liquid metals in gasification reactions with blast furnace slags has already been reported in the literature, this effect has not yet been fully understood for pure liquid metal oxides. Hence, one potential gap for future work is to study the catalytic effect of liquid metal oxides in the gasification of renewable energy resources such as biomass.

8.2.2. Plausible application of concentrated solar thermal energy

With the advancements in concentrated solar thermal energy, its application broadens to different industrial sectors. The liquid chemical looping gasification system offers potential to be hybridised with solar thermal energy. This is because the reactions in the gasifier are

endothermic for some of the liquid metals such as lead, antimony and bismuth oxides, as identified in this project. Therefore, the energy required to drive the reactions can be met with concentrated solar thermal energy. To achieve this, a thermodynamic assessment should be conducted on the process to obtain the fraction of solar thermal energy contribution; exergetic and energetic performance of the system, together with the fuel upgrade parameter. Likewise, a hybrid system has the potential to be connected to a power cycle, since it has two high-temperature streams of syngas (from the gasification reactor) and hot vitiated air (from the air reactor). Thus, the first law thermodynamic efficiency, together with an exergy analysis, needs to be conducted for different configurations of power cycles including steam turbine, gas turbine and supercritical steam power to identify the most suitable configuration for the co-production of heat, power and syngas.

8.2.3. Heat and mass transfer within a bubbling regime

A chemical looping gasification system employs two bubble columns as the air and the fuel reactors. The gaseous feedstock and the gasifying agent bubble within the bed of the liquid metal. Thus, the behaviour of the bubbles, their size and the frequency of generation of bubbles in the liquid metal are some key parameters influencing the rate of heat and mass transfer. Moreover, both the pressure drop and hold up can influence the residence time of the bubbles in the bed, the gas-liquid, gas-gas, gas-solid contacts and mixing performance of the reactors. Hence, a systematic study is highly recommended to understand the behaviour of bubbles in different liquid metals, at various temperatures and for different injection characteristics, including the nozzle diameter, injection angle and gas superficial velocity (Chisti & Moo-Young, 1989; Kantarci, Borak, & Ulgen, 2005).

8.2.4. Development of an ash separator

Reaction of biomass feedstock, natural gas and coal with liquid metal creates a massive amount of ash, including unreacted carbon. For biomass, the ash content can be as high as 10% of the total content of the reactor. Therefore, due to the considerable differences between the density of ash and liquid metal, ash can be accumulated on top of the liquid metal in the form of a porous layer, which needs to be removed. Over several successive cycles of operation, the ash content increases and creates some challenges, including agglomeration and a reduction in the rate of mixing in the reactor. Therefore, there is a need to develop a robust and efficient ash separator to separate ash contents from the liquid metal oxide. Although some ash separators have already been developed in the literature, none of them has been tested for liquid metals (Kinto, 1996; Weniger, 1947).

8.2.5. Fabrication of a small-scale reactor and LCLG plant

By undertaking the above recommendations, the main steps will be taken towards the fabrication of a small-scale chemical looping gasification plant. To achieve this, a robust system must be developed for the injection of steam into liquid metal. In addition, the containment of liquid metal and material constraint challenges must be addressed for the pipes, reactors and injection system before the small-scale plant is fabricated. Importantly, a high-fidelity system for the circulation of liquid metal oxides must be developed. The University of Adelaide has already developed a cold prototype for the circulation of a viscous liquid between two bubble column reactors. However, it needs further development for high temperature applications. Additionally, using the equilibrium models developed in the present research and the kinetics information, a molten metal reactor should be designed and optimised. To do so, a material selection is recommended to be performed to identify the plausible fabrication materials for the reactor, which can tolerate thermal expansion, creep and thermal stress.

References

- Abad, A., Adánez, J., García-Labiano, F., Luis, F., Gayán, P., & Celaya, J. (2007). Mapping of the range of operational conditions for Cu-, Fe-, and Ni-based oxygen carriers in chemical-looping combustion. *Chemical Engineering Science*, 62(1-2), 533-549.
- Abánades, A., Rathnam, R. K., Geißler, T., Heinzl, A., Mehravaran, K., Müller, G., . . . Stoppel, L. (2016). Development of methane decarbonisation based on liquid metal technology for CO₂-free production of hydrogen. *International Journal of Hydrogen Energy*, 41(19), 8159-8167.
- Abdulally, I., Edberg, C., Andrus, H., Chiu, J., Thibeault, P., & Lani, P. (2011). *ALSTOM's chemical looping combustion prototype for CO₂ capture from existing pulverized coal-fired power plants*. Paper presented at the Proceedings of Department of Energy National Energy Technology Laboratory CO₂ Capture Technology Meeting.
- Adánez, J., Abad, A., Garcia-Labiano, F., Gayan, P., & Luis, F. (2012). Progress in chemical-looping combustion and reforming technologies. *Progress in energy and combustion science*, 38(2), 215-282.
- Adánez, J., de Diego, L. F., García-Labiano, F., Gayán, P., Abad, A., & Palacios, J. (2004). Selection of oxygen carriers for chemical-looping combustion. *Energy & Fuels*, 18(2), 371-377.
- Adánez, J., García-Labiano, F., de Diego, L., Gayán, P., Abad, A., & Celaya, J. (2005). Development of oxygen carriers for chemical-looping combustion. *Carbon dioxide capture for storage in deep geologic formations-Results from the CO₂ Capture Project*, 1, 587-604.
- Adánez, J., García-Labiano, F., de Diego, L. F., Gayán, P., Celaya, J., & Abad, A. (2006). Nickel–copper oxygen carriers to reach zero CO and H₂ emissions in chemical-looping combustion. *Industrial & Engineering Chemistry Research*, 45(8), 2617-2625.
- Adánez, J., Gayán, P., Celaya, J., de Diego, L. F., García-Labiano, F., & Abad, A. (2006). Chemical looping combustion in a 10 kW_{th} prototype using a CuO/Al₂O₃ oxygen carrier: Effect of operating conditions on methane combustion. *Industrial & engineering chemistry research*, 45(17), 6075-6080.
- Ahmad, A. A., Zawawi, N. A., Kasim, F. H., Inayat, A., & Khasri, A. (2016). Assessing the gasification performance of biomass: A review on biomass gasification process conditions, optimization and economic evaluation. *Renewable and Sustainable Energy Reviews*, 53, 1333-1347.
- Bach, R. D., & Nagel, C. J. (1986). Destruction of toxic chemicals: Google Patents.
- Brandvoll, O. y., & Bolland, O. (2002). *Inherent CO₂ capture using chemical looping combustion in a natural gas fired power cycle*. Paper presented at the ASME Turbo Expo 2002: Power for Land, Sea, and Air.
- Brown, T., Dennis, J., Scott, S., Davidson, J., & Hayhurst, A. (2010). Gasification and chemical-looping combustion of a lignite char in a fluidized bed of iron oxide. *Energy & fuels*, 24(5), 3034-3048.
- Burke, P., & Gull, S. (2002). *HISmelt[®]-The Alternative Ironmaking Technology*. Paper presented at the Proceedings of International Conference on Smelting Reduction for Ironmaking, Jouhari, AK, Galgali, RK, Misra, VN, Eds.
- Burnard, K., & Bhattacharya, S. (2011). Power generation from coal.
- Cao, Y., & Pan, W.-P. (2006). Investigation of chemical looping combustion by solid fuels. 1. Process analysis. *Energy & Fuels*, 20(5), 1836-1844.
- Chang, A. C., Chang, H.-F., Lin, F.-J., Lin, K.-H., & Chen, C.-H. (2011). Biomass gasification for hydrogen production. *International Journal of Hydrogen Energy*, 36(21), 14252-14260.

- Change, I. C. (2007). Mitigation of climate change. *Summary for Policymakers*, 10(5.4).
- Chisti, Y., & Moo-Young, M. (1989). On the calculation of shear rate and apparent viscosity in airlift and bubble column bioreactors. *Biotechnology and bioengineering*, 34(11), 1391-1392.
- Cho, P., Mattisson, T., & Lyngfelt, A. (2005). Carbon formation on nickel and iron oxide-containing oxygen carriers for chemical-looping combustion. *Industrial & engineering chemistry research*, 44(4), 668-676.
- Cho, P., Mattisson, T., & Lyngfelt, A. (2006). Defluidization conditions for a fluidized bed of iron oxide-, nickel oxide-, and manganese oxide-containing oxygen carriers for chemical-looping combustion. *Industrial & Engineering Chemistry Research*, 45(3), 968-977.
- Conti, J., Holtberg, P., Diefenderfer, J., LaRose, A., Turnure, J. T., & Westfall, L. (2016). *International Energy Outlook 2016 With Projections to 2040*.
- Corella, J., Aznar, M. P., Delgado, J., & Aldea, E. (1991). Steam gasification of cellulosic wastes in a fluidized bed with downstream vessels. *Industrial & Engineering Chemistry Research*, 30(10), 2252-2262.
- Cuadrat, A., Abad, A., Adánez, J., De Diego, L., García-Labiano, F., & Gayán, P. (2012). Behavior of ilmenite as oxygen carrier in chemical-looping combustion. *Fuel Processing Technology*, 94(1), 101-112.
- Daniel, T. (1931). Production of hydrogen: Google Patents.
- De Diego, L. F., García-Labiano, F., Adánez, J., Gayán, P., Abad, A., Corbella, B. M., & Palacios, J. M. a. (2004). Development of Cu-based oxygen carriers for chemical-looping combustion. *Fuel*, 83(13), 1749-1757.
- De Diego, L. F., Gayán, P., García-Labiano, F., Celaya, J., Abad, A., & Adánez, J. (2005). Impregnated CuO/Al₂O₃ oxygen carriers for chemical-looping combustion: avoiding fluidized bed agglomeration. *Energy & Fuels*, 19(5), 1850-1856.
- de Noronha, R. F., Miranda, M. A., Cavalca, K. L., Memmott, E. A., & Ramesh, K. (2014). 43rd Turbomachinery & 30th Pump Users Symposia (Pump & Turbo 2014) September 23-25, 2014| Houston, TX| pumpturbo. tamu. edu.
- Dunn, W., Bonilla, C., Ferstenberg, C., & Gross, B. (1956). Mass transfer in liquid metals. *AIChE journal*, 2(2), 184-189.
- Eatwell-Hall, R., Sharifi, V., & Swithenbank, J. (2010). Hydrogen production from molten metal gasification. *International Journal of Hydrogen Energy*, 35(24), 13168-13178.
- Energy, D. (2009). HydroMax—Advanced gasification technology.
- Fan, L., Li, F., & Ramkumar, S. (2008). Utilization of chemical looping strategy in coal gasification processes. *Particuology*, 6(3), 131-142.
- Gaffney, J. S., & Marley, N. A. (2009). The impacts of combustion emissions on air quality and climate—From coal to biofuels and beyond. *Atmospheric Environment*, 43(1), 23-36.
- Gao, N., Li, A., Quan, C., & Gao, F. (2008). Hydrogen-rich gas production from biomass steam gasification in an updraft fixed-bed gasifier combined with a porous ceramic reformer. *International Journal of Hydrogen Energy*, 33(20), 5430-5438.
- Gayán, P., Forero, C. R., Abad, A., de Diego, L. F., García-Labiano, F., & Adánez, J. (2011). Effect of support on the behavior of Cu-based oxygen carriers during long-term CLC operation at temperatures above 1073 K. *Energy & Fuels*, 25(3), 1316-1326.
- Gayán, P., Luis, F., García-Labiano, F., Adánez, J., Abad, A., & Dueso, C. (2008). Effect of support on reactivity and selectivity of Ni-based oxygen carriers for chemical-looping combustion. *Fuel*, 87(12), 2641-2650.

- Geißler, T., Abánades, A., Heinzl, A., Mehravaran, K., Müller, G., Rathnam, R., . . . Stückrad, S. (2016). Hydrogen production via methane pyrolysis in a liquid metal bubble column reactor with a packed bed. *Chemical Engineering Journal*, 299, 192-200.
- Geißler, T., Plevan, M., Abánades, A., Heinzl, A., Mehravaran, K., Rathnam, R., . . . Stückrad, S. (2015). Experimental investigation and thermo-chemical modeling of methane pyrolysis in a liquid metal bubble column reactor with a packed bed. *International Journal of Hydrogen Energy*, 40(41), 14134-14146.
- Georgakis, C., Chang, C., & Szekely, J. (1979). A changing grain size model for gas—solid reactions. *Chemical Engineering Science*, 34(8), 1072-1075.
- Greenwalt, R. B. (1997). Method of providing fuel for an iron making process: Google Patents.
- Gulevich, A., Martynov, P., Gulevsky, V., & Ulyanov, V. (2008). Technologies for hydrogen production based on direct contact of gaseous hydrocarbons and evaporated water with molten Pb or Pb–Bi. *Energy conversion and management*, 49(7), 1946-1950.
- Guo, Q., Cheng, Y., Liu, Y., Jia, W., & Ryu, H.-J. (2013). Coal chemical looping gasification for syngas generation using an iron-based oxygen carrier. *Industrial & Engineering Chemistry Research*, 53(1), 78-86.
- Halloran, J. W. (2008). Extraction of hydrogen from fossil fuels with production of solid carbon materials. *International Journal of Hydrogen Energy*, 33(9), 2218-2224.
- Hatanaka, T., Matsuda, S., & Hatano, H. (1997). A new-concept gas-solid combustion system “MERIT” for high combustion efficiency and low emissions. Paper presented at the Energy Conversion Engineering Conference, 1997. IECEC-97., Proceedings of the 32nd Intersociety.
- He, F., Galinsky, N., & Li, F. (2013). Chemical looping gasification of solid fuels using bimetallic oxygen carrier particles—Feasibility assessment and process simulations. *International Journal of Hydrogen Energy*, 38(19), 7839-7854.
- Herguido, J., Corella, J., & Gonzalez-Saiz, J. (1992). Steam gasification of lignocellulosic residues in a fluidized bed at a small pilot scale. Effect of the type of feedstock. *Industrial & Engineering Chemistry Research*, 31(5), 1274-1282.
- Holcombe, T. C., & Malone, D. P. (2002). Two-zone molten metal hydrogen-rich and carbon monoxide-rich gas generation process: Google Patents.
- Hossain, M. M., & de Lasa, H. I. (2008). Chemical-looping combustion (CLC) for inherent CO₂ separations—a review. *Chemical Engineering Science*, 63(18), 4433-4451.
- Hoteit, A., Chandel, M. K., & Delebarre, A. (2009). Nickel-and Copper-Based Oxygen Carriers for Chemical Looping Combustion. *Chemical engineering & technology*, 32(3), 443-449.
- Huang, Z., Zhang, Y., Fu, J., Yu, L., Chen, M., Liu, S., . . . Zhao, K. (2016). Chemical looping gasification of biomass char using iron ore as an oxygen carrier. *International Journal of Hydrogen Energy*, 41(40), 17871-17883.
- IEA. (2017). *World Energy Outlook 2017*: Organisation for Economic Co-operation and Development, OECD.
- Irfan, M. F., Usman, M. R., & Kusakabe, K. (2011). Coal gasification in CO₂ atmosphere and its kinetics since 1948: A brief review. *Energy*, 36(1), 12-40.
- Ishida, M., & Jin, H. (1994). A novel combustor based on chemical-looping reactions and its reaction kinetics. *Journal of Chemical Engineering of Japan*, 27(3), 296-301.
- Ishida, M., Jin, H., & Okamoto, T. (1998). Kinetic behavior of solid particle in chemical-looping combustion: suppressing carbon deposition in reduction. *Energy & Fuels*, 12(2), 223-229.
- Jafarian, M., Arjomandi, M., & Nathan, G. J. (2014). Influence of the type of oxygen carriers on the performance of a hybrid solar chemical looping combustion system. *Energy & fuels*, 28(5), 2914-2924.

- Jafarian, M., Arjomandi, M., & Nathan, G. J. (2017). Thermodynamic potential of high temperature chemical looping combustion with molten iron oxide as the oxygen carrier. *Chemical Engineering Research and Design*, *120*, 69-81.
- Jerndal, E., Mattisson, T., & Lyngfelt, A. (2009). Investigation of different NiO/NiAl₂O₄ particles as oxygen carriers for chemical-looping combustion. *Energy & fuels*, *23*(2), 665-676.
- Jin, H., Okamoto, T., & Ishida, M. (1998). Development of a novel chemical-looping combustion: synthesis of a looping material with a double metal oxide of CoO– NiO. *Energy & fuels*, *12*(6), 1272-1277.
- Johansson, E., Lyngfelt, A., Mattisson, T., & Johnsson, F. (2003). Gas leakage measurements in a cold model of an interconnected fluidized bed for chemical-looping combustion. *Powder Technology*, *134*(3), 210-217.
- Johnson, J. (1974). Kinetics of bituminous coal char gasification with gases containing steam and hydrogen. In: ACS Publications.
- Joshi, A., Lou, X., Neuschaefer, C., Chaudry, M., & Quinn, J. (2012). *Development of Computational Approaches for Simulation and Advanced Controls for Hybrid Combustion-Gasification Chemical Looping*.
- Kalinci, Y., Hepbasli, A., & Dincer, I. (2009). Biomass-based hydrogen production: a review and analysis. *International Journal of Hydrogen Energy*, *34*(21), 8799-8817.
- Kantarci, N., Borak, F., & Ulgen, K. O. (2005). Bubble column reactors. *Process biochemistry*, *40*(7), 2263-2283.
- Karimipour, S., Gerspacher, R., Gupta, R., & Spiteri, R. J. (2013). Study of factors affecting syngas quality and their interactions in fluidized bed gasification of lignite coal. *Fuel*, *103*, 308-320.
- Kern, S., Pfeifer, C., & Hofbauer, H. (2013). Gasification of wood in a dual fluidized bed gasifier: Influence of fuel feeding on process performance. *Chemical Engineering Science*, *90*, 284-298.
- Kim, S. D., Go, K. S., Jeon, Y. W., & Park, C. S. (2010). Chemical-looping steam methane reforming for hydrogen production in a circulating fluidized bed reactor.
- Kinto, K. (1996). Ash melting system and reuse of products by arc processing. *Waste Management*, *16*(5-6), 423-430.
- Kirubakaran, V., Sivaramakrishnan, V., Nalini, R., Sekar, T., Premalatha, M., & Subramanian, P. (2009). A review on gasification of biomass. *Renewable and Sustainable Energy Reviews*, *13*(1), 179-186.
- Kolbitsch, P., Pröll, T., Bolhar-Nordenkamp, J., & Hofbauer, H. (2009). Design of a chemical looping combustor using a dual circulating fluidized bed (DCFB) reactor system. *Chemical engineering & technology*, *32*(3), 398-403.
- Kronberger, B., Johansson, E., Löffler, G., Mattisson, T., Lyngfelt, A., & Hofbauer, H. (2004). A two-compartment fluidized bed reactor for CO₂ capture by chemical-looping combustion. *Chemical engineering & technology*, *27*(12), 1318-1326.
- Kronberger, B., Lyngfelt, A., Löffler, G., & Hofbauer, H. (2005). Design and fluid dynamic analysis of a bench-scale combustion system with CO₂ separation– chemical-looping combustion. *Industrial & Engineering Chemistry Research*, *44*(3), 546-556.
- Ku, Y., Shiu, S.-H., Liu, Y.-C., Wu, H.-C., Kuo, Y.-L., & Lee, H.-Y. (2017). Liquid sintering behavior of Cu-based oxygen carriers for chemical looping process. *Catalysis Communications*, *92*, 70-74.
- Kumar, A., Jones, D. D., & Hanna, M. A. (2009). Thermochemical biomass gasification: a review of the current status of the technology. *Energies*, *2*(3), 556-581.
- LaMont, D. C., Seaba, J., Latimer, E. G., & Platon, A. (2010). Liquid-phase chemical looping energy generator: Google Patents.

- Leion, H., Lyngfelt, A., Johansson, M., Jerndal, E., & Mattisson, T. (2008). The use of ilmenite as an oxygen carrier in chemical-looping combustion. *Chemical Engineering Research and Design*, 86(9), 1017-1026.
- Leion, H., Mattisson, T., & Lyngfelt, A. (2009). Use of ores and industrial products as oxygen carriers in chemical-looping combustion. *Energy & Fuels*, 23(4), 2307-2315.
- Li, F., & Fan, L.-S. (2008). Clean coal conversion processes—progress and challenges. *Energy & Environmental Science*, 1(2), 248-267.
- Li, F., Kim, H. R., Sridhar, D., Wang, F., Zeng, L., Chen, J., & Fan, L.-S. (2009). Syngas chemical looping gasification process: oxygen carrier particle selection and performance. *Energy & fuels*, 23(8), 4182-4189.
- Li, F., Zeng, L., Velazquez-Vargas, L. G., Yoscovits, Z., & Fan, L. S. (2010). Syngas chemical looping gasification process: Bench-scale studies and reactor simulations. *AIChE journal*, 56(8), 2186-2199.
- Lieuwen, T., Yetter, R., & Yang, V. (2009). *Synthesis gas combustion: fundamentals and applications*: CRC Press.
- Liu, G., Liao, Y., Wu, Y., & Ma, X. (2018). Application of calcium ferrites as oxygen carriers for microalgae chemical looping gasification. *Energy conversion and management*, 160, 262-272. doi: <https://doi.org/10.1016/j.enconman.2018.01.041>
- Luis, F., Garcá, F., Gayán, P., Celaya, J., Palacios, J. M., & Adánez, J. (2007a). Operation of a 10 kWth chemical-looping combustor during 200 h with a CuO–Al₂O₃ oxygen carrier. *Fuel*, 86(7-8), 1036-1045.
- Luis, F., Garcá, F., Gayán, P., Celaya, J., Palacios, J. M., & Adánez, J. (2007b). Operation of a 10kWth chemical-looping combustor during 200h with a CuO–Al₂O₃ oxygen carrier. *Fuel*, 86(7), 1036-1045.
- Lyngfelt, A., Kronberger, B., Adanez, J., Morin, J., & Hurst, P. (2004). *The GRACE project. Development of oxygen carrier particles for chemical-looping combustion. Design and operation of a 10KW chemical-looping combustor*: na.
- Lyngfelt, A., Leckner, B., & Mattisson, T. (2001). A fluidized-bed combustion process with inherent CO₂ separation; application of chemical-looping combustion. *Chemical Engineering Science*, 56(10), 3101-3113.
- Lyngfelt, A., & Thunman, H. (2005a). Construction and 100 h of operational experience of a 10-kW chemical-looping combustor. *Carbon Dioxide Capture for Storage in Deep Geologic Formations; Results from the CO₂ Capture Project*, 1, 625-645.
- Lyngfelt, A., & Thunman, H. (2005b). Construction and 100 h of operational experience of a 10-kW chemical-looping combustor. *Carbon dioxide capture for storage in deep geologic formations-results from the CO₂ capture project*, 1, 625-645.
- Martynov, P., Gulevich, A., Orlov, Y. I., & Gulevsky, V. (2005). Water and hydrogen in heavy liquid metal coolant technology. *Progress in Nuclear Energy*, 47(1-4), 604-615.
- Mattisson, T., Johansson, M., Jerndal, E., & Lyngfelt, A. (2008). The reaction of NiO/NiAl₂O₄ particles with alternating methane and oxygen. *The Canadian Journal of Chemical Engineering*, 86(4), 756-767.
- Mattisson, T., Johansson, M., & Lyngfelt, A. (2004). Multicycle reduction and oxidation of different types of iron oxide particles application to chemical-looping combustion. *Energy & Fuels*, 18(3), 628-637.
- Mattisson, T., Johansson, M., & Lyngfelt, A. (2006). The use of NiO as an oxygen carrier in chemical-looping combustion. *Fuel*, 85(5-6), 736-747.
- McGlashan, N. (2008). Chemical-looping combustion—a thermodynamic study. *Proceedings of the Institution of Mechanical Engineers, Part C: Journal of Mechanical Engineering Science*, 222(6), 1005-1019.

- Monazam, E. R., Siriwardane, R., Breault, R. W., Tian, H., Shadle, L. J., Richards, G., & Carpenter, S. (2012). Kinetics of the reduction of CuO/bentonite by methane (CH₄) during chemical looping combustion. *Energy & Fuels*, 26(5), 2779-2785.
- Noorman, S., van Sint Annaland, M., & Kuipers, J. (2010). Experimental validation of packed bed chemical-looping combustion. *Chemical Engineering Science*, 65(1), 92-97.
- Ono, H., Yoshida, S., Nezuka, M., Sano, T., Tsuji, M., & Tamaura, Y. (1999). Kinetics and simulation on a high-temperature solar thermochemical energy conversion process on the Boudouard reaction. *Energy & fuels*, 13(3), 579-584.
- Ortiz, M., Abad, A., Luis, F., García-Labiano, F., Gayán, P., & Adánez, J. (2011). Optimization of hydrogen production by chemical-looping auto-thermal reforming working with Ni-based oxygen-carriers. *International Journal of Hydrogen Energy*, 36(16), 9663-9672.
- Outlook, A. E. (2007). with Projections to 2030. *US Energy Information Administration*.
- Owusu, P. A., & Asumadu-Sarkodie, S. (2016). A review of renewable energy sources, sustainability issues and climate change mitigation. *Cogent Engineering*, 3(1), 1167990.
- Pan, Y., Velo, E., Roca, X., Manya, J., & Puigjaner, L. (2000). Fluidized-bed co-gasification of residual biomass/poor coal blends for fuel gas production. *Fuel*, 79(11), 1317-1326.
- Paxman, D., Trottier, S., Nikoo, M., Secanell, M., & Ordorica-Garcia, G. (2014). Initial experimental and theoretical investigation of solar molten media methane cracking for hydrogen production. *Energy Procedia*, 49, 2027-2036.
- Plevan, M., Geißler, T., Abánades, A., Mehravaran, K., Rathnam, R., Rubbia, C., . . . Wetzler, T. (2015). Thermal cracking of methane in a liquid metal bubble column reactor: Experiments and kinetic analysis. *International Journal of Hydrogen Energy*, 40(25), 8020-8033.
- Plewa, J., & Skrzypek, J. (1989). Kinetics of the reduction of copper oxide with carbon monoxide. *Chemical Engineering Science*, 44(12), 2817-2824.
- Prathap, C., Ray, A., & Ravi, M. (2008). Investigation of nitrogen dilution effects on the laminar burning velocity and flame stability of syngas fuel at atmospheric condition. *Combustion and Flame*, 155(1-2), 145-160.
- Richter, H. J., & Knoche, K. F. (1983). *Reversibility of combustion processes*. Paper presented at the ACS Symposium series.
- Riedel, T., Claeys, M., Schulz, H., Schaub, G., Nam, S.-S., Jun, K.-W., . . . Lee, K.-W. (1999). Comparative study of Fischer–Tropsch synthesis with H₂/CO and H₂/CO₂ syngas using Fe- and Co-based catalysts. *Applied Catalysis A: General*, 186(1-2), 201-213.
- Rostrup-Nielsen, J. R. (2002). Syngas in perspective. *Catalysis today*, 71(3), 243-247.
- Rydén, M., Lyngfelt, A., & Mattisson, T. (2008). Chemical-looping combustion and chemical-looping reforming in a circulating fluidized-bed reactor using Ni-based oxygen carriers. *Energy & Fuels*, 22(4), 2585-2597.
- Ryu, H.-J., Bae, D.-H., & Jin, G.-T. (2003). Effect of temperature on reduction reactivity of oxygen carrier particles in a fixed bed chemical-looping combustor. *Korean Journal of Chemical Engineering*, 20(5), 960-966.
- Ryu, H.-J., Jin, G.-T., & Yi, C.-K. (2005). -Demonstration of inherent CO₂ separation and NO_x emission in a 50kW chemical-looping combustor: Continuous reduction and oxidation experiment. In *Greenhouse Gas Control Technologies 7* (pp. 1907-1910): Elsevier.
- Ryu, H., Jo, S.-H., Park, Y. C., Bae, D., & Kim, S. (2010). *Long term operation experience in a 50 kWth chemical looping combustor using natural gas and syngas as fuels*. Paper presented at the 1st International Conference on Chemical Looping.

- Sarafraz, M., Jafarian, M., Arjomandi, M., & Nathan, G. (2017). Potential use of liquid metal oxides for chemical looping gasification: a thermodynamic assessment. *Applied energy*, 195, 702-712.
- Sarafraz, M., Jafarian, M., Arjomandi, M., & Nathan, G. (2018). Potential of molten lead oxide for liquid chemical looping gasification (LCLG): a thermochemical analysis. *International Journal of Hydrogen Energy*, 43(9), 4195-4210.
- Sarafraz, M., Jafarian, M., Arjomandi, M., & Nathan, G. (2019a). Experimental investigation of the reduction of liquid bismuth oxide with graphite. *Fuel Processing Technology*, 188, 110-117.
- Sarafraz, M., Jafarian, M., Arjomandi, M., & Nathan, G. (2019b). The thermo-chemical potential liquid chemical looping gasification with bismuth oxide. *International Journal of Hydrogen Energy*.
- Sarafraz, M., Jafarian, M., Arjomandi, M., & Nathan, G. J. (2017). The relative performance of alternative oxygen carriers for liquid chemical looping combustion and gasification. *International Journal of Hydrogen Energy*, 42(26), 16396-16407.
- Sato, A., Aragane, G., Kamihira, K., & Yoshimatso, S. (1987). Reducing rates of molten iron oxide by solid carbon or carbon in molten iron. *Transactions of the Iron and Steel Institute of Japan*, 27(10), 789-796.
- Schenk, S. (2007). *HydroMax: Breakthrough Molten-Metal Coal Gasification Technology*. Paper presented at the Presentation at the Gasification Technology Conference, San Francisco, CA.
- Schultz, I., & Agar, D. W. (2015). Decarbonisation of fossil energy via methane pyrolysis using two reactor concepts: Fluid wall flow reactor and molten metal capillary reactor. *International Journal of Hydrogen Energy*, 40(35), 11422-11427.
- Schwebel, G., Wiedenmann, F., & Krumm, W. (2010). *Reduction performance of ilmenite and hematite oxygen carriers in the context of a new CLC reactor concept*. Paper presented at the 1st International Conference on Chemical Looping: An Alternative Concept for Efficient and Clean Use of Fossil Resources.
- Scott, S., Dennis, J., Hayhurst, A., & Brown, T. (2006). In situ gasification of a solid fuel and CO₂ separation using chemical looping. *AIChE journal*, 52(9), 3325-3328.
- Seaton, C. E., Rodriguez, A. A., Gonzalez, M., & Manrique, M. (1983). The Rate of Dissolution of Pre-reduced Iron in Molten Steel. *Transactions of the Iron and Steel Institute of Japan*, 23(1), 14-20.
- Serban, M., Lewis, M. A., Marshall, C. L., & Doctor, R. D. (2003). Hydrogen production by direct contact pyrolysis of natural gas. *Energy & Fuels*, 17(3), 705-713.
- Shen, L., Gao, Y., & Xiao, J. (2008). Simulation of hydrogen production from biomass gasification in interconnected fluidized beds. *Biomass and bioenergy*, 32(2), 120-127.
- Shen, L., Wu, J., Xiao, J., Song, Q., & Xiao, R. (2009). Chemical-looping combustion of biomass in a 10 kWth reactor with iron oxide as an oxygen carrier. *Energy & fuels*, 23(5), 2498-2505.
- Steinberg, M. (1999). Fossil fuel decarbonization technology for mitigating global warming. *International Journal of Hydrogen Energy*, 24(8), 771-777.
- Szekely, J., Lin, C., & Sohn, H. (1973). A structural model for gas—solid reactions with a moving boundary—V an experimental study of the reduction of porous nickel-oxide pellets with hydrogen. *Chemical Engineering Science*, 28(11), 1975-1989.
- Turn, S., Kinoshita, C., Zhang, Z., Ishimura, D., & Zhou, J. (1998). An experimental investigation of hydrogen production from biomass gasification. *International Journal of Hydrogen Energy*, 23(8), 641-648.

- Udomsirichakorn, J., & Salam, P. A. (2014). Review of hydrogen-enriched gas production from steam gasification of biomass: the prospect of CaO-based chemical looping gasification. *Renewable and Sustainable Energy Reviews*, 30, 565-579.
- Upadhy, K. (1986). Kinetics of reduction of lead oxide in liquid slag by carbon in iron. *Metallurgical Transactions B*, 17(2), 271-279.
- Velazquez-Vargas, L. G. (2007). *Development of chemical looping gasification processes for the production of hydrogen from coal*. The Ohio State University.
- Wang, K., Yu, Q., Qin, Q., Hou, L., & Duan, W. (2015). Thermodynamic analysis of syngas generation from biomass using chemical looping gasification method. *International Journal of Hydrogen Energy*.
- Wang, K., Yu, Q., Qin, Q., Hou, L., & Duan, W. (2016). Thermodynamic analysis of syngas generation from biomass using chemical looping gasification method. *International Journal of Hydrogen Energy*, 41(24), 10346-10353.
- Weniger, J. K. (1947). Ash and dust separator: Google Patents.
- Wolf, J., Anheden, M., & Yan, J. (2001). *Performance analysis of combined cycles with chemical looping combustion for CO₂ capture*. Paper presented at the Proceedings of 18th Pittsburg Coal Conference, December.
- Woolcock, P. J., & Brown, R. C. (2013). A review of cleaning technologies for biomass-derived syngas. *Biomass and bioenergy*, 52, 54-84.
- Wu, J., Shen, L., Hao, J., & Gu, H. (2010). *Chemical looping combustion of coal in a 1 kWth reactor*. Paper presented at the 1st International Conference on Chemical Looping.